UNIVERSITY OF BAHRAIN

College of Engineering

Department of
Civil Engineering

Shear Behavior of Ultra-High Strength Concrete Beams Reinforced with High Strength Steel Bars

A Thesis Submitted in Partial Fulfillment of the Requirements for the Ph.D. Degree in Civil Engineering

Prepared by

Mohammed Moosa Mohammed Meqdadi

University Number: 20150098

Supervised by

Prof. Mustafa Aytekin
Professor
University of Bahrain

Dr. Md Shah Alam
Assistant Professor
University of Bahrain

Kingdom of Bahrain

January 2023

UNIVERSITY OF BAHRAIN

College of Engineering

Department of Civil Engineering

Shear Behavior of Ultra-High Strength Concrete Beams Reinforced with High Strength Steel Bars

A Thesis Submitted in Partial Fulfillment of the Requirements for the Ph.D. Degree in Civil Engineering

Prepared by

Mohammed Moosa Mohammed Meqdadi

University Number: 20150098

Supervised by

Prof. Mustafa Aytekin
Professor
University of Bahrain

Dr. Md Shah Alam
Assistant Professor
University of Bahrain

Kingdom of Bahrain

January 2023

بسم الله الرحمن الرحيم

University of Bahrain
Deanship of Graduate Studies
And scientific Research

جامعة البحرين
عمادة الدراسات العليا والبحث العلمي

Thesis Discussion Committee Decision

Student Name: Mohammed Moosa Mohammed Meqdadi	Student ID: 20150098
Department: **Civil Engineering**	College: **Engineering**
Program: **PhD in Civil Engineering**	
Thesis Title: Shear Behavior of Ultra-High Strength Concrete Beams Reinforced with High Strength Steel Bars	
Supervisor Name: **Prof. Mustafa Aytekin & Dr. MD Shah Alam**	Student GPA: **3.43**

The Discussion Committee met on 06-Mar-23 In Room 29-107. Upon discussing the student whose details are stated above in public, the discussion committee recommends the following:

The student is awarded a grade A- in the thesis subject.

☐ Without making any changes to the thesis.

☒ After making the modifications attached with this decision.

Discussion Committee Members Approval:

Name		Signature
1. Prof. Mustafa Aytekin&Dr.MD.S.Alam	(Advisor)	Click here to enter text.
2. Prof. Ghulam Hussain	(Internal Examiner)	Click here to enter text.
3. Prof. Erkan Dogan	(External Examiner)	

Approved at the University Council 6th meeting, 2013
In accordance with Decision No. 736/2013 dated 14/3/2013
Modified by University Council Decision No. 2043/2013 dated 20/11/2013.

Abstract

Ultra-High Strength Concrete (UHSC) reinforced with High Strength Steel (HSS) bars is a composite material utilized as a structural member that reduces cross-sectional dimensions causing the reduction of the structure's self-weight and cost. To avoid the shear failure of reinforced concrete beams, it is important to investigate the shear behavior of a structural member. Shear failure is considered a major structural problem because it usually occurs without warning. Hence, the aim of this thesis is to study the shear behavior of (UHSC) reinforced with (HSS) bars without web reinforcement.

In this study the shear behavior of UHSC reinforced with HSS is investigated experimentally and numerically. Three groups of beams were examined, three for each group with nine beams, combined with three cubes as a control specimen for each beam. The beams have been experimentally tested, numerically compared using the analysis tool ANSYS, and theoretically compared to international codes ACI 318, BS 8110, and Eurocode 2.

The span-to-depth ratio (a/d), flexural reinforcement ratio (ρ), and compressive strength of concrete (f_{cu}) are the main variables investigated in this study. The values for the first variable (a/d) in G1 taken as 2.62, 3.16 and 4.21 with ρ equal to 0.041 (= 1.088 ρ_b) and f_{cu} Grade C110. On the other hand, the values for the second variable (ρ) in G2 taken as 0.019, 0.031, and ρ = 0.041 (= 0.521 ρ_b, 0.838 ρ_b, and 1.088 ρ_b respectively) with a/d = 4.21 and f_{cu} Grade C110. While the values for the third variable (f_{cu}) in G3 are 76.8 MPa, 102.2 MPa and 112.8 MPa with a/d = 2.63, and ρ = 0.041 (= 1.088 ρ_b). All the beams were casted without stirrups to investigate (a/d), (ρ), and (f_{cu}) respectively. The behavior of the tested beams was studied in terms of crack pattern, failure mechanisms, load deflection relationships, and shear strength of beams.

The experiment results indicate that at the same load level, as (a/d) ratio increases, deflection increase and shear strength decreases. Further, as ρ or f_{cu} increases, deflection decrease and shear strength increases. The experimental study on shear strengths of ultra-high strength concrete reinforced with high strength steel bars without web reinforcement was compared with ACI 318, BS 8110, and Eurocode 2 equations. The results show that the measured shear strength was larger than those predicted by code equations by varying the amount depending on (a/d), (ρ) and (f_{cu}); hence, these codes were underestimated in this investigation and instead increase for the identified type of concrete.

The Finite Element Analysis (FEA) results show a linear relationship for the beams with higher steel ratio ($\rho / \rho_b > 1$) and lower ($a/d < 4.21$), where the relationship shows linear up to 60 to 80% then non-linear for lower steel ratio ($\rho / \rho_b < 1$) and higher ($a/d \geq 4.21$). The FEA results also indicate that for the same load level, increasing the (a/d) ratio increases the deflection and decreases the shear strength. Furthermore, increasing (ρ) or (f_{cu}) decreases the deflection and increases the shear strength. This is consistent with experiment results. The shear strength of FEA is about 6% higher than the experiment results.

Publications

Dedication

To my parents, wife, kids, brothers, and sisters

Acknowledgments

I would like to express my appreciation to my thesis supervisor, Dr. Md Shah Alam for his excellent supervision, assistance, and encouragement throughout the entire study and Prof. Mustafa Aytekin for providing me support and for orienting me on academic procedures until the completion of this thesis. Similarly, my sincere appreciation and respect to the head of the Civil Engineering Department, Dr. Nuha Alzayani for the great support provided particularly in following up the progress of my PhD thesis.

My great and special gratitude to my wife and to all my family members: the kids, brothers, and sisters for their moral support during the study and research period.

Gratitude is also extended to Engineer Waheed Ghuloom for his valuable help during the conduct of experimental work in the structural lab of the Civil Engineering Department. Moreover, I thank my friends and colleagues at the University of Bahrain and at the Ministry of Works, Municipalities Affairs and Urban Planning for their moral encouragement.

Finally, I would like to thank Bahrain Precast Concrete Company for casting the beams in their yard and Alhoty Materials Testing Laboratories for testing the steel reinforcement bars and concrete cubes. Moreover, many thanks to the Materials Engineering Directorate Laboratories of the Ministry of Works for providing guidance and information relevant to my study.

Table of Contents

Thesis Discussion Committee Decision ..... B
Abstract C
Publications and Participations ..... E
Dedication ..... F
Acknowledgments ..... G
Table of Contents ..... H
List of Tables ..... M
List of Figures ..... N
List of Abbreviations ..... R
Chapter 1 Introduction 1
1.1 General 2
1.2 Ultra High Strength Concrete 3
1.3 High Strength Steel 5
1.4 Ultra-High-Strength Reinforced Concrete Beams 5
1.5 Finite Element Method 7
1.6 Research Problem 7
1.7 Research Questions 8
1.8 Research Objectives 8
1.9 Research Significance 9
1.10 Research Scope 9
1.11 Definition of Terms 9
1.12 Research Outline 11
Chapter 2 Literature Review 12
2.1 Introduction 13
2.2 Flexure Behavior of Ultra-High Strength cCncrete 14
2.2.1 Design Formulas for Rectangular Beam Using ACI 318 code 14
2.2.2 Design Formulas for rRctangular Beam Using BS 8110 code 17
2.2.3 Design Formulas for Rectangular Beam Using Eurocode 2 18
2.2.4 Design Formulas for Rectangular Beam Using Canadian Code ..... CSA A23.3 19

2.3 Cracking Moments ans Stresses in Reinforced Concrete Beams 20
2.4 Shear Behavior of Reinforced Concrete Beams 23
2.5 Codes Prediction for Reinforced Concrete Beams in Shear 24
2.5.1 American Code ACI 318-2019 24
2.5.2 British Code BS 8110-1-1997 25
2.5.3 Eurocode 2 EN 1992-1-2-2004 25
2.5.4 Canadian Code CSA S6-09 Addendum 26
2.6 Shear Behavior of Ultra-High Strength Concrete Beams 27
Chapter 3 Experimental Works 39
3.1 Introduction 40
3.2 Materials 41
3.2.1 Cement 41
3.2.2 Aggregate 41
3.2.2.1 Coarse Aggregate 41
3.2.2.2 Fine Aggregate 42
3.2.3 Water 43
3.2.4 Chemical Admixture 43
3.2.5 Slag 43
3.2.6 Micro Silica 43
3.2.7 Reinforcing Steel 43
3.3 Concrete Mix Proportions 44
3.4 Test Specimen Details 47
3.5 Preperation of Test Specimens 51
3.5.1 Patching 51
3.5.2 Mixing 52
3.5.3 Fabrications 54
3.5.3.1 Before Concreting 54
3.5.3.2 Concreting Operation 56
3.5.3.3 After Concreting 63
Chapter 4 Experimental Works 69
4.1 General 70
4.2 Beams testing 70

4.2.1 Test Loading Equipment 71
4.2.2 Test Instrumentation 74
4.2. 3 Test Procedure 75
4.3 Test Results 76
4.3.1 Test Results for Steel Bars 77
4.3.2 Test Results for Concrete Cube 80
4.3.3 Beam Test Results 83
4.4 General Behavior 91
4.5 Shear Load Deflection Relationships 92
4.5.1 Shear Span-to-Depth Ratio 93
4.5.2 Longitudinal Steel Ratio 94
4.5.3 Compressive Strength of Concrete 95
Chapter 5 Finite Element Analysis 96
5.1 General 97
5.2 History of Finite Element Analysis 97
5.3 Finite Element Analysis (FEA) Softwares 98
5.4 Modeling Using ANSYS 99
5.4.1 Element Types Used 99
5.4.2 Materials Properties Used 100
5.4.2.1 Concrete 100
5.4.2.2 Flexural Steel Reinforcement 106
5.4.2.3 Steel Plate Bearing 107
5.4.3 Geometry of the Beams 109
5.4.4 Meshing for the Model 111
5.4.5 Loading and Boundary Conditions for the Beams 112
5.4.6 FE Analysis Setting 114
5.5 Comparing the Model Result with the Litrature Results 115
5.6 Final Setting up of the model 120
5.6.1 Mesh Size 121
5.6.2 Steps Control 122
5.7 FEA Results for the Full Size Beams 123
5.7.1 Shear Span-to-Depth Ratio Variable (G1) 124

5.7.1.1 Comparing with Experimental Results 124
5.7.1.2 Effect of Shear Span-to-Depth Ratio 129
5.7.2 Flexural Steel Reinforcement Variable (G2) 129
5.7.2.1 Comparing with Experimental Results 130
5.7.2.2 Effect of Flexural Steel Reinforcement Ratio 134
5.7.3 Compressive Strength of Concrete Variable (G3) 135
5.7.3.1 Comparing with Experimental Results 135
5.7.3.2 Effect of Compressive Strength of Concrete 140
5.8 Summary of ultimate load results using FEM 141
5.9 Result Using Other Models 142
5.9.1 Bruker Prager Model 142
5.9.2 Using Biaxial Test Data 143
5.9.3 Menetrey-Wiliam Model after Changing the Boundary Conditions 145
Chapter 6 Data Analysis and Results Discussion 147
6.1 Introduction 148
6.2 Crack Patterns and General Behavior 149
6.3 Calculation of Cracking Moments and Stresses 156
6.4 Load Deflection Relationships 157
6.4.1 Shear Span-to-Depth Ratio 158
6.4.2 Longitudinal Steel Ratio Ratio 159
6.4.3 Compressive Strength of Concrete 160
6.5 Shear Strength of Beams without Web Reinforcement 161
6.5.1 General 161
6.5.2 Effect of Shear Span-to-Depth Ratio 164
6.5.3 Effect of Longitudinal Steel Ratio Ratio 168
6.5.4 Effect of Compressive Strength of Concrete 171
6.6 Data Analysis and Discussion for FEM Results 176
6.6.1 General 176
6.6.2 Materials and Modelling 177
6.6.3 Shear Load Deflection Relationships 178
6.6.3.1 Effect of Shear Span-to-Depth Ratio 178
6.6.3.2 Effect of Longitudinal Steel Ratio Ratio 178

6.6.3.3 Effect of Compressive Strength of Concrete 179
6.6.4 Shear Strength of Beams without Web Reinforcement 179
6.6.4.1 Effect of Shear Span-to-Depth Ratio 179
6.6.4.2 Effect of Longitudinal Steel Ratio Ratio 180
6.6.4.3 Effect of Compressive Strength of Concrete 181
6.6.5 FEM Results and Experimental Results Comparison 181
6.6.5.1 Load Deflection Relationships 181
6.6.5.2 Shear Strength of Beams 183
6.6.6 Linear Relationship from Litrature for the Shear Load Defleflection Curve186
Chapter 7 Conclusions, Recommendations and Future Works 188
7.1 Conclusions 189
7.3 Recommendations and Future Works 191
References 193
Summary in Arabic (الملخص بالعربية) 207
Appendix 211

List of Tables

Table 2.1 Values of β_1 as per ACI code 16
Table 3.1 Concrete mix proportions 46
Table 3.2 Concrete slump class specification to BS 8500 47
Table 3.3 Details of test beam specimen 48
Table 3.4 Nominal strength Calculations as per BS 8110 & ACI equations 51
Table 3.5 Properties of fresh concrete 62
Table 4.1 Tensile steel reinforcement test results 78
Table 4.2 Concrete cubes compressive strength test results 81
Table 4.3 Nominal strength calculations as per BS 8110 and ACI equations 83
Table 4.4 Experimental load, shear, and moment at different stages for tested beams 84
Table 5.1 Concrete properties to use in FEA 105
Table 5.2 Steel properties to use in FEA 107
Table 5.3 Beams dimensions 109
Table 5.4 Mesh size effect on Δ_u of mid span deflection of B4G2 beam 121
Table 5.5 comparison of experimental and FEA ultimate load 141
Table 6.1 Cracking, failure Load, shear, and moment for the tested beams 155
Table 6.2 Cracking moment and stresses calculation 156
Table 6.3 Experiment and FEA comparison of hear strength with codes 162
Table 6.4 Comparison the effect of a/d, ρ, and fcu on shear strength with FEA and Codes in terms of $(Vc/(bw\ d\ \sqrt{fc})$ 163
Table 6.5 Comparison the effect of a/d, ρ, and f_{cu} on shear strength with FEA and Code 163

List of Figures

Figure 2.1 Strain and Stress Distribution in rectangular reinforced concrete beam ACI15
Figure 2.2 Simplified stress block for concrete at ultimate limit state 17
Figure 2.3 Singly reinforced section with rectangular stress block 19
Figure 2.4 Stress block parameters for rectangular sections 20
Figure 2.5 Uncracked transformed beam 21
Figure 2.6 Cracked transformed section and stresses on the section 22
Figure 3.1 Grading for coarse aggregate 42
Figure 3.2 Grading for fine aggregate 42
Figure 3.3 Rebars texture image 44
Figure 3.4 Combined Grading for f_{cu} = 120 Mpa 45
Figure 3.5 Combined Grading for f_{cu} = 100 Mpa 45
Figure 3.6 Combined Grading for f_{cu} = 80 Mpa 46
Figure 3.7 Slump test apparatus based on BS 8500 47
Figure 3.8 Details of test beam specimen 49
Figure 3.9 Batching of materials for the mix 52
Figure 3.10 Concrete mixer machine 53
Figure 3.11 Concrete Mixing 53
Figure 3.12 Steel plate forms 54
Figure 3.13 The form ready for casting 55
Figure 3.14 Conveying of the concrete mix 56
Figure 3.15 Conveying of the concrete mix using central type 57
Figure 3.16 Placing of the concrete in to the form 58
Figure 3.17 Placing of the concrete in to the form using central type mixer 59
Figure 3.18 Concrete after consolidation 60
Figure 3.19 Beam after finishing of the concrete level 61
Figure 3.20 Cubes 100 mm as concrete contro; specimen 62
Figure 3.21 Beam after removing the form 63
Figure 3.22 The beams are ready for curing and storage 64
Figure 3.23 Curing of the beams 65
Figure 3.24 Storage of the beams 65
Figure 3.25 Curing and storage of the control specimens (Cubes) 66
Figure 3.26 Transporting and storing the beams in the Lab 67
Figure 3.27 The beams after white painting 68
Figure 4.1 Hydraulic testing machine 71
Figure 4.2 Beam setup for testing 72
Figure 4.3 Beam roller supports 73
Figure 4.4 Arrangement for two-point loads with spreader steel beam 73
Figure 4.5 Dial gage for measuring midspan deflection 74
Figure 4.6 Typical beam test arrangement 75
Figure 4.7 Testing machine for steel bars tensile strength 77

Figure 4.8 Load vs elongation curves for steel bars 79
Figure 4.9 Testing machine for concrete compressive strength 80
Figure 4.10 Crack pattern and failure for B2G1/ B3G3 beam..... 85
Figure 4.11 Crack pattern and failure for B3G1 beam 86
Figure 4.12 Crack pattern and failure for B4G2 beam 87
Figure 4.13 Crack pattern and failure for B5G2 beam 88
Figure 4.14 Crack pattern and failure for B6G2/B4G1 beam..... 89
Figure 4.15 Crack pattern and failure for B1G3 beam 90
Figure 4.16 Crack pattern and failure for B2G3 beam 91
Figure 4.17 Load vs deflection curves for G1 beams (a/d ratio). 93
Figure 4.18 Load vs deflection curves for G2 beams (ρ flexural steel ratio). 94
Figure 4.19 Load vs deflection curves for G3 beams (f_{cu} compressive strength of concrete). 95
Figure 5.1 Different models comparison for concrete strength 101
Figure 5.2 Different models comparison for concrete strength 100 MPa..... 101
Figure 5.3 Different models comparison for concrete strength 120 MPa..... 102
Figure 5.4 Properties for concrete used in ANSYS software 106
Figure 5.5 Properties for steel used in ANSYS software..... 108
Figure 5.6 Properties for the steel plate used in ANSYS software for B3G..... 108
Figure 5.7 Sketch for typical half beam, (a) isometric view (b) right side view and (c) front side view..... 110
Figure 5.8 Meshing for typical half beam..... 112
Figure 5.9 Typical loading and support locations (a) top view (b) side view and (c) bottom view 114
Figure 5.10 Analysis setting details..... 115
Figure 5.11 UB-5 beam cross section detail and layout of UHPFRC 116
Figure 5.12 Comparison of load deflection curve using ANSYS and experimental (Kodur) 117
Figure 5.13 Load vs deflection curve comparison using ABAQUS and experimental118
Figure 5.14 Cross section detail and layout of Wang beam L0..... 119
Figure 5.15 Comparison of load deflection curve using ANSYS and experiments (Wang) 120
Figure 5.16 Mesh sizes comparison..... 121
Figure 5.17 The three sub steps numbers comparison..... 123
Figure 5.18 Minimum and maximum deflection areas by ANSYS for B2G1 beam... 125
Figure 5.19 Comparison between FEA and experimental results of the load of deflection relationships for beam B2G1 125
Figure 5.20 Location of the minimum and maximum deflection areas by ANSYS for B3G1 beam 126
Figure 5.21 FEA and experimental results comparison forthe load deflection relationships for beam B3G1 127
Figure 5.22 Location of minimum and maximum deflection areas by ANSYS for B4G1 beam 128

Figure 5.23 Comparison between FEA and experimental results of the load deflection relationships for beam B4G1 128
Figure 5.24 Load vs deflection curves for G1 beams (a/d ratio). 129
Figure 5.25 Areas of minimum and maximum deflection by ANSYS for B4G2 130
Figure 5.26 Comparison between FEA and experimental results of the load deflection relationships for beam B4G2 131
Figure 5.27 Location of minimum and maximum deflection areas by ANSYS for B5G2 beam 132
Figure 5.28 FEA and experimental results comparison for the load deflection relationships for beam B5G2 132
Figure 5.29 Location of minimum and maximum deflection areas by ANSYS for B6G2 beam 133
Figure 5.30 FEA and experimental results comparison for the load deflection relationships for beam B6G2 134
Figure 5.31 Load vs deflection curves for G2 beams (ρ) 135
Figure 5.32 Location of minimum and maximum deflection areas by ANSYS for B1G3 beam 136
Figure 5.33 FEA and experimental results comparison for the load deflection relationships for beam B1G3 136
Figure 5.34 Location of minimum and maximum deflection areas by ANSYS for B2G3 beam 137
Figure 5.35 FEA and experimental results comparison for the load deflection relationships for beam B2G3 135
Figure 5.36 Location of minimum and maximum deflection areas by ANSYS for B3G3 beam 139
Figure 5.37 FEA and experimental results comparison for the load deflection relationships for beam B3G3 139
Figure 5.38 Load vs deflection curves for G3 beams (f_{cu}) 140
Figure 5.39 Input data or B3G1 using Bruker Prager Model l. 142
Figure 5.40 Load vs deflection curves for B3G1 using Bruker Prager Model. 143
Figure 5.41 Data or B3G1 Using biaxial test data.. 144
Figure 5.42 Load deflection curve for B3G1 Using biaxial test data 144
Figure 5.43 Data for B3G1 Using MW with changing the BC. 145
Figure 5.44 Load vs deflection curve for B3G1 Using MW with changing the BC. .. 146
Figure 6.1 Crack pattern and failure in the beam B2G1/B3G3. 151
Figure 6.2 Cracks pattern and failure in the beam B3G1 152
Figure 6.3 Crack pattern and failure in the beam B4G1/B6G2 152
Figure 6.4 Crack a pattern and failure in the beam B4G2 153
Figure 6.5 Crack pattern and failure in the beam B5G2). 153
Figure 6.6 pattern in the beam B1G3. 154
Figure 6.7 Crack pattern and failure in the beam B2G3. 154
Figure 6.8 The effect of shear span to depth ratio (a/d) on shear strength. 164

Figure 6.9 The effect of shear span to depth ratio (a/d) on shear strength with comparison with codes). 165
Figure 6.10 The effect of shear span to depth ratio (a/d) on concrete shear strength beam $v_{c, test}$ / $v_{c, BS}$, $v_{c, test}$ / $v_{c, ACI}$, and $v_{c, test}$ / $v_{c, EC2}$ 166
Figure 6.11 The effect of Steel ratio (ρ) on shear strength 168
Figure 6.12 The effect of steel ratio (ρ) on shear strength with comparison with codes168
Figure 6.13 The effect of steel ratio (ρ) on concrete shear strength beam $v_{c, test}$ / $v_{c, BS}$, $v_{c, test}$ / $v_{c, ACI}$, and $v_{c, test}$ / $v_{c, EC2}$. 170
Figure 6.14 The effect of compressive strength of concrete (f_{cu}) on shear strength.... 172
Figure 6.15 The effect of compressive strength of concrete (f_{cu}) on shear strength with comparison with codes V_c 173
Figure 6.16 The effect of compressive strength of concrete (f_{cu}) on concrete shear strength beam $v_{c, test}$ / $v_{c, BS}$, $v_{c, test}$ / $v_{c, ACI}$, and $v_{c, test}$ / $v_{c, EC2}$ 174
Figure 6.17 The effect of shear span to depth ratio (a/d) on shear strength 179
Figure 6.18 The effect of steel ratio (ρ) on shear strength 180
Figure 6.19 The effect of compressive strength of concrete (f_{cu}) on shear strength 181
Figure 6.20 Comparison the effect of shear span to depth ratio (a/d) on shear strength between Exp. & FEM 183
Figure 6.21 Comparison thee ffect of longitudinal steel ratio (ρ) on shear strength between Exp. & FEM 184
Figure 6.22 Comparison thee ffect of concrete compressive strength (f_{cu}) on shear strength between Exp. & FEM 185
Figure 6.23 Load vs deflection for concrete reinforced with steel and NiTi 186
Figure 6.24 Load vs deflection curves for models with discrete reinforcement..... 187

List of Abbreviations

ACI	American Concrete Institute
ASTM	American Society for Testing and Materials
BS	British Standard
CSA	Canadian Standards Association
EN	European Standards (Norm in Germany)
FEM	Finite Element Method
FEA	Finite Element Analysis
HPC	High Performance Concrete
HPSCC	High-Performance Self-Compacting Concrete
HSC	High-Strength Concrete
HSS	High-Strength Steel
LFEA	Linear Finite Element Analysis
NLFEA	Nonlinear Finite Element Analysis
NSC	Normal Strength Concrete
RC	Reinforced Concrete
UAE RAK	United Arab Emirates Ras Al Khaimah
UHPC	Ultra-High-Performance Concrete
UHSC	Ultra-High Strength Concrete
UHPFRC	Ultra-High Performance Fiber Reinforced Concrete

Chapter 1
Introduction

Chapter 1

Introduction

1.1 General

Reinforced concrete is a combination of two materials referring to plain concrete possessing high compressive but with little tensile strength and reinforcing steel rods embedded in the concrete that support and strengthen concrete under tension. Buildings, dams, tanks, reservoirs, viaducts, retaining walls, tunnels, conduits, marine are structures built out of reinforced concrete.

Concrete is a universal building material. It has a high fire and weather resistance. The constituent materials for concrete are available locally at the construction site at a low cost. A concrete of high compressive strength is suitable for structural members subjected to compression such as columns and arches.

Concrete is a brittle material whose tensile strength is minor compared to its compressive strength and this prevents its economical use in structural members that are subject to tension over all or over a part of their cross sections such as beams or other flexural members. Reinforcement steel with its high-tensile strength is used in those places where its small-tensile strength would limit the carrying capacity of the member. The reinforcement has a round shape with appropriate surface deformation to provide interlocking. Reinforced Concrete members are subjected to axial force, bending moments, shear, torsion, or a combination of these forces. On the one hand, beams are structural elements that transport transverse external loads causing bending moments and shear forces along their length.

Most reinforced concrete beams' failure is caused by one of the two mechanisms, either the effect of internal flexural moment or the effect of internal

shear force. The proportion of beam, placement of load, and the presence of transverse and longitudinal reinforcement also generally play a significant role in failure mechanism.

1.2 Ultra-High Strength Concrete

The word high is a relative term. Sixty years ago, 40 MPa (5800 psi) concrete was considered of high strength. High strength concrete has been defined as having a compressive strength ranging from 41 to 83 MPa (6000 to 12000 psi). Nowadays, high-strength concrete is used in cast-in-place and precast constructions.

Concrete is established to be a universal building material because of its high compressive strength and its adaptability to take any form and shape. Reinforced concrete (RC) is being used extensively in the construction industry all over the world. The concrete in which common ingredients such as aggregate, water, cement is used is known as normal-strength concrete (NSC) and has a compressive strength ranging from 20 to 60 MPa. The adoption of high-strength concrete (HSC) has increased to its obvious advantages: Increased modulus of elasticity, chemical resistance, freeze thaw resistance, lower creep, lower drying shrinkage, and lower permeability, to name a few. UHSC is usually proportioned with a low water-to-cementitious material ratio and has a high compressive strength ranging from 83 to 150 MPa. The supplementary cementitious materials may include blast furnace slag, fly ash, or silica fume, which is used either as cement replacement or as additive to the concrete mixture.

In the recent decades, concrete is the most extensively used building material and many researchers show interest in it by innovating its material design material, examining its behavior, and solving some of its limitations such as large cross-section, low tensile strength, and low resistance to aggressive environment attacks.

Such innovation led to the production of a new type of concrete called Ultra-High-Performance Concrete (UHPC), a cement composite with an average compressive strength of 150 MPa (21,570 psi). According to Khaksefidi, et al. (2021), UHPC was pioneered by Richard and Cheyrezy in the early 1990s in France and several types were later introduced by other researchers. UHPC as compared to NSC has unique mechanical features that contribute to new techniques in construction, repair, and renovation of concrete structures. It is durable and creative in design. But design standards are often based on NSC; thus, being challenged in UHPC and for this reason, further research is required to understand the performance of the structures in this material.

UHPC and NSC differ in composition. UHPC has ultra-high strength, high toughness, and durability. It is now considered as an alternative to NSC due to its shear performance with steel bars. It is popularly used in the field of engineering, particularly in the construction of bridge structure, airport runway, high-speed railway, repair work, etc. UHPC is preferred than NSC due to its excellent properties that has an economic benefit (Wang et al., 2021).

According to Tibea et al. (2020), UHPC surpasses the performance of a normal or high-strength concrete due to slenderer and more efficient RC structures. However, UHSC in a building offers an advantage because of the reduction in beam and column size allowing the increase in building height and stories. With UHSC, construction cost of a building is reduced resulting to extra space and greater span for the beam. UHSC gains increased interest for practical reasons; hence, further research is necessary to determine the possibilities of producing these concretes and identifying their properties.

1.3 High Strength Steel

In the United States, the Reinforced Concrete (RC) structures' design for seismic applications using deformed steel bars with specified yield strength, f_y, *of* 415 MPa (60 ksi) dominated for many years. The use of steel bars with *fy* greater than 415 MPa (60 ksi) allows designers to reduce the amount of required reinforcement, which results to savings on material, shipping, and handling costs. A reduced amount of reinforcement also enables concrete placement and improves construction quality (Tavallali et al., 2014).

The HSS's definition is dependent on the country's codes. In Canada and Germany, the recent limitation of yield stress f_y for reinforcement bars is equal to 500 N/mm^2 while 550 N/mm^2 is the code limit in the USA, and 600 N/mm^2 is permitted in some European countries. High-strength reinforcement satisfies all reinforcement requirements including high ductility, good bond behavior, low relaxation, and low stress corrosion risk and surpasses the common reinforcement's strength parameters. Bond strength of high-strength reinforcement is significantly higher compared to common reinforcement in normal strength concrete and is slightly higher than UHPC. In fact, the qualities of high ductility and post-failure load capacity are the advantages of using high-strength reinforcement (Florian et al., 2018).

1.4 Ultra-High Strength Reinforced Concrete Beams

RC is a concrete that includes reinforcing bars or other types of reinforcement to enhance one or more properties of the concrete. Cracking occurs when the tensile stress of concrete in a member reaches its tensile strength due to external loads, temperature changes, or shrinkage. Concrete members without any type of

reinforcement usually fail suddenly after the first tension cracks form as there is nothing to prevent the cracks from spreading throughout the members.

According to Rewers (2019), buildings are being designed more boldly; therefore, materials with higher strength parameters need to be used such as the reinforced concrete structures, both high strength concrete and high strength steel.

UHSC or UHPC is formulated by adding fibers to the HSC mix; thus, represents a major step when compared to the conventional NSC and HSC due to the achievement of extremely high strength and extremely low permeability.

Beams are known as horizontal members carrying lateral loads. The loads on the beams produce a significant bending effect as opposed to twisting or having axial effect. Bending moments produce bending strains on the beam and consequently compressive and tensile stresses. Under positive moments (as is normally the case), compressive stresses are produced on top of the beam and tensile stresses are produced at the bottom; bending members must resist both compressive and tensile stresses. In a reinforced concrete beam, three different failure modes may occur, and these are compression, tension, and shear failures.

In general, UHSC can be applied in tall building, long-span bridge, marine structure, elevated structure, precast and pre-stressed products, and construction where durability is critical; thus, the performance of structural elements made with such type of concrete can be a major concern.

In Bahrain, as in many other countries, UHSC is still not in use. Before using such material in construction in the future, it is essential to study and understand the behavior of members made from this type of material.

This study entitled "Shear Behavior of Ultra-High Strength Concrete Beams Reinforced with High Strength Steel Bars without Stirrups" deals with the

experimental and theoretical application of numerical technique through Finite Element Method (FEM) and the comparison of the experimental results with analytical formulas using the codes of ACI-3182019 and BS 8110-1-97.

1.5 Finite Element Method

FEM is a numerical analysis method where the structural element divides into smaller parts and simulates static loading conditions to evaluate concrete response. With tremendous advances in engineering and technology, this method is being used increasingly. This method also responds well to non-linear analysis as each component possesses different stress-strain behavior. Each element' response is indicated through a finite number of degrees of freedom specified at a set of nodal points.

The method in evaluating structures as well as predicting the component's response subjected to different structural loads refers to the Finite Element Analysis (FEA). FEA is the common preference used in studying concrete behavior because results are shown faster, and it is cheaper as compared to the experimental method. On the other hand, FEM, an advanced numerical analysis tool, allows to model the reinforced concrete beams' complex behavior using finite element modeling. The common problems encountered in concretes are non-linear in nature; hence, non-linear analysis can be used in obtaining precise problem solutions (Badiger, 2017).

1.6 Research Problem

UHSC is a composite and new material used as structural element reinforced with high strength steel. The behavior of UHSC is different from the NSC due to its brittle behavior and crushing through the aggregate, which is different when normal strength steel is used as a reinforcement for the element.

The main problem in this study deals with the shear behavior of UHSC beams reinforced with HSS bars. It intends to apply the common best practices for the study of shear behavior through beam cracking patterns, failure modes, shear-load deflection relationships, shear strength experiment, and comparison of numerical results using finite element analysis in addition to the comparison of the results of shear strength with the code equations.

1.7 Research Question

The study seeks to answer the following questions:

- How do the UHSC beams reinforced with HSS bars behave due to shear?
- Can the code equations of ACI and BS be used for the design of UHSC beams reinforced with HSS bars?

1.8 Research Objectives

The objectives of this study are as follows:

- Investigate the shear behavior of UHSC beams reinforced with HSS bars without stirrups.
- Compare the simulation results conducted through FEA with the experimental results and with other data from literature for analytical investigation.
- Evaluate the applicability of the current code equations of ACI and BS.
- Present recommendations in designing UHSC beams reinforced with HSS bars for shear.

1.9 Research Significance

UHPC is described as a cement composite with an average compressive strength that reached about 150 MPa. As cited by Khaksefidi et al. (2021) the distinctive mechanical features of UHPC are considered as chances for development of new techniques in the repair, renovation, and construction of concrete structures. However, the use of common design standards, often based on NSC, is being challenged in this type of concrete. Therefore, further research is needed to understand the performance of the structure of this material.

In this thesis, the shear behavior of UHSC beams reinforced with HSS bars is studied experimentally to investigate the crack patterns in the UHSC, the mode of failure of the beams, and the load deflection relationship. The results are compared using code equations and numerical techniques through FEA.

1.10 Research Scope

The scope of the study included the casting of the UHSC beams at the Bahrain Precast Concrete Company (BPC) yard and testing conducted at the University of Bahrain laboratory where a large-scale experiment was performed to study the shear behavior of UHSC beams reinforced with HSS.

1.11 Definition of Terms

Beams: Horizontal members carrying lateral loads.

Bending: The action of supporting an external load perpendicular to the longitudinal axis of the beam (Nm. or lb. ft.).

Compression: is the action, force, or state of being crushed (opposite tension).

Cracks: Refer to concrete shrinkage. Shrinkage is the decrease in volume of the concrete after hardening.

Ductility: Refers to a structural feature dominated by fracture and depends on the size of the structure.

Failure: Refers to the loss of structural integrity, i.e. is the loss of the load_carrying the capacity of components and members of a structure, or of the structure itself. Beam failure occurs when a material is stressed beyond its strength limit, resulting to fracture or extreme deformations.

Failure Load: The magnitude of the load on the beam at the time of failure.

FEM: Finite Element Method is a numerical analysis method that divides the structure's elements into smaller parts.

Flexure: It refers to bending.

Force: An action caused by the load (N or lb.).

Load: The weights supported by the beam (N or lb.).

Moment: The moment of force refers to a measure of its tendency that prompts a body to rotate to a specific point or axis (= force multiply by its arm).

Ultimate Load: The maximum load that the beam reaches before failure.
Reinforcement: Refers to the addition of steel bars to the concrete.

Shear: It refers to the unbalanced vertical force on the right or left side of the beam.

Strain: Strain is defined as "deformation of a solid due to stress" and can be expressed as change in length divided by the original length.

Stress: Stress is "*force per unit area,*" the ratio of applied force (F) to the cross-section area, described as the "force per area N/mm^2"

Tension: It is the action, force, or state of being stretched up (Positive).

Workable: ASTM (American Society for Testing and Materials) defines it as the "Property determining the effort required to manipulate a freshly mixed quantity of concrete with minimum loss of homogeneity".

1.12 Research outline

The thesis comprises of seven chapters. Chapter 1 presents the introduction of the study, chapter 2 theoretical framework and literature review, chapter 3 refers to the experimental works, chapter 4 deals with testing and results, chapter 5 exhibits the finite element analysis, chapter 6 shows the data analysis and discussion, and finally, chapter 7 presents the summary, conclusions, and recommendations of the study.

Chapter 2
Theoretical Framework
and
Literature Review

Chapter 2

Theoretical Framework and Literature Review

2.1 Introduction

RC beams are commonly subject to the combined effects of flexural and shear loads. The current design philosophy requires an artificial detachment between the shear resistance and moment capacity of the reinforced concrete beams. In fact, most studies on shear and flexural behavior were carried out either separately or together.

The provisions for flexure and shear design specification were grounded on experimental results through concrete with compressive strength of less than 41 MPa (6000 psi), and with normal shear span-to-depth ratio ($a/d<6$). However, concrete of higher compressive strength, both reinforced and prestressed concretes, has been produced successfully and used gradually in different countries. With the recent development of high-strength concrete, the behavior of structural members of this type of concrete necessitates information dissemination.

Existing formulas are semi-empirical and are based on ordinary concrete. With HSC and UHSC being brittle compared to NSC, it necessitates that the semi-empirical models are to be developed through experiments. In current practice, many calculation parameters and equations in the design codes are derived from experimental research programs on concretes with compressive strength not exceeding 40 MPa. Therefore, it is but logical that validity of these equations be verified for concretes with strength above 40 MPa, just like HSC and UHSC (Tahenni et al., 2022).

2.2 Flexural Behavior of Reinforced Concrete Beams

Previous research on reinforced concrete beams under flexure indicated that beams fail due to flexure failure, which is either tension or compression failure. Tension failure takes place when moderate amount of reinforcement is used where the steel starts to yield and stretch, and the tension cracks in the concrete widens and propagates upwards with concurrent significant deflection of the beam then the strength in the remaining compression zone of the concrete increases causing concrete crushing. On the other hand, compression failure transpires when a large amount of reinforcement is used. The concrete fails by crushing specifically when the strain becomes large before the steel yields. Usually, compression failure through concrete crushing is sudden and it occurs without warning.

The basic assumption of deriving a general theory for the flexure strength of reinforced concrete sections are as follows:

1. Plane section stays the same before and after bending,

2. The stress-strain curve for the steel is known,

3. The tensile strength of concrete may be disregarded, and

4. The stress-strain curve for concrete, defending the magnitude and distribution of compressive stress, is recognized (Park and Paulay., 2009).

2.2.1 Design Formulas for Rectangular Beams Using American code (ACI 318-2019)

The current design specification of ACI 318-2019 is based on experimental results using normal strength concrete. Figure 2.1A presents a rectangular singly reinforced concrete beam with a width of b and effective depth of d.

Figure 2.1B shows the distribution of internal strains and figure 2.1C displays the distribution of internal stresses when the beam is about to fail. One desires a method to calculate that moment M_n (nominal moment) at which the beam will fail either by tension yielding of the steel or by crushing of the concrete in the outer compression fiber. The criterion for the first mode of failure is that the steel stress equals the yield point ($f_s = f_y$).

According to Nilson et al. (2016), Whitney first proposed the American Concrete Institute (ACI) code, which uses an equivalent rectangular stress distribution to replace an actual shape of a concrete compressive stress block as shown in figure 2.1C. The flexural strength, using the equivalent stress block distribution is presented in figure 2.1D.

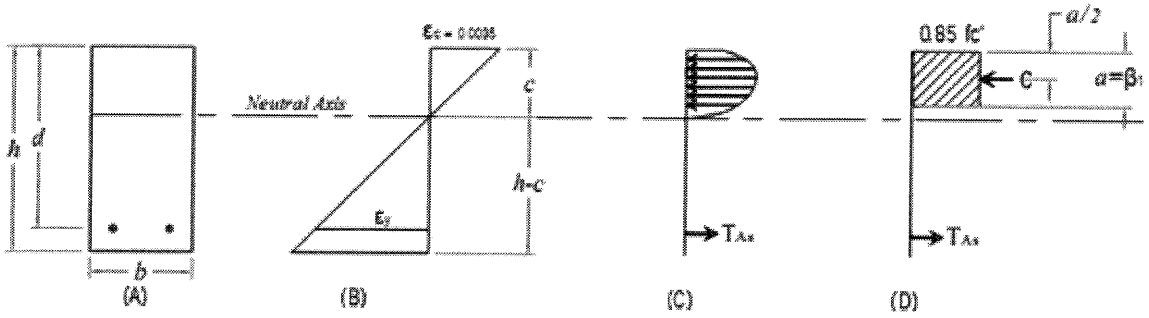


Figure 2.1 Strain and stress distribution in rectangular reinforced concrete beam by ACI-318 (Khalil et al., 2013)

The compression force $C = 0.85\, f'_c\, b\, a$ ... (2.1)

Where f'_c is the compressive strength of concrete and b is the width of the beam, further, a is the depth of compression zone.

The tension force $T = A_s\, f_y$ ... (2.2)

Where A_s is the area of steel reinforcement and f_y is the yield strength of the reinforcing bars

The nominal flexural strength $M_n = A_s f_y \left(d - \frac{a}{2}\right)$ ... (2.3)

and the depth of compression zone (a) is

$$a = \frac{A_s f_y}{0.85 f'_c b} \quad \text{... (2.4)}$$

While the balanced steel ratio found in tension zone is

$$\rho_b = 0.85 \beta_1 \frac{f'_c}{f_y} \frac{600}{600 + f_y} \quad \text{... (2.5)}$$

Noting that the minimum steel ratio

$$\rho_{min} = \left(\frac{1.38}{f_y}\right) \quad \text{... (2.6)}$$

Values of β_1 were shown in Table 2.1 for different concrete compressive strengths.

Table 2.1 Values of β_1 as per ACI code

f'_c MPa	≤ 27.6	34.5	41.4	48.3	≥ 55.2
β_1	0.85	0.80	0.75	0.70	0.65

ACI 318-2019 is the required ACI building code for reinforced concrete. ACI proposes that the utmost usable strain of the extreme compression fiber of a concrete at ultimate is 0.003. Furthermore, ACI recommends the utilization of an equivalent rectangular concrete stress distribution for the reinforced concrete beams' strength prediction.

2.2.2 Design Formulas for Rectangular Beams Using British Code (BS 8110-1-1997)

British Standard BS 8110-1-1997 or BS 8110 used the following formulas for the design of reinforced concrete rectangular beam (Limit State Design) based on the simplified stress block as shown in figure 2.2.

K' = 0.156 where redistribution does not exceed 10 % (this implies a limitation of the neutral axis depth to $d/2$); or

$$K' = 0.402(\beta_b - 0.4) - 0.18(\beta_b - 0.4)^2 \qquad \ldots (2.7)$$

where redistribution exceeds 10 %, and

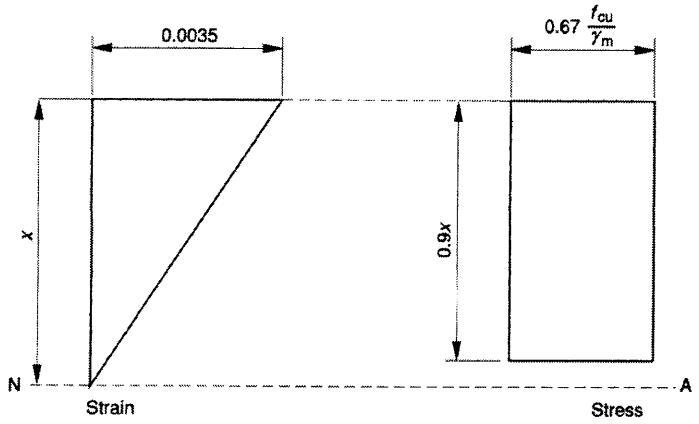


Figure 2.2 Simplified stress block for concrete at ultimate limit state (BS 8110-1-1997)

$$K = M/bd^2 f_{cu} \qquad \ldots (2.8)$$

Where, A_s = area of tension reinforcement, b = width of the beam, d = effective depth of the tension reinforcement, M = design ultimate moment, x = depth to the neutral axis, f_{cu} = the compressive strength of concrete, and

β_b = the ratio $\frac{\text{(moment at the section after redistribution)}}{\text{(moment at the section before redistribution)}}$

For singly reinforced concrete beams $K = K'$ and:

$$z = d\,(0.5+\sqrt{(0.25 - K/0.9)}) \quad \ldots \quad (2.9)$$

But not greater than $0.95d$, where z refers to the lever arm,

$$x = (d - z)/0.45 \qquad \ldots (2.10)$$

$$A_s = M/0.95 f_y\ z \qquad \ldots (2.11)$$

Where f_y signifies the yield strength of the reinforcing bars

2.2.3 Design Formulae for Rectangular Beams Using Eurocode 2 (EN 1992-1-2-2004)

European Standard EN 1992-1-2-2004 or Eurocode 2 applies the following formulas in the design of reinforced concrete rectangular beam (Limit State Design) based on the equivalent rectangular stress block presented in figure 2.3.

$$K = M/bd^2 f_{ck} \quad < K_{bal} = 0.167 \qquad \ldots (2.12)$$

$$Z = d\,[0.5+\sqrt{(0.25 - K/1.134)}] \qquad \ldots (2.13)$$

$$A_s = M/0.87 f_{yk}\ z \qquad \ldots (2.14)$$

Where f_{ck} = the concrete's compressive strength and f_{yk} is the reinforcing bars' yield strength

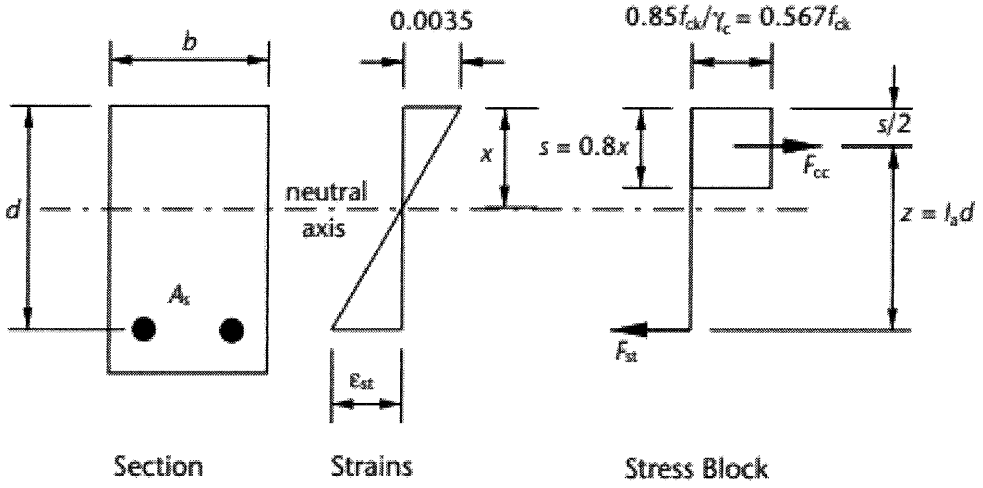


Figure 2.3 Singly reinforced section with rectangular stress block (European Standard EN 1992-1-2-2004)

2.2.4 Design Formulae for Rectangular Beams Using Canadian Code (CSA-A23.3-2019)

Canadian Standards Association (A23.3-2019) design of concrete structures used the following formulas for the design of reinforced concrete rectangular beam based on the equivalent rectangular stress block in figure 2.4.

$$\alpha_1 = 0.85 - 0.0015 f_c' \geq 0.67 \quad \ldots (2.15)$$

$$\beta_1 = 0.97 - 0.0025 f_c' \geq 0.67 \quad \ldots (2.16)$$

$$a = \frac{\varphi_r A_s f_y}{\alpha_1 \varphi_c f_c' b} \quad \ldots (2.17)$$

$$M_r = \varphi_r A_s f_y \left(d - \frac{a}{2}\right) \quad \ldots (2.18)$$

Where φ_c = Concrete resistance factor and φ_r = Reinforcement resistance factor

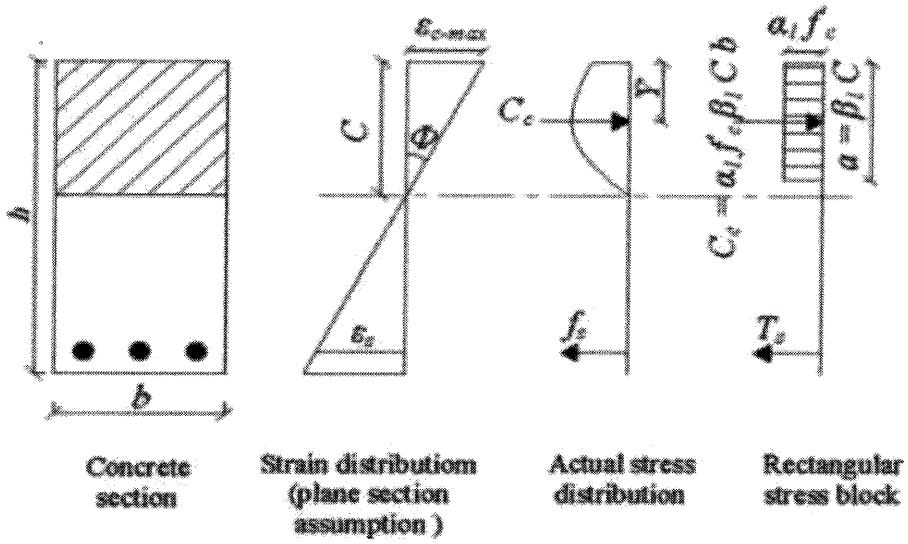


Figure 2.4 Stress block parameters for rectangular sections (CSA-A23.3-2019)

2.3 Cracking Moment and Stresses in Reinforced Concrete Beams

The cracks in reinforced concrete beams start below the applied service load level. Flexural cracking due to loads is inevitable; thus, it is necessary to provide reinforcement effectively. Prior to the flexural crack formation, the steel stress is no more than *n* times the stress in the adjacent concrete.

$$n = \frac{E_s}{E_c} \qquad \ldots (2.19)$$

where *n* is the modular ratio, Es is the modulus of elasticity of steel, and Ec is the modulus of electricity of concrete.

$$E_c = 4700\sqrt{f'_c} \qquad \ldots (2.20)$$

Flexural cracks, also called hairline cracks, are usually fine and are invisible to an observer. They permit little if there is any corrosion in the reinforcement. The

number and the width of cracks increased with the increasing loads beyond the crack loads. With further increase in loads, the number of cracks remained stable, but not the width of the cracks which continue to increase observation (Nilson et al., 2016).

Calculation of the cracking moment through ACI code, SI units (ACI 318-2019)

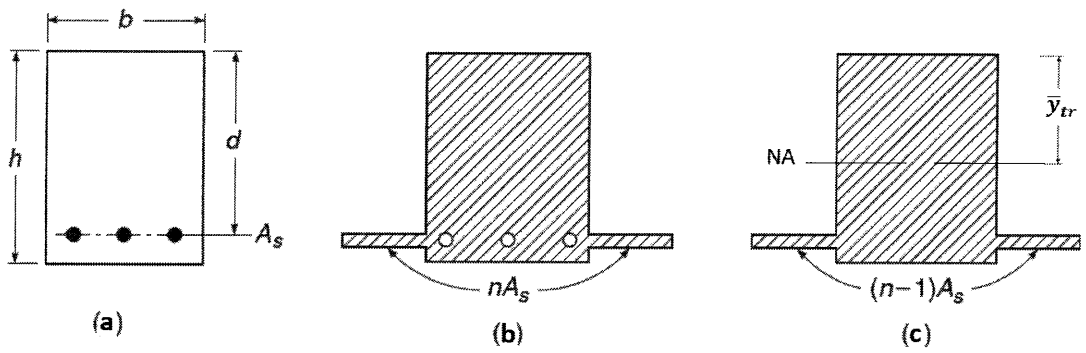


Figure 2.5 Un-cracked transformed beam (Darwin et al., 2016)

The rectangular section is revealed in Figure 2.5 with height (h) and width (b)

$$M_{cr} = \frac{f_r . I_{un,tr}}{h - \bar{y}_{tr}} \qquad (2.21)$$

Where M_{cr} refers to the cracking moment, f_r represents the modulus of rupture and $I_{un,tr}$ is the moment of inertia for uncracked section and $\bar{y}_{tr}$ is the calculated distance of the transformed section of concrete and steel bars from the top of the beam to the neutral axis.

$$f_r = 0.7\,\lambda\sqrt{f'_c} \qquad \ldots (2.22)$$

Where f'_c is the concrete's compressive strength in MPa and $\lambda = 1$ is the concrete's normal weight

The stresses in the concrete σ_c and steel σ_s before cracking are as follows:

$$\sigma_c = M_{cr} \cdot \frac{\bar{y}_{tr}}{I_{un,tr}} \qquad \ldots (2.23)$$

$$\sigma_{cs} = n\, M_{cr} \cdot \frac{d - \bar{y}_{tr}}{I_{un,tr}} \qquad \ldots (2.24)$$

Where d is the effective depth of the beam (h-concrete cover)

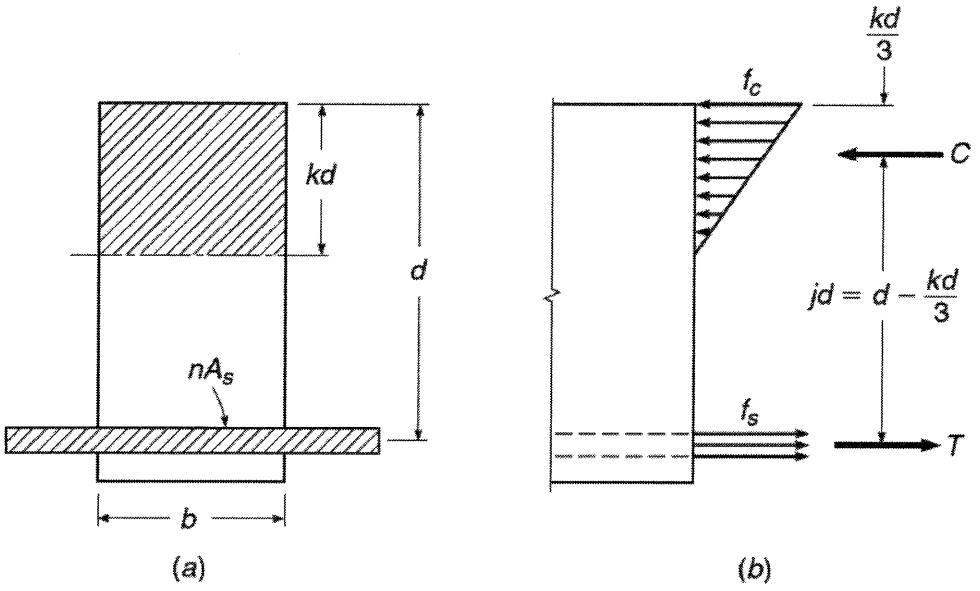


Figure 2.6_Cracked transformed section and stresses on the section (Darwin et al., 2016)

Figure 2.6 illustrates the stresses in the concrete σ_c and steel σ_s after cracking as follows:

$$\sigma_c = M_{cr} \cdot \frac{\bar{y}_{cr,tr}}{I_{cr,tr}} \qquad \ldots (2.25)$$

$$\sigma_{cs} = n\, M_{cr} \cdot \frac{d - \bar{y}_{cr,tr}}{I_{cr,tr}} \qquad \ldots (2.26)$$

Where $\bar{y}_{cr,tr} = kd$ is the calculated distance of the cracked section from the top of the beam to the neutral axis, and $I_{cr,tr}$ is the cracked section's moment of inertia.

2.4 Shear Behavior of Reinforced Concrete Beams

The design of reinforced concrete beams is protected against shear failure and flexural failure. Shear failure happens only when shearing force and bending moment are combined and if shear failure happens, it is expected to be quick and brittle than flexural failure. Thus, beam strength is reduced below flexural capacity and ductility of the element is lessened making it undesirable. Through the occurrence of inclined cracks, shear failure of the beam is shown where in some cases, inclined cracking is immediately followed by member failure and in other cases, inclined cracks are stabilized, and more shear force is applied before the member fails. Moreover, inclined cracks in the beam web are developed prior to a flexural crack in the surrounding area or an extension of a previously developed flexural crack. Inclined cracks are of two types: The web-shear crack and the flexural shear crack. The flexural crack that causes the inclined cracks is referred to as the initiating one. Besides the primary cracks including flexural and two types of inclined cracks, is the secondary crack caused by the splitting forces from the deformed bars especially when there is a slip between concrete and steel reinforcement, or from the dowel action force in the longitudinal bars transferring shear across the cracks (Meqdadi.,1993). Shear strength of beams depends partly on tensile strength of concrete in which it is more variable and more difficult to measure than compressive strength. Therefore, safety and care are important in the design to withstand shear and flexure.

2.5 Codes Prediction for Reinforced Concrete Beams in Shear

2.5.1 ACI 318-2019

Current specification beam refers to the sum of the shear that is carried by the concrete V_c and the web reinforcement that represents the sum of at least three separate components including the Dowel action of longitudinal reinforcement, aggregate interlock, and shear carried across the un-cracked concrete in the flexural compression zone. The term V_s represents the vertical component of the force carried by shear reinforcement across an assumed 45° failure crack. The nominal shear strength contributed by the concrete V_c is computed using the ACI equation in SI units (ACI 318-2019).

$$V_c = \lambda \times \left(0.16\sqrt{f'_c} + 17.2\rho_w \frac{V_u d}{M_u}\right) b_w d \qquad \ldots (2.27)$$

Where λ=1 for normal concrete

and the nominal shear strength contributed by shear reinforcement V_s is computed by:

$$V_s = \frac{A_v f_y d}{s} \qquad \ldots . (2.28)$$

The nominal shear strength of the reinforced concrete beam, V_n is expressed as the sum of the individual contribution of the concrete V_c and the shear reinforcement V_s. (ACI 318-2019).

$$V_n = V_c + V_s \qquad \ldots (2.29)$$

$V_s = 0$ for the beams without web reinforcement.

To compare the analytical prediction with the experimental results, it is more useful to express the above equation in terms of shear stress by dividing the shear with the width of the web (b_w) and the effective depth of the beam (d).

2.5.2 BS 8110-1-1997

In British specification BS8110 (BS 8110-1-1997), the design shear V_c for normal weight concrete is represented in SI units.

$$V_c = 0.79\left(\frac{100A_s}{bd}\right)^{\frac{1}{3}}\left(\frac{400}{d}\right)^{\frac{1}{4}}\left(\frac{f_{cu}}{25}\right)^{\frac{1}{3}}/\Upsilon_m \quad \ldots(2.30)$$

Where A_s is the area of steel, b refers to the breadth of the web, d deals with the effective depth, f_{cu} is the characteristic concrete cube strength, which would not exceed 40 Mpa, and Υ_m denotes the material partial safety factor taken as 1.25. The value of $\left(\frac{100A_s}{bd}\right)$ should not be taken as greater than 3.

The ACI building code [ACI 318-2019] considers that the nominal shear strength is proportional to $(f'_c)^{1/2}$ while BS 8110 code [BS 8110-1, (1997)] and some investigations concludes that the shear strength is proportional to $(f_{cu})^{1/3}$.

2.5.3 Eurocode 2 EN 1992-1-2-2004

The shear capacity of the concrete using Eurocode 2 European Standard (EN 1992-1-2-2004), $V_{Rd,c}$ is exemplified through the empirical expression below:

$$V_{Rd,c} = \left[0.12\, k(100\rho_1 f_{ck})^{\frac{1}{3}}\right] b_w d \quad \ldots(2.31)$$

with a minimum value of:

$$V_{Rd,c} = \left[0.0035\ (k)^{\frac{3}{2}}(f_{ck})^{\frac{1}{2}}\right] b_w d \qquad \ldots (2.32)$$

where:

$V_{Rd,c}$ = design shear resistance of the section without shear reinforcement

$$k = \left(1 + \sqrt{\frac{200}{d}}\right) \leq 2.0 \qquad \ldots (2.33)$$

With d expressed in mm

$$\rho_1 = \frac{A_{s1}}{b_w d} \leq 0.02 \qquad \ldots . (2.34)$$

A_{sl} = the area of tensile reinforcement extending beyond the section by at least a full anchorage length and an effective depth (d) b_w = the smallest width of the section in the tensile area (mm).

2.5.4 Canadian Code CSA S6-09 Addendum

The shear capacity of the concrete using Canadian Standards Associations (CSA S6-09 Addendum), V_c is illustrated in the following expressions:

$$V_c = 2.5\ \beta\ \varphi_c\ f_{cr}\ b\ d_v \qquad \ldots . (2.33)$$

$$f_{cr} = 2.5\sqrt{f'_c} \qquad \ldots . (2.34)$$

$$d_v \geq \{0.9d \qquad \ldots (2.35)$$

$$\{0.72h$$

$$\beta = \frac{0.4}{(1 + 1500\,\varepsilon_x)} \times \frac{1300}{(1000 + s_{ze})} \qquad \ldots (2.36)$$

$$\varepsilon_x = \frac{\left[\left(\frac{M_f}{d}\right) + V_f + 0.5N_f\right]}{2(E_{f1}A_{f1})} \leq 0.003 \qquad \ldots (2.37)$$

Where φ_c is a resistance factor for concrete = 0.75, f_{cr} refers to the cracking strength of concrete, f'_c *is the* compressive strength of concrete, s_{ze} represents the effective crack spacing for members without stirrups = 300 mm, ε_x stands for the longitudinal strain at mid-height of the cross section, M_f is the bending moment, V_f expresses the shear load, N_f is the factored axial load normal to the cross-section occurring simultaneously with V_f including the effects of tension due to creep and shrinkage (taken as positive for tension and negative for compression), E_{f1} indicates the modulus of elasticity of longitudinal reinforcement, and A_{f1} is the area of longitudinal reinforcement.

2.6 Shear Behavior of Ultra-High Strength Concrete Beams

The following search platforms such as Science Direct, Engineering Village, ASCE Journal, and ACI Journal stipulate research data on the shear behavior of UHSC beam. Numerous investigations carried out and literature published are focused on shear behavior of normal strength and high-strength concrete using the experimental and analytical model through the codes but there is dearth of research on UHSC.

Further, an extensive body of literature is available on the shear behavior of RC beams, from both analytical and experimental stand points; however, there is no methodological study previously conducted on calculation.

Hung et al. (2021) presented a review of developments and challenges for UHPC in structural engineering and summarized the developments, analysis, and design approaches of reinforced ultra-high-performance concrete (R/UHPC) elements under axial forces, shear forces, and bending moments with emphasis on the shear behavior of ultra-high strength concrete beams using high strength steel bars without stirrups. Further, they highlighted the advantages and limitations of these approaches for different structural elements including beams, slabs, columns, joists, shear wall, and bridge system using normal and high strength concrete with high tensile yield strength of steel.

The current design codes for RC stipulate that slender R/UHPC beams without stirrups can attain a shear strength greater than the concrete design shear strength. To resolve an unfavorable behavior or failure modes such as excessive crack width, splitting failure, pre-mature concrete crushing, and buckling of steel bars, that occur when high-strength steel rebars are used in normal-strength concrete members, combined high-strength steel reinforcing bars and UHPC are feasible to be used.

Using UHPC resulted in less steel reinforcement ratio and flexural failure only occurs when using minimum steel ratio. In addition, using a high amount of reinforcement kept small deformation in the bars while using high-steel reinforcement ratio gave low tension control behavior.

As stated by Yousef et al. (2018) increase in the concrete strength results to increase in the shear strength using R/UHPC. On the one hand, the majority of the codes in shear equations were underestimated.

Tahenni et al. (2021) conducted an experimental study of 16 RC beams made of NSC and HSC under shear using a four-point loading. In their study, the shear capacity of the tested beams was evaluated, diagonal cracking behavior was examined, numerical analysis of shear and diagonal cracks were performed through ANSYS to show the effect on the behavior of RC beams made of NSC and HSC, with and without transverse reinforcement, and results were compared with the different models from other studies. The beams without web reinforcement made of HSC demonstrate brittle behavior while the mode of failure of the tested beams changed from shear to flexure, particularly with web reinforcement. Moreover, the ultimate load capacity of the beams increased.

The experimental investigation and the theoretical values presented in literature on the comparison of ultimate shear strength of the beams without web reinforcement can be considered acceptable. The FE predicted results of the load–deflection response, the ultimate load, the cracking load, the ultimate deflection, and the maximum diagonal crack widths coincided with the data as a result of the experiment.

In the study of Wang et al. (2020) on the shear performance of reinforced UHPC (eight without web reinforcement and four with web reinforcement) rectangular section beams with different shear span ratio, stirrup ratio, steel fiber volume ratio, reinforcement ratio, and longitudinal reinforcement strength, the results demonstrate that increase in the beams' shear span ratio at a certain range resulted in the decrease of the beams' shear capacity. Moreover, increase in the beams' stirrup, reinforcement ratios and the longitudinal reinforcement strength at a certain range resulted to the slight increase in the beams' shear capacity while beams without web reinforcement display diagonal compression failure with less shear

span-to-depth ratio and shear compression failure with higher shear span-to-depth ratio.

Another study using experimental performance of Ultra-High-Performance Steel Fiber-Reinforced Concrete (UHPSFRC) beams where the concrete parts of the beams were modelled using eight-node solid element was conducted by Tibea et al. (2020). They tested six beams that were subjected to loads at low shear span-to-depth ratios. The test results showed that a higher fiber content caused an increase in ultimate capacity and some enhancement in ductility. The findings further provided an understanding of the ultimate response including shear strength and failure mode of structural elements that integrate various fiber contents.

The experimental and numerical results revealed that the shear strength and failure mode of such members are influenced by the flexural reinforcement ratio, fiber content, and location of loading.

With the goal of building a numerical model, Rewers (2019) describes a four-point bending test of a beam with steel reinforcement with created model from ABAQUS software using the Concrete Damage Plasticity (CDP) material model for concrete. However, the beam failed due to concrete crushing and top reinforcement buckling. Specifically, the experiment failed due to bending, concrete crushing, and steel yielding. The numerical model serves as a duplicate with the assumed dilation angle of not less than 25 degrees. Those with smaller angles of dilation have failure mode that does not correspond with reality.

Hence, it is also shown that the shear strength and failure mode of such members is dependent on the fiber content, flexural reinforcement ratio, and location of loading as indicated in the experimental and numerical results.

Wakjira et al. (2020) experimented on the effect of the shear span-to-depth (a/d) ratio in the shear behavior of Steel Reinforced Grout (SRG) and strengthened RC beams. During the experiment, there were 12 beams that were casted in four series of three specimens where each was tested as part of the support system. The findings showed the intensified efficacy of SRG for deficient beams in shear. In particular, the SRG significantly increased with an increase in a/d. Hence, it was recommended that an analytical model for predicting the shear capacity of SRG strengthened beams be used to record the effect of the a/d ratio.

Ahmed et al. (2019) studied the shear behavior of UHPC beams reinforced with HSS bars and investigated the effects of key structural parameters on the shear behavior of non-pre-stressed UHPC beams passively reinforced with high-strength steel bars taking into consideration several parameters (steel-fiber volume ratio V_f, compressive strength of concrete fc', longitudinal reinforcement ratio ρ, stirrups spacing s, and shear span-effective depth ratio a/d). Under a four-point loading configuration, ten beam specimens with cross-section were quasi-statically loaded to failure on a simple span. The researchers found that the shear capacity increased with an increase in both V_f and ρ, but with a decrease in a/d.

All beams failed in pure shear, and the longitudinal steel bars did not yield during beam failure. At the time of failure, concrete crushing did not occur at the top of UHPC beams. At a higher shear span to effective depth ratio (a/d), the shear load capacity and mid-span deflection were found to be lower. The findings further exhibit that decrease in shear load capacity and mid-span deflection with increase in a/d was more at a lower longitudinal reinforcement ratio.

The shear strength of UHPC beams without stirrups showed that its shear capacity increased with the expansion of the steel bars' compressive strength and volume ratio while the failure mode is altered from shear tension to shear

compression. In addition, research on the use of steel fibers as shear reinforcement in High Strength Concrete (HSC) beams revealed that the HSC beams' shear strength improved with the addition of steel fibers to the HSC mixture.

Another study by Nikbakhta et al. (2019) is focused on the shear and flexural behavior of High-Performance Self-Compacting Concrete (HPSCC) beams with no coarse aggregate and compressive strength of above 100 MPa. They experimented on the casting of six HPSCC beams of different longitudinal reinforcement ratios and shear span-depth ratios for both casted and experimented cases using three-point loads (simply supported beam with concentrated load at the center of beam). It was found that beam specimens without transverse reinforcement were designed; thus, they fail in shear.

The experiment results showed that in the beam specimens without transverse shear reinforcement, the beams with Hooked Steel Fibers (HSF) had a greater ultimate load and deformation capacity. Moreover, it was proven that specimens with HSF and a lower longitudinal reinforcement ratio displayed greater shear strength and deformation capacity. Nikbakhta et al. (2019) further indicated that the influence of the type of steel fiber is more evident than that of the longitudinal reinforcement ratio in HPSCC beams, which were set to shear loads. The results showed that increase in the longitudinal reinforcement causes an intensified strength of the beams and reduction in the deformation capacity.

The shear behavior of fiber-reinforced ultra-high-performance concrete beams was examined by Meszoly et al. (2018) through an experiment. Twenty I-shaped beams made of (UHPC) of different steel fiber content and with varying degrees of shear reinforcement (with or without stirrups) were tested in shear with the mean compressive strength of the concrete at 170 MPa. The study examined the traditional transverse shear reinforcement, the fiber reinforcement effects on the shear behavior

as well as the interaction of both parameters such as shear capacity and breakdown mechanisms. The results showed that all tests failed in shear.

Twenty UHP(FR)C beams reinforced longitudinally with high-grade steel bars were tested in for the shear behavior of UHP(FR)C beams; however, all tests ended up with shear failure.

Kodur et al. (2018) analyzed the failure characteristics of Ultra High-Performance Fiber Reinforced Concrete (UHPFRC) beams without stirrups under flexural and shear loading. Four large scale beams with low tensile reinforcement ratio and with no shear reinforcement were tested to check on the structural behavior of UHPFRC members. Two tested under flexural loading while the other two under shear loading. The findings showed that UHPFRC beams exhibit a cracking pattern, specifically multiple microcracks at the initial stages and scattered single macrocrack at the critical section with increased loading at the later stages. The comparison of results also revealed the absence of shear reinforcement in UHPFRC beams in which the beam's ductility or moment capacity under dominant shear loading did not reduce.

Bae et al. (2016) conducted a study on the flexural strength of reinforced concrete members, specifically models made up of compression and tension stress blocks with steel fiber reinforced ultra-high strength concrete using ACI code formulas. On the compression side, rectangular stress block, triangular stress block, and real distribution shape of stress were utilized. The rectangular stress block was used in the partial and whole area of tension side. The comparison of results showed that the triangular compression stress block and strain-softening type tension stress block models can be used as solution for UHPC on the other hand, the modified rectangular stress block model can be utilized with strain softening type tension stress block.

The structural behavior of Ultra-High -Performance Fiber Reinforced Concrete (UHPFRC) with Normal Strength Concrete (NSC) or High Strength Concrete (HSC) composite member was experimented by Hussain et al. (2015). The test results showed that the bond strength between concrete material layers of UHPFRC and NSC/HSC was significantly high and hence revealed that the performance of the proposed composite system, in terms of flexural and shear capacity, was successfully enhanced.

Hawileh (2015) constructed a Finite Element (FE) model of reinforced concrete beams with a hybrid combination of steel and aramid reinforcement of 30 MPa (NSC) and 65 MPa (HSC) using ANSYS program for UHSC. In the study, there are 21 3D non-linear FE models developed to simulate the response of concrete beams reinforced with a hybrid combination of Fiber Reinforced Polymer (FRP) and steel. Six models were used to validate the accuracy of the results through the comparison of the predicted load against the mid-span deflection response values with the experimental results obtained from a previous study while the remaining 15 models were used to analyze the effect of AFRP bar size, FRP reinforcement material type, reinforcement bond–slip action, and concrete compressive strength on the performance of the RC beam specimens.

Moreover, Hawileh (2015) developed three-dimensional (3D) FE models that predicted the load versus mid-span deflection response of tested RC beams with a hybrid combination of steel and AFRP bars. The FE models account for the constituent material non-linearities and bond–slip behavior between the reinforcing bars and adjacent concrete surfaces. Based on the findings, it was concluded that the developed models can accurately capture the behavior and predict the load-carrying capacity of such RC members.

A study was conducted by Badiger et al. (2017) on the reinforced concrete beam (NSC) by finite element analysis using ANSYS 13.0 for formal Strength Concrete. A four-point bending analysis was implemented using reinforced concrete beam. Results were based on the analysis of the beam with reference to mesh density, varying depths, use of steel cushions for support and loading points, effect of shear reinforcement on flexure behavior, and impact of tension reinforcement on the behavior of the beam.

Xia et al. (2011) conducted a shear failure analysis, particularly the mechanism of the deck strip shear failure on ultra-high-performance concrete beams reinforced with high strength steel. Experiments with material characterization, tests on bond strength, small-scale prism, and full-scale beam were conducted and specimens with traditional shear strengthening techniques were tested. Results were compared and the researchers concluded that in UHPC beams reinforced with passive HSS rebar, shear failure is more critical if there is no transverse reinforcement. Further, the actual flexural load capacity based on the ultimate tensile strength of HSS rebar surpassed the design value, which was predicted on the nominal yielding stress of HSS based on the 0.2% offset rule. A considerable amount of shear reinforcement was required to increase the shear resistance that is higher than the actual flexural capacity to avoid the domination of shear failure in UHPC–HSS beams. The addition of transverse reinforcement is not practical and economical.

Xia et al. (2011) further pointed out that like normal reinforced concrete, shear failure of UHPC–HSS beam does not indicate any brittle response or catastrophic load reduction. Therefore, this shear failure mode is regarded as acceptable but additional shear resistance due to localized deformation of the longitudinal reinforcement is not proposed for design capacity formulas.

Choi et al. (2009) studied the shear strength of a slender reinforced concrete beams without web reinforcement and found that a reliable shear strength model for slender reinforced concrete beams without web reinforcement is described based on fuzzy set theory. A fuzzy-based model was developed to deal with the interaction between the shear modeling parameters and the random and non-random reservations on these parameters. The compressive strength, effective depth, and tension reinforcement ratio are essential parameters to determine the modeling shear strength in slender reinforced concrete beams without web reinforcement. The shear strength predicted by the fuzzy-based model is compared to that predicted by current shear strength model suggested by design codes such as the Eurocode 2, EC2; American code, ACI 318-05; and Canadian code, CSA A23.3-04.

Hamrat et al. (2009) in their study presented the shear behavior of RC beams without stirrups made of normal strength and high-strength concretes and covered the compressive strengths at the range of 40 MPa to 104 MPa.

Sixteen reinforced concrete beams without transverse stirrups were experimented for failure to investigate the influences of the shear-span/depth ratio (a/d), longitudinal steel ratio (ρ), and compressive strength of concrete (f'_c) on the global behavior in shear for beams made of NSC as well as HSC. Using a digital video recording, crack development and propagation were monitored for shear cracking and results showed that the shear capacity depends more on the shear-span/depth ratio (a/d) and the longitudinal steel ratio (ρ) and less on the compressive strength (f'_c) in the case of HSC. Based on the findings and data collected from other studies, a shear formula was proposed for the computation of the shear strength of concrete beams without stirrups. Comparison between different models in the design codes to present the contribution of concrete to the shear resistance of beams and to show that the beams without stirrups was made through the proposed formula. The

findings revealed that those made of HSC exhibit a brittle behavior and with the increase in strength capacity the compressive strength of the concrete also increases. The increase in longitudinal steel ratio also increases the ultimate shear capacity but reduces the deflection at mid-span where the steel percentage increases and the ultimate load decreases as *a/d* increases. In the same manner, mid-span deflections at ultimate load increase as the values of *a/)* increase. The tests also demonstrated that as the ratio *Pu/)* decreases, *a/d* increases.

Hassan et al. (2008) conducted a study on the shear behavior of large concrete beams reinforced with high-strength steel by testing six large-size concrete beams reinforced with either conventional or high-strength steel and further tested up to failure. The beams were built without web reinforcement to ensure the evaluation of the nominal shear strength provided by the concrete.

The influence of the shear span-to-depth ratio, concrete compressive strength, and the type and amount of longitudinal steel reinforcement were investigated. The study showed that using high-strength steel alters the failure mode from diagonal tension to shear compression failure and resulting in higher shear strength compared to using conventional steel. Moreover, the influence of the shear span-to-depth ratio a/d and the type and amount of longitudinal steel reinforcement were also examined. The findings showed that high-strength steel strongly influenced the shear behavior of the concrete beams tested in the current study and constructed without web reinforcement, the diagonal cracking strength is the measure of the concrete contribution at ultimate for members reinforced with conventional steel and constructed without web reinforcement. Such relationship is inappropriate for high-strength steel as the behavior is strongly influenced by the a/d and the stress level in the bars, concrete beams reinforced with Grade 420 MPa (60 ksi) steel and constructed without web reinforcement exhibited a very brittle failure due to

yielding of the longitudinal steel reinforcement. Shear failure occurred shortly after the initial shear crack.

The ACI 318-05 simplified expression for the shear contribution of concrete is unconservative for large-size concrete beams without web reinforcement. The expression needs to account for the size effect and the reinforcement characteristics.

From the above review, it can be observed that most of the data focused on the discussion of the shear behavior of normal strength and high strength concrete using experiments and comparison of analytical model through codes. There are insufficient studies on the behavior of high strength concrete using numerical methods. There are also limited investigations related to ultra-high strength concrete reinforced with high-strength steel bars without stirrups, and these studies have not used the numerical method either. With these observations, the researcher intends to examine the shear behavior of ultra-high strength concrete beams reinforced with high-strength steel bars without stirrups using experimental and numerical approaches.

Chapter 3

Experimental Works

Chapter 3

Experimental Works

3.1 Introduction

The main objective of the present study is to investigate the shear behavior of ultra-high strength concrete beams reinforced with high-strength steel bars without stirrups.

Three variable were selected for this study. the span-to-depth ratio (a/d), flexural reinforcement ratio (ρ), and compressive strength of concrete (f_{cu}). The basis for selecting these variable as follows:

1- Normal span-to-depth ratio $2 \leq (a/d) \leq 6$ and the three beams in this range.

2- Flexural reinforcement ratio, one with $\rho \leq \rho_b$, second beam with ρ approximately equal ρ_b, and the third one with $\rho \geq \rho_b$.

3- Compressive strength of concrete (f_{cu}). Ultra high strength concrete (UHSC) has been defined as having a compressive strength ranging from 83 to 150 MPa, therefore the first one selected below the lower limit, the second and the third one selected in the range of the definition of UHSC.

To achieve this objective, an experimental program is carried out testing the beams at the structural laboratory of the Civil Engineering Department of the University of Bahrain and casting the beam at Bahrain Precast Concrete CO. W.L.L. In addition to taking samples of cubes for 28 days, testing the steel bar strength is performed at the Al Hoty Analytical Services W.L.L. Prior to the start of the experimental works, Numerous preparations and tests are made in relation to material proportion, preparation of the molds, test set up, measurements, and

machine operation. The experimental work included casting and testing of several beams designed to fail by shear.

3.2 Materials

The production of UHSC that consistently meets the workability and strength development requirements is important in material selection. UHSC was produced using material of high quality and low water cement ratio based on the trial mixtures' result. Also, a water reducing admixture is used to decrease the quantity of water and increase workability that results in strength increase.

3.2.1 Cement

The cement used in all beams is from one shipment ordinary Portland cement, which is in accordance with BS 12 and ASTM C 150 Type I.

3.2.2 Aggregate

Approximately three quarters of the volume of concrete is occupied by the aggregate. The aggregate limits not only the concrete's strength but its properties may affect its durability and structural performance (Neville, 2011). BS and ASTM standard specifications were followed to determine the physical properties of aggregates.

3.2.2.1 Coarse Aggregate

Crushed limestone from United Arab Emirates (UAE RAK Aggregate) with nominal maximum size of 20 mm was used in ultra-high strength concrete. Figure 3.1 shows the sieve analysis for the coarse aggregate.

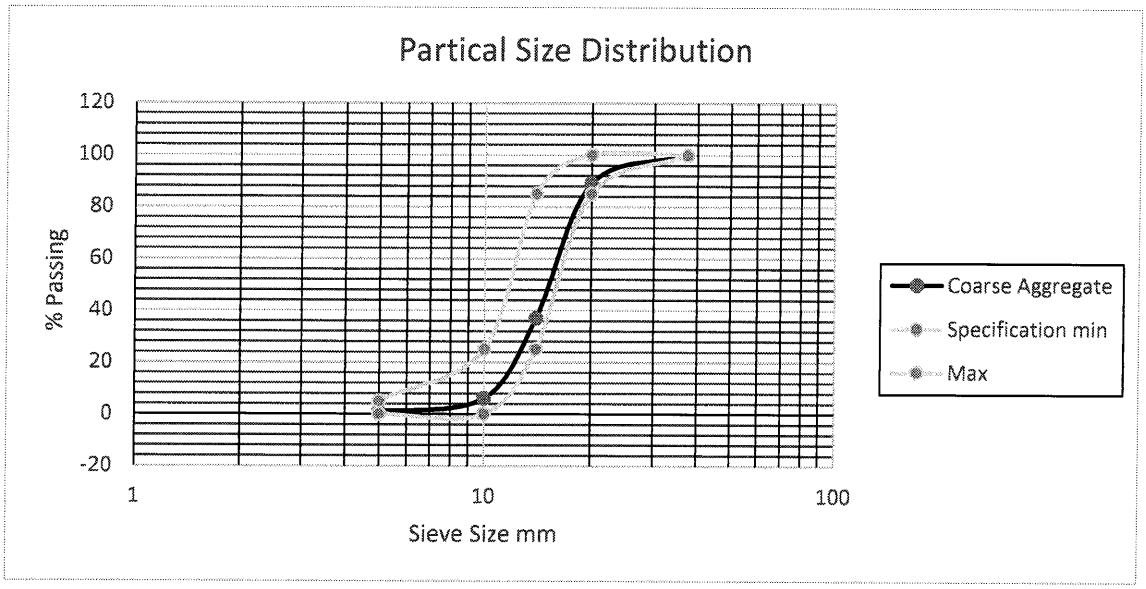


Figure 3.1 Grading for coarse aggregate

3.2.2.2 Fine Aggregate

Blended/Marine sand in accordance with BS 882 was used as fine aggregate to produce ultra-high strength concrete. Figure 3.2 shows the sieve analysis for fine aggregate.

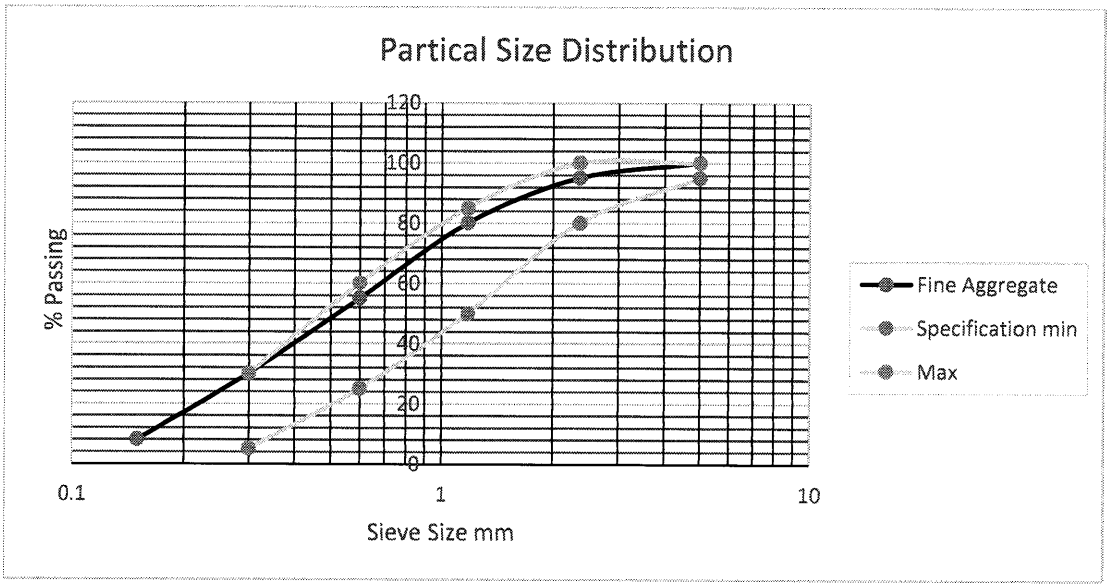


Figure 3.2 Grading for fine aggregate

3.2.3 Water

Filtered water was used.

3.2.4 Chemical Admixture

Water reducing admixtures were added to the high strength and ultra-high strength concrete mix to increase workability, decrease the water content for the same workability, and increase the strength of the concrete. Water reducing admixtures PC-331 F was used to produce ultra-high strength concrete and high strength concrete.

3.2.5 Slag

Slags are waste products of iron, alloy steel, and phosphate industries (Haynes 2017) and these were used to produce ultra-high strength concrete.

3.2.6 Micro silica

Micro silica was used in ultra-high concrete to improve the concrete strength, provide more uniform distribution and greater volume of hydration products, and decrease the average size of pores in the concrete.

The advantages of using micro silica can be significant as it reduces thermal cracking caused by the heat of cement hydration and can improve durability to avoid attack by sulfate and acidic waters (Bubshait et al., 2007).

3.2.7 Reinforcing Steel

The reinforcing steel used in the beams was high-strength deform bars Grade 500 BS / Grade 72.5 ASTM (f_y =500 MPa) in accordance with BS 4449:2005 +

A2:2009, ASTM A955/A955M-2009 standard for different bar diameters to get the properties of the reinforcement bars with modulus of elasticity (E_s = 200 GPa).

In this research, two samples were used, one for 25 mm dia and another for 32 mm dia, the rebars texture image shown in figure 3.3. Other the details are shown in the next chapter (chapter 4 Testing and Results).

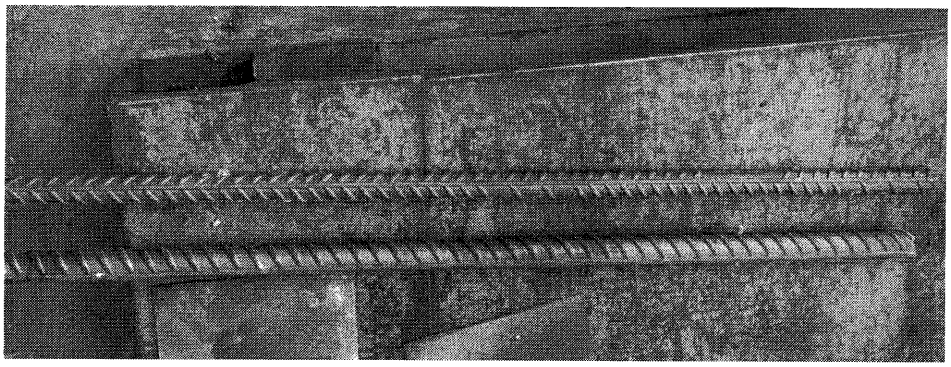


Figure 3.3 Rebars texture image

3.3 Concrete Mix Proportions

Three types of concrete mixes were made, namely, ultra-high strength concrete with compressive strength of f_{cu} = 120 MPa and 100 MPa and high strength concrete with compressive strength of f_{cu} = 80 MPa.

The grading was a combination of fine and coarse aggregates to ensure that a satisfactory amount of aggregate with a minimum void space is obtained in the mix. This will enable the use of a minimum amount of paste (water and cementitious material) in concrete, improving its dimensional stability and durability.

The combined grading for the three mixes is shown in figures 3.3, 3.4, and 3.5.

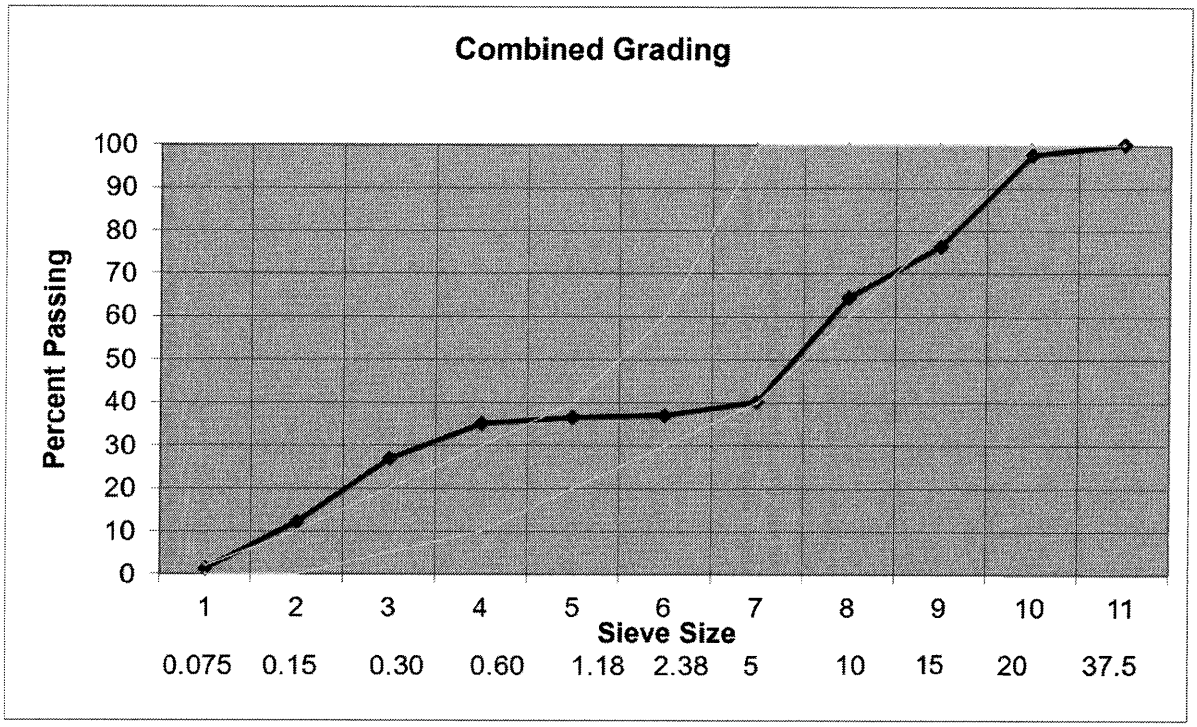


Figure 3.4 Combined Grading for f_{cu} = 120 Mpa

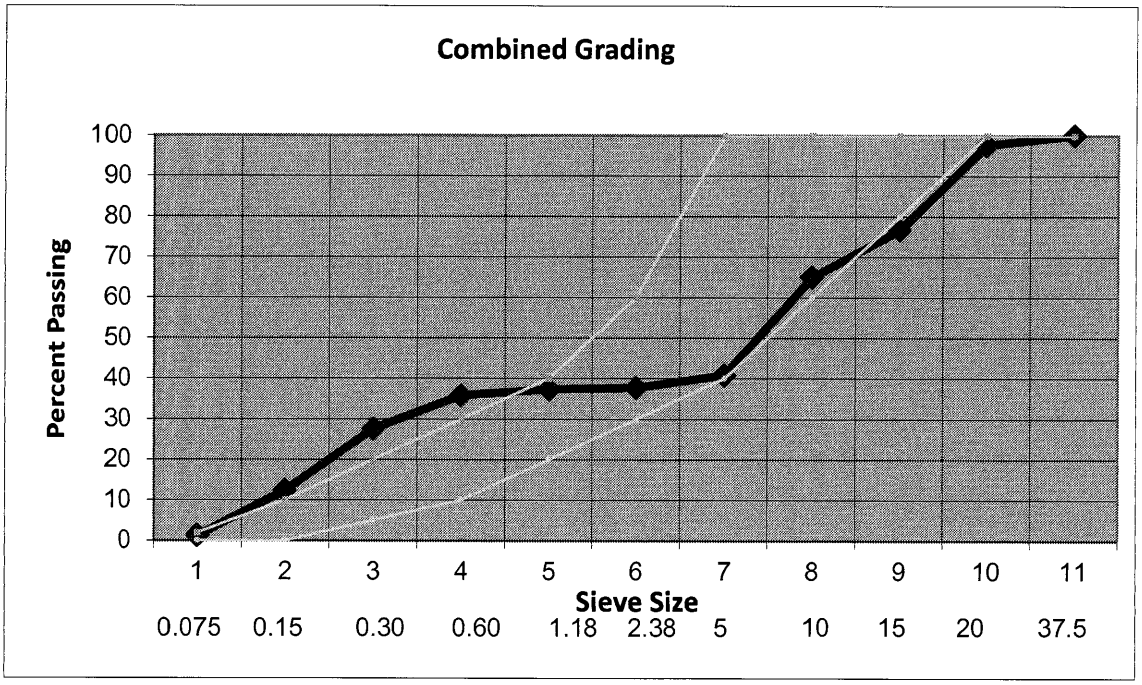


Figure 3.5 Combined Grading for f_{cu} = 100 Mpa

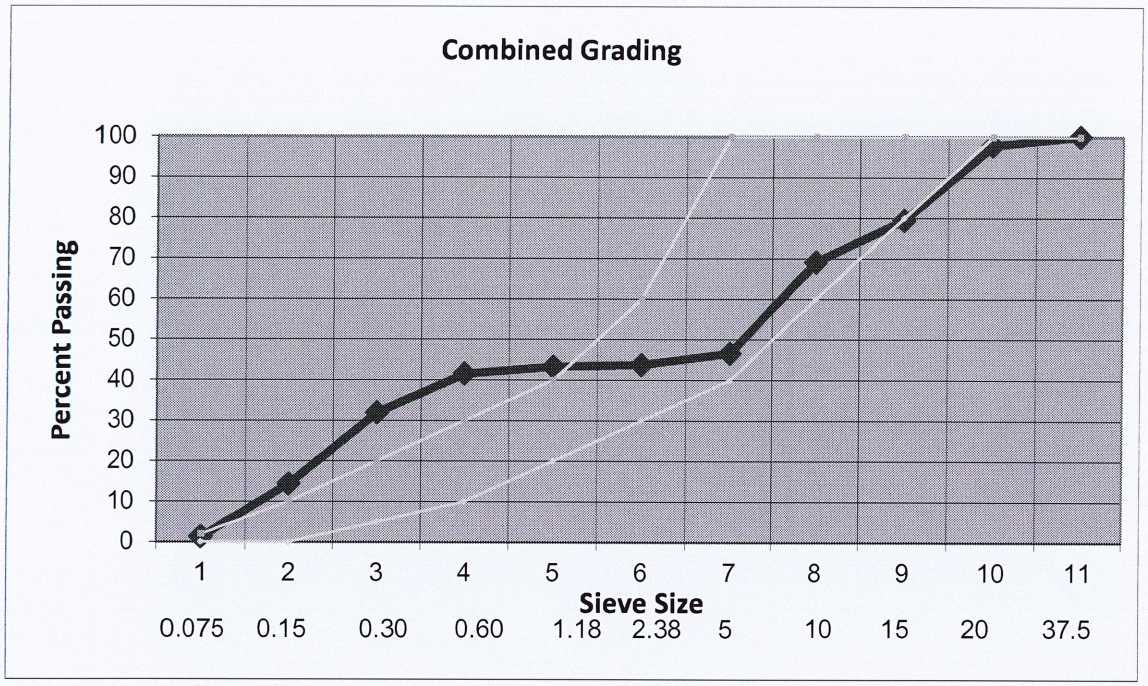


Figure 3.6 Combined Grading for f_{cu} = 80 Mpa

The concrete mix proportion for the three mixes (by weight) are given in table 3.1. Their slumps were measured according to BS 8500 in figure 3.6. For high workability, S5 class is 220 mm for all the mixes as shown in table 3.2.

Table 3.1 Concrete mix proportions

Concrete Strength MPa	Cement Content kg/m^3	Water Cement Ratio W/C	Coarse Aggregate kg/m^3	Fine Aggregate kg/m^3	Slag kg/m^3	Micro Silica kg/m^3	Admixture kg/m^3
120	499	0.19	1120	656	63	63	15
100	470	0.28	1160	700	0	47	9.5
80	470	0.34	1235	793	0	0	7.9

Table 3.2 Concrete slump class specification to BS 8500

Specified Slump Class	Requirement		Target (mm)
	Not less than (mm)	Not more than (mm)	
S1	0	50	20
S2	40	100	70
S3	90	160	130
S4	150	220	180
S5	210	NA	220

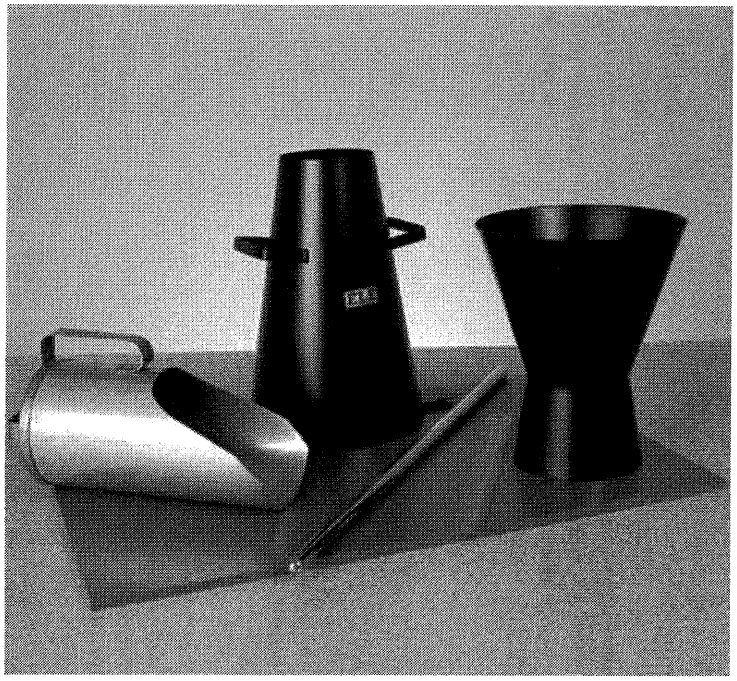


Figure 3.7 Slump test apparatus based on BS 8500

3.4 Test Specimen Details

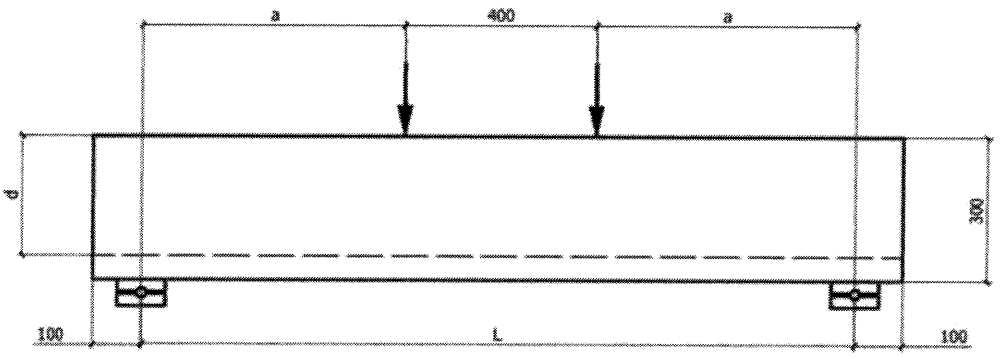
Shear tests consist of three sample groups of beams (Group 1 [G1], Group 2 [G2], and Group 3[G3]). The main variables of each group are the shear span-to-depth ratio (a/d) in G1, the flexural reinforcement ratio (ρ) in G2, and the compressive strength of concrete (f_{cu}) in G3. The beams were singly reinforced with

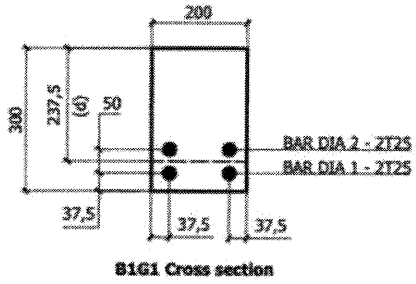
double layers of G72.5 as per ACI code; G500 as per BS code reinforcing bars which had a yield stress (f_y) of 500 MPa (72.5 Ksi).

All beams are designed according to ACI 318-19 and BS 8110 part 11997 requirements with compressive strength of concrete f_{cu} of 120 MPa (17.5 Ksi) except the beams in G3 that are designed with f_{cu} of 80 MPa (11.7 Ksi) and 100 Mpa (14.6 Ksi). In addition to the beam of 120 MPa (17.5 Ksi), all beams in all groups are Mpa and are without stirrups. The beams with 200 mm wide (b) have a total depth (h) of 300 mm. The beams were simply supported and loaded by two-point loads. Each beam specimen was intentionally designed to have calculated a nominal bending moment capacity M_n that was greater than the calculated moment required to cause a shear failure. Table 3.2 and figure 3.4 summarize the specimen details. Table 3.3 shows the calculated moment capacity M_n as per ACI code, noting that using f'_c (Cylinder) = 0.8 f_{cu} (Cubes) for ACI equations and as per BS code.

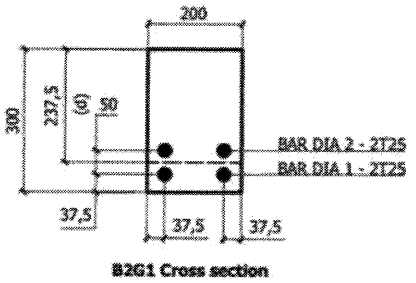
Table 3.3 Details of test beam specimen

No.	Beam No.	b mm	h mm	d mm	L m	a mm	L/h	a/d	Flexural Reinforcement		ρ $= \frac{As}{b\,d}$
									No. of bars	(As) mm2	
1	B1G1	200	300	237.5	1.4	500	4.67	2.11	4 φ 25	1964.29	0.041
2	B2G1	200	300	237.5	1.65	625	5.50	2.63	4 φ 25	1964.29	0.041
3	B3G1	200	300	237.5	1.90	750	6.33	3.16	4 φ 25	1964.29	0.041
4	B4G1	200	300	237.5	2.4	1090	8	4.21	4 φ 25	1964.29	0.041
5	B1G2	200	300	237.5	1.65	625	5.50	2.63	4 φ 25	1964.29	0.041
6	B2G2	200	300	230.5	1.65	625	5.50	2.71	2 φ 25 2 φ 32	2591	0.056
7	B3G2	200	300	230.5	1.65	625	5.50	2.71	4 φ 32	3218	0.064
8	B4G2	200	300	262.5	2.61	1105	8.7	4.21	2 φ 25	982.14	0.019
9	B5G2	200	300	259	2.58	1090	8.6	4.21	2 φ 32	1609.14	0.031
10	B6G2	200	300	230.5	1.65	625	5.50	2.71	4 φ 32	3218	0.064
11	B1G3	200	300	237.5	1.65	625	5.50	2.63	4 φ 25	1964.29	0.041
12	B2G3	200	300	237.5	1.65	625	5.50	2.63	4 φ 25	1964.29	0.041
13	B3G3	200	300	237.5	1.65	625	5.50	2.63	4 φ 25	1964.29	0.041

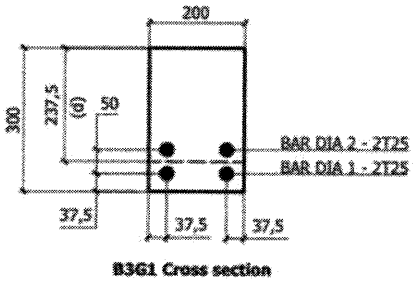




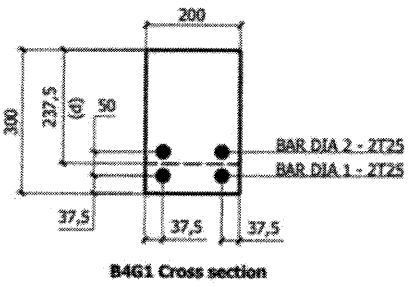
B1G1 Cross section



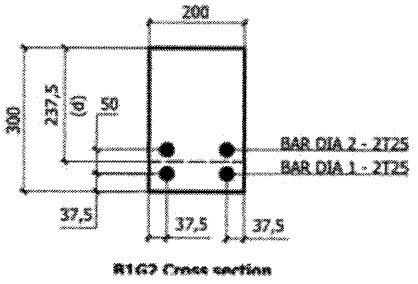
B2G1 Cross section



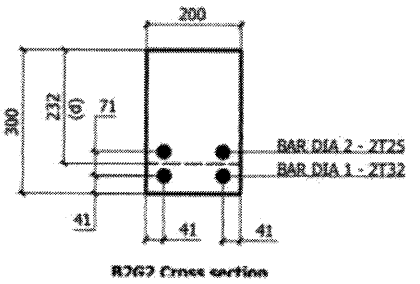
B3G1 Cross section



B4G1 Cross section



B1G2 Cross section



B2G2 Cross section

Figure 3.8 Details of test beam specimen

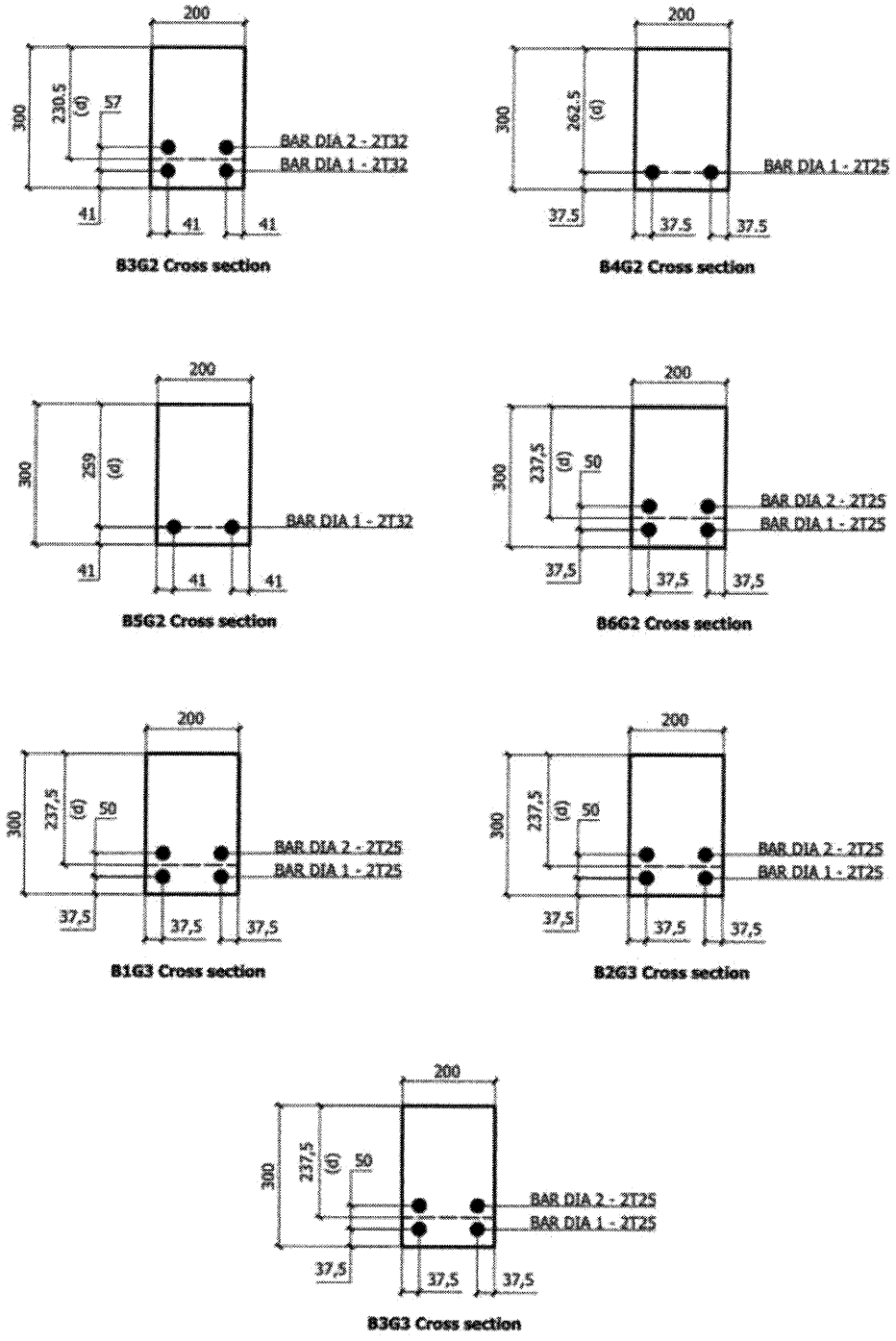


Figure 3.8 Details of test beam specimen (Cont'd)

Table 3.4 Nominal strength calculation as per BS 8110 and ACI equations

No.	Beam No.	a/d	ρ	f_y MPa	f_{cu} MPa	f_c' MPa	ρ_b	ρ / ρ_b	Calculated Nominal strength BS equations				Calculated Nominal strength ACI equations			
									Shear		Flexure		Shear		Flexure	
									Vn KN	P KN	Mn KN.m	P KN	Vn KN	P KN	Mn KN.m	P KN
1	B1G1	2.11	0.041	500	120	96	0.058	0.71	92.6	185.19	172.16	688.62	90.51	181.3	203.71	814.82
2	B2G1	2.63	0.041	500	120	96	0.058	0.71	92.6	185.19	172.16	550.9	87.3	174.61	203.71	651.86
3	B3G1	3.16	0.041	500	120	96	0.058	0.71	92.6	185.19	172.16	459.08	85.16	170.33	203.71	543.22
4	B4G1	4.21	0.041	500	120	96	0.058	0.71	92.6	185.19	172.16	344.31	82.49	164.98	203.71	407.41
5	B1G2	2.63	0.041	500	120	96	0.058	0.71	92.6	185.19	172.16	710.02	87.3	174.61	203.71	651.86
6	B2G2	2.7	0.056	500	120	96	0.058	0.97	100.57	201.15	221.88	875.99	89.3	178.6	249.2	797.45
7	B3G2	2.7	0.07	500	120	96	0.058	1.21	107.81	215.62	173.75	550.9	92.68	185.37	291.58	933.05
8	B4G2	4.21	0.019	500	120	96	0.058	0.32	76.728	153.25	95.14	172.2	86.32	172.36	121.52	219.94
9	B5G2	4.21	0.031	500	120	96	0.058	0.54	89.83	179.65	153.8	282.2	87.78	175.56	188.55	345.97
10	B6G2	4.21	0.041	500	120	96	0.058	0.71	92.6	185.19	172.16	344.31	82.49	164.98	2-3.71	407.41
11	B1G3	2.63	0.041	500	80	64	0.039	1.07	80.89	161.78	172.16	550.9	73.64	147.28	188.93	604.57
12	B2G3	2.63	0.041	500	100	80	0.048	0.86	87.14	174.27	172.16	550.9	80.82	161.63	197.8	632.95
13	B3G3	2.63	0.041	500	120	96	0.058	0.71	92.6	185.19	172.16	550.9	87.3	174.61	203.71	651

3.5 Preparation of Test Specimen

The preparation includes batching, mixing, and fabrication.

3.5.1 Batching

Batching involves the collection, storage, and proportion of the concrete constituents before mixing. Batching is done by weight for accuracy. All operations of weighing and batching of the concrete ingredients were done by hand. All materials were weighed using a sensitive scale. Cement, slug, micro silica, fine and coarse aggregate, water, and admixtures were measured accurately and fed to the mixer in a similar flow to produce a uniform quality of concrete.



Figure 3.9 Batching of materials for the mix

3.5.2 Mixing

The concrete was mixed in a drum type mechanical mixer as shown in figure 3.9.

For the higher quantities of concrete, a central type of concrete mixer machine was used as shown in figure 3.10.

Before the mixing operation, the mixer was cleaned and checked to ensure that it is in good condition. The materials were uniformly distributed throughout the mixtures and all aggregate surface was coated with cement paste. The mixer was meticulously designed, not overloaded, charged correctly, and operated at the optimum speed as recommended by the manufacturer. The time of mixing required was according to ASTM C-94 and BS standard.

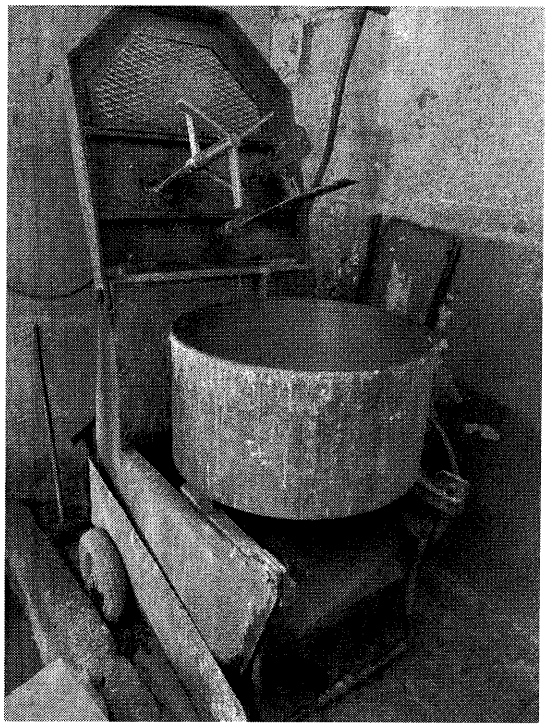
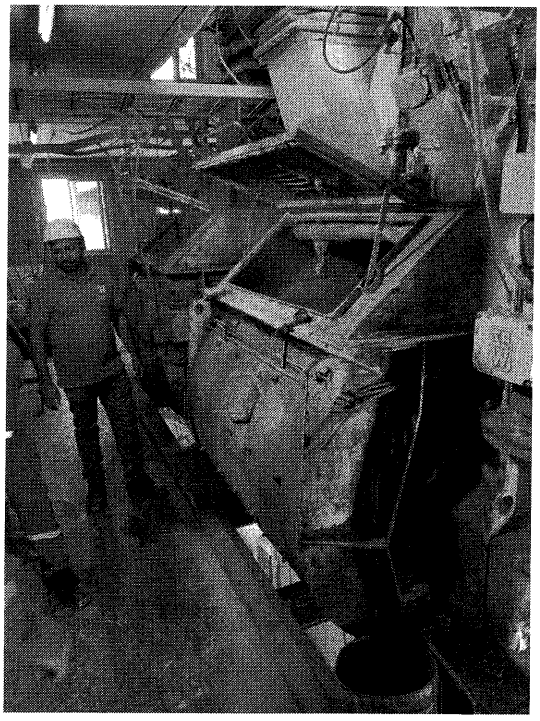
(a)  (b) 

Figure 3.10 Mixer machine (a) Drum type mechanical mixer, (b) Central type concrete mixer

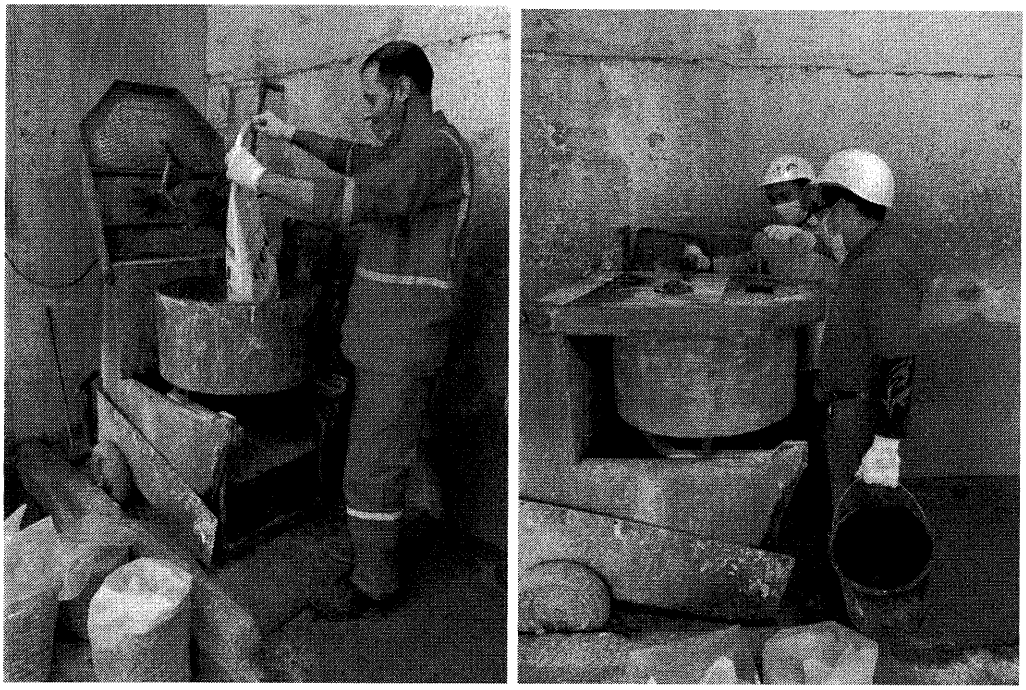


Figure 3.11 Concrete Mixing

3.5.3 Fabrication

The fabrication steps include fabrication before concreting, concreting operation, and after concreting.

3.5.3.1 Before Concreting

Fabrication before concreting includes fixing the forms, fixing the reinforcement, and checking out the forms.

Forms

The forms were made of steel plates as shown in figure 3.12 and were reused several times for the 10 beams. The forms have the same cross section and have smooth inside surface to facilitate the observation of cracks. Before placing the concrete, the forms were oiled as a precaution against sticking of the concrete forms.

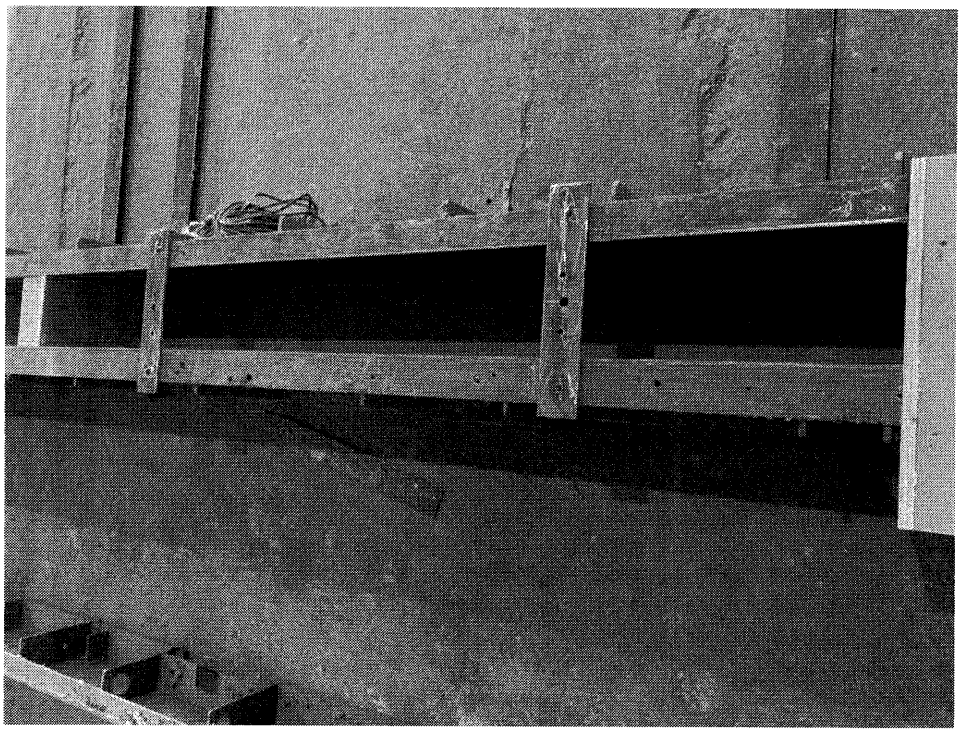


Figure 3.12 Steel plate forms

Reinforcement

The longitudinal reinforcement was placed in two layers in all beams. To hold the reinforcement in its proper position with respect to the bottom of beam, supporting steel chairs with the necessary depth were tied to the layers of the longitudinal bars, in addition to the concrete that covers the necessary depth to support the longitudinal bars with the sides of the forms.

Checkout Forms

Before the concreting operation, the forms were checked and braced against collapsing. In addition, the enforcement steels were checked. Figure 3.13 shows that the form is ready for casting.

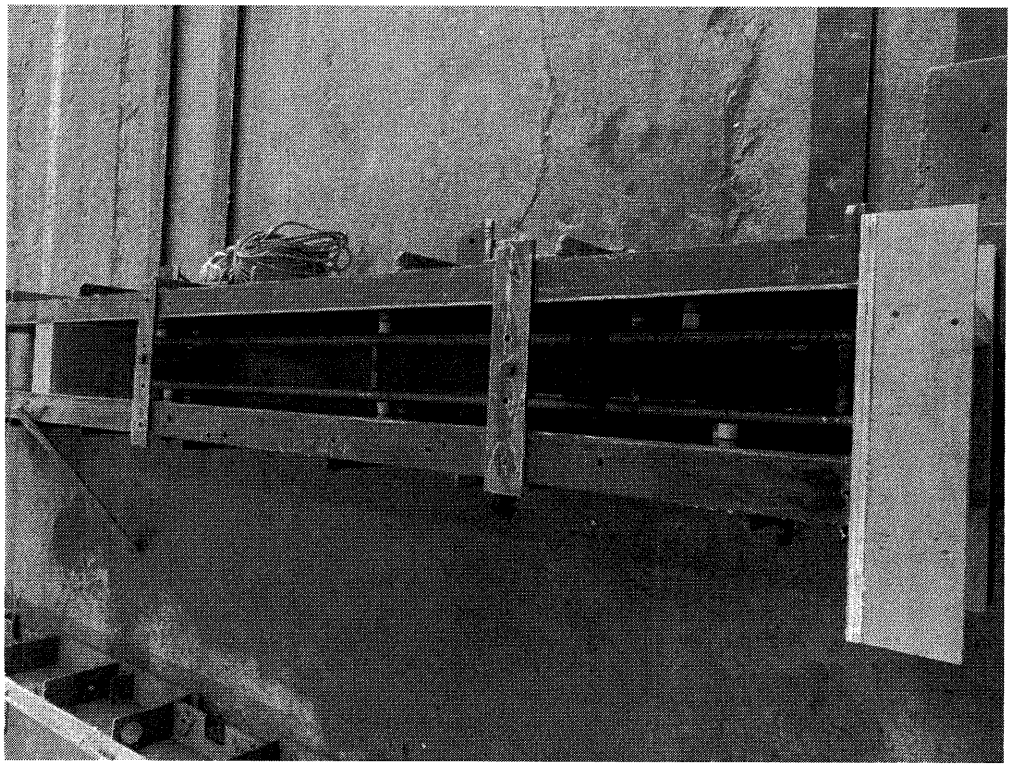


Figure 3.13 The form ready for casting

3.5.3.2 Concreting Operation

After batching and mixing operations were completed, the concrete was conveyed, placed, and consolidated without segregation; testing of fresh concrete and taking samples for testing the concrete strength also transpired.

Conveying

The concrete was dumped into metal container and then shoveled into the form.



Figure 3.14 Conveying of the concrete mix

Placing

The concrete was placed uniformly into the form by layers using a spread trowel. Each layer was spread to a uniform depth over the full length of the beam. The concrete was kept uniform and freed from obvious imperfection.

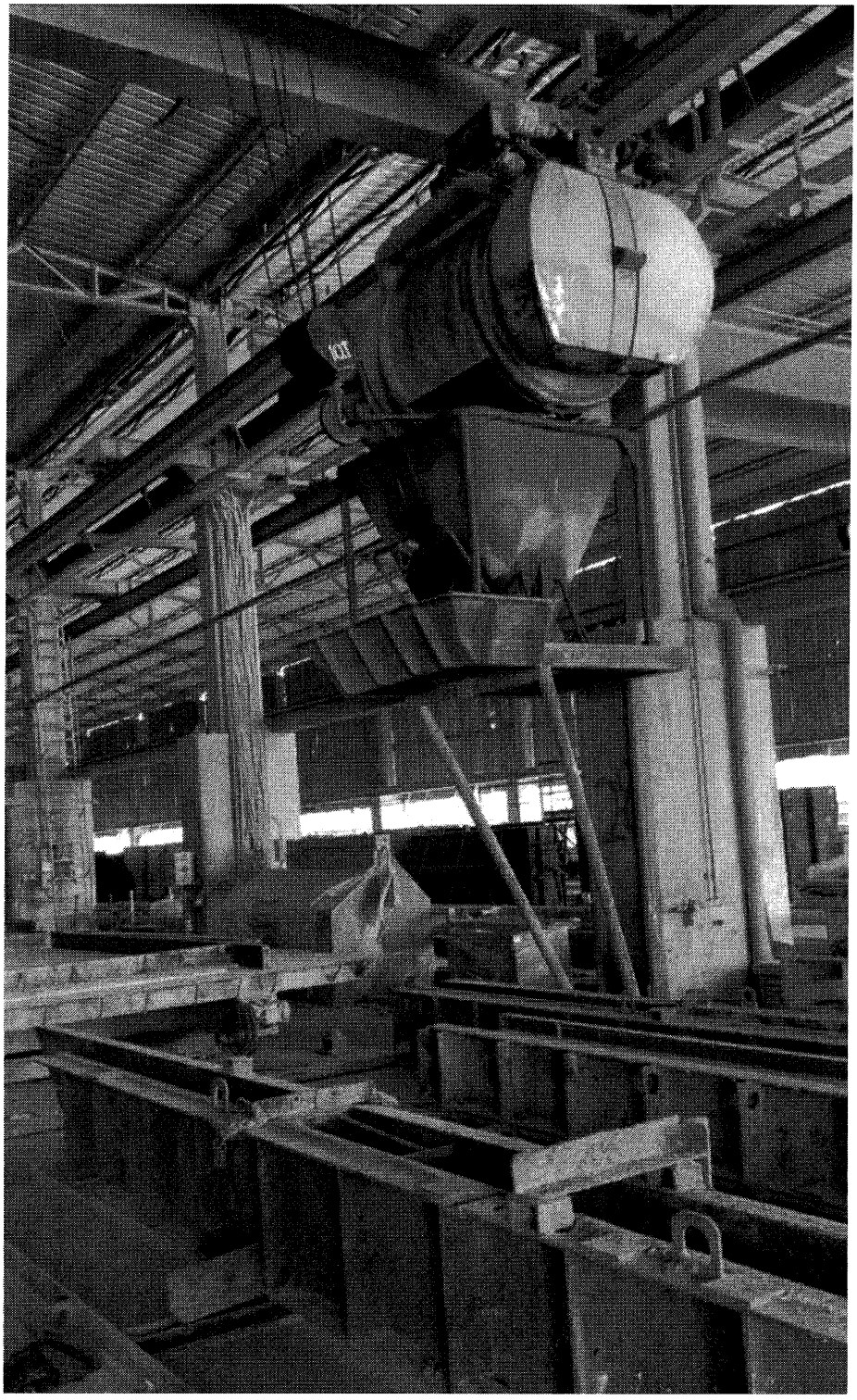


Figure 3.15 Conveying of the concrete mix using central type mixer

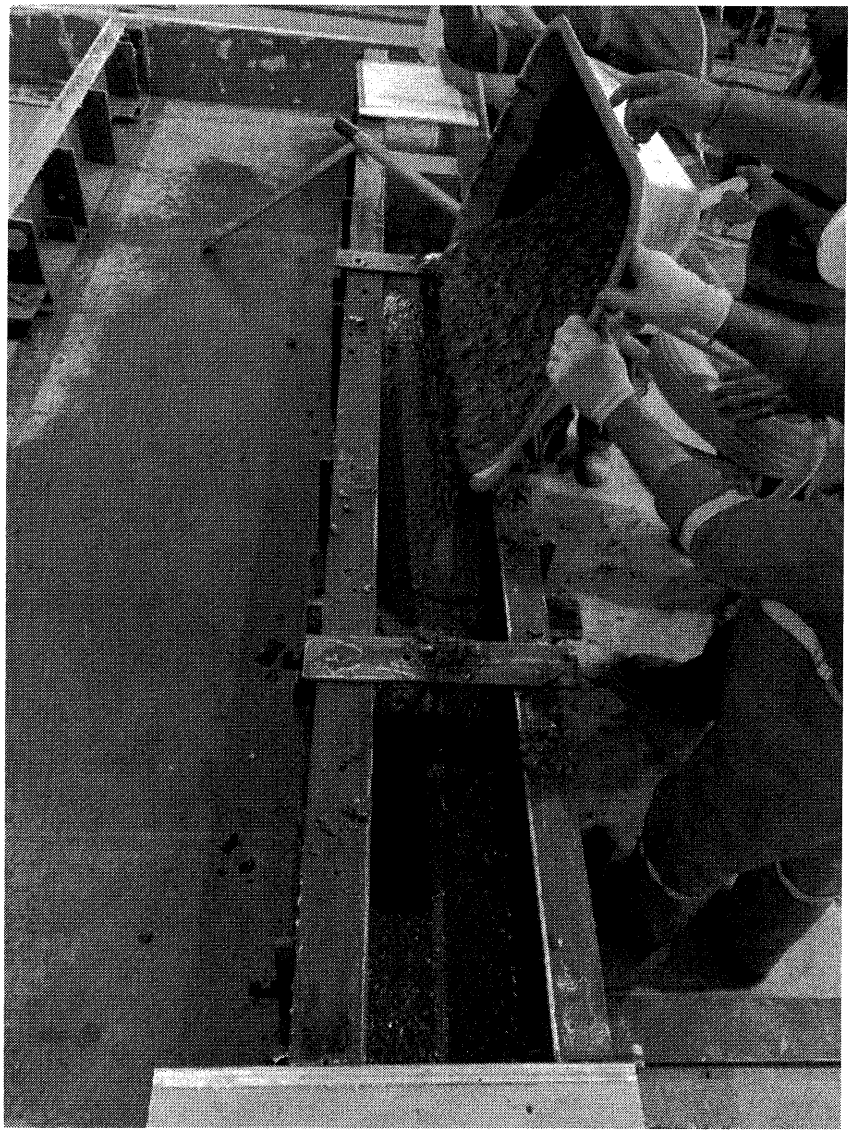


Figure 3.16 Placing of the concrete into the form

Consolidation

After the concrete was placed, the consolidation was done by means of electrical vibrator to secure a dense beam and close the bond with reinforcement and smooth surface. The concrete worked around reinforcement and embedded fixtures

and into the corner of the forms and operated continuously so that no holes were left in the concrete for forms to flow, because such practice usually caused segregation.



Figure 3.17 Placing of the concrete into the form using central type mixer



Figure 3.18 Concrete after consolidation

Test of Fresh Concrete

Immediately after mixing, a slum test was performed in accordance with ASTM C134 and BS 5328, BS 8110 to ensure workability. Unit weight was performed in accordance with ASTM C138 and BS 5328. Table 3.5 shows the results of these tests.



Figure 3.19 Beam after finishing of the concrete level

Table 3.5 Properties of fresh concrete

No.	Beam No.	BPC No.	Date of Casting	*Required* f_{cu} (MPa)	Slump (mm)	Unit Weight (Kg/m^3)	Note
1	B1G1	BE-11-300	13-Mar-2022	120	300	2475	
2	B2G1	BE-11-301	07-Mar-2022	120	300	2423	
3	B3G1	BE-11-302	06-Mar-2022	120	300	2447	
4	B4G1	BE-11-402	05-Jun-2022	120	230	2470	Additional Beam
6	B1G2	BE-11-301	07-Mar-2022	120	300	2423	B2G1
6	B2G2	BE-11-303	08-Mar-2022	120	300	2436	
7	B3G2	BE-11-304	09-Mar-2022	120	300	2560	
8	B4G2	BE-11-400	02-Jun-2022	120	190	2493	Additional Beam
9	B5G2	BE-11-401	04-Jun-2022	120	230	2480	Additional Beam
10	B6G2	BE-11-402	05-Jun-2022	120	230	2470	Additional Beam B2G4
11	B1G3	BE-11-100	12-Mar-2022	80	300	2436	
12	B2G3	BE-11-200	10-Mar-2022	100	300	2439	
13	B3G3	BE-11-301	07-Mar-2022	120	300	2423	B2G1

Concrete Control Specimen (Cubes)

Six 100 mm cube specimens were casted along with each beam prepared according to BS 1881 to investigate the uniaxial compressive strength of concrete for 7 and 28 days.

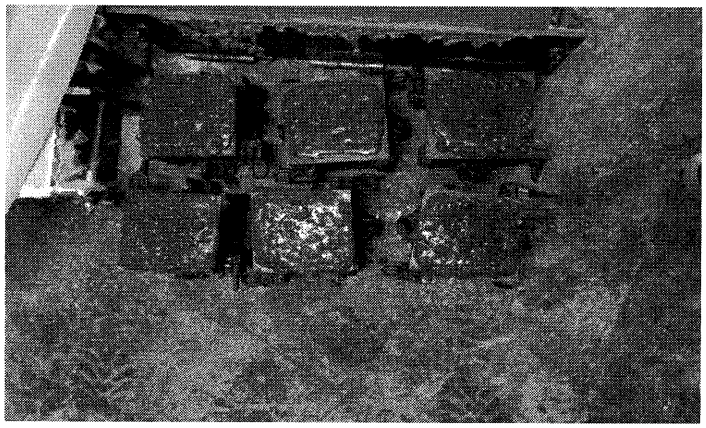


Figure 3.20 Cubes 100 mm as Concrete Control Specimen

3.5.3.3 After Concreting

The process includes the removal of forms, storage, cure, transport, and paint.

Removal of Forms

The sides of steel forms of the beams were removed one day after casting. Also cube molds were removed 24 hours after casting.



Figure 3.21 Beam after removing the form

Storage and Curing

All beams and control specimens (cubes) were cured in the curing yard of Bahrain Precast Concrete Company. The typical arrangement of curing and storage

of the beams were shown in figures 3.23 and 3.24. The beams were covered with standard towels and saturated daily with water for 28 days, while the cubes were immersed in water in a big container for 28 days as shown in figure 3.25.



Figure 3.22 The beams are ready for curing and storage

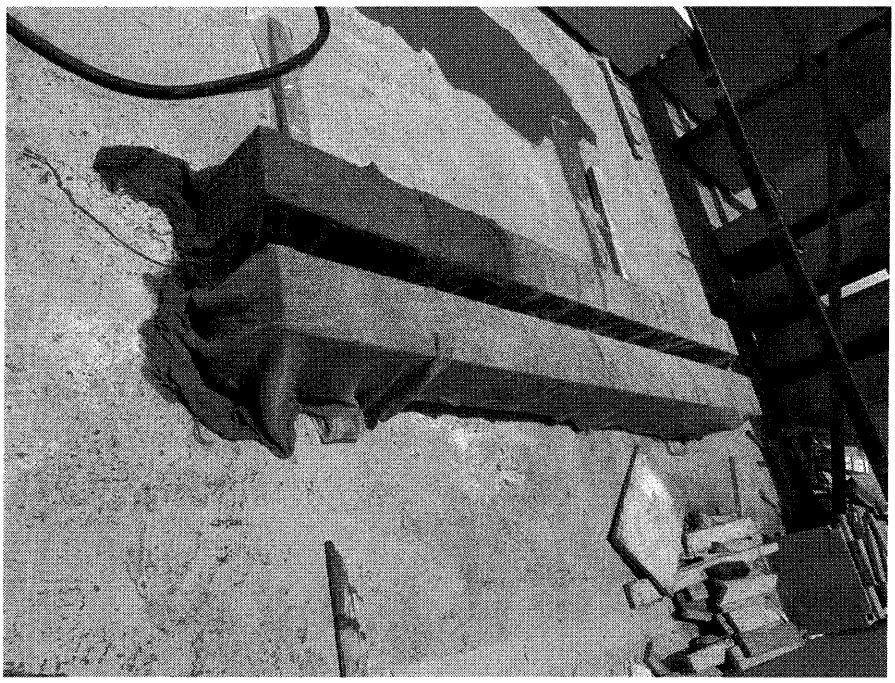


Figure 3.23 Curing of the beams



Figure 3.24 Storage of the beams

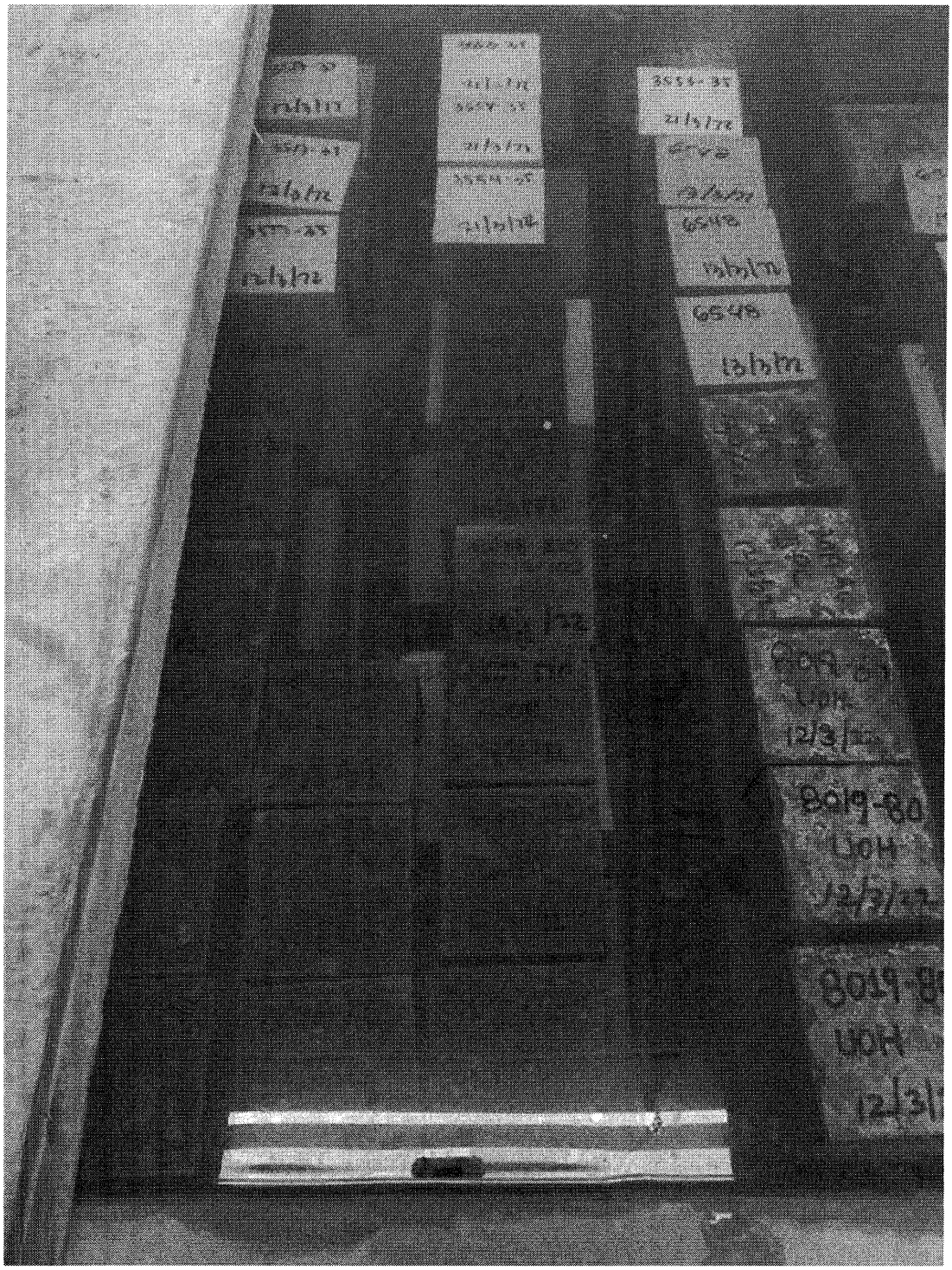


Figure 3.25 Curing and storage of the control specimens (Cubes)

Transportation of the Beams

The beams were transported to the structural lab at the University of Bahrain for testing as shown in figure 3.26.



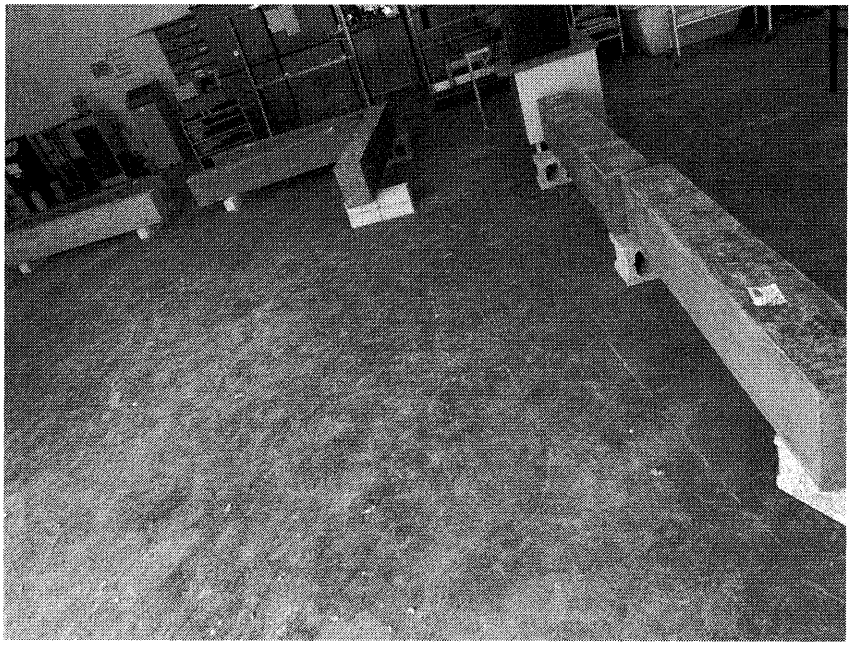


Figure 3.26 Transporting and storing the beams in the Lab

Painting of the Beams

The beams were coated with white to observe cracking patterns during the test as shown in figure 3.27.

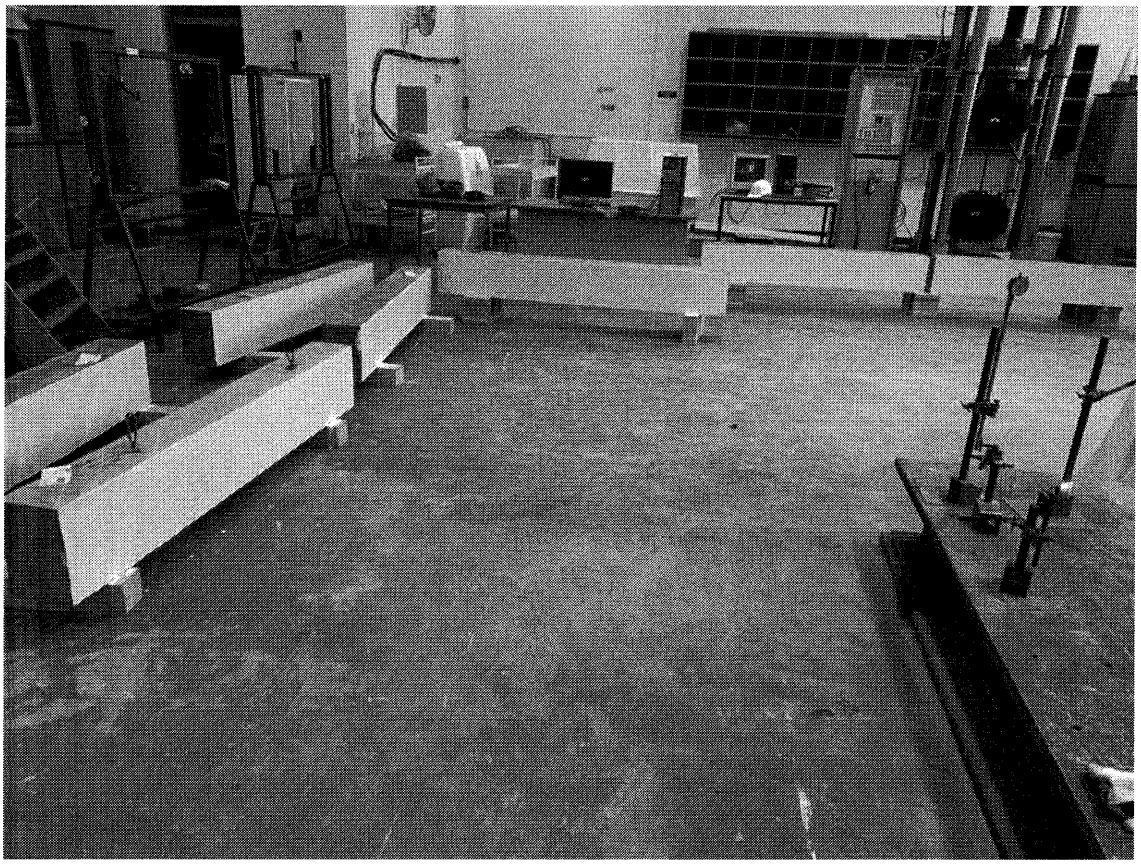


Figure 3.27 The beams after white painting

Chapter 4

Testing and Results

Chapter 4

Testing and Results

4.1 General

To achieve the goals of the experimental program, nine reinforced concrete beams were designed to fail in shear in three groups. Each group has three beams; one beam is common between groups. Seven reinforced concrete beams were casted at Bahrain Precast Concrete (BPC) company yard for the researcher to study their shear behavior. All beams have the same width (b=200 mm) and the same total depth (h=300 mm). The effective depth (d=230.5 to 237.5 mm) depends on the longitudinal steel reinforcement arrangement. The variables; however, with shear span-to-depth ratio (a/d) vary from 2.11 to 3.16, the flexural reinforcement ratio (ρ) vary from 0.041 to 0.064, and the compressive strength of concrete f_{cu} vary from 80 MPa to 120 MPa. For each beam, six concrete control specimen cubes were casted.

Before testing, the beams and their respective cubes were taken out from the storage room and were coated with white paint to facilitate the observation of the cracks during testing.

4.2 Beams Testing

The beams were tested using hydraulic load testing machine in the structural laboratory of the University of Bahrain. The machine is shown in figure 4.1.



Figure 4.1 Hydraulic testing machine

4.2.1 Test Loading Equipment

The beams were supported by a free roller at both ends to eliminate any axial forces during testing. All beams were loaded symmetrically with two equal concentrated monotonically increasing loads and were tested under static loading until the ultimate stage defined as the maximum load carrying capacity. The load was transferred from the head of the hydraulic load to the concrete beam by spreader

steel beam with free roller at both ends. The two-point loads were placed with the support of spreader steel beam at 200 mm on both sides at the center of the reinforced concrete beam, noting that the distance between the end of the RC beam and center of its support is 100 mm for both ends.

This arrangement of loads produced a constant moment and zero shear in the central 400 mm. Figure 4.2 shows the beam test setup, Figure 4.3 manifests the roller supports and figure 4.4 exhibits the two-point load arrangement, respectively.

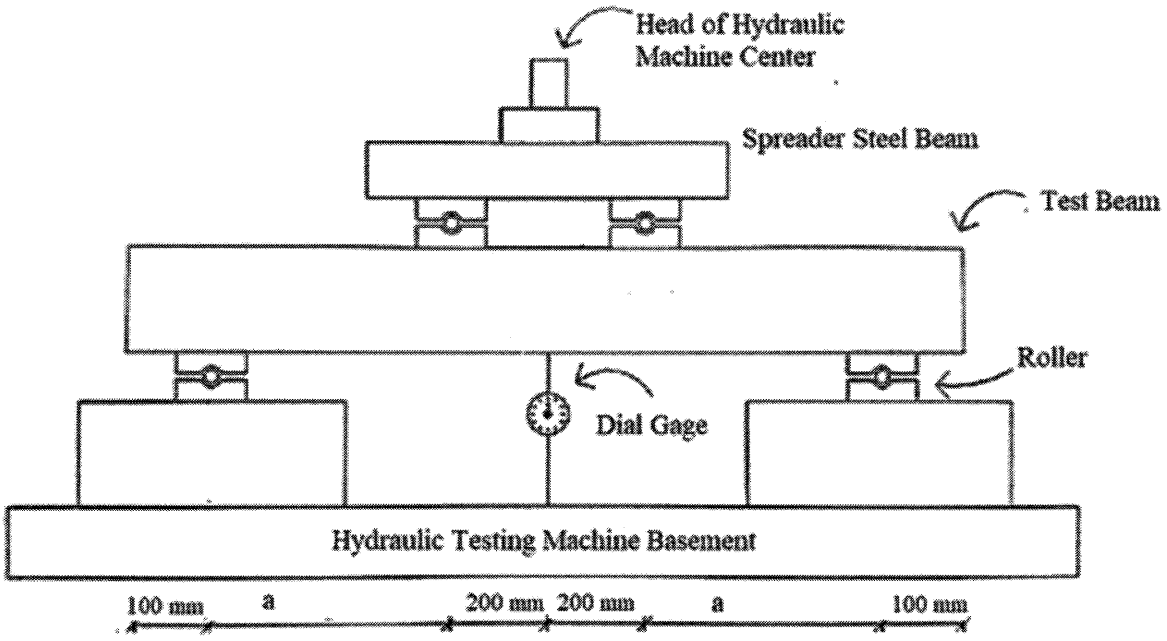
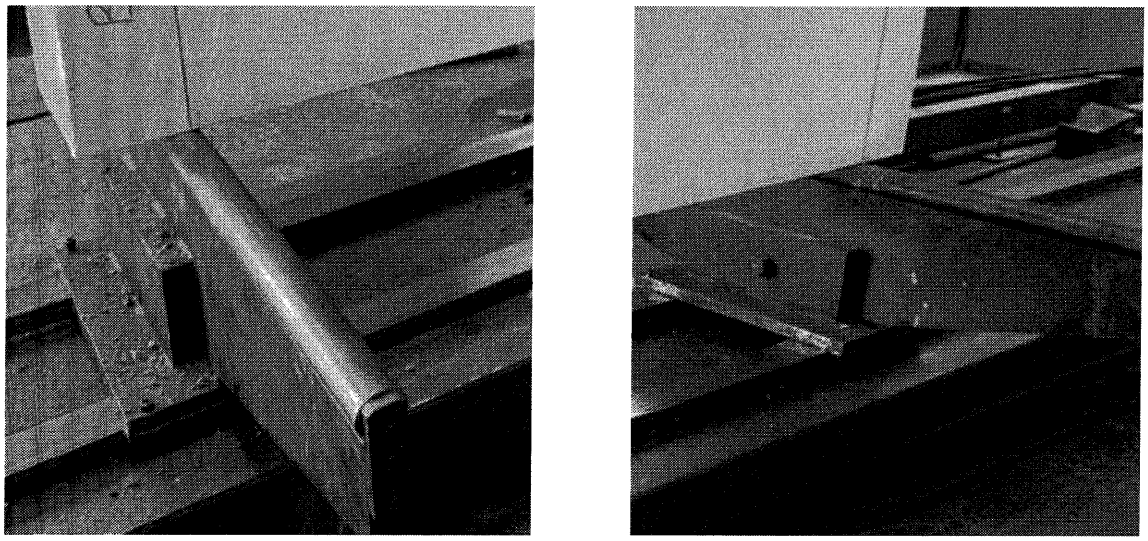


Figure 4.2 Beam setup for testing



(a) Left side (b) Right side

Figure 4.3 Beam roller supports

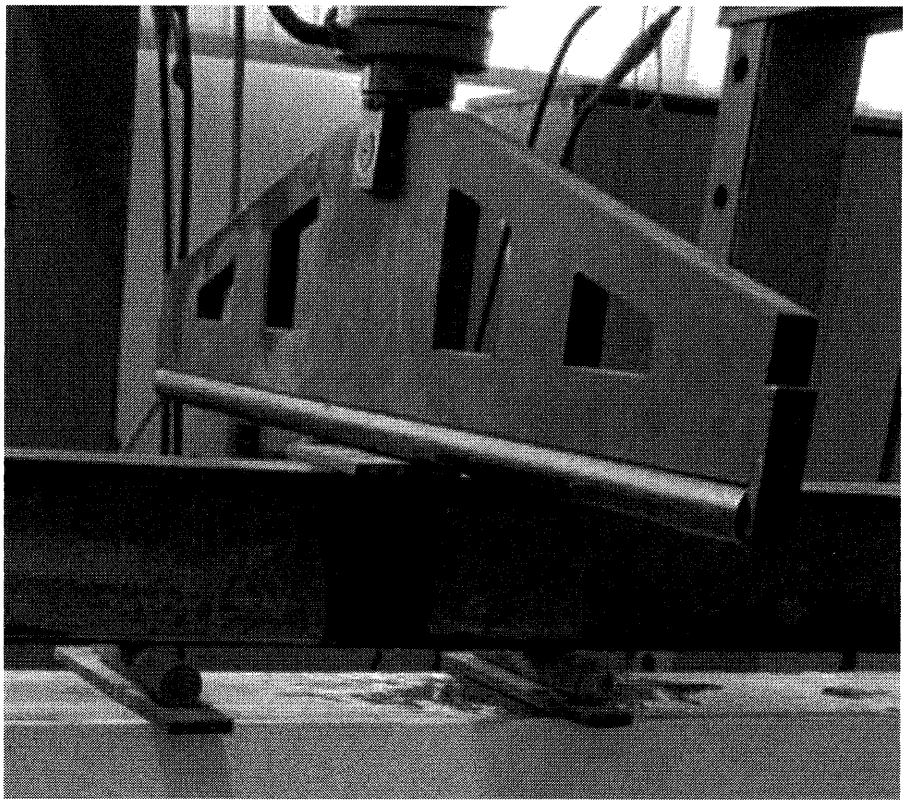


Figure 4.4 Arrangement for two-point loads with spreader steel beam

4.2.2 Test Instrumentation

Dial gage was used to measure deflection with precision of measuring the nearest 0.01 mm fixed under the bottom of the mid-span of the tested beam to determine the mid-span deflection.

Figure 4.2 shows the position of the dial gage that measures the mid-span deflection and the beam test setup and figure 4.5 displays the dial gage used during the test.

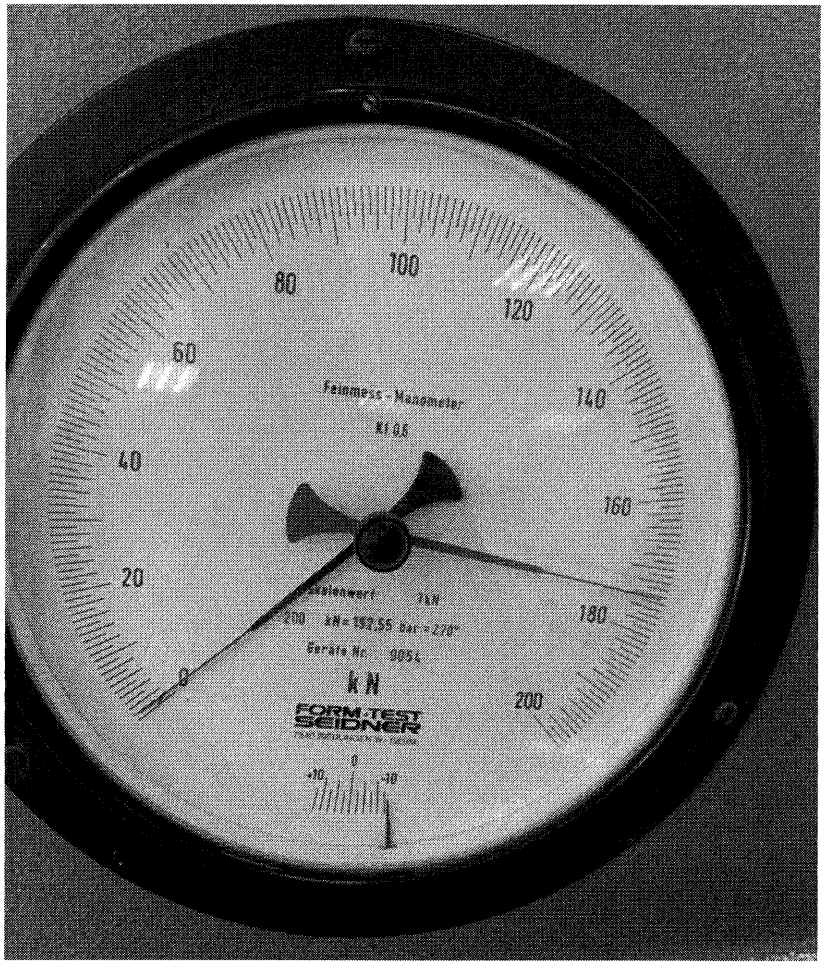


Figure 4.5 Dial gage for measuring midspan deflection

4.2.3 Test Procedure

The beam test specimen was placed for loading in the test machine after which the dial gage was fixed under the test beam in the basement of the testing machine through a holding tool. The typical arrangement of specimen under test is shown in figure 4.6. The dial gage was set to zero reading prior to testing.

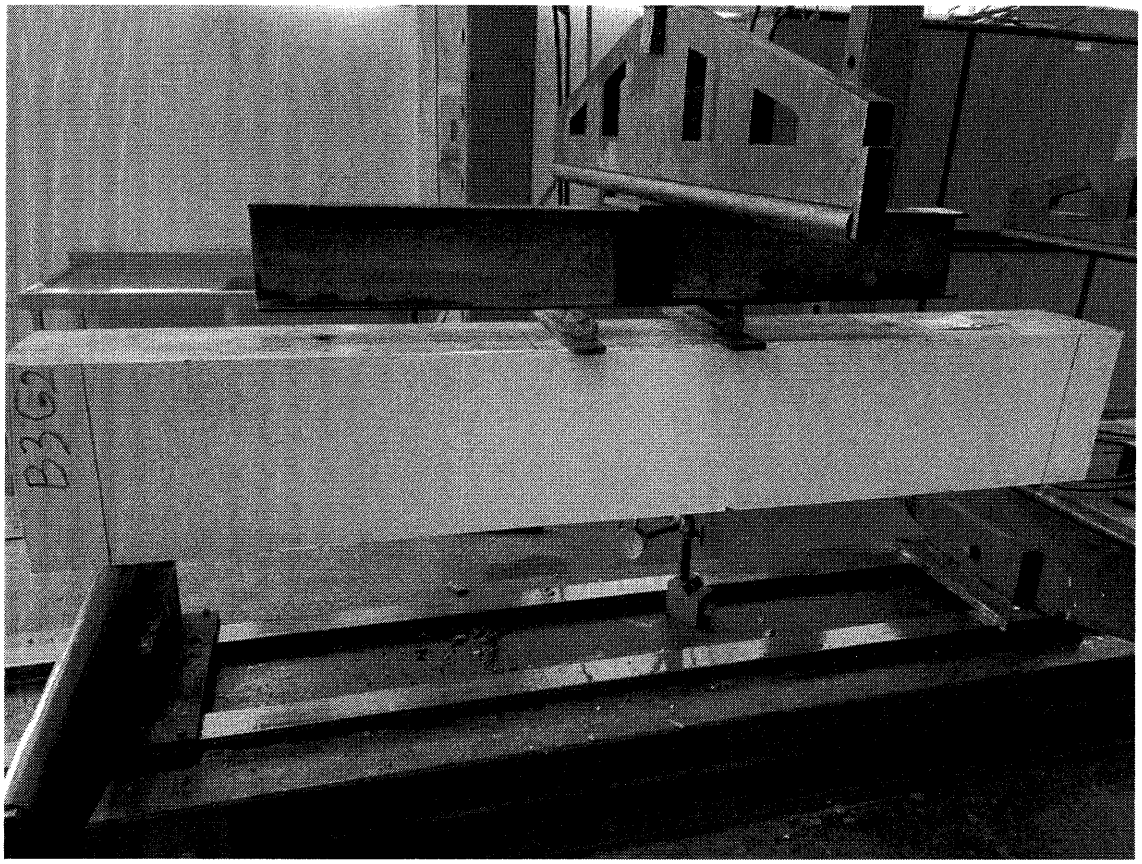


Figure 4.6 Typical beam test arrangement

The load was applied with increment of 5 KN until the appearance of the first crack, then the load was increased to 10 KN up to 70 percent of the estimated

ultimate load of the beam, after which the increment was reduced to 5 KN up to failure. At each load increment, deflection readings were recorded through the dial gage, cracks were checked, traced with color tipped pen, identified with the load at which they formed. Before failure of the beam, the mid-span dial gage was taken off, and a ruler was used to read the deflection at failure.

The time required for testing each beam is the time between initial load and failure. It varies depending on the estimated ultimate load but may take about 60 to 90 minutes.

The control specimen (cubes) for each beam was tested to determine the compressive strength of concrete and steel bars and to determine the yield strength of reinforcing bars.

4.3 Test Results

The main objective of the present study is to investigate the shear behavior of ultra-high strength concrete beams reinforced with high strength steel. The parameters for the study are beam deflection, cracking, strength, and failure mechanisms.

All efforts have been made to record all measurements up to failure. Beam deflection was recorded through the dial gage, cracks were marked, and failure load was recorded from the testing machine.

The beam test results, the control specimen results, and steel bars are presented in the following sections.

4.3.1 Test Results for Steel Bars

Two samples of steel reinforcement bars were used in the research, one sample for 25 mm dia steel and another sample for 32 mm dia steel. The method of testing is according to BS 4449:2005+A3:2016/BS EN 15630-1:2019. Figure 4.7 shows the steel reinforcement bars testing machine.

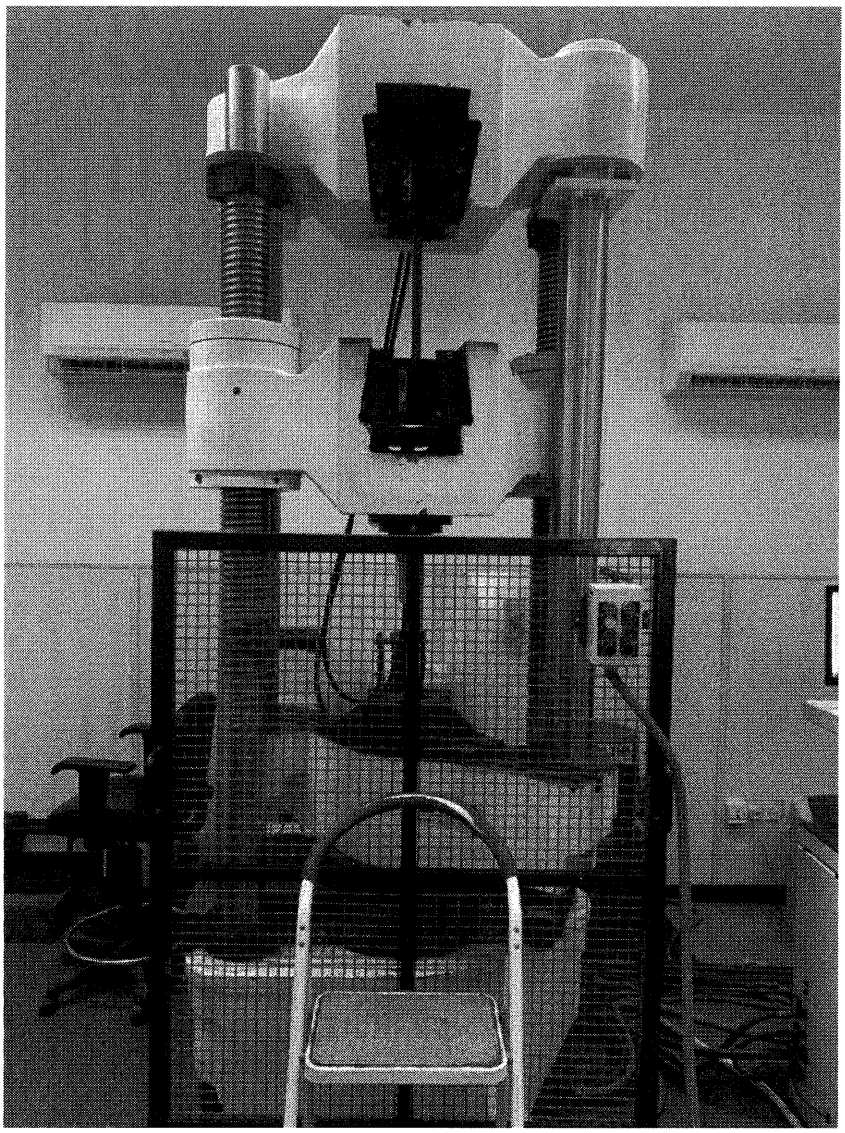
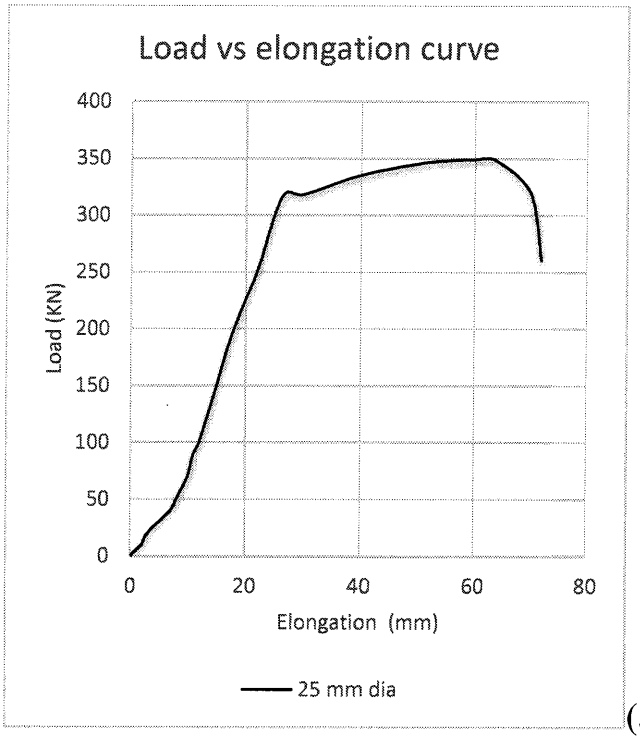


Figure 4.7 Testing machine for steel bars tensile strength

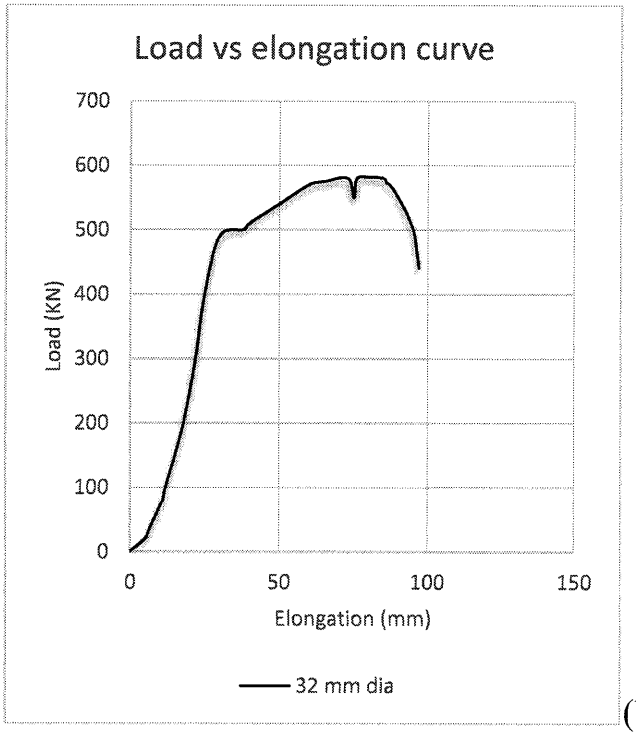
Table 4.1 presents the details of the test results for the steel rebars both in 25 mm dia and 32 mm dia, and figure 4.8 shows the load elongation curve for 25 mm dia and 32 mm dia, respectively.

Table 4.1 Tensile Steel reinforcement test results

Results		Sample No. 1 25 mm dia	Sample No. 2 32 mm dia
Condition of the sample		Satisfactory	Satisfactory
Length	(m)	0.596	0.699
Mass	(kg)	2.239	4.331
Mass per meter	(kg/m)	3.757	6.196
Area	(mm^2)	478.56	789.3
Nominal diameter	(mm)	25	32
Temperature at test	(°c)	23	23
Yield stress (Re)	(N/mm^2)	636.469	623.097
Tensile stress (Rm)	(N/mm^2)	727.298	731.231
Stress ratio Rm/Re)		1.14	1.17
Initial gage length	(mm)	100	100
Final gage length	(mm)	121.32	129.65
Elongation at fracture	(%)	21.32	29.65



(a)



(b)

Figure 4.8 load vs elongation curve for (a) 25 mm dia (b) 32 mm dia

4.3.2 Test Results for Concrete Cubes

Three cubes were taken from each batch of concrete. The concrete cubes were prepared according to BS 1881-125:1986 and tested according to BS 1881116:1983. Figure 4.9 shows the concrete compressive testing machine.



Figure 4.9 Testing machine for concrete compressive strength

Table 4 presents the average cubic compressive strength results (f_{cu}) and cylinder compressive strength of concrete ($f'_c = 0.8 f_{cu}$).

Table 4.2 Concrete cubes compressive strength test results

No.	Beam No.	Date of casting	Date of Testing	Age (Days)	*Average* f_{cu} (Mpa)	*Average* f'_c (Mpa)	Selected Grade as (BS)
1	B1G1	13/03/22	17/04/22	35	108.70	86.96	C110
2	B2G1	07/03/22	17/04/22	41	112.80	90.24	C110
3	B3G1	06/03/22	29/03/22	28	111.40	89.12	C110
4	B4G1	05/06/22	02/07/22	28	106.5	85.2	C110
5	B1G2/B2G1	07/03/22	17/04/22	41	112.80	90.24	C110
6	B2G2	08/03/22	17/04/22	40	109.70	87.76	C110
7	B3G2	09/03/22	17/04/22	39	109.50	87.60	C110
8	B4G2	02/06/22	28/06/22	28	107.5	86	C120
9	B5G2	04/06/22	02/07/22	28	106.6	85.28	C110
10	B6G2/B4G1	05/06/22	02/07/22	28	106.5	85.2	C110
11	B1G3	12/03/22	17/04/22	36	76.80	61.44	C80
12	B2G3	10/03/22	17/04/22	38	102.20	81.76	C100
13	B3G3/B2G1	07/03/22	17/04/22	41	112.80	90.24	C110

Noting that, the concrete compressive strength takes 99% of it is strength at the age of 28 days with very less increase after that. It is customary to assume the 28 days' strength as full strength of concrete so that the age after will not affect the strength of the concrete.

4.3.3 Beams Test Results

Thirteen reinforced concrete beams have been assigned for the investigation of shear behavior, and they failed in shear. They were divided into three groups, each designed for the researcher to study one variable's effect.

The parameters included shear span-to-depth ratio (a/d) ranging from 2.11 to 3.16 in addition to one with (a/d =4.21) in group No.1; flexural reinforcement ratio ρ ranging from 0.041 to 0.07 in addition to three numbers with (a/d = 4.21); different steel ratio from 0.019 to 0.041 in group No.2; and compressive strength of concrete f_{cu} ranging from 76.8 to 112.8 Mpa in group No.3.

Table 4.3 summarizes the beam details and the nominal ultimate strength calculations as per BS 8110 part 1,1997 and ACI 318-19 equations.

The first seven beams were tested, four failed in shear and three did not fail because their strength exceeded the machine's capacity. To keep the three beams for each variable, these beams were replaced by another new three beams. A summary of the test results is presented in table 4.4, which includes the load, shear moment capacity, load at first flexural cracks and first inclined cracks, and the ultimate stage of the beams, with the mode of failure. Figure 4.10 to figure 4.16 show the cracking and failure of all beams. More details are discussed in chapter 6 (Data Analysis and Discussion).

Table 4.3 Nominal strength calculations as per BS 8110 & ACI equations

Beam No.	a/d	ρ	f_y MPa	f_{cu} MPa	f_c' MPa	ρ_b	ρ / ρ_b	Calculated Nominal strength BS equations				Calculated Nominal strength ACI equations			
								Shear		Flexure		Shear		Flexure	
								Vn KN	P KN	Mn KN.m	P KN	Vn KN	P KN	Mn KN.m	P KN
B1G1	2.11	0.041	636.5	108.7	86.96	0.037	1.129	89.59	179.19	219.15	876.61	86.92	173.84	244.07	976.28
B2G1	2.63	0.041	636.5	112.8	90.24	0.038	1.088	90.71	181.41	219.15	701.29	85.03	170.06	245.99	787.17
B3G1	3.16	0.041	636.5	111.4	89.12	0.038	1.102	90.33	180.66	219.15	584.41	82.45	164.9	245.35	654.27
B4G1	4.21	0.041	636.5	106.5	85.2	0.039	1.048	88.98	177.97	219.15	438.31	78.18	156.35	242.98	485.95
B1G2 B2G1	2.63	0.041	636.5	112.8	90.24	0.038	1.088	90.71	181.44	219.15	894.34	85.03	170.06	245.99	787.17
B2G2	2.7	0.056	629.8	109.7	87.76	0.038	1.487	97.91	195.22	279.48	1091.65	86.11	172.21	289.42	926.14
B3G2	2.7	0.064	623.1	109.5	87.6	0.038	1.832	104.57	209.14	341.14	701.29	89.45	178.9	327.71	1047.1
B4G2	4.21	0.019	636.5	107.5	86	0.036	0.521	73.66	147.32	121.11	219.21	81.58	163.82	150.62	272.62
B5G2	4.21	0,031	636.5	106.6	93.68	0.037	0.838	86.32	172.65	191.66	351.67	83.08	166.23	225.02	412.81
B6G2 B4G1	4.21	0,041	636.5	106.5	85.2	0.039	1.487	88.98	177.97	219.15	438.31	78.18	156.35	242.98	485.95
B1G3	2.63	0.041	636.5	76.8	61.44	0.026	1.598	79.8	159.59	219.15	701.29	72.41	144.82	222.11	710.75
B2G3	2.63	0.041	636.5	102.2	81.76	0.034	1.201	87.77	175.54	219.15	701.29	81.56	163.12	240.71	770.26
B3G3 B2G1	2.63	0.041	636.5	112.8	86.96	0.038	1.088	90.71	181.41	219.15	701.29	85.03	170.06	245.99	787.17

Table 4.4 Experimental load, shear, and moment at different stages for tested beams

No.	Beam No.	Date of Casting	Date of Testing	Age	At First flexure cracking			At First inclined cracking			At Ultimate (failure)			Failure Mode
					P (KN)	V= P/2 (KN)	M= Pa/2 (KN)	P (KN)	V= P/2 (KN)	M= Pa/2 (KN)	P (KN)	V= P/2 (KN)	M= Pa/2 (KN.m)	
1	B1G1	13/03/2022	24/04/2022	42	-	-	-	-	-	-	-	-	-	-
2	B2G1 B1G2 B3G3	07/03/2022	13/04/2022	37	100	50	31.5	190	95	59.38	220	110	68.75	SF
3	B3G1	06/03/2022	13/04/2022	38	65	32.5	24.38	170	85	63.75	210	105	78.75	SF
4	B2G2	08/03/2022	24/04/2022	47	-	-	-	-	-	-	-	-	-	-
5	B3G2	09/03/2022	13/04/2022	35	-	-	-	-	-	-	-	-	-	-
6	B4G2	02/06/2022	06/09/2022	96	40	20	22.1	150	75	88.4	160	80	88.4	SF
7	B5G2	04/06/2022	05/09/2022	93	70	35	38.15	170	85	92.65	180	90	98.1	SF
8	B6G2 B4G1	05/06/2022	07/09/2022	94	90	45	45	190	95	95	200	100	100	SF
9	B1G3	12/03/2022	14/04/2022	33	90	45	45	180	90	56.25	200	100	62.5	SF
10	B2G3	10/03/2022	24/04/2022	45	95	47.5	47.5	185	92.5	57.81	210	105	65.63	SF

Noting that, in (Table 4.4) above, three beams B1G1, B2G2, and B3G2 were not tested and replaced by additional beams B4G1, B4G2, and B5G2.

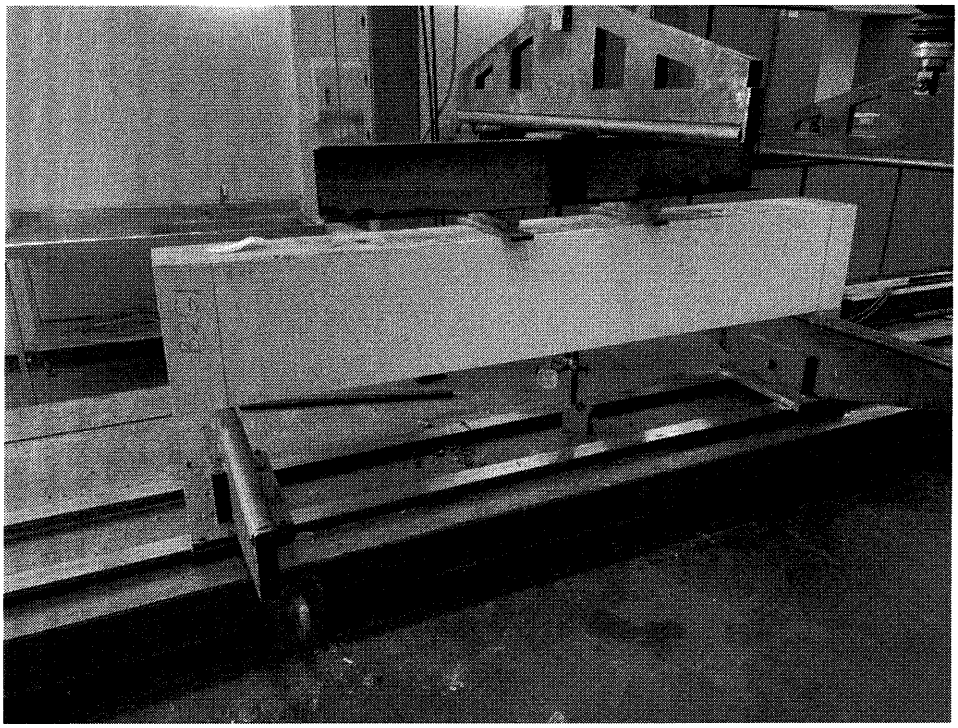


Figure 4.10 (a) B2G1/B3G3 beam before starting the testing



Figure 4.10 (b) Crack pattern and failure for B2G1/B3G3 beam

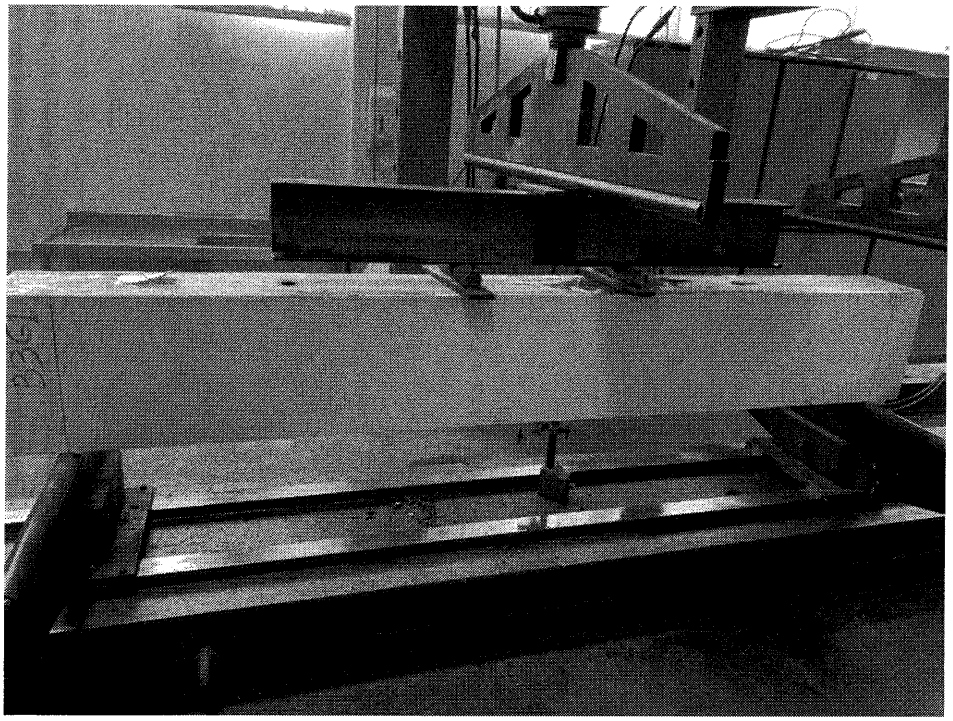


Figure 4.11 (a) B3G1 beam before starting the testing

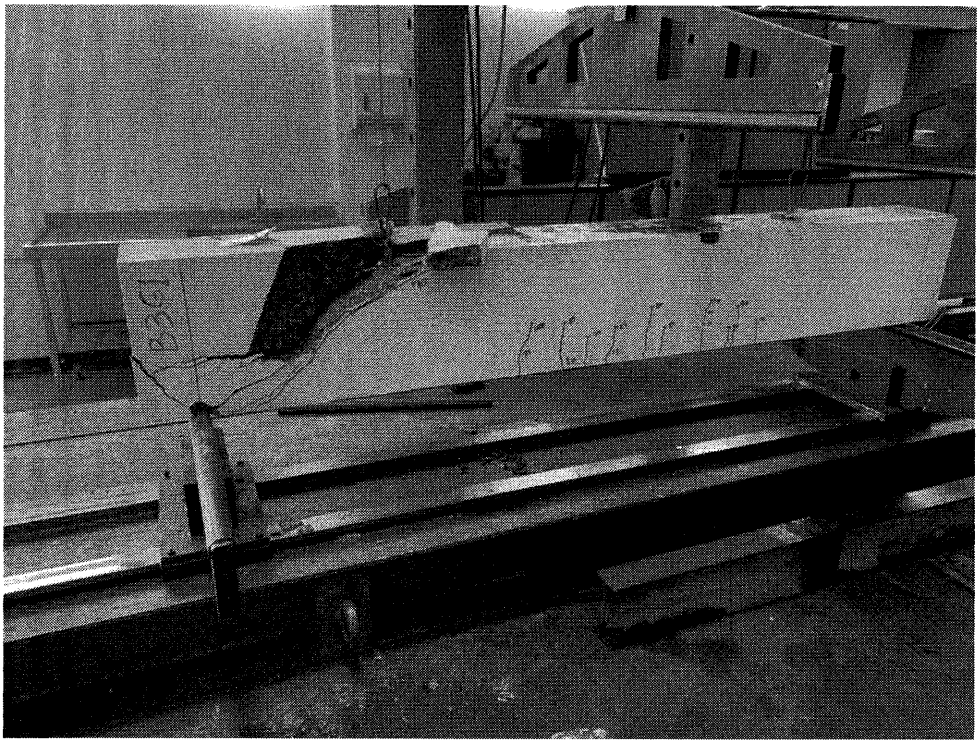


Figure 4.11 (b) Crack pattern and failure for B3G1 beam

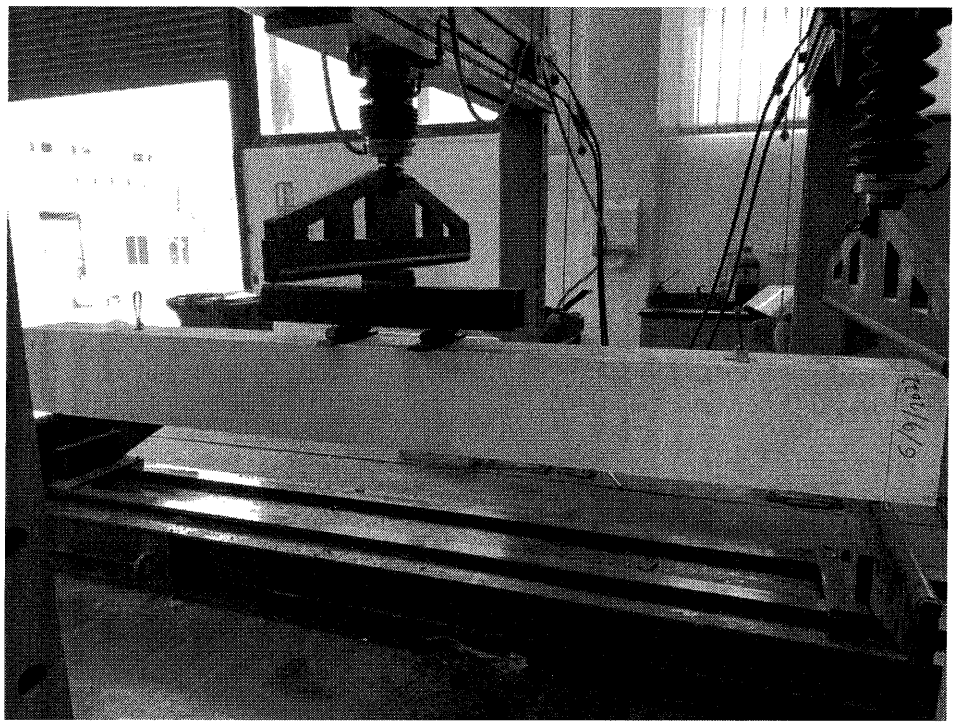


Figure 4.12 (a) B4G2 beam before starting the testing

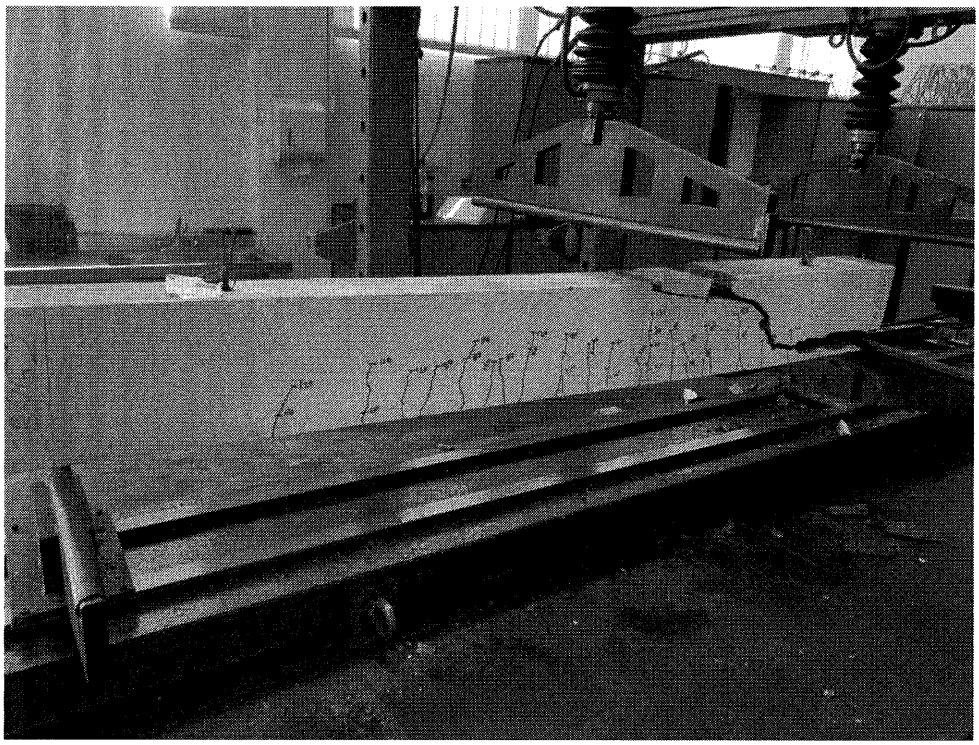


Figure 4.12 (b) Crack pattern and failure for B4G2 beam

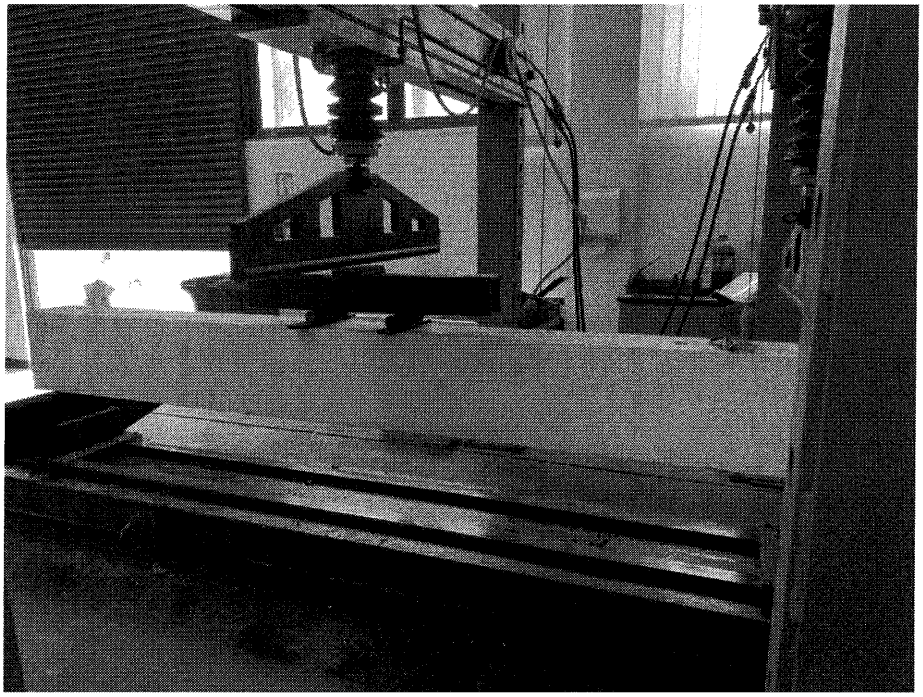


Figure 4.13 (a) B5G2 beam before starting the testing



Figure 4.13 (b) Crack pattern and failure for B5G2 beam



Figure 4.14 (a) B6G2/B4G1 beam before starting the testing



Figure 4.14 (b) Crack pattern and failure for B6G2/B4G1 beam



Figure 4.15 (a) B1G3 beam before starting the testing



Figure 4.15 (b) Crack pattern for B1G3 beam

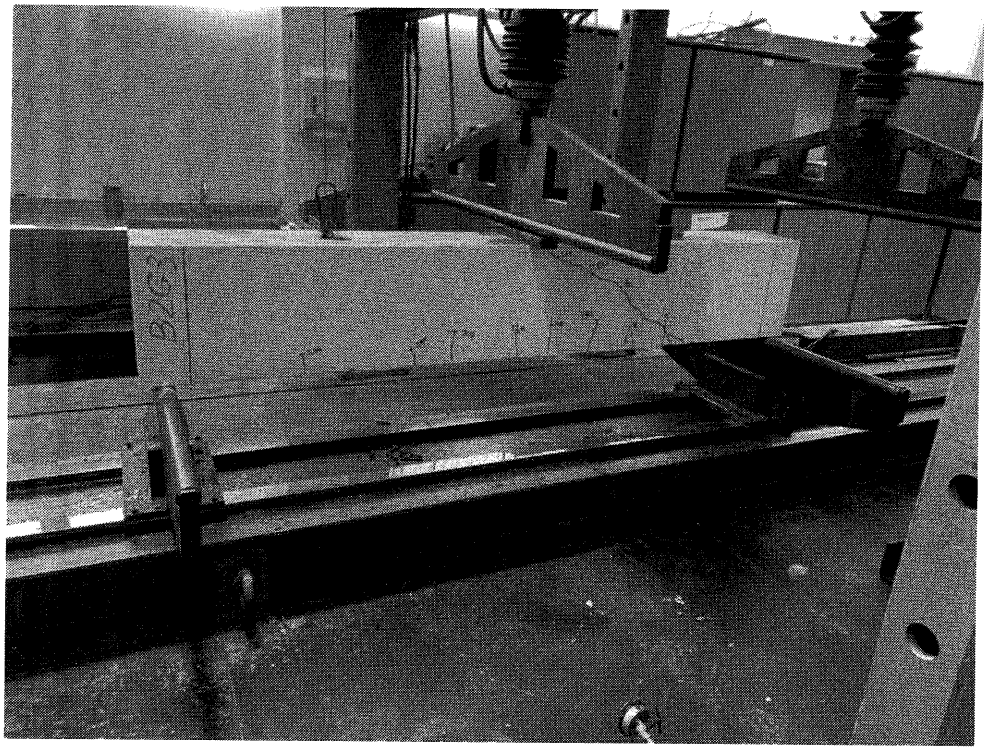


Figure 4.16 Crack pattern and failure for B2G3 beam

4.4 General Behavior

All beams were tested to failure in the same manner. The results of the tests conducted are shown in section 4.3.3. In the early stage of loading, the beams were free of cracks and acted as homogeneous composite members composed of concrete and steel. As the beam was loaded, flexural cracks formed in the tension face of the region with pure bending at the load level of about 35 to 40% of the ultimate capacity of each beam. Under further loading, additional flexural cracks formed in the central region and new ones were formed in the shear spans between loads and support. With further increase of load, flexural cracking increased, and inclined cracks developed at about 85% of the ultimate capacity of each beam with an angle of about 45◦, curving towards the loading points. After cracking, the behavior of the beam depended on a/d, ρ, and f_{cu}.

Failure took place at load greater than the load of which the initial inclined cracks occur.

4.5 Shear Load Vs Deflection Relationships

The vertical deflection of the tested beams was obtained from the dial-gage reading placed at the mid-span. The deflection at failure was determined from the roller reading, because the dial gages were taken off before the beam failed to prevent dial gage damage. The factors effecting the deflections were the magnitude and direction of load, condition of the restraint, section properties, amount and extent of flexural cracking, and span length.

In this study, the major variables that effect the load deflection relationship were the span-to-depth ratio a/d, flexural reinforcement ρ, and compressive strength of concrete f_{cu}. Figures 4.17. 4.18, and 4.19 show the load deflection curves for these variables in G1, G2, and G3. The load deflection curves of all the beams show that there are three stages for each beam curve. Pre-cracking stage, post-cracking stage, and failure stage, so that, the load deflection curves may be used to classify the failure type. In the pre-cracking stage, the deflection increases linearly with the loading because the strains in the steel and concrete are small and both materials are in elastic portion of their respective response. In the post-cracking stage, there is a change of slope in the load deflection curve due to cracking, but the deflection again increases linearly while increasing the load before failure. The third portion was exceedingly small because the failure occurs at this stage, the load deflection curves in this portion exhibit some change in slope. Table 4.4 presents beam deflections at various stages. The main variables that affected the load deflection behavior are discussed in the next sections.

4.5.1 Shear Span-to-Depth Ratio (a/d)

Load deflection curve for G1 which includes beams B2G1, B3G1, and B4G1 is shown in figure 4.17, where the beam without shear reinforcement has the same longitudinal steel ratio ρ, and compressive strength of concrete f_{cu} but with different shear span-to-depth ratio (a/d). The figure shows that the beam with lower a/d ratio has a stiffer response in terms of load deflection behavior. For the same load level as a/d ratio, the deflection increased. This is because the depth of the beam is constant, while the shear span increased as a/d ratio increased.

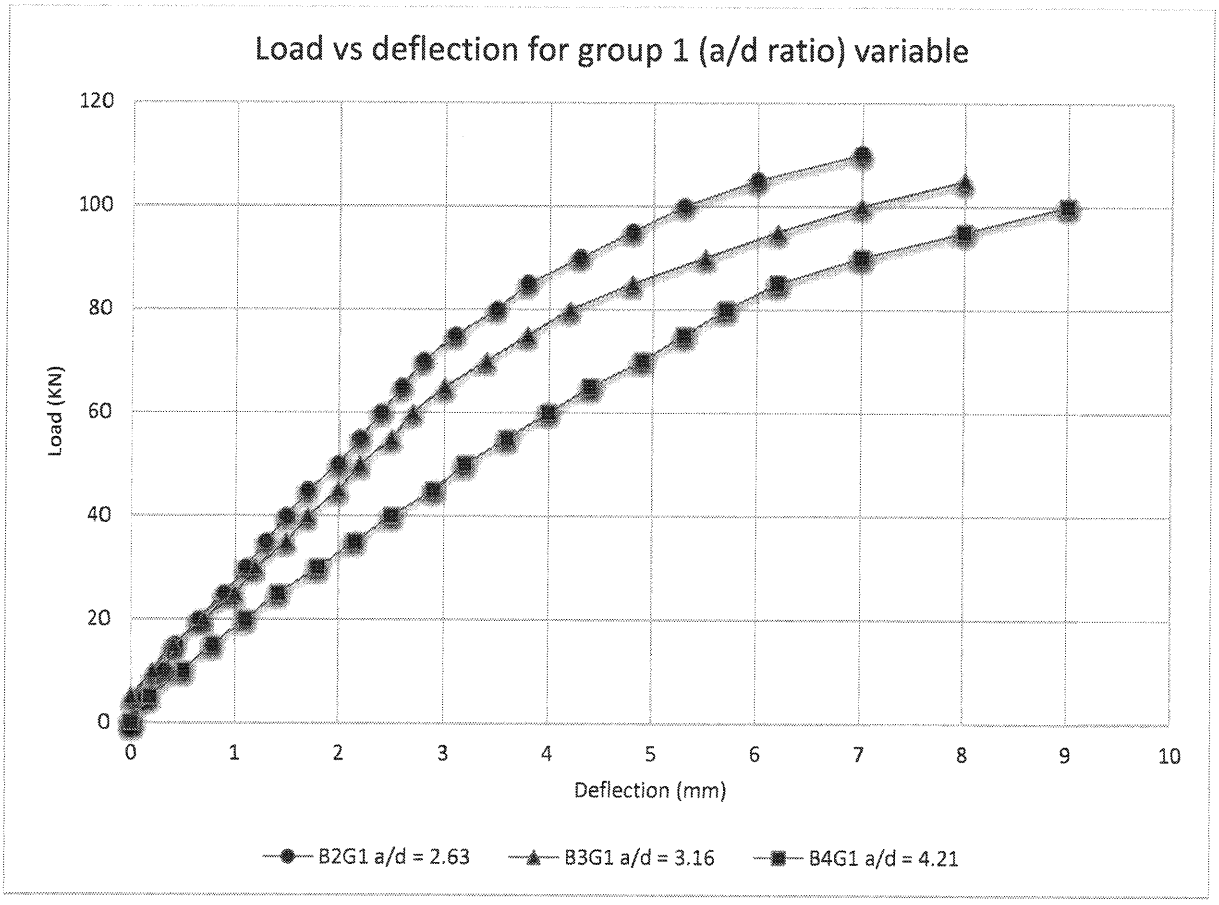


Figure 4.17 Load vs deflection curves for G1 beams (a/d ratio)

4.5.2 Longitudinal Steel Ratio (ρ)

Figure 4.18 shows the comparison of load deflection curves of G2 which include B4G2, B5G2, and B6G2 beams without shear reinforcement and the same f_{cu} and a/d ratio, but with different amount of longitudinal reinforcement ρ. The figure discloses that the beam with higher steel content has a stiffer response in terms of load deflection behavior. This trend is due to the larger effective moment of inertia and the large amount of tensile reinforcement. For the same load level, the deflection increased as the tensile steel ratio decreased as shown in the same figure.

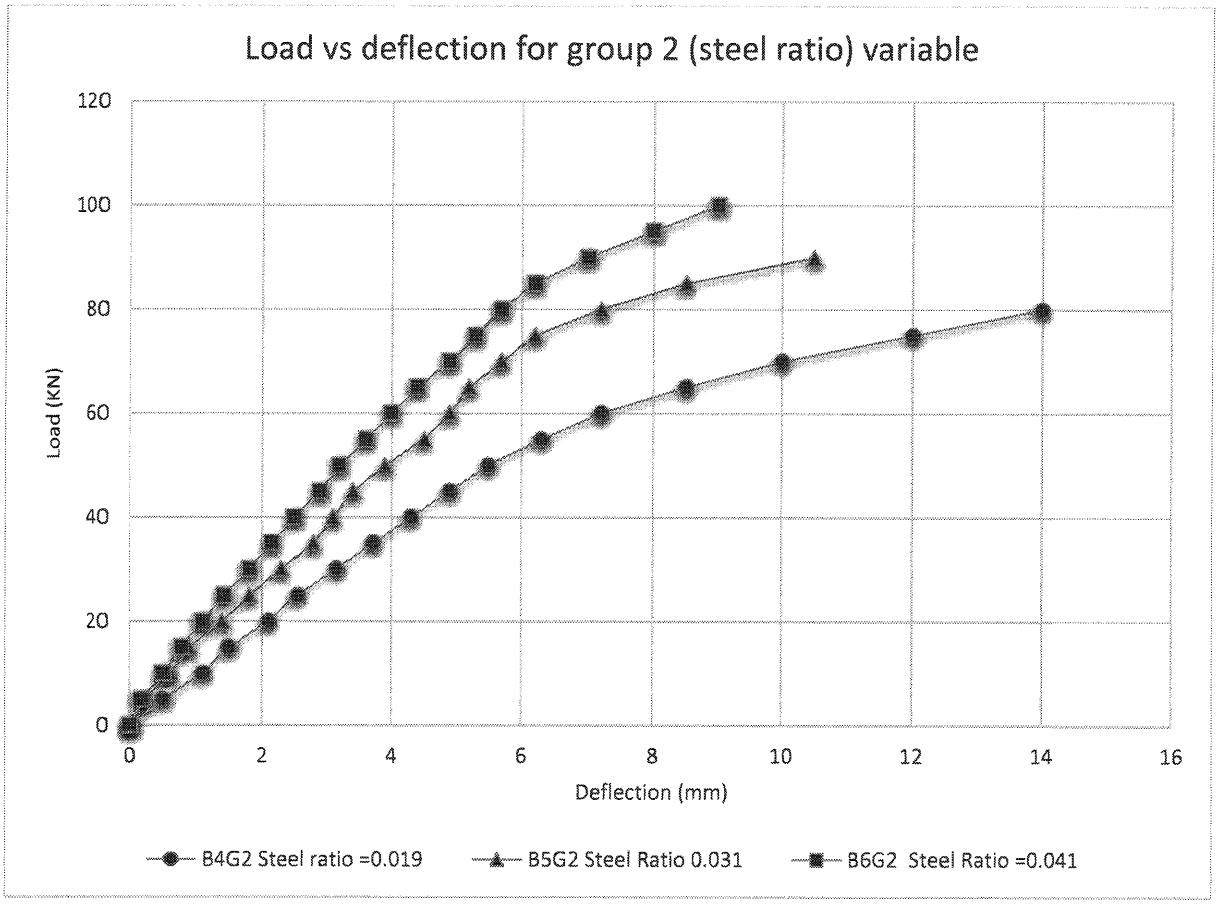


Figure 4.18 Load vs deflection curves for G2 beams (ρ flexural steel ratio)

4.5.3 Compressive Strength of Concrete (f_{cu})

Figure 4.19 shows the comparison of load deflection curves for the three beams in G3 which include B1G3, B2G3, and B3G3 beams without shear reinforcement and having the same longitudinal steel ratio ρ, and shear span-to-depth ratio a/d, but with different concrete strength. The figure shows that the beam with higher strength concrete suffers less deflection than the similar member with lower strength concrete at the same load level, which may be attributed to the fact that higher strength concrete beams are stiffer than lower strength concrete beams since the modulus of elasticity of concrete is larger for the higher strength concrete than for the lower.

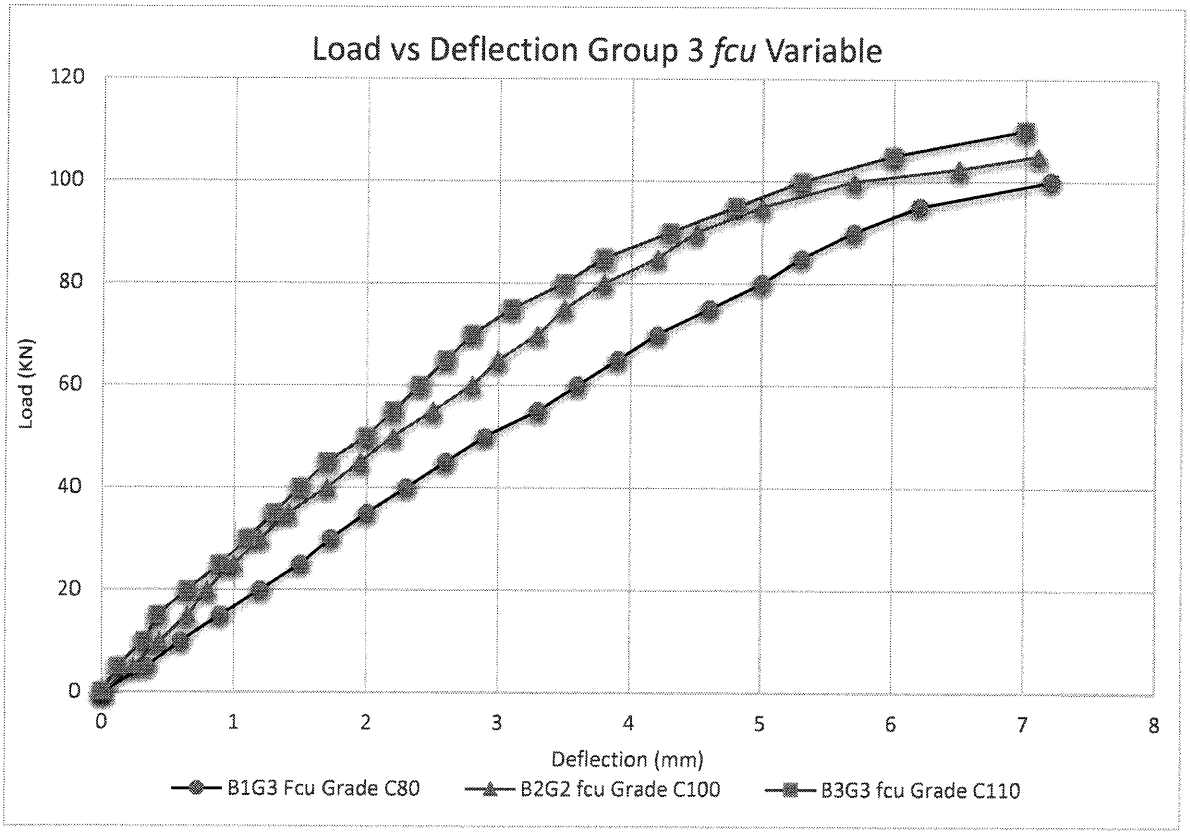


Figure 4.19 Load vs deflection curves for G3 beams (f_{cu} compressive strength of concrete)

Chapter 5

Finite Element Analysis

Chapter 5

Finite Element Analysis

5.1 General

The Finite Element Method (FEM) is a numerical technique used to perform a Finite Element Analysis (FEA) to solve problems of any given physical phenomenon in engineering and mathematical fields. FEM is used to model several mechanical applications including one of the most problematic areas, which is the structural analysis of reinforced concrete structures.

Reinforced concrete structures are employed in engineering. The applications and design procedures are based on experimental data. Further, FEM is utilized to ensure safety in the reinforced concrete structures.

The basic concept of FEM is to split the computational domain of the members into individual small patches and find local solutions to problems. FEM is a great tool which can be used to solve problems involving complicated geometry, loading, and material property.

This chapter's main objective is to compare the results of FEM solution with the experimental results in chapter 4.

5.2 History of Finite Element Analysis

Hrennikoff (1941) and Courant (1942) started to employ FEA in structural engineering in the 1950s when the solution of simultaneous equations is facilitated through digital computer (Farooq et al., 2014). FEM, however, was invented by Clough in his book The Finite Element Method in Plane Stress Analysis in the early 1960s. Turner et al. (1956) as cited by Pradhan et al. (2019) explained that finite

elements have been used in the analysis of aircraft structures and since then contributed to the development of FEM.

The development of the FEM is divided into four time periods: 1 (1941-1965) early years of FEM; 2 (1966-1991) golden age of FEM; 3 (1992-2017) large scale, industrial applications of FEM and development of material modeling, and 4 (2018) the state-of-the-art FEM technology for the current and future eras of FEM research (Liu et al., 2022).

5.3 Finite Element Analysis (FEA) Softwares

1. ABAQUS
2. Sap2000
3. LS-DYNA
4. Cosmos/M
5. Algor
6. Gt-Strudl
7. Marc
8. Mcs/Nastran
9. Nisa
10. Pro/Mechanica
11. Stardyne
12. Open Foam
13. SimScale
14. Autodesk/CFD

The most common software in finite element analysis is ANSYS mechanical software which is used in this research because it is available, easy to use, and gives

an exactly accurate and reliable simulation results that enable to solve complex structural engineering problems.

5.4 Modeling Using ANSYS

The behavior of reinforced concrete beams is studied by full-scale experimental investigations. The results are compared to theoretical calculations that estimate deflections. Finite element analysis, as used in structural engineering, determines the overall behavior of a structure by dividing it into several simple elements, each of which has well-defined mechanical and physical properties. ANSYS 2021/R2 is used in this study through structural statics.

5.4.1 Element Types Used

1. Solid element concrete

In modeling concrete, ANSYS uses an eight-node solid element named Solid65. The solid element has eight nodes, each with three degrees of freedom translations in the nodal x, y, and z directions (Kachlakev et al., 2001). In the model input data for concrete, ANSYS requires input data for material properties as follows: elastic modulus E_c, ultimate uniaxial compressive strength f_{cu}, and ultimate uniaxial tensile strength (modulus of rupture) f_r, poison's ratio ν (Dahmani et al., 2010).

2. Solid element reinforcement (Rebar)

For modeling steel, ANSYS provided an element named Link180, used to model steel reinforcement. Two nodes are required for this element with each node having three degrees of freedom and translations in the nodal x, y, and z directions (Kachlakev et al., 2001).

3. Solid element steel plates (Bearing)

For modeling of bearing, ANSYS provided an element named as, Solid45, with an eight-node solid element, which was used for the steel plates as support in the beam models.

5.4.2 Materials Properties

5.4.2.1 Concrete

The uniaxial compressive strength of concrete, referring to normal, high, and ultra-high strength, is higher as compared to tensile strength. The tensile strength of concrete is typically 8-15% of the compressive strength while the stress-strain curve of concrete is linearly elastic up to 30% of the maximum compressive strength. The stress increases gradually up to the maximum compressive strength (Shah et al., 1995).

Figures 5.1, 5.2, and 5.3 show the comparison between some stress strain curve models such as Comite Euro-International Du Beton CEB Code (1995), Hognestad (1951), Carreira and Chu et al. (1985), Wee et al. (1996), the concept of "Fuzzy set" as introduced by Zadeh (1976), and the experiments on high strength concrete 80 MPa and ultra-high strength concrete 100 MPa and 120 MPa (Kadir et al., 2012).

Due to non-availability of testing machine in the lab to get results showing the stress strain diagram for concrete, therefore literature results were used, because these relations needed in the ANSYS program. The fuzzy model was utilized in experimental data on the stress–strain behavior of high and ultra-high strength concrete in the ascending and descending curves. The fuzzy model through ANSYS is used in this research to obtain engineering data on concrete.

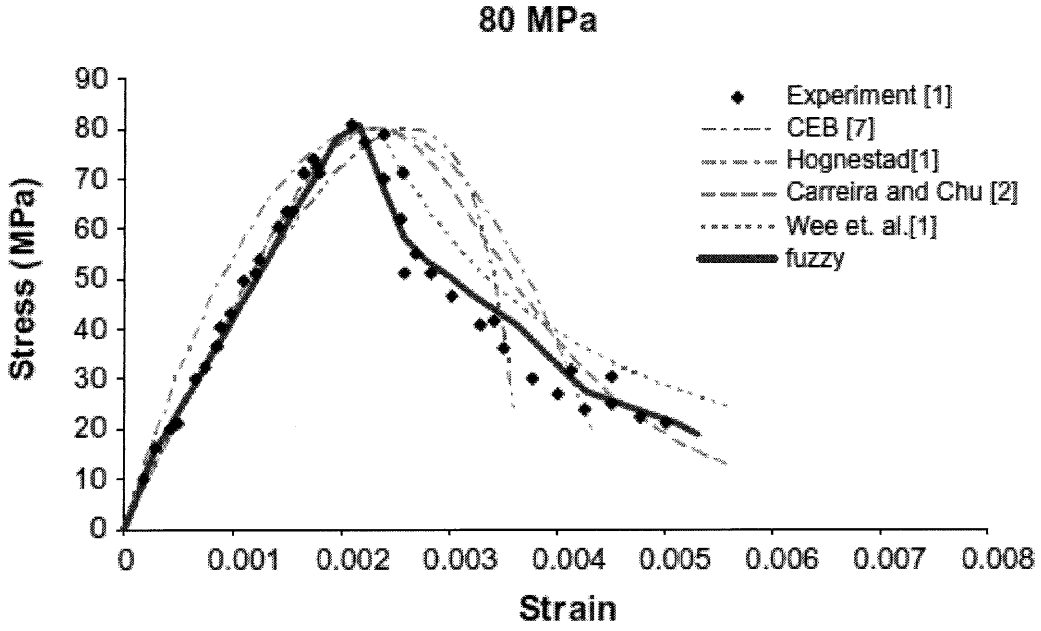


Figure 5.1 Different models comparison for concrete strength 80 MPa

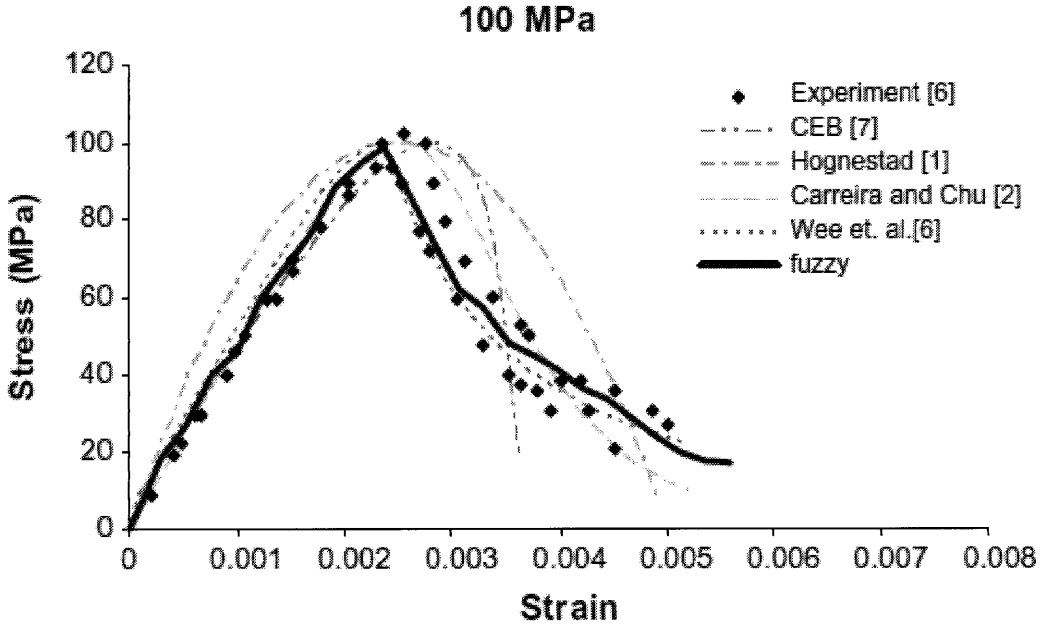


Figure 5.2 Different models comparison for concrete strength 100 MPa

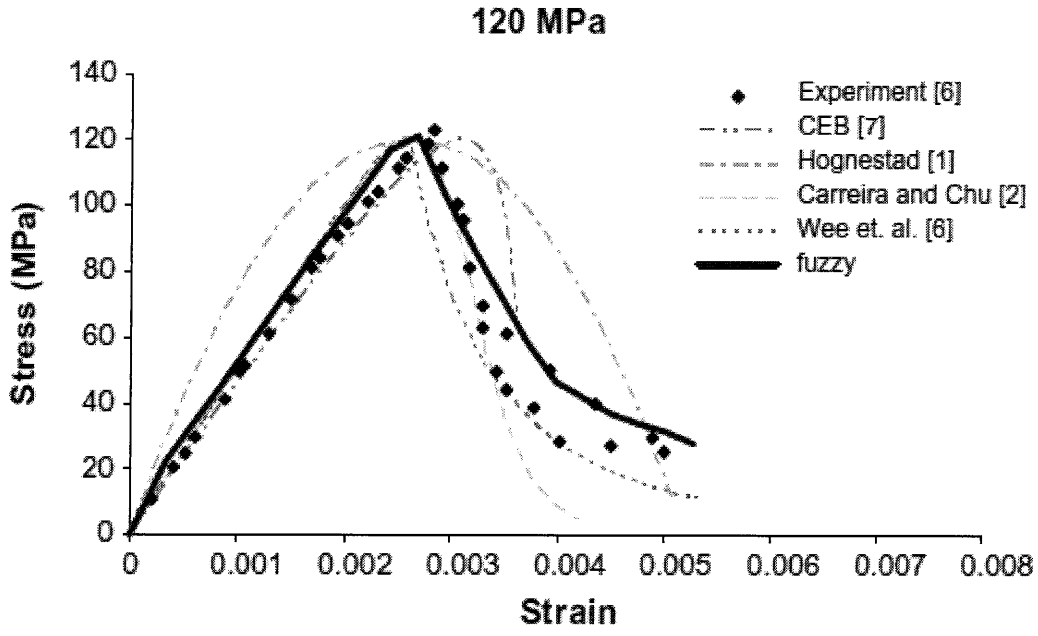


Figure 5.3 Different models comparison for concrete strength 120 MPa

FEM Input Data

ANSYS requires input data for material properties for concrete and these are as follows:

Elastic modulus (E_c)

Ultimate uniaxial compressive strength (f'_c)

Ultimate uniaxial tensile strength (modulus of rupture, f_r)

Poisson's ratio (ν)

Compressive uniaxial stress-strain relationship for concrete

Using Menetrey-Wiliam model and softening, the following parameters are needed:

Uniaxial compressive strength (f'_c)

Uniaxial tensile strength (modulus of rupture, f_r)

Biaxial compressive strength (f_{2c2})

Dilatancy angle (15 to 30 degrees)

Dilatancy angle describes inclination of the failure angle. Unlike in conventional concrete, it exhibits a nearly linear behavior up to almost 70% of the compressive strength (Solhmirzaei Roya et al., 2021).

Biaxial strain at uniaxial compressive strength (K_{cm})

Ultimate effective plastic strain in compression

Relative stress at start of nonlinear hardening

Residual compressive relative stress

Plastic strain limit in tension

Residual tensile relative stress

The secant modulus of elasticity for high-strength concrete is estimated by the equation (5.1) (ACI 363R-10 2010).

$$Ec = 3320\sqrt{f'_c} + 6900 \ldots . \ in\ Mpa \qquad (5.1)$$

The uniaxial cracking stress for high-strength concrete is assumed equal to the modulus of rapture obtained by the equation (5.2) (ACI 363R-10 (2010).

$$fr = 0.94\sqrt{f'_c} \ldots. \ in\ Mpa \qquad (5.2)$$

Both equations for 21 MPa < f'_c < 83 MPa

The relationships between modulus of rupture and compressive strength of UHPC shown in the formula below (Arafa., 2010)

$$fr = 0.98\sqrt{f'_c} \ldots. \ in\ Mpa \qquad (5.3)$$

UHPC achieves a mean modulus of rupture of 11.7 MPa at 28 days.

The Poisson's ratio of normal-density HSCs (with compressive strengths ranging from 8000 to 11,600 psi [55 to 80 MPa]) is between 0.20 and 0.28. (ACI 363R-10 (2010)).

Biaxial compressive strength f_{2c2} (per fib MC 2010 section 5.1.6 Commentary).

$$f2c2 = \left(1.2 - \left(\frac{f'_c}{1000}\right)\right) f'_c \ \ldots in\ Mpa \qquad (5.4)$$

Biaxial strain at uniaxial compressive strength K_{cm}

$$Kcm = \varepsilon cm - \left(\frac{f'_c}{Ec}\right) \ \ldots in\ Mpa \qquad (5.5)$$

Where εcm is the strain at peak compression from stress strain diagram

Concrete properties of all beams that need to use FEA software are shown in Table 5.1 depending on the experimental results, but for the strain depend on the above literatures. Figure 5.4 shows the concrete properties for one of the beams.

Table 5.1 Concrete properties to use in FEA

No.	Beam No.	f_{cu} (Mpa)	f'_c (Mpa)	E_c (MPa)	f_r (Mpa)	f_{2c2} (Mpa)	ε_{cm}	K_{cm}	ν
1	B2G1	112.80	90.24	38438.25	9.31	100.14	0.00290	0.00055	0.2
2	B3G1	111.40	89.12	38241.93	9.25	99.00	0.00290	0.00057	0.2
3	B4G1	106.50	85.20	37544.88	9.05	94.98	0.00290	0.00063	0.2
4	B4G2	107.50	86.00	37688.41	9.09	95.8	0.00290	0.00062	0.2
5	B5G2	106.60	85.28	37559.26	9.05	95.06	0.00290	0.00063	0.2
6	B6G2	106.50	85.20	37544.88	9.05	94.98	0.00290	0.00063	0.2
7	B1G3	76.80	61.44	32923.38	7.68	69.95	0.00230	0.00043	0.2
8	B2G3	102.20	81.76	36919.85	8.86	91.43	0.00250	0.00029	0.2
9	B3G3	112.80	90.24	38438.25	9.31	100.14	0.00290	0.00055	0.2

Assuming Linear softening parameters

Ultimate effective plastic strain in compression = 0.01

Relative stress at start of nonlinear hardening = 0.7

Residual compressive relative stress = 0.2

Plastic strain limit in tension = 0.01

Residual tensile relative stress =0.2

Dilatancy angle assumed for widespread practice = 30°

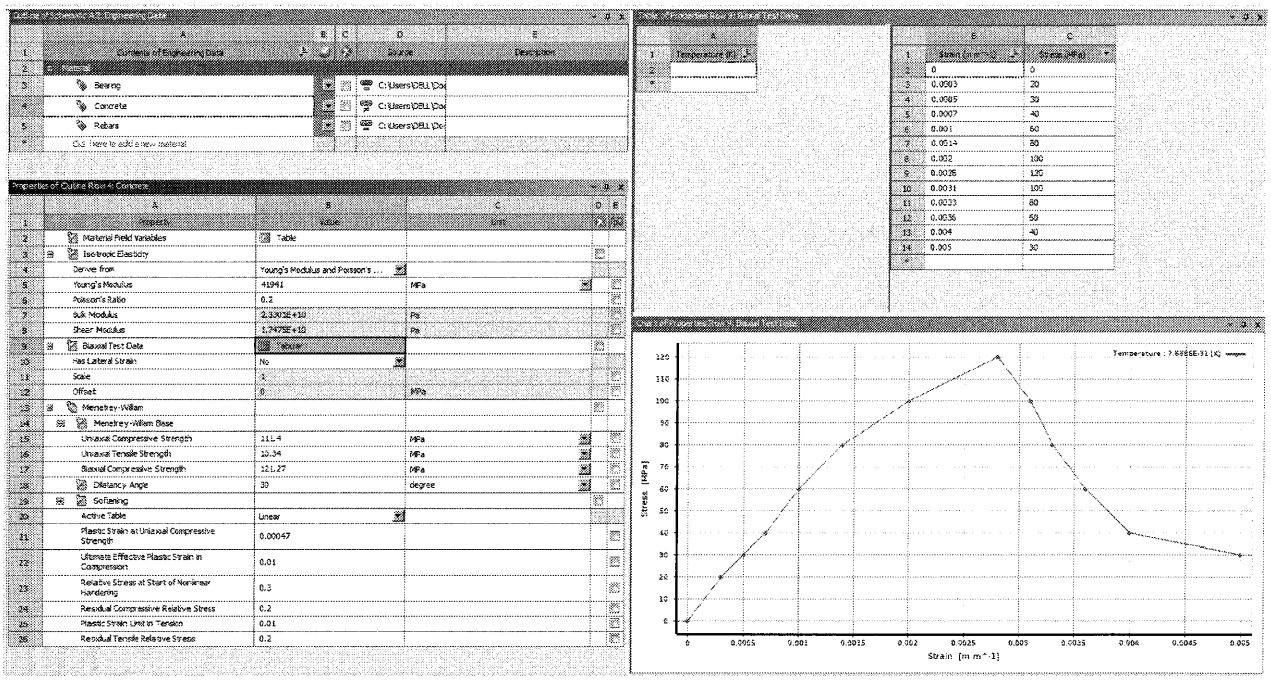


Figure 5.4 Properties for concrete used in ANSYS software

5.4.2.2 Flexural Steel Reinforcement

Steel reinforcement in the experimental beams was constructed with typical with f_y = 636.5 MPa (for 25 mm diameter bars) and 623.1 MPa (for 32 mm diameter bars) steel reinforcing bars as described in chapter 4. Properties, i.e., elastic modulus and yield stress, for the steel reinforcement used in this FEM study follow the design material properties used in the experiment.

Material properties for the steel reinforcement are as follows:

Elastic modulus, *Es* = 200,000 MPa

Yield stress, f_y = 636.5 MPa (for 25 mm diameter bars) and 623.1 MPa (for 32 mm diameter bars).

Poisson's ratio, ν = 0.3

Table 5.2 shows the steel properties of all beams that need to use FEA and figure 5.5 shows the properties for 25 mm dia bars.

Table 5.2 Steel properties to use in FEA

No.	Beam No.	f_y (Mpa)	E_s (Mpa)	ν	Rebar	A_s (mm^2)	ρ	ρ/ρ_b
1	B2G1	636.5	200000	0.3	4 φ 25	1964.29	0.041	1.088
2	B3G1	636.5	200000	0.3	4 φ 25	1964.29	0.041	1.102
3	B4G1	636.5	200000	0.3	4 φ 25	1964.29	0.041	1.048
4	B4G2	636.5	200000	0.3	2 φ 25	982.14	0.041	0.521
5	B5G2	623.1	200000	0.3	2 φ 32	1609.14	0.019	0.838
6	B6G2	636.5	200000	0.3	4 φ 25	1964.29	0.031	1.487
7	B1G3	636.5	200000	0.3	4 φ 25	1964.29	0.041	1.598
8	B2G3	636.5	200000	0.3	4 φ 25	1964.29	0.041	1.201
9	B3G3	636.5	200000	0.3	4 φ 25	1964.29	0.041	1.088

5.4.2.3 Steel Plates Bearing

Steel plates (50 mm x 25 mm) were used as bearing added at support locations in the finite element models (as in the actual beams) to provide a more even stress distribution in the support areas for the two-point loading supports. An elastic modulus equal to 69,000 MPa and Poisson's ratio of 0.5 were used for the plates. The steel plates were assumed to be linear elastic materials.

Noting that ANSYS define that the steel reinforcement bonding with concrete and work together as a composite called reinforced concrete, while the body of the steel plate were split from the whole body and not working with them.

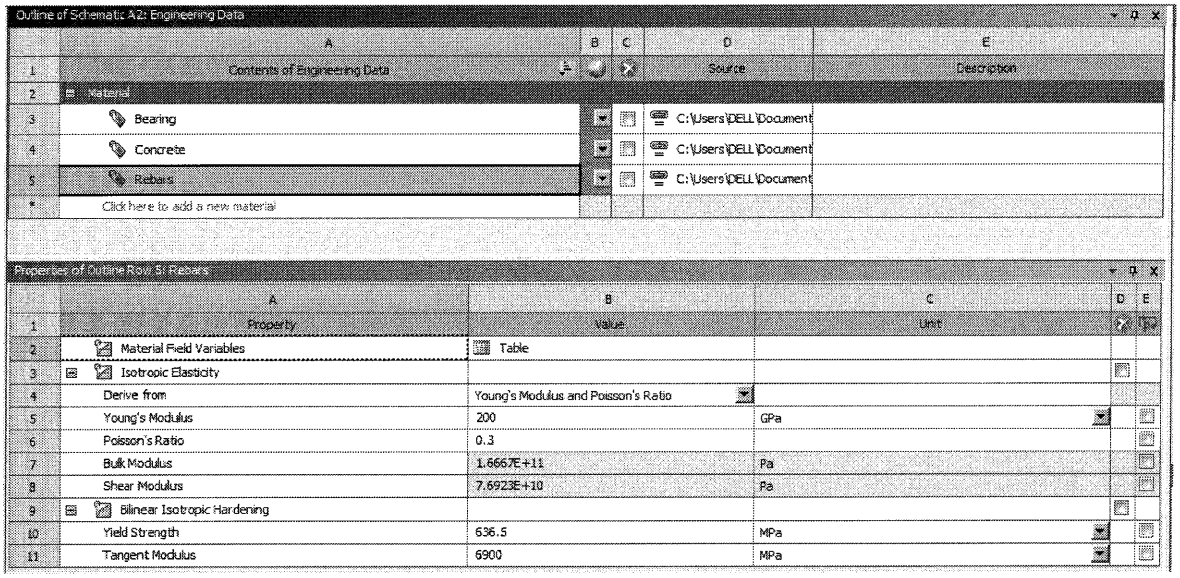


Figure 5.5 Properties for steel used in ANSYS software

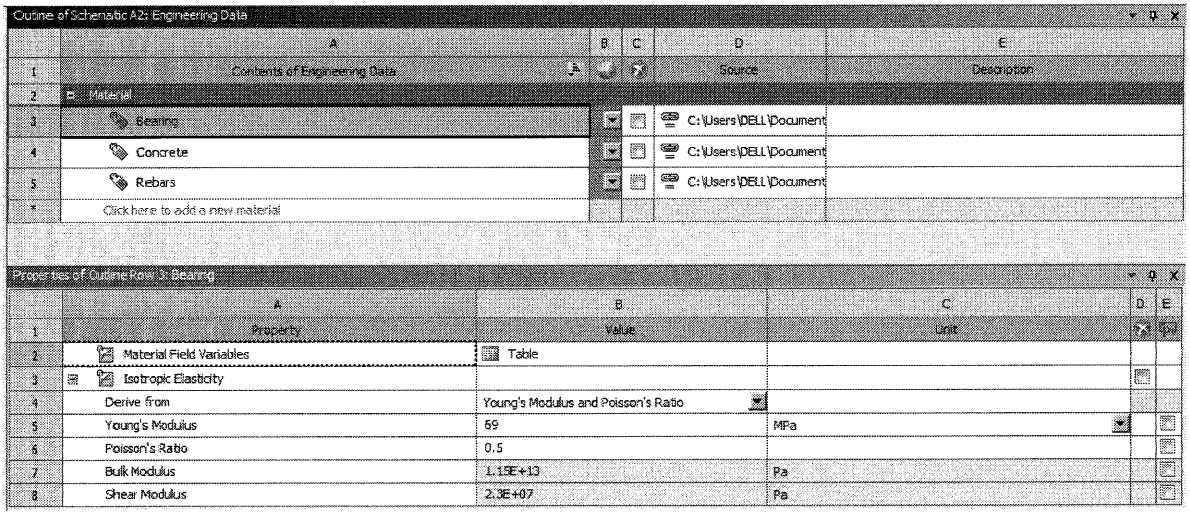


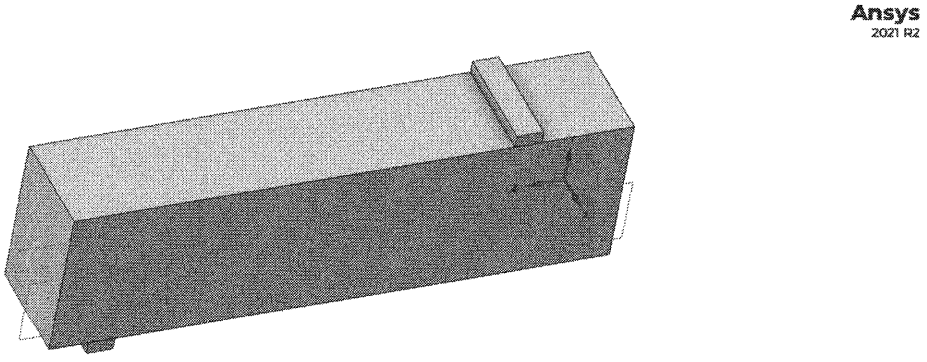
Figure 5.6 Properties for the steel plate used in ANSYS software

5.4.3 Geometry of the Beams

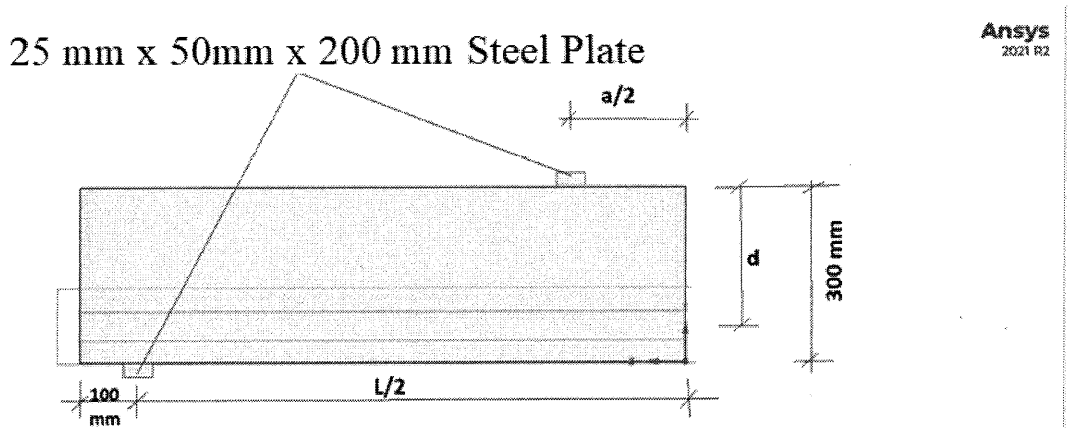
The dimensions of the full-size beams are 200 mm x 300 mm with length depending on the group ranging between 1.85 m to 2.81m. The clear span between the two supports as shown in table 5.3 ranges between 1.65 m to 2.61m. The distance between the two-point load is 400 mm. Figure 5.7 shows the typical sketch of half of one beam, taking advantage of the symmetry used for modeling. This approach reduced the computational time and computer disk space requirements significantly.

Table 5.3 Beams dimensions

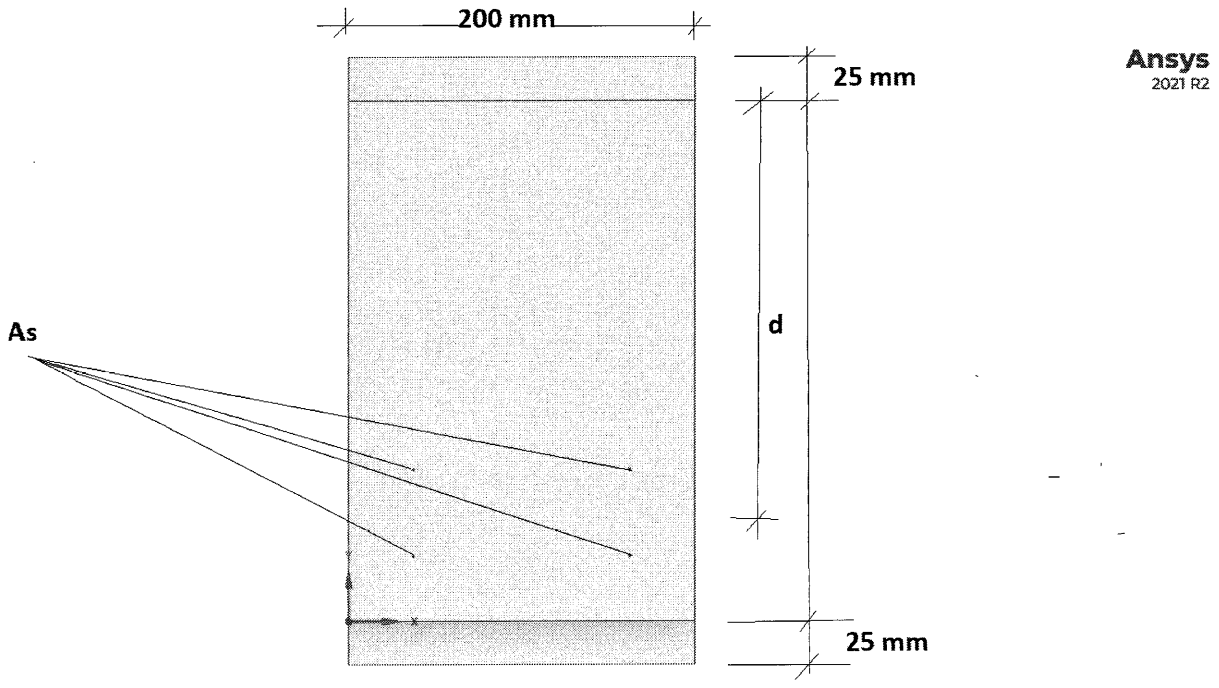
No.	Beam No.	b (mm)	h (mm)	d (mm)	L_{Clear} (mm)	L_{Total} (mm)	a (mm)
1	B2G1	200	300	237.5	1650	1850	625
2	B3G1	200	300	237.5	1900	2100	750
3	B4G1	200	300	237.5	2400	2600	1000
4	B4G2	200	300	262.5	2610	2810	1105
5	B5G2	200	300	259	2580	2780	1090
6	B6G2	200	300	237.5	2400	2600	1000
7	B1G3	200	300	237.5	1650	1850	625
8	B2G3	200	300	237.5	1650	1850	625
9	B3G3	200	300	237.5	1650	1850	625



(a) Isometric view



(b) Right side view

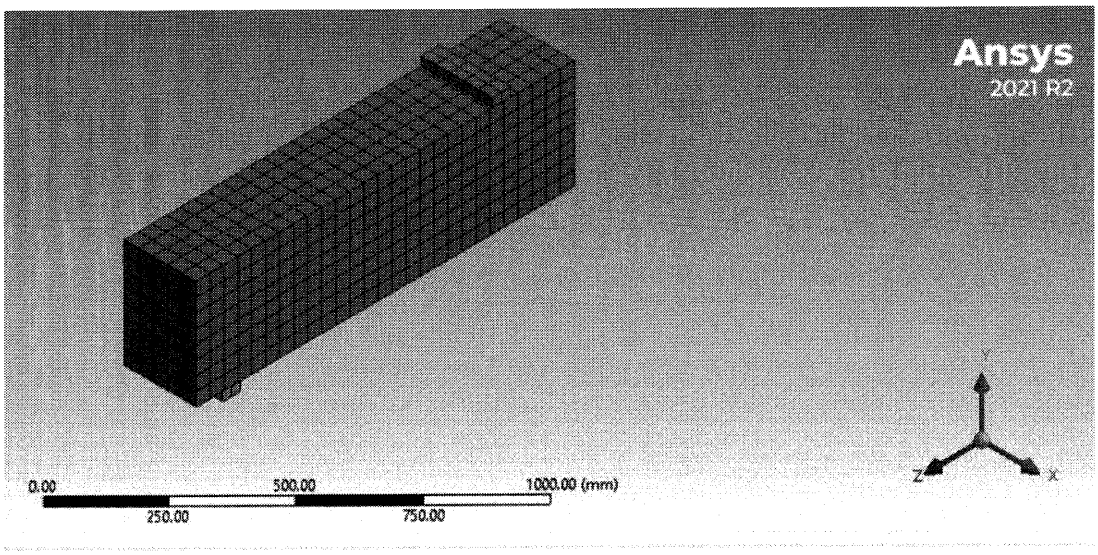


(b) front side view

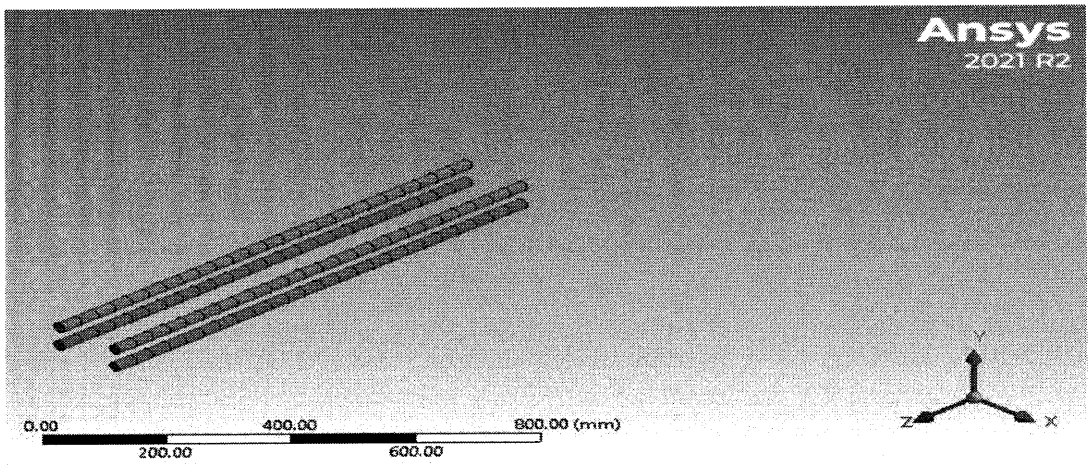
Figure 5.7 Sketch for typical half beam, (a) isometric view, (b) right side view, and (c) front side view

5.4.4 Meshing for the Model

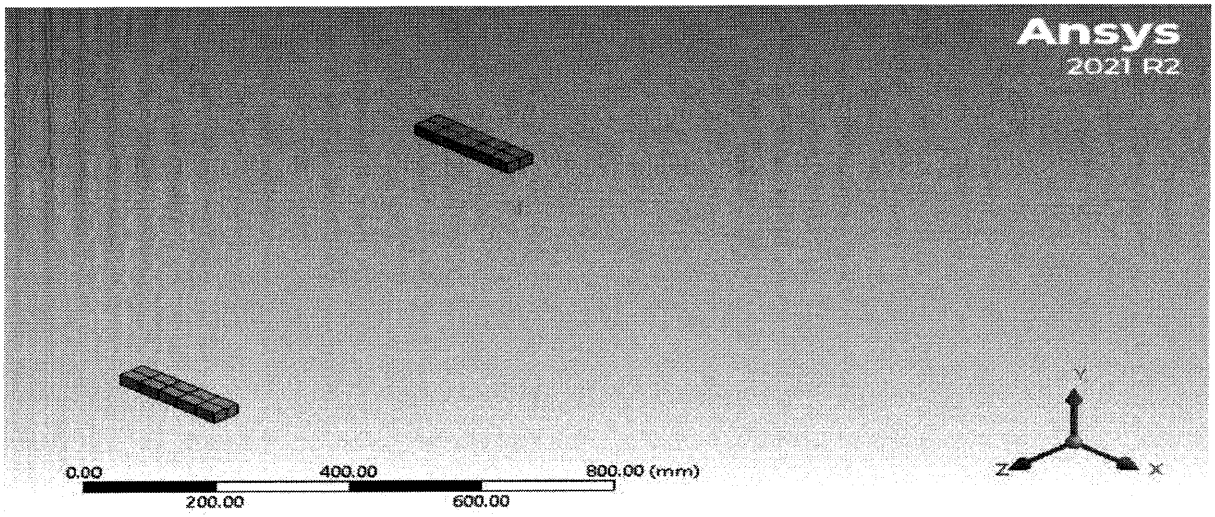
Finite Element Analysis (FEA) requires meshing of the model, and the model is divided into several small elements, linear or quadratic or program control. If linear, different shapes may be used such as square, rectangle, triangle, and others. In this study, square elements are used with an element size of 30 mm, 40 mm, and 45 mm. Figure 5.8 shows the meshing for typical half of the beam.



(a) Meshing for typical half beam



(b) Meshing for steel bars

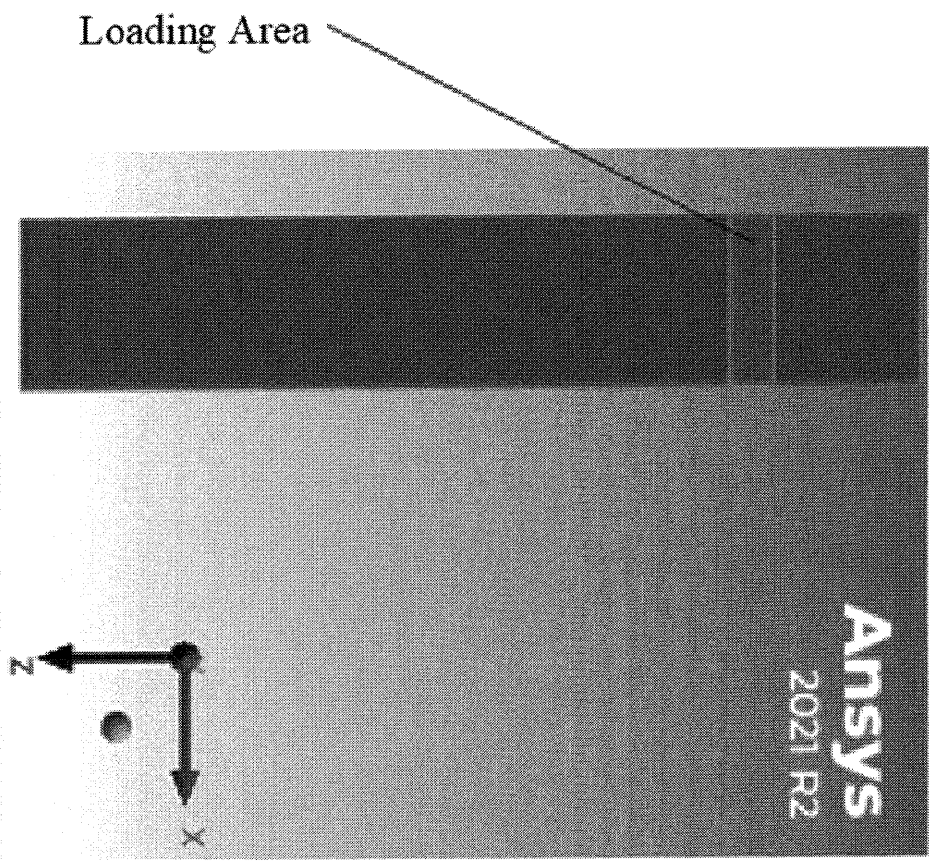


(c) Meshing for the steel plates

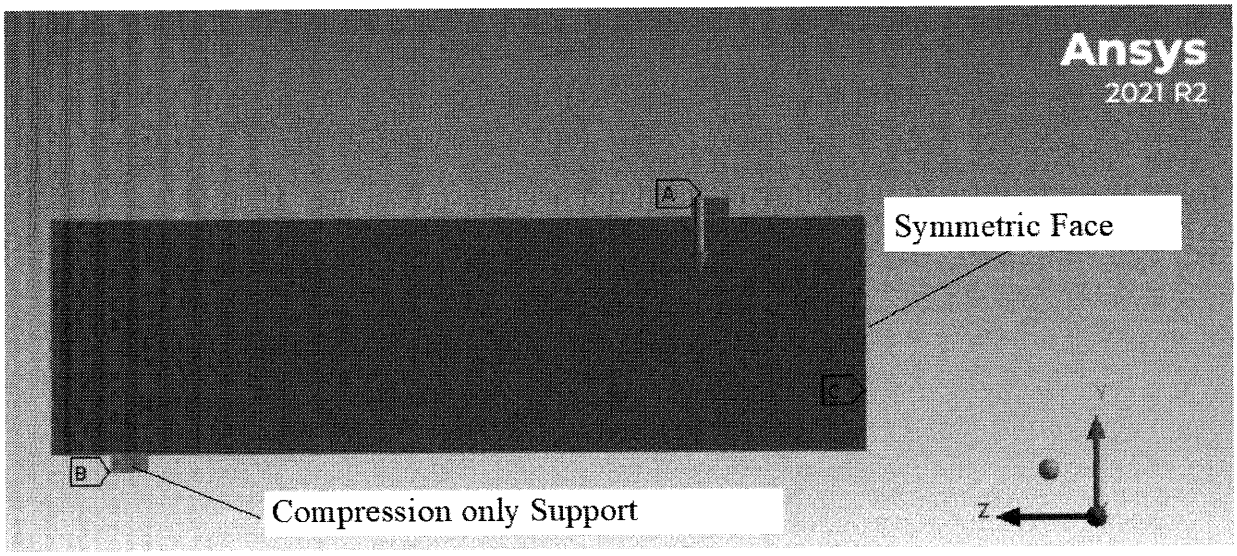
Figure 5.8 (a) Meshing for typical half beam, (b) Meshing for steel bars, and (c) Meshing for the steel plates

5.4.5 Loading and Boundary Conditions for the Beam

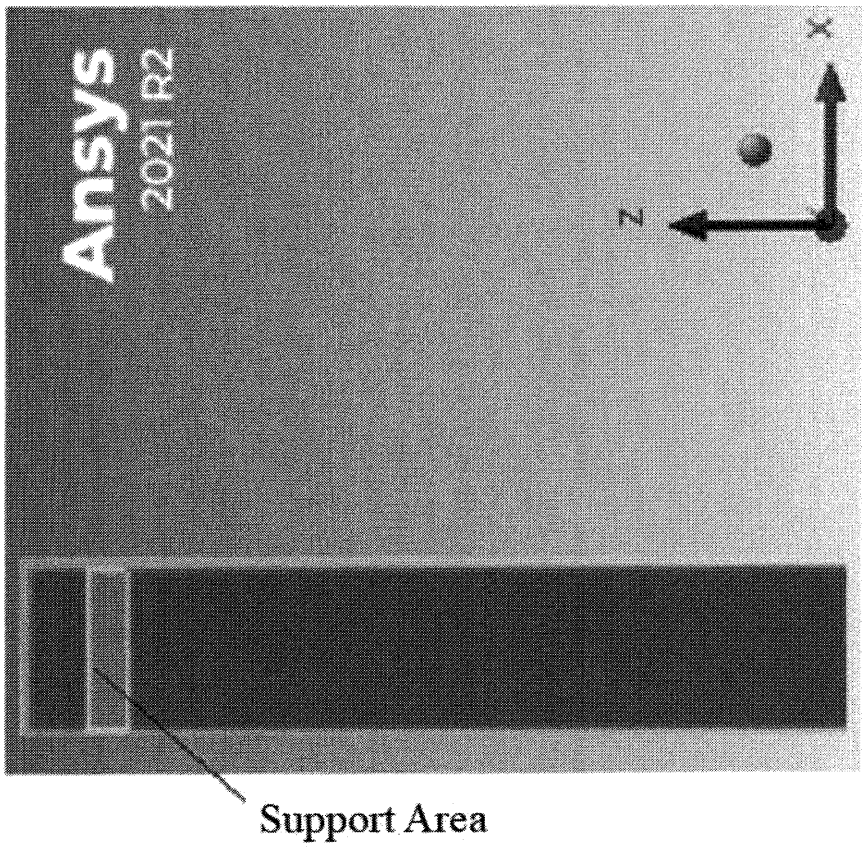
All full-size beams were tested, as shown in figure 5.9. The finite element models were loaded at the same locations as the full-size beams in the experiment. A 25mm thick steel plate was added at the support location to avoid stress concentration problems. This provided an even more stressful distribution over the support area.



(a) Top view



(b) Side view



(c) Bottom view

Figure 5.9 Typical loading and support locations (a) top view, (b) side view, and (c) bottom view

5.4.6 FE Analysis Setting

The ANSYS program predicts, and controls load step sizes for the non-linear analysis, which means that there is an automatic time stepping. Figure 5.10 presents the FE analysis setting of this study. Only initial sub-steps set by 200, minimum sub-step by 200 and maximum sub-step by 10000, the rest of other setting is left for program control.

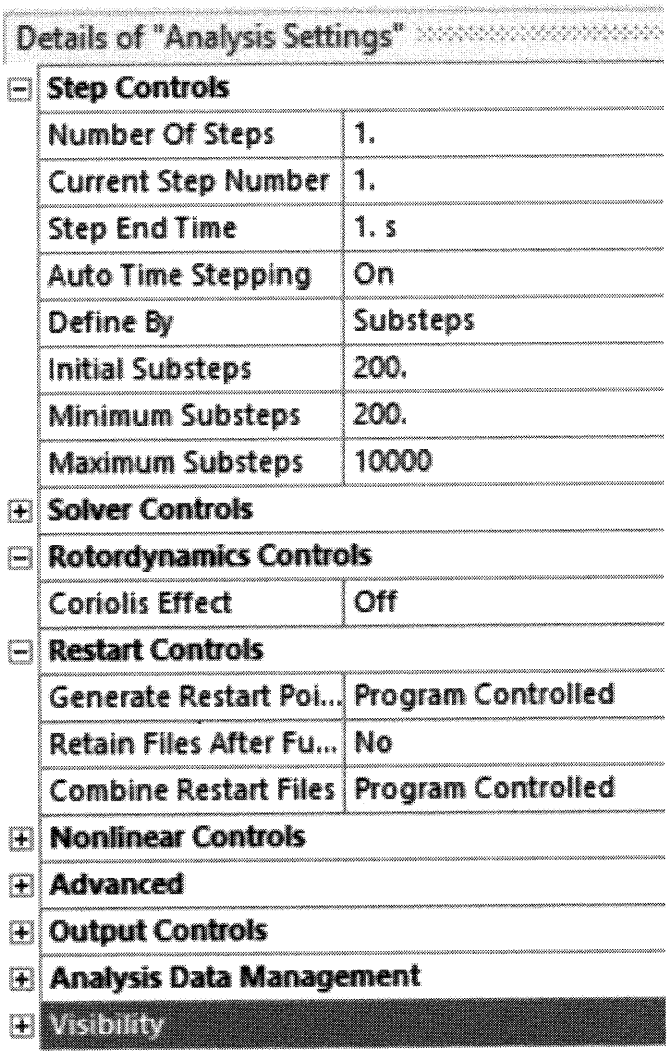


Figure 5.10 Analysis setting details

Noting that failure load was noted by ANSYS after many trial done, so that the program will not run after this load.

5.5 Comparison the Model Results with Literature Results

To evaluate the results of the model in this research, experimental results or laboratory results from various research and literature were considered for comparison with the data obtained from experiments.

Kodur et al. (2018), prepared an experimental analysis of flexural and shear resistance of Ultra-High-Performance Fiber Reinforced Concrete (UHPFRC) beams without stirrups. Cross section detail and layout of UHPFRC beam, U-B5 is shown in figure 5.11 where all dimensions are in mm.

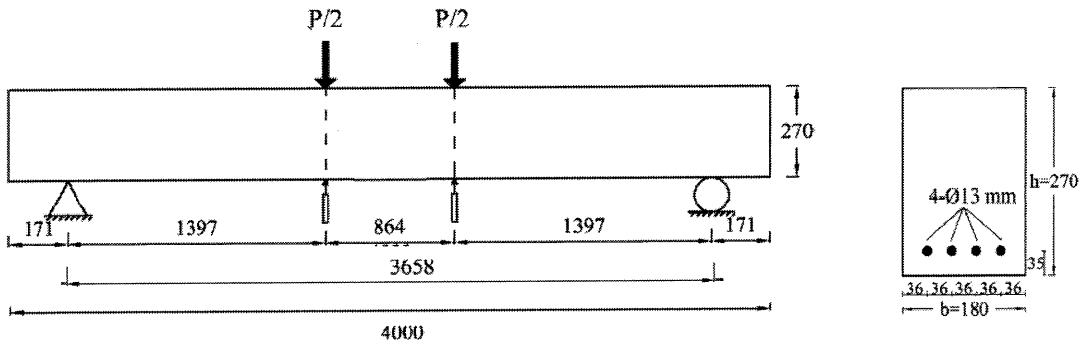


Figure 5.11 U-B5 beam cross section detail and layout of UHPFRC (Kodur et al., 2018)

Materials data used for this beam

Ultimate uniaxial compressive strength of concrete f'_c = 167 MPa

Modulus of elasticity for concrete E_c. = 40615 MPa,

Yield strength for reinforcing steel f_y = 436 Mpa

Modulus of elasticity for concrete E_s = 210000 MPa,

Flexural reinforcement ratio ρ = 0.012

The maximum deflection in the experimental load deflection curve is 70 mm at maximum load of 123. By using the displacement base of 70 mm, the model does not work, again by using the load base of 123 KN does not work. The model only

run at 55 mm deflection and that gives a maximum load of 105.5 KN and a maximum deflection of 57.85 mm. The results are shown in figure 5.12.

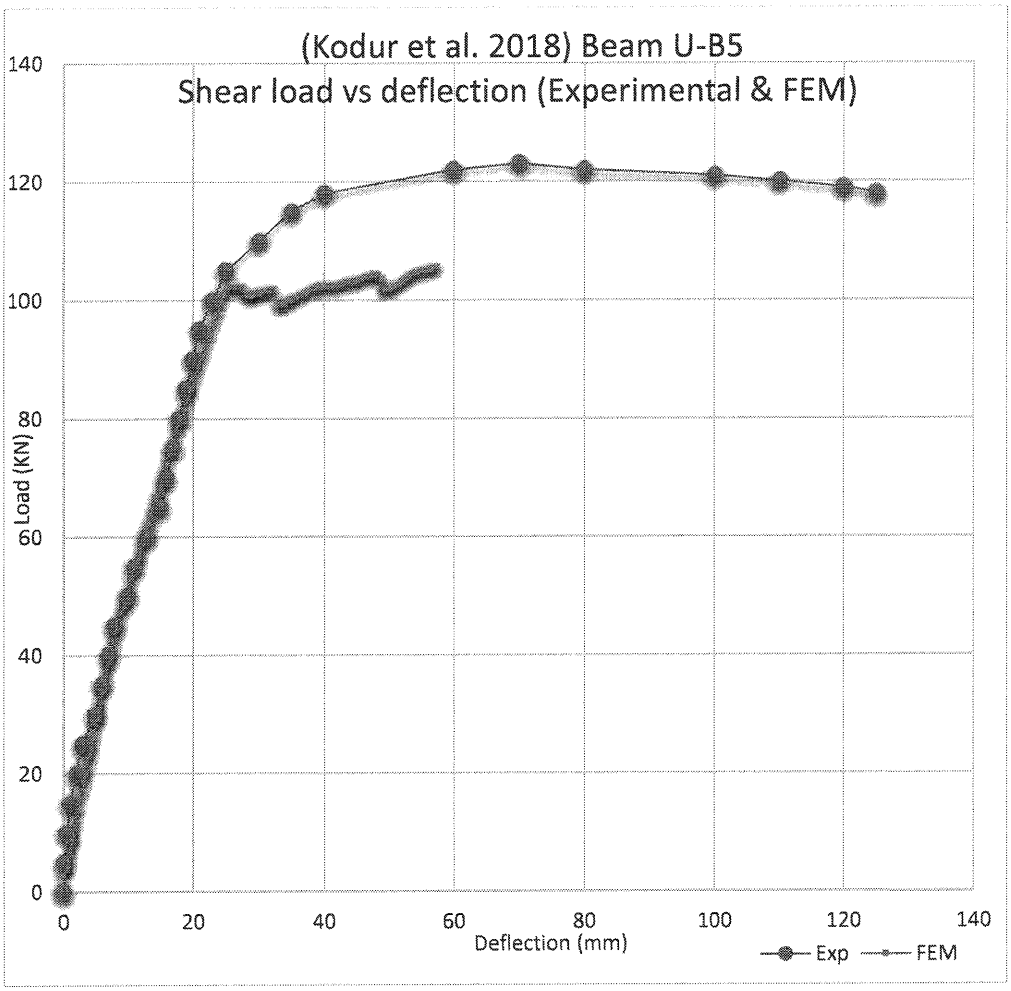


Figure 5.12 Comparison of load deflection curve using ANSYS and experimental (Kodur et al., 2018)

It can be seen from the above load-deflection behavior in figure 5.12 that the prediction from the numerical model was in line with the measured data in the linear part, elastic stage until yielding in steel reinforcing bars, but FEA shows lower results during plastic deformation stage until failure.

Solhmirzaei et al. (2021) worked at the same beam U-B5 using FEA ABAQUS software as shown in figure 5.13 below.

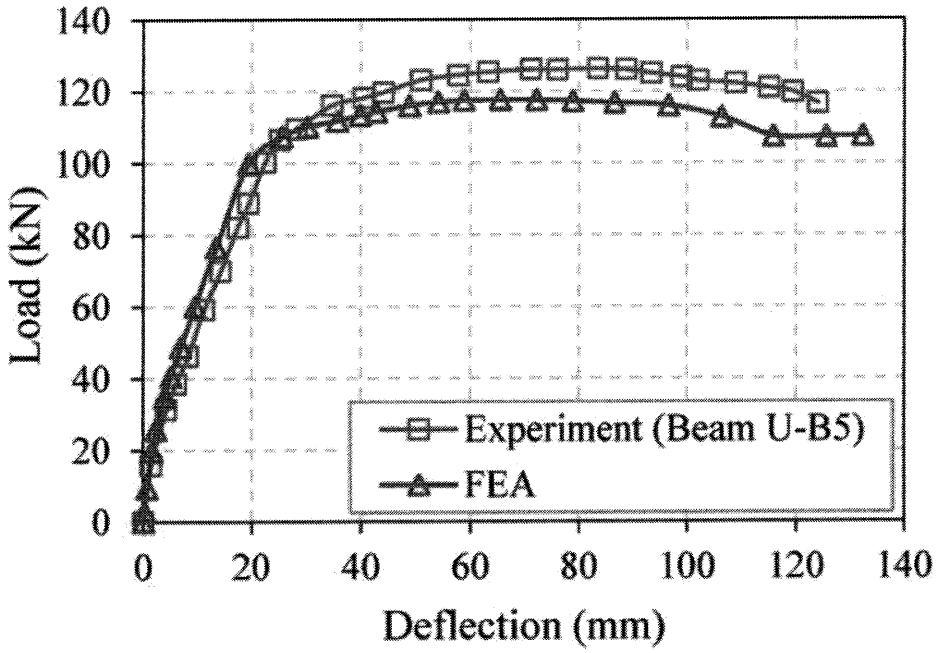


Figure 5.13 Load vs deflection curve comparison using ABAQUS and experimental (Solhmirzaei et al., 2021)

The above load-deflection behavior in figure 5.13 shows that the prediction from the numerical model compares well with the measured data in various stages: elastic stage till tensile cracking initiation, post-cracking stage with the propagation of cracks, yielding in steel reinforcing bars, and plastic deformation stage including softening until failure.

The experimental study was conducted by Wang et al. (2018) on the shear performance of reinforced ultra-high-performance concrete rectangular section beams. Cross section detail and layout of beam L0 is shown in figure 5.14 where all the dimensions are in mm.

Materials data used for this beam

Ultimate uniaxial compressive strength of concrete f'_c = 127.1 MPa

Modulus of elasticity for concrete E_c. = 41 MPa

Yield strength for reinforcing steel f_y = 522 Mpa

Modulus of elasticity for concrete E_s = 210000 MPa

Flexural reinforcement ratio ρ = 0.0658

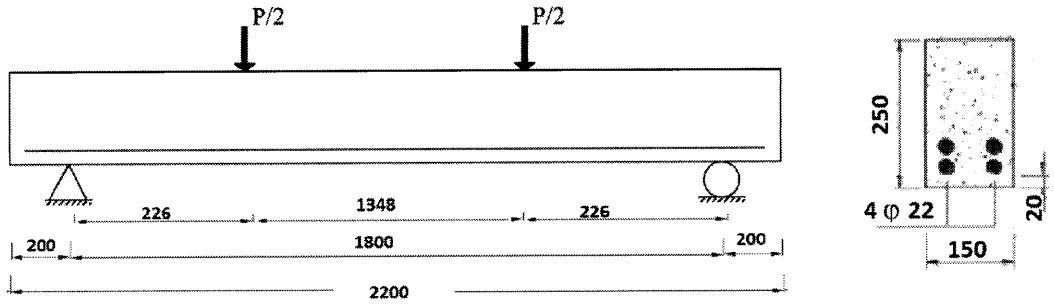


Figure 5.14 Cross section detail and layout of Wang beam L0 (Wang et al., 2018)

The experimental results against the results of this model through ANSYS are presented in figure 5.15.

The maximum deflection in the experimental load deflection curve is 20 mm. By using this magnitude in Ansys, it shows that the model does not work even when the number of steps decrease to 100, still, the model does not work. The model only works at 17 mm deflection with a mesh size of 40 mm and that gives a maximum load of 209.5 KN and a maximum deflection of 1.84 mm. The results are shown in figure 5.15.

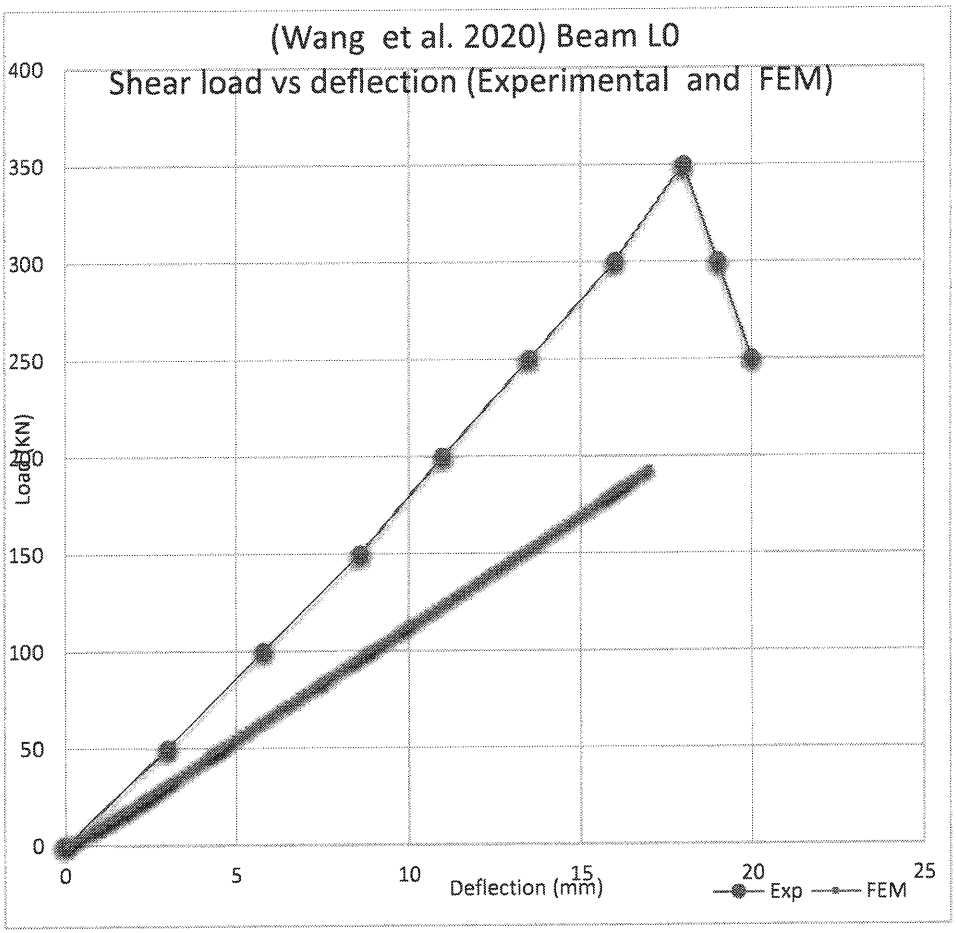


Figure 5.15 Comparison of load deflection curve using ANSYS and experiment (Wang et al., 2018)

As a result of the experiment, the above load-deflection behavior in figure 5.15 shows a linear relationship up to 17 mm deflection in the elastic range then inelastic up to failure at 20 mm deflection. The result of the numerical model shows a linear relationship lower than the experimental results.

5.6 Final Setting up of the Model

Before running the program, some sensitive items were finalized such as mesh size and step control.

5.6.1 Mesh Size

Linear element order was selected and to finalize the element mesh size, three sizes are compared (30 mm, 40 mm, and 45 mm) on the same beam. The comparison of the results of load deflection related to the mesh size is shown in figure 5.16.

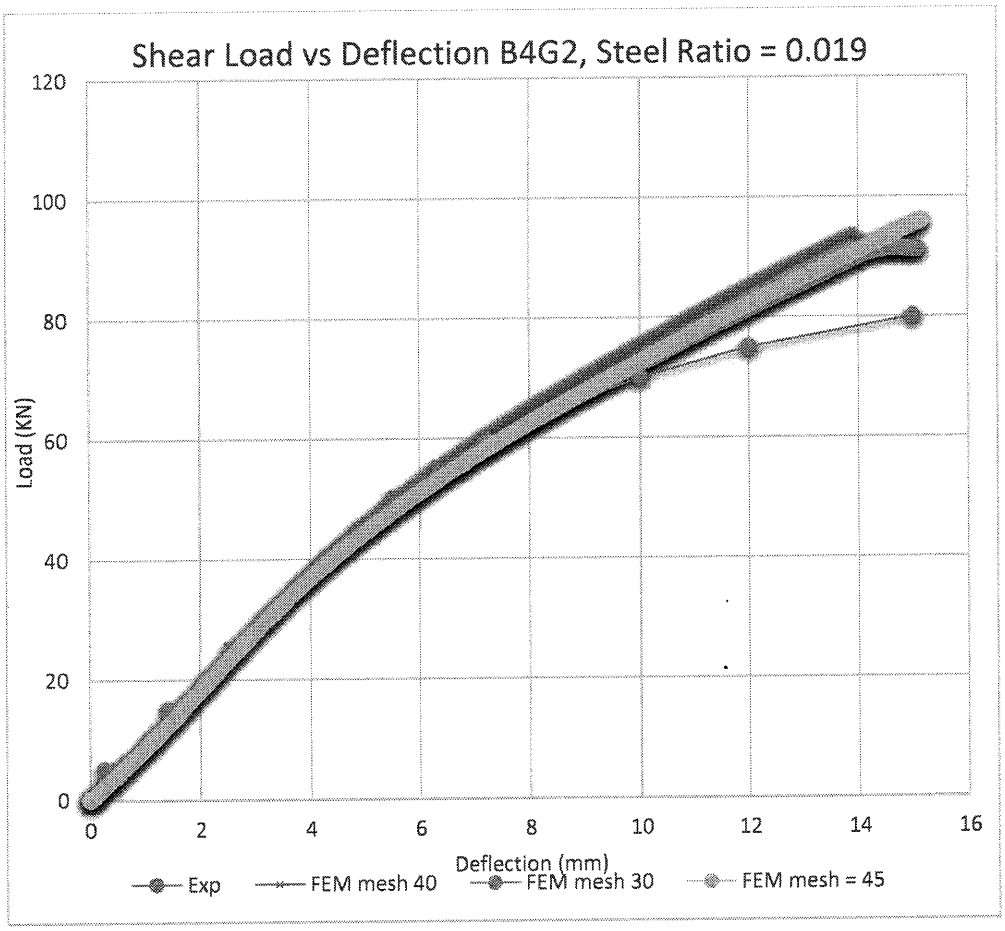


Figure 5.16 Mesh sizes comparison

Table 5.4 Mesh size effect on Δ_u of mid span deflection of B4G2 beam

No.	Mesh size (mm)	Experimental Δ_u (mm)	Numerically Δ_u (mm)	$\frac{\text{Exp} - \text{Num}}{\text{Exp}}$
1	30	15	15.588	-3.92%
2	40	15	15.588	-3.92%
3	45	15	15.575	-3.83%

Figure 5.16 and table 5.4 show that the results are remarkably close to each other in the three cases, except at the end as shown in the graph. Before the ultimate load occurs, there is a slight difference of 30 mm and 40 mm in the results and 40 mm is considered the best which does not require a longer time during the operation of the program unlike 30 mm.

5.6.2 Step Control

To finalize the sub-steps that complete the iteration process, three iterations are selected as follows:

1- Initial sub steps = 100, minimum sub steps =100, and maximum sub steps = 5000
2- Initial sub steps = 200, minimum sub steps =200, and maximum sub steps = 10000
3- Initial sub steps = 300, minimum sub steps =300, and maximum sub steps = 20000

Comparison of the results of load deflection related to the sub-steps are shown in figure 5.17. Figure 5.17 indicates that the results are remarkably close to each other in the three cases, except at the end. Before the ultimate load occurs, there is a slight difference, and 200 steps mm is the best which does not require a longer time during the operation of the program unlike 300 steps.

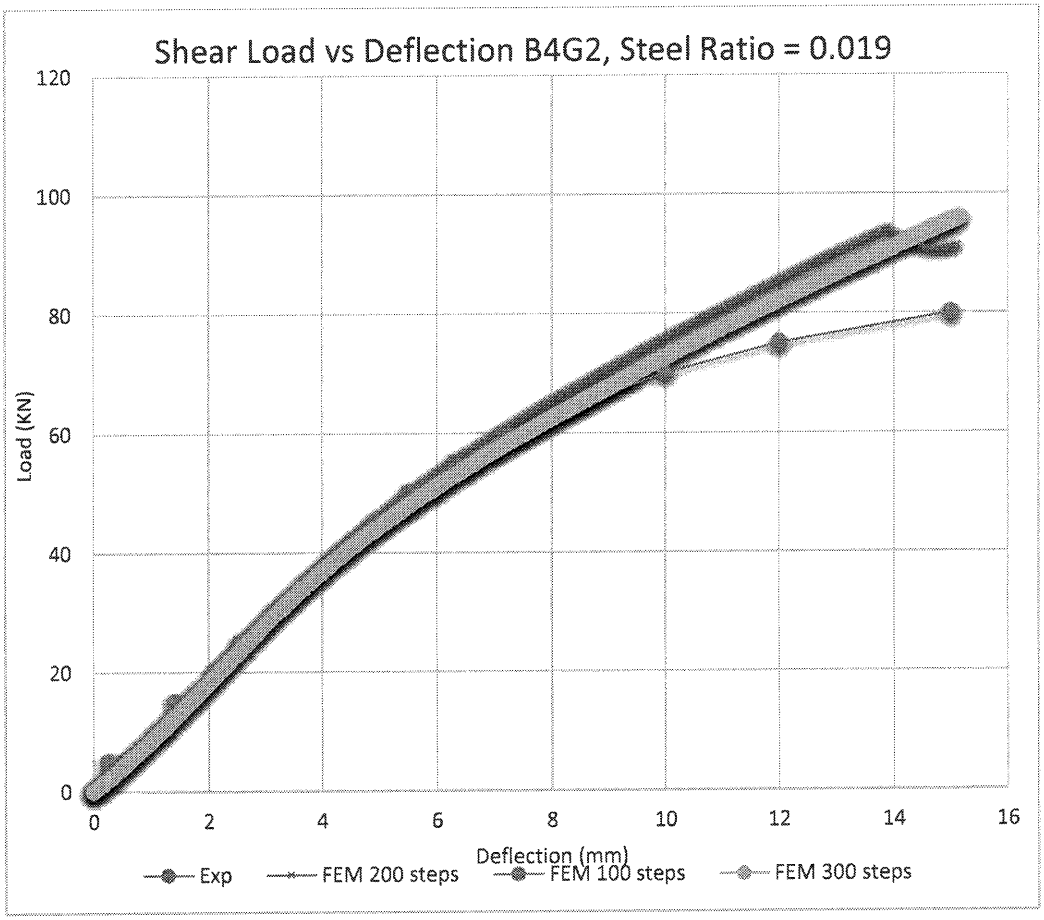


Figure 5.17 The three sub steps numbers comparison

5.7 FEA Results for the Full-Size Beams

This section presents the results of the ANSYS finite element analysis and the comparison of the experimental data on the nine full-size beams. The data used for the FEA were collected from the experiments of the full-size beams in addition to some information from the literature and codes for the missing information. Noting that the compressive strength of concrete for cylinder (f'_c) were used in the program.

The main subject for comparison is the load deflection curves. Dial gage was used directly to measure the deflections of the experimental beams at mid-span in

the center bottom face of the beams. In ANSYS, deflections are measured at the same location as for the experimental beams.

The following sections show the load-deflection plots from the finite element analyses and the comparison of the experimental results for all groups of beams.

5.7.1 Shear Span-to-Depth Ratio Variable (G1)

All the beams in this group have the same specifications and dimensions, with flexural steel reinforcement ratio of $\rho = 0.041 > \rho_b$ and compressive strength of concrete f_{cu} = Grade C110. The shear span-to-depth ratio a/d is the variable in this group.

5.7.1.1 Comparing with Experimental Results B2G1

This beam has the t a/d ratio which is 2.63. Figure 5.18 shows the minimum and maximum deflection areas for the half of the beam B2G1using Ansys. There are some variations between the results of FEA and the experiment. FEA shows a linear relationship between load and deflection in all stages, but the experiment results changed at 75% of the ultimate load of the test results. The finite element analysis ultimate load results are seen at 20% more than the experimental results, and the same for the deflection. The comparison between FEA and experimental results of the shear load deflection relationships is shown in figure 5.19.

These variations between experimental results and finite element results may be due to some assumption using Menetrey-Wiliam model for ultra-high strength concrete stress strain relationship and softening stage.

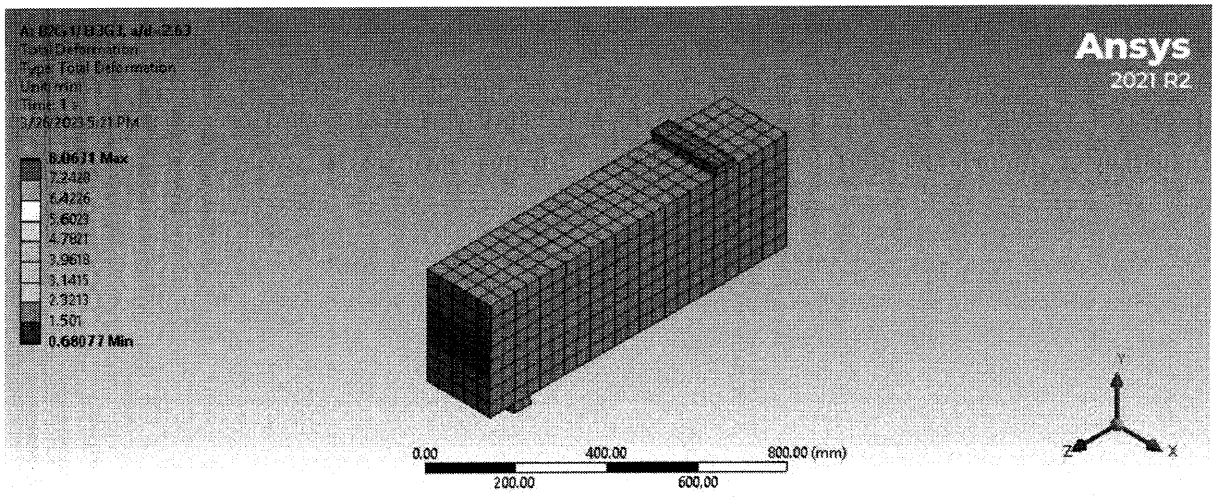


Figure 5.18 Minimum and maximum deflection areas by ANSYS for B2G1 beam

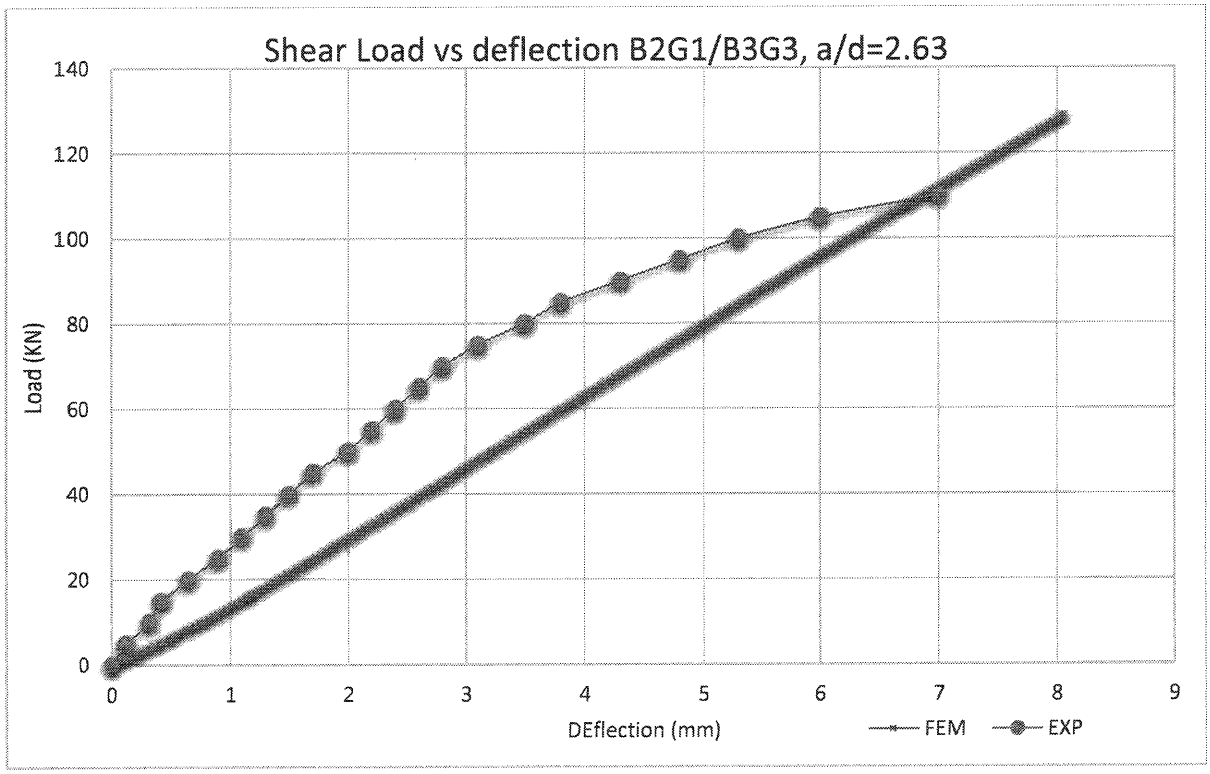


Figure 5.19 Comparison between FEA and experimental results of the load deflection relationships for beam B2G1

B3G1

B3G1 has the a/d ratio which is 3.16. The minimum and maximum deflection areas for the half of the beam B3G1using Ansys is shown in figure 5.20. There are some variations between the results of FEA and the experiment. FEA shows a linear relationship between load and deflection in all stages, but the experiment results changed at 60% of the ultimate load of the test results. The finite element analysis ultimate load results are seen at 30% more than the experimental results, and the same for the deflection. Figure 5.21 shows the comparison between FEA and experimental results of the load deflection relationship.

These variations between experimental results and finite element results are assumed to be of the same reasons mentioned in beam B2G1 and the linearity is that Menetrey-Wiliam model is not applicable in using high steel ratio $\rho > \rho_b$ and lower a/d ratio.

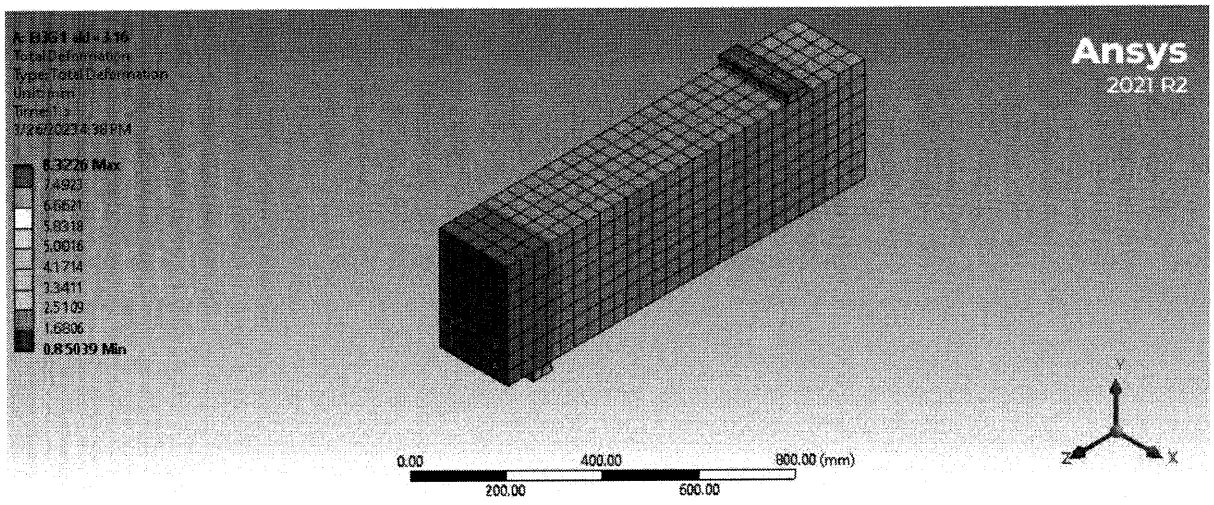


Figure 5.20 Location of the minimum and maximum deflection areas by ANSYS for B3G1 beam

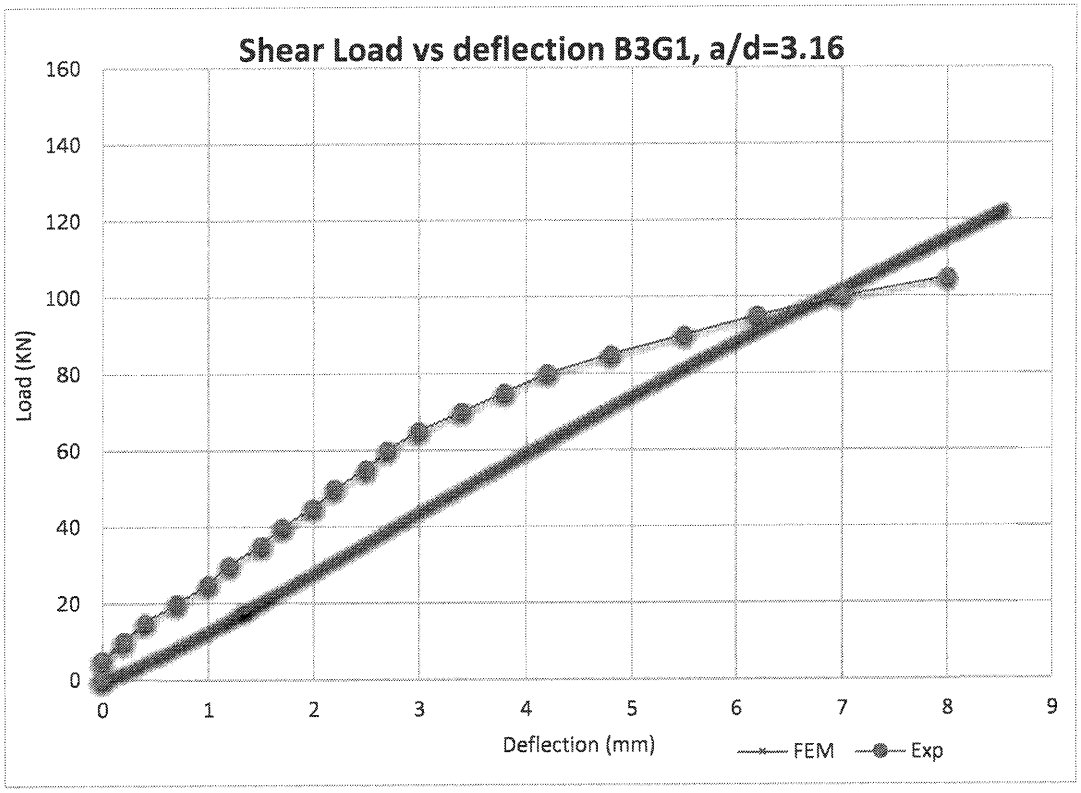


Figure 5.21 FEA and experimental results comparison for the load deflection relationships for beam B3G1

B4G1

The last beam in this group has an a/d ratio of 4.21. Figure 5.22 shows the location of minimum and maximum deflection areas for half of the beam B4G1 using ANSYS. The results show that around 90% is in line with the results between the FEA and the experiment. Both FEA and experimental results show that the linear relationship is up to 75% of the ultimate load. The finite element analysis ultimate load results are seen at 15% more than the experimental results, and around 10% more for the deflection. The comparison between FEA and

experimental results for the shear load deflection relationship is shown in figure 5.23.

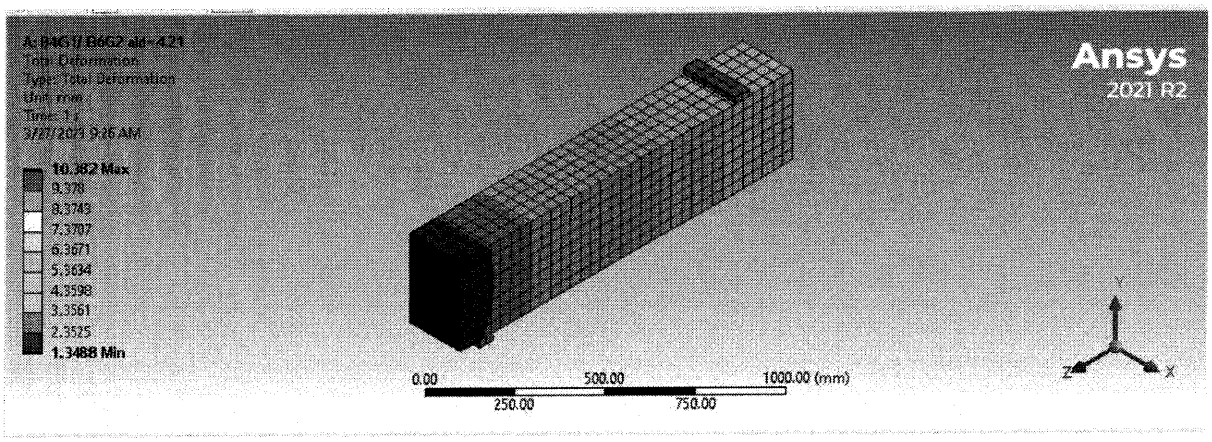


Figure 5.22 Location of minimum and maximum deflection areas by ANSYS for B4G1 beam

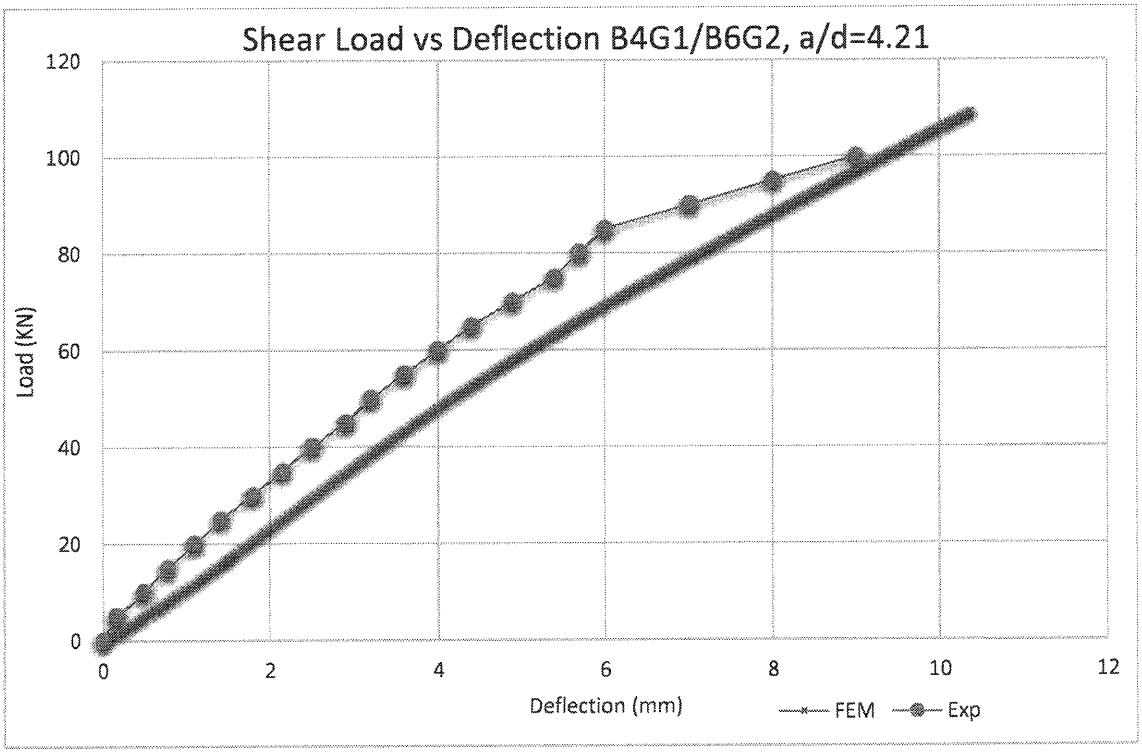


Figure 5.23 FEA and experimental results comparison for the load deflection relationships for beam B4G1

5.7.1.2 Effect of Shear Span-to-Depth Ratio *(a/d)*

Figure 5.24 shows that the beam with lower a/d ratio has a stiffer response in terms of load deflection behavior. For the same load level as a/d ratio, the deflection increased. This is because the depth of the beam is constant, the shear load was decreased as a/d ratio increased, and this is in line with the experimental results.

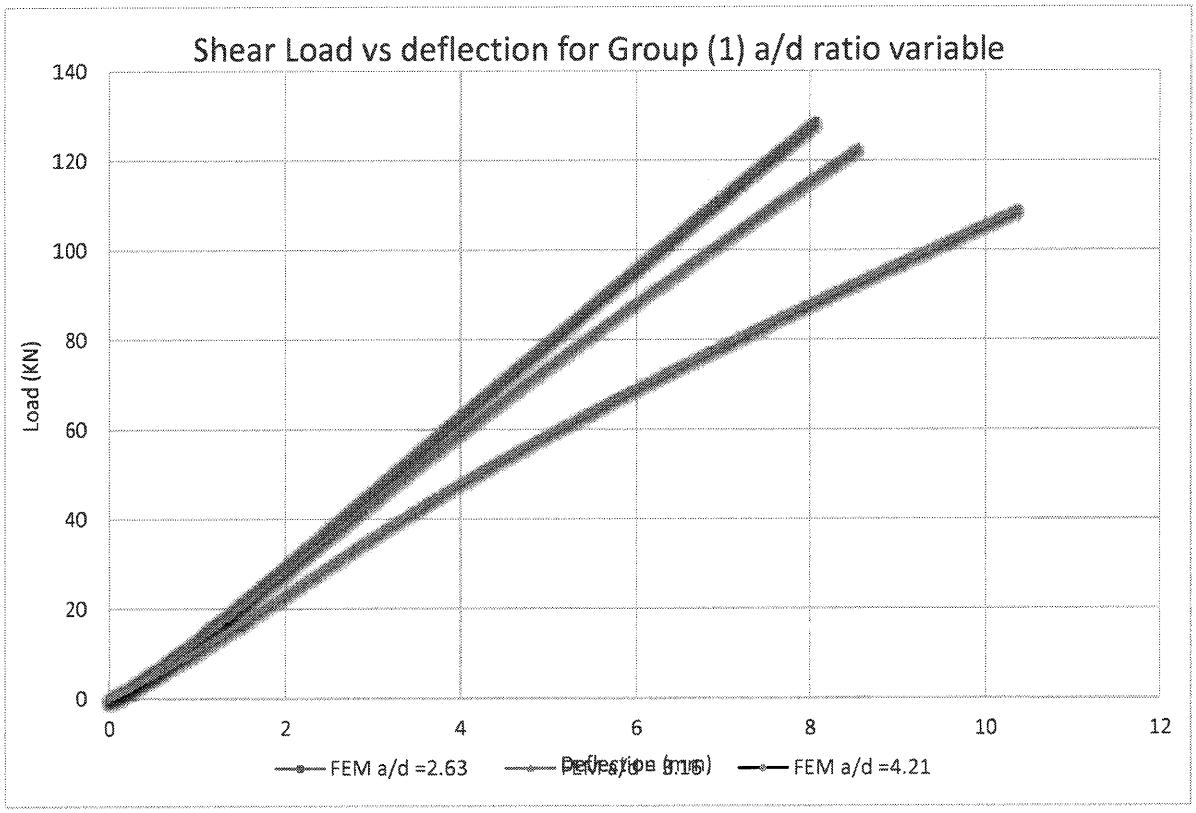


Figure 5.24 Load vs deflection curves for G1 beams (a/d ratio)

5.7.2 Flexural Steel Reinforcement (ρ) Variable (G2)

All the beams in this group have the same specifications and dimensions with shear span-to-depth ratio (a/d = 4.21) and compressive strength of concrete (f_{cu} = Grade C110). The variable in this group is the flexural steel reinforcement ratio ρ

5.7.2.1 Comparing with Experimental Results

B4G2

The first beam in this group has the steel reinforcement ratio of 0.019, ($\rho < \rho_{max}$, noting that $\rho_{max} = 0.75\ \rho_b$). Figure 5.25 shows the location of minimum and maximum deflection areas for half of the beam B4G2 using Ansys. The FEA results show that up to the linear portion, findings are in line with the experimental results. Both FEA and experimental results show that the linear relationship is up to 50% of the ultimate load. The finite element analysis ultimate load results are seen at 25% more than the experimental results, and around 4% more for the deflection. Figure 5.26 presents the comparison between FEA and experimental results of the shear load deflection relationships.

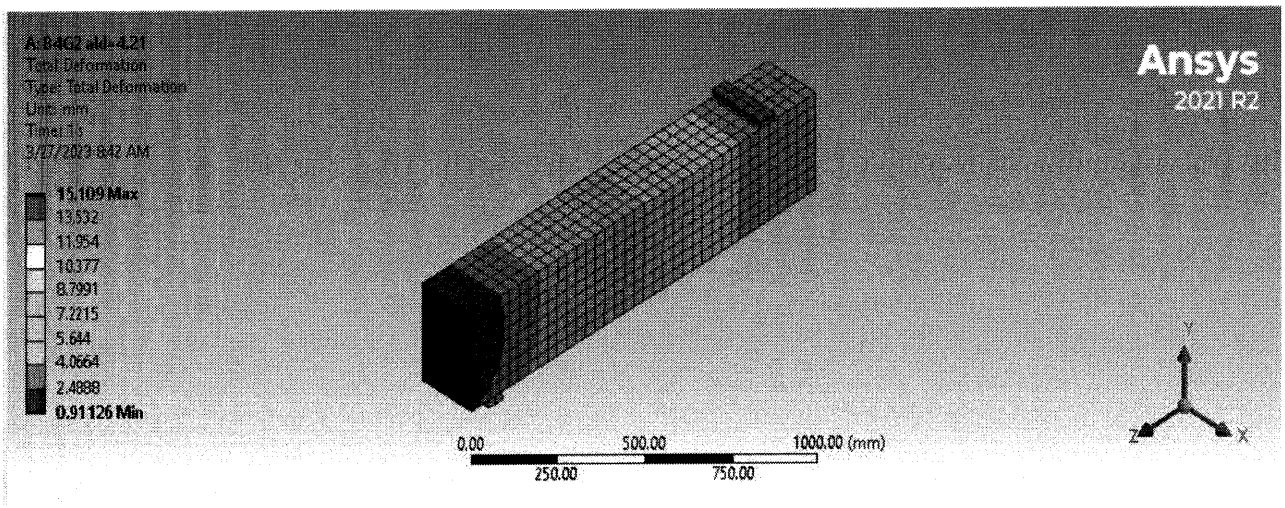


Figure 5.25 Areas of minimum and maximum deflection by ANSYS for B4G2



Figure 5.26 FEA and experimental results Comparison for the load deflection relationships for beam B4G2

B5G2

This beam has the middle steel reinforcement ratio of 0.031, ($\rho_{max} < \rho < \rho_b$). Figure 5.27 shows the location of minimum and maximum deflection areas for the half of the beam B4G1using Ansys. The FEA results show that 75% are in line with the experimental results. Both FEA and experimental results present that the linear relationship is up to 50% of the ultimate load. The finite element analysis ultimate load results are seen at 20% more than the experimental results, and around 6% more for the deflection. Figure 5.28 shows the comparison between FEA and experimental results for the shear load deflection relationships.

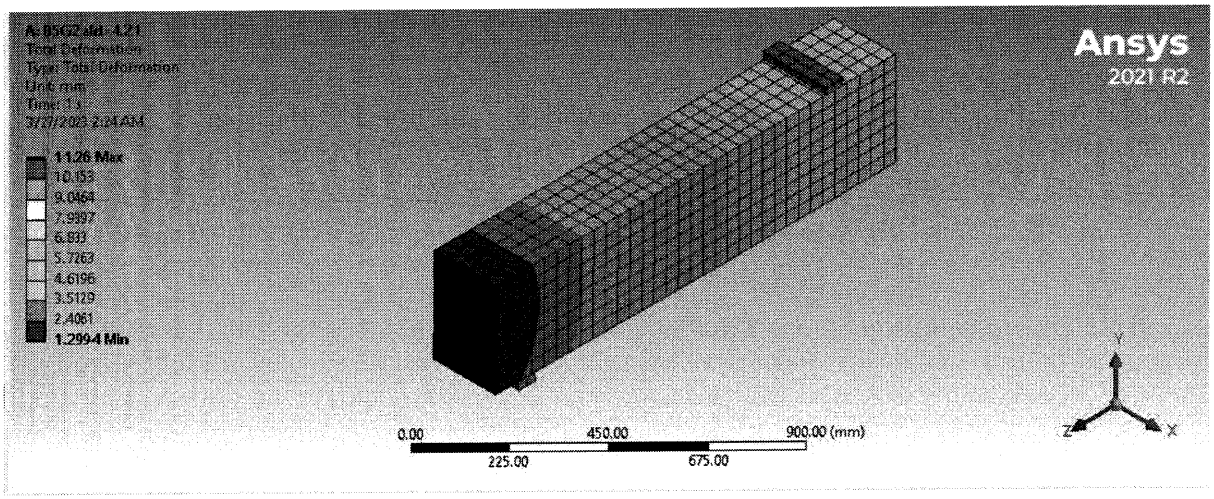


Figure 5.27 Location of minimum and maximum deflection areas by ANSYS for B5G2 beam



Figure 5.28 FEA and experimental results comparison for the load deflection relationships for beam B5G2

B6G2

This beam has the higher steel reinforcement ratio of 0.041, ($\rho > \rho_b$). Figure 5.29 shows the location minimum and maximum deflection areas for the half of the beam B4G1using Ansys. The results indicate that around 90% are in line with the FEA and experimental results. Both FEA and experimental results show that the linear relationship is up to 75% of the ultimate load. The finite element analysis ultimate load results are seen at 15% more than the experimental results, and around 10% more for the deflection. Figure 5.30 shows the comparison between FEA and experimental results for the shear load deflection relationships.

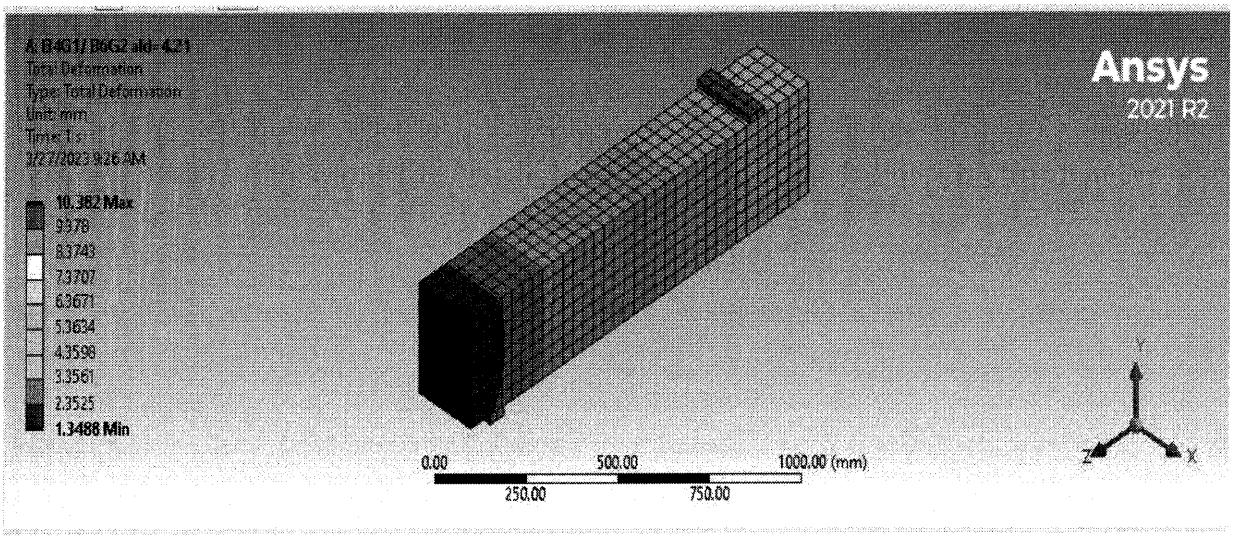


Figure 5.29 Location of minimum and maximum deflection areas by ANSYS for B6G2 beam

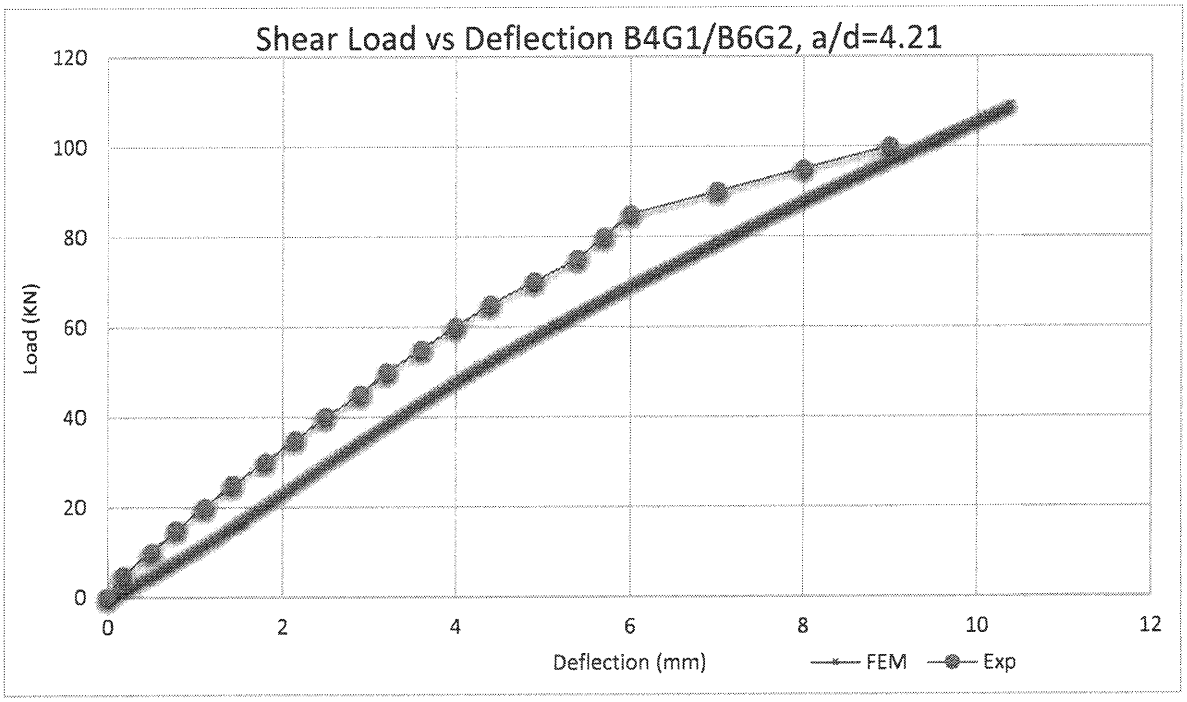


Figure 5.30 FEA and experimental results comparison for the load deflection relationships for beam B6G2

5.7.2.2 Effect of Flexural Steel Reinforcement (ρ)

Figure 5.31 shows that the beam with higher steel content has a stiffer response in terms of load deflection behavior and this trend is due to the larger effective moment of inertia and the large amount of tensile reinforcement. For the same load level, the deflection has increased as the tensile steel ratio decreased as shown in the same figure, and this is in line with the experimental results.

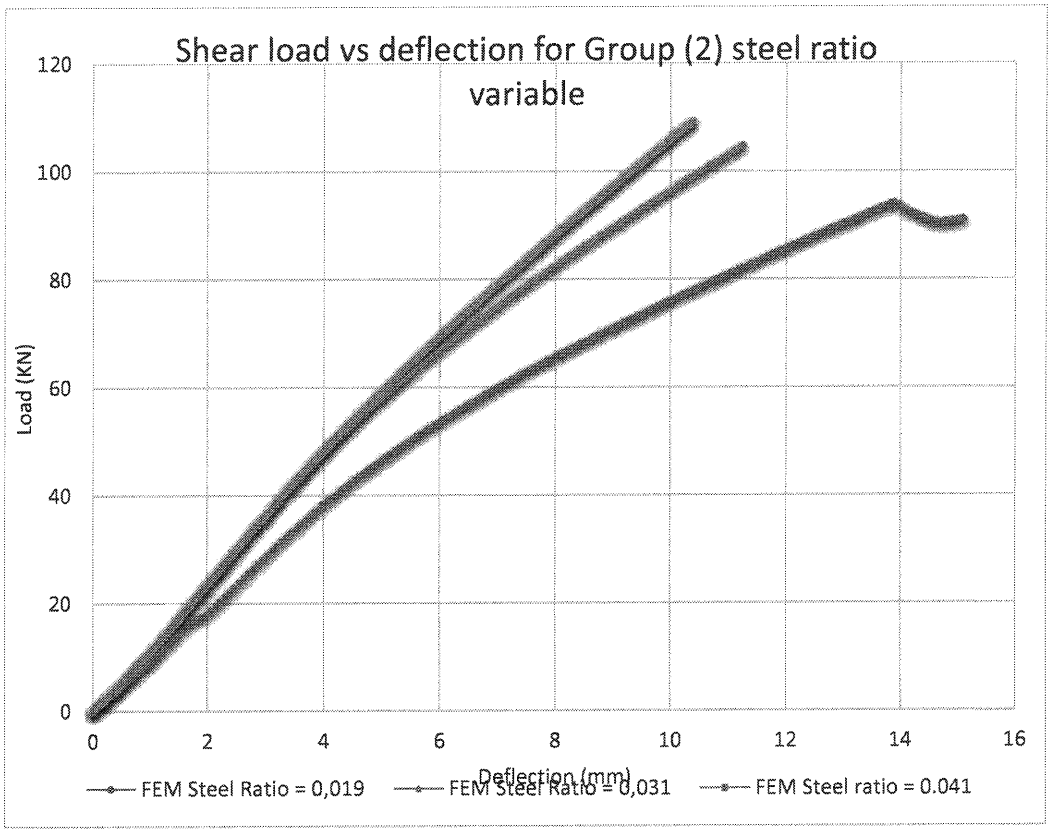


Figure 5.31 Load vs deflection curves for G2 beams (ρ)

5.7.3 Compressive Strength of Concrete (f_{cu}) Variable (G3)

All the beams in this group have the same specifications and dimensions with the same flexural steel reinforcement ratio ($\rho = 0.041 > \rho_b$) and shear span-to-depth ratio (a/d =2.63). The variable in this group is the compressive strength of concrete (f_{cu}).

5.7.3.1 Comparing with Experimental Results

B1G3

This beam has the compressive strength of high-strength concrete (f_{cu} Grade C80). Figure 5.32 shows the location of minimum and maximum deflection areas for half of the beam B1G3 using ANSYS. FEA shows a linear relationship between

shear load and deflection in all stages. 95% of the experimental results show linear and this part is in line with the results of FEA. The finite element analysis ultimate load results are seen at 30% more than the experimental results and 15% more for the deflection. Figure 5.39 shows the comparison between FEA and experimental results for the shear load deflection relationship.

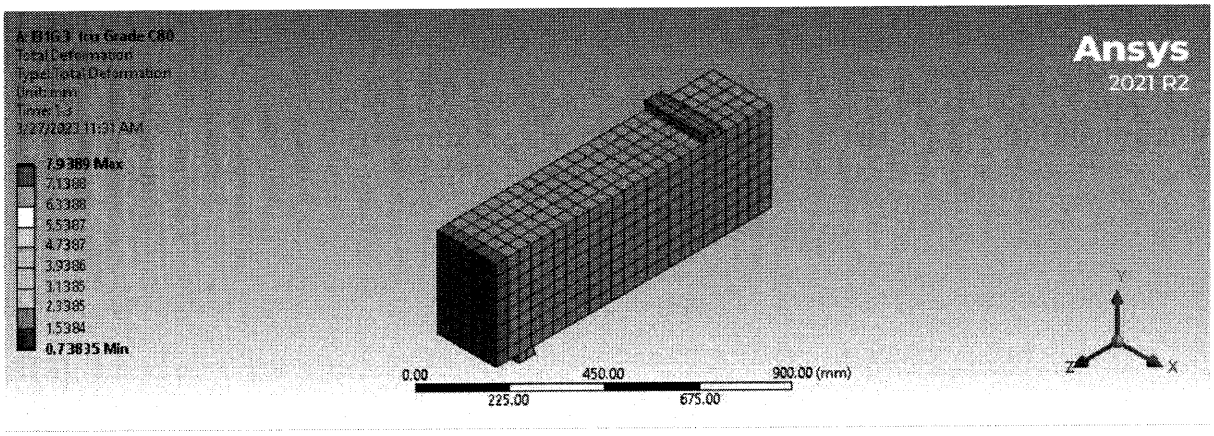


Figure 5.32 Location of minimum and maximum deflection areas by ANSYS for B1G3 beam

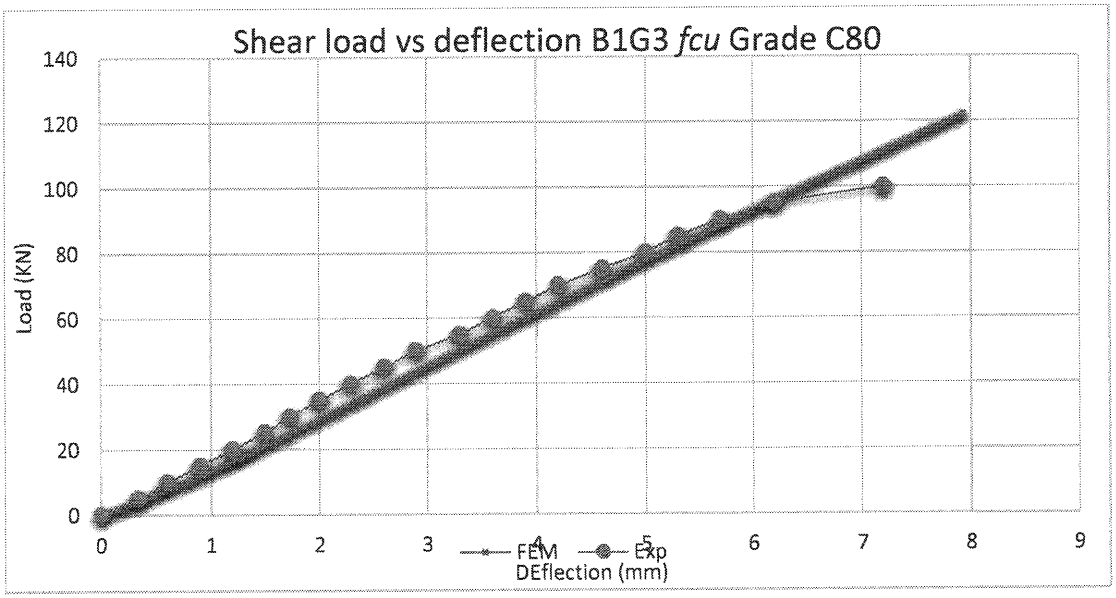


Figure 5.33 FEA and experimental results comparison for the load deflection relationships for beam B1G3

B2G3

B2G3 has the ultra-high compressive strength of concrete (f_{cu} Grade C100). Figure 5.34 shows the location of minimum and maximum deflection areas for the half of the beam B2G3 using ANSYS. There is a variation between FEA and experimental results. FEA shows a linear relationship between load and deflection in all stages, but experiment results changed at 80% in the ultimate load of the test results. The finite element analysis ultimate load results are seen at 30% more than the experimental results, and 20% more for the deflection. Figure 5.35 shows the comparison between FEA and experimental results for the shear load deflection relationships.

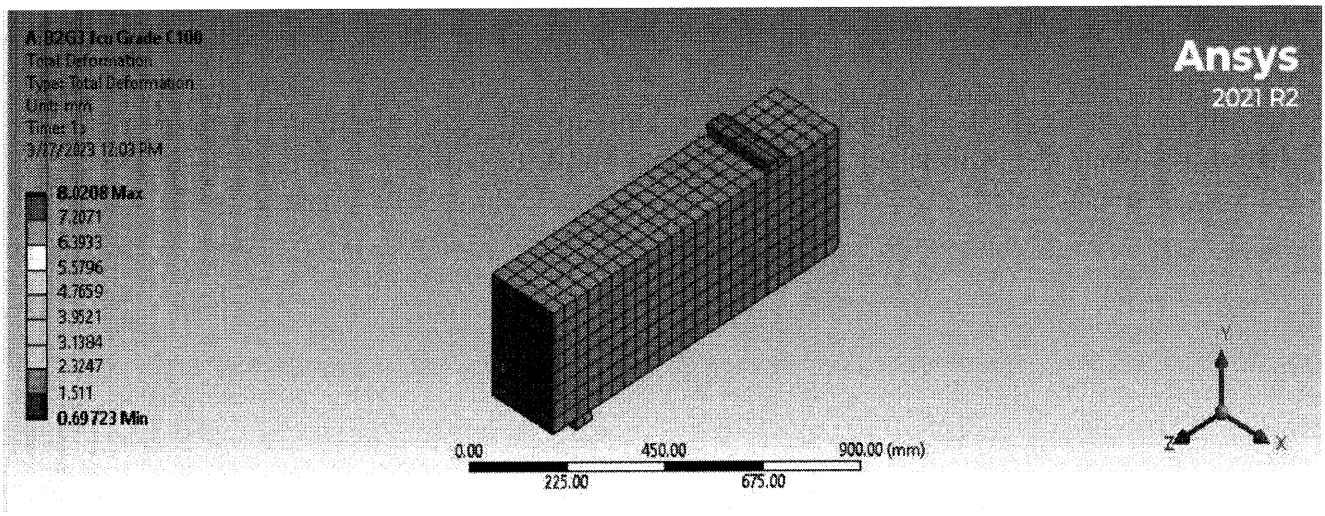


Figure 5.34 Location of minimum and maximum deflection areas by ANSYS for B2G3 beam

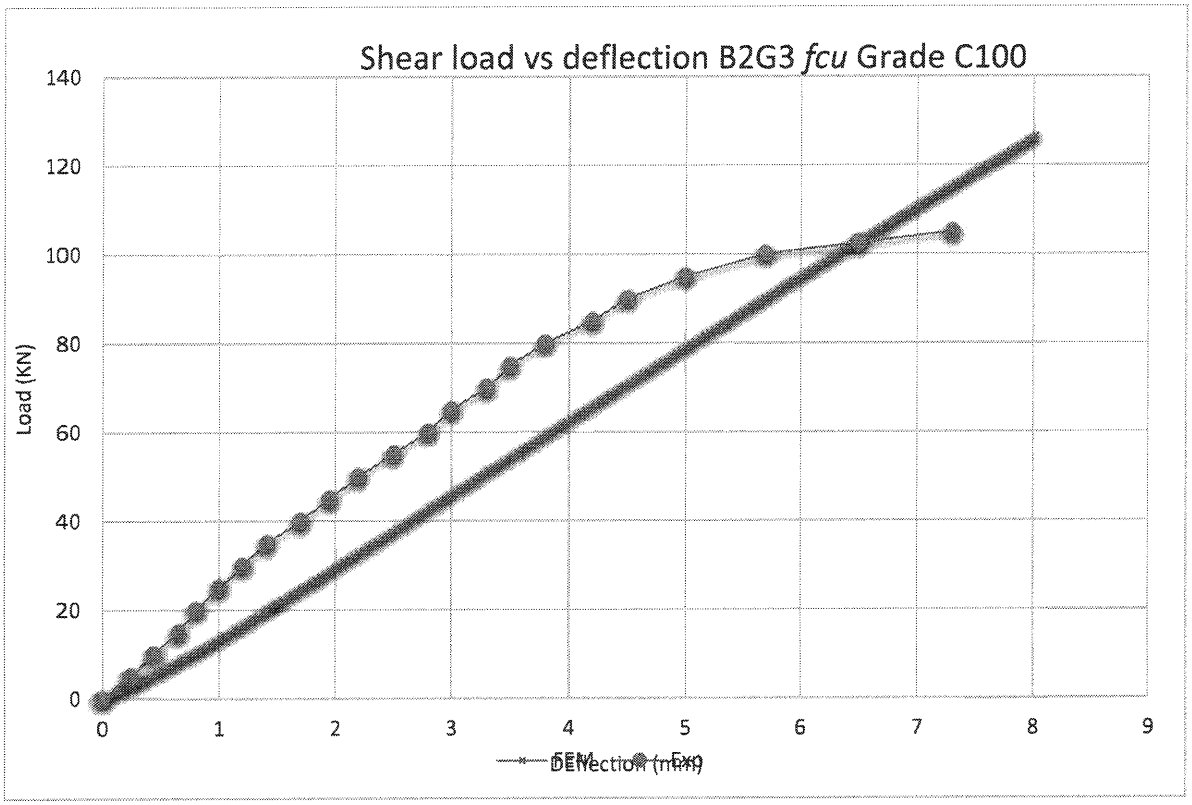


Figure 5.35 FEA and experimental results comparison for the load deflection relationships for beam B2G3

B3G3

The last beam has the ultra-high compressive strength of concrete (f_{cu} Grade C110). Figure 5.36 shows the location of minimum and maximum deflection areas for half of the beam B3G3 using ANSYS.

Variation between the FEA and experimental results is observed. FEA shows a linear relationship between load and deflection in all stages, but experiment results changed at 75% in the ultimate load of the test results. The finite element analysis ultimate load results are seen at 20% more than the experimental results, and the

same for the deflection. Figure 5.37 shows the comparison between FEA and experimental results for the shear load deflection relationships.

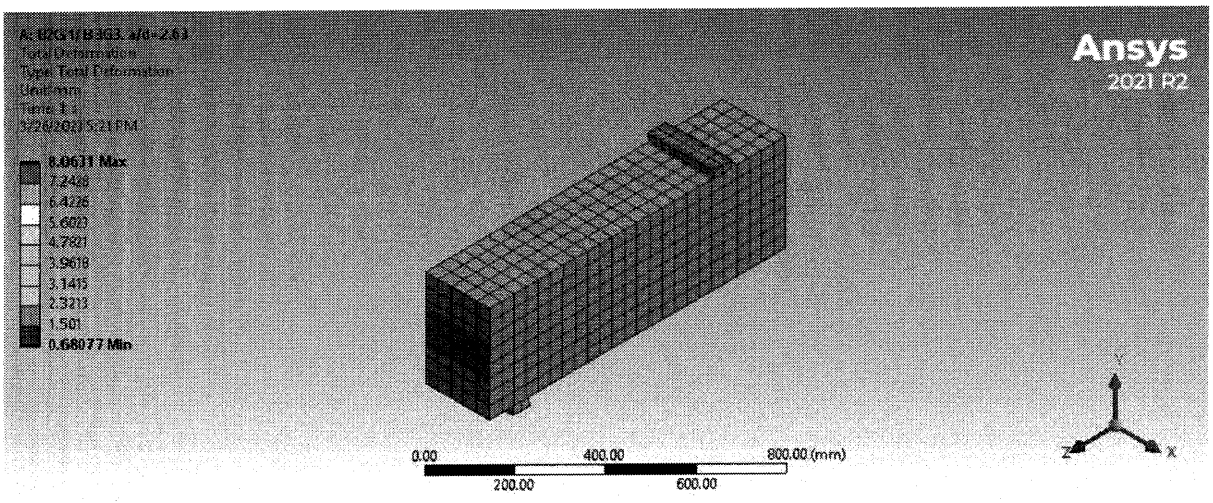


Figure 5.36 Location of minimum and maximum deflection areas by ANSYS for B3G3 beam

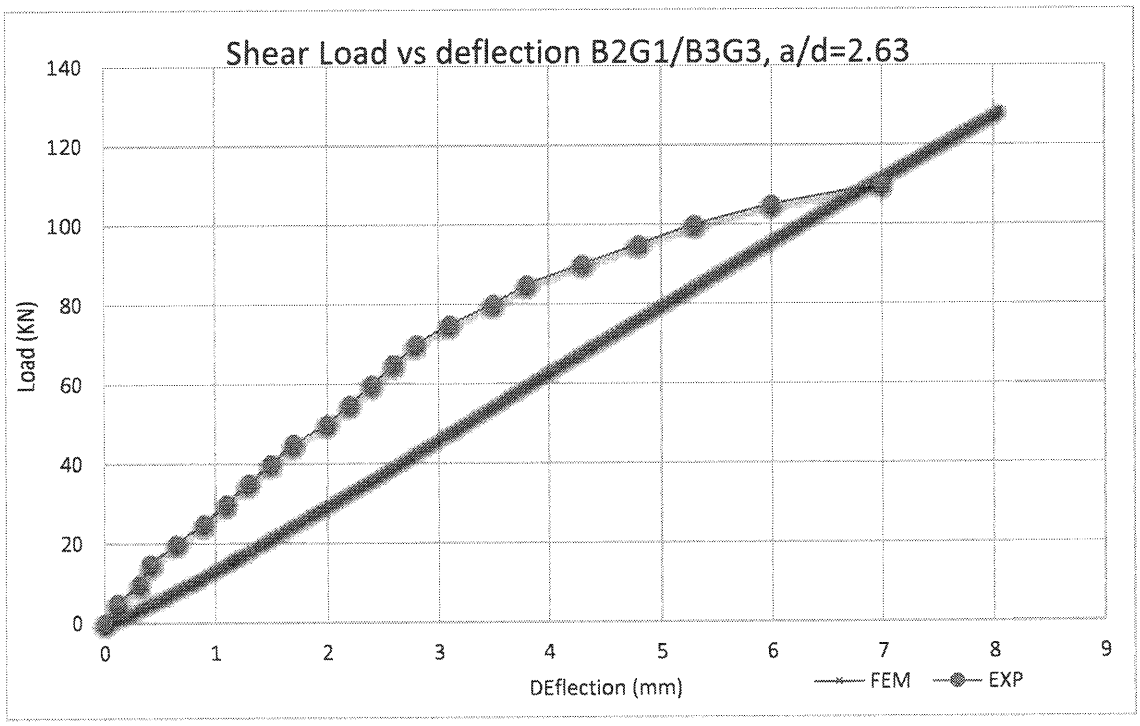


Figure 5.37 FEA and experimental results comparison for the load deflection relationships for beam B3G3

5.7.3.2 Effect of Compressive Strength of Concrete (f_{cu})

Figure 5.38 shows that all results are similar but the beam with higher strength concrete suffers less deflection than a similar member with lower strength concrete at the same load level, which may be attributed to the fact that higher strength concrete beams are stiffer than lower strength concrete beams since the modulus of elasticity of concrete is larger for the higher strength concrete than that of the lower strength concrete. This is in line with the experimental results.

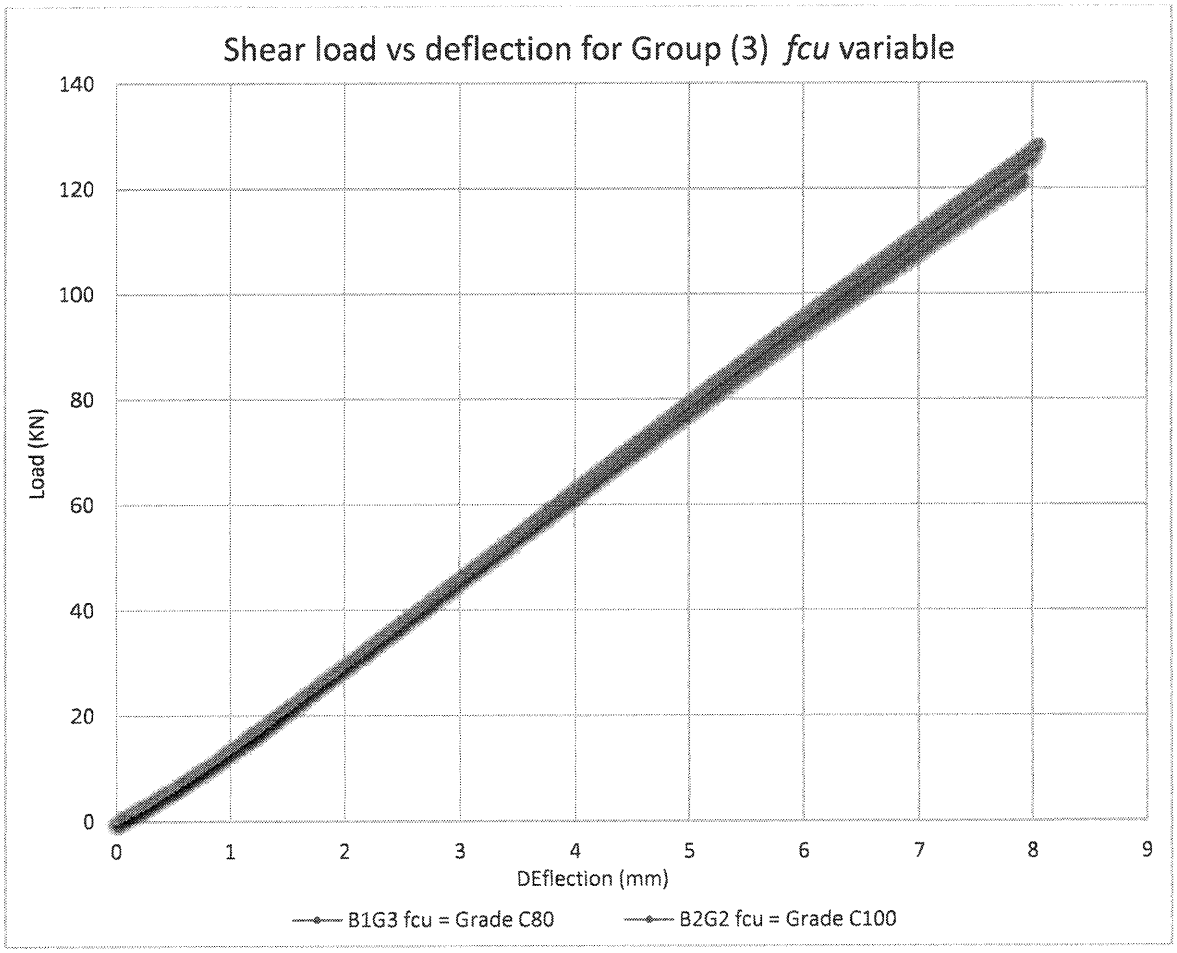


Figure 5.38 Load vs deflection curves for G3 beams (f_{cu})

5.8 Summary for ultimate load results using FEM

The ultimate load using FEA is considered a peak load of the beam depends on the load deflection curve shown in the above figures.

For group No. (1), and group No. (3) the load deflection relation of the FEA results approximately linear relationships, therefore depends on the maximum deflection in the experimental result, the load can be read direct from the load deflection relationship of the FEA Figures (5.19, 5.21,5.23, 5.33, and 5.35).

For group No.2, the load deflection relation of the FEA results for beam B4G2, the ultimate load shown in the curve, therefore, the load can be read direct from the load deflection relationship of the FEA Figure 5.26, while the beam B5G2 Figure 5.28 will use the same way of group No. (1).

The summary of the results shown in table 5.5 below

Table 5.5 Comparison of experiment and FEA ultimate load

No.	**Beam** No.	***a/d***	**ρ**	f_{cu} MPa	**Test**		**FEA**
					P (KN)	**V=P/2 (KN)**	**V (KN)**
1	B2G1	2.63	0.041	112.8	220	110	110
2	B3G1	3.16	0.041	111.4	210	105	105
3	B4G1	4.21	0.041	106.5	200	100	100
4	B4G2	4.21	0.019	106.6	160	80	90
5	B5G2	4.21	0,031	117.1	180	90	95
6	B6G2	4.21	0,041	106.5	200	100	100
7	B1G3	2.63	0.041	76.8	200	100	106
8	B2G3	2.63	0.041	102.2	210	105	108
9	B3G3	2.63	0.041	112.8	220	110	110

5.9 Results Using Other Models

The following beams B2G1, B3G1, B3G1, and B2G3 show the linear relationship of shear-load deflection. The results are based on Menetrey-Wiliam model and softening of concrete. One of the abovementioned beams, B3G1 is calculated using other base models, noting the results with the use of Menetrey-Wiliam Model as shown in figure 5.19 of section 5.7.3.

5.9.1 Bruker Prager Model

Figure 5.39 shows the input data for B3G1 using Bruker Prager Model and figure 3.40 shows the load deflection curve.

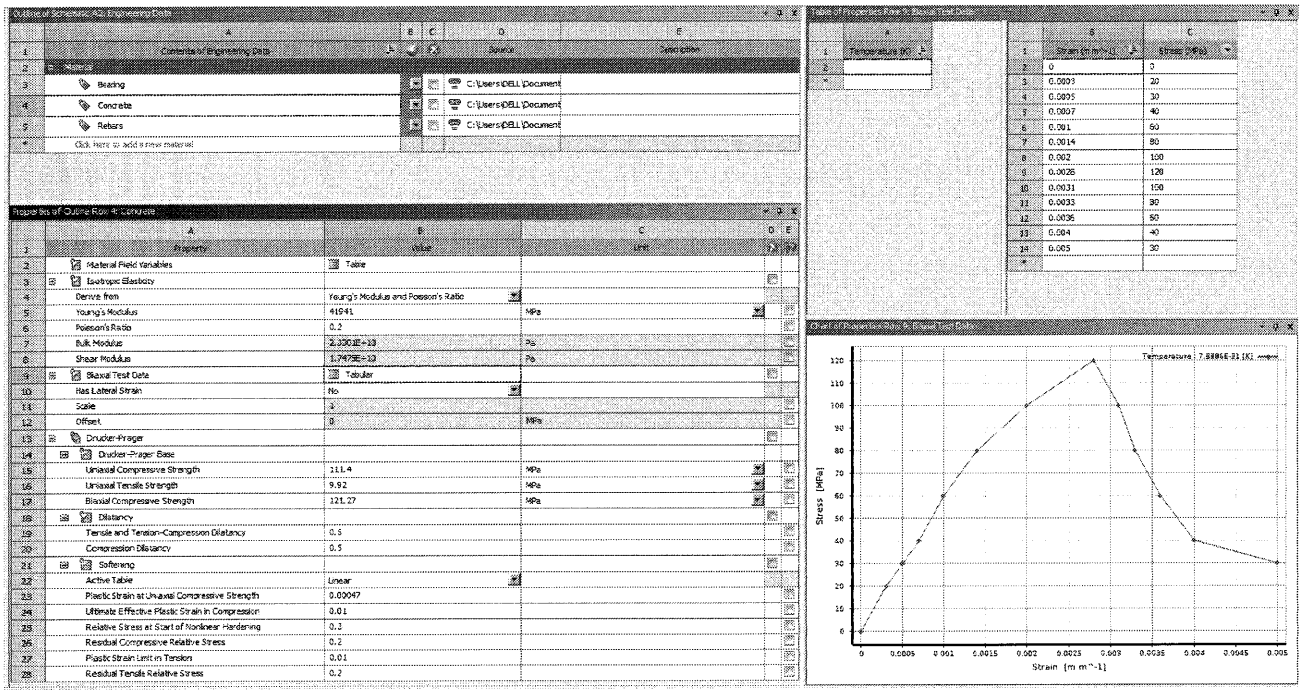


Figure 5.39 Input data for B3G1 using Bruker Prager model

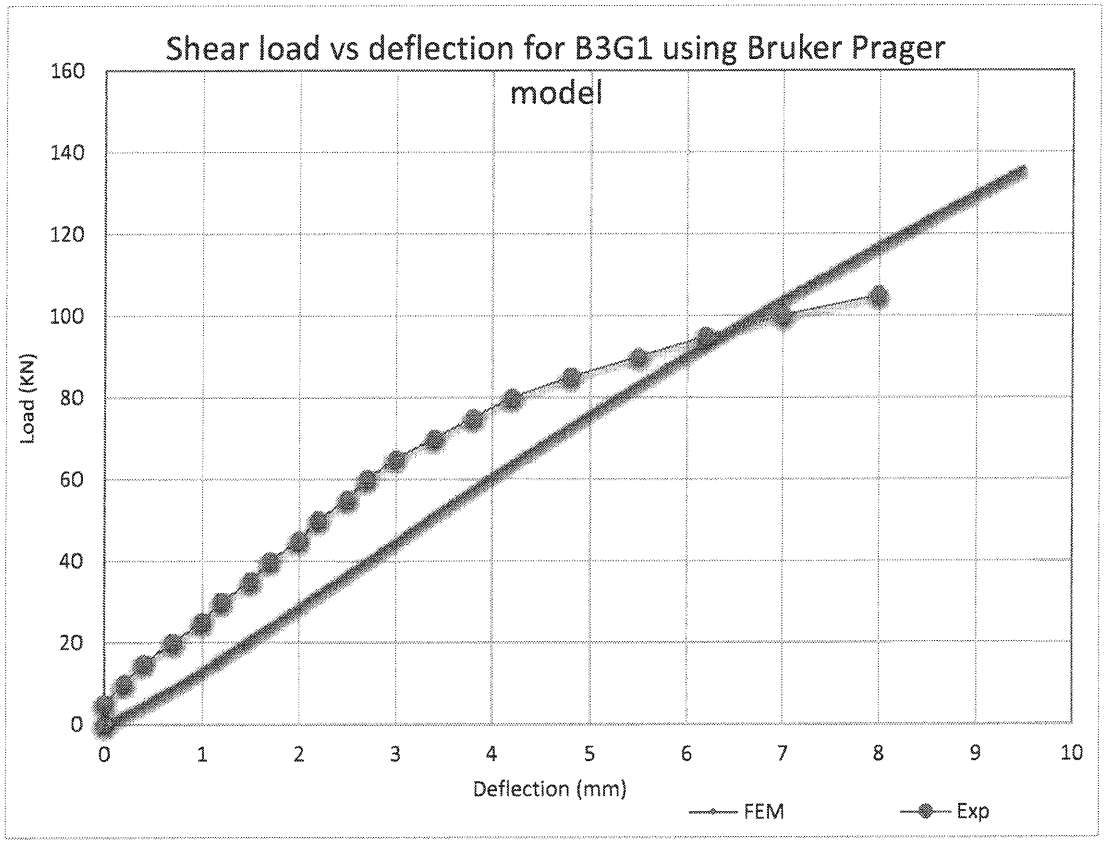


Figure 5.40 Load vs deflection curve for B3G1 using Bruker Prager model

5.9.2 Using Biaxial Test Data

Figure 5.41 presents the input data for B3G1 using Bruker Prager Model and figure 3.42 shows the load deflection curve.

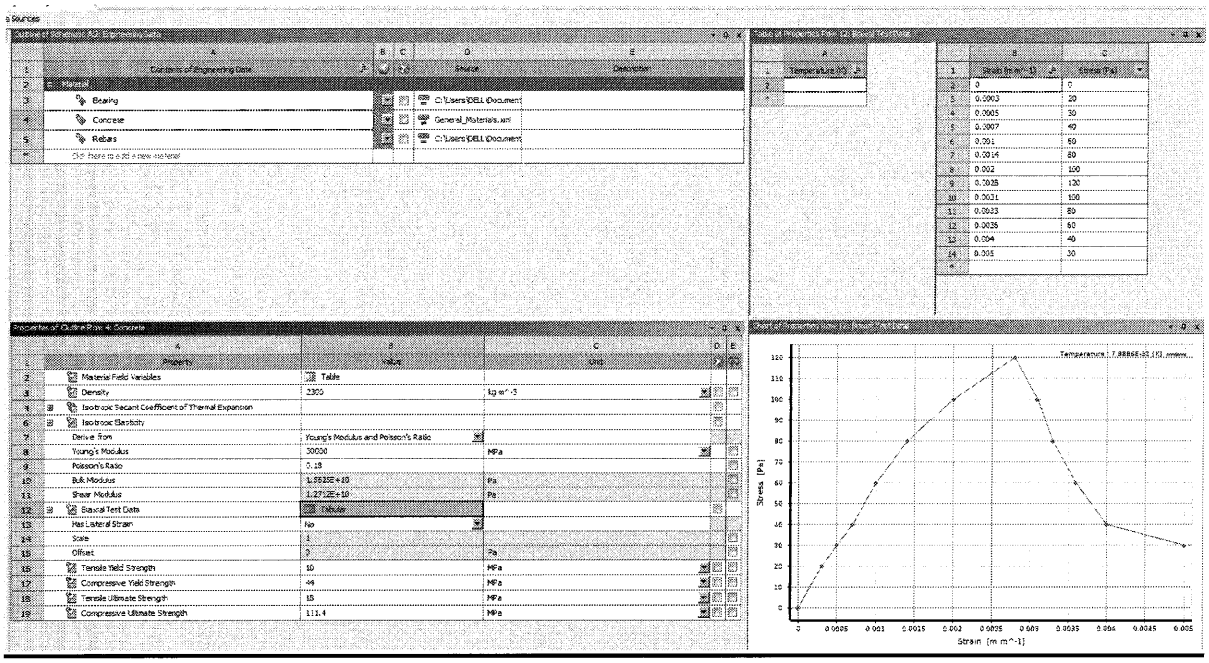


Figure 5.41 Data for B3G1 using biaxial test data

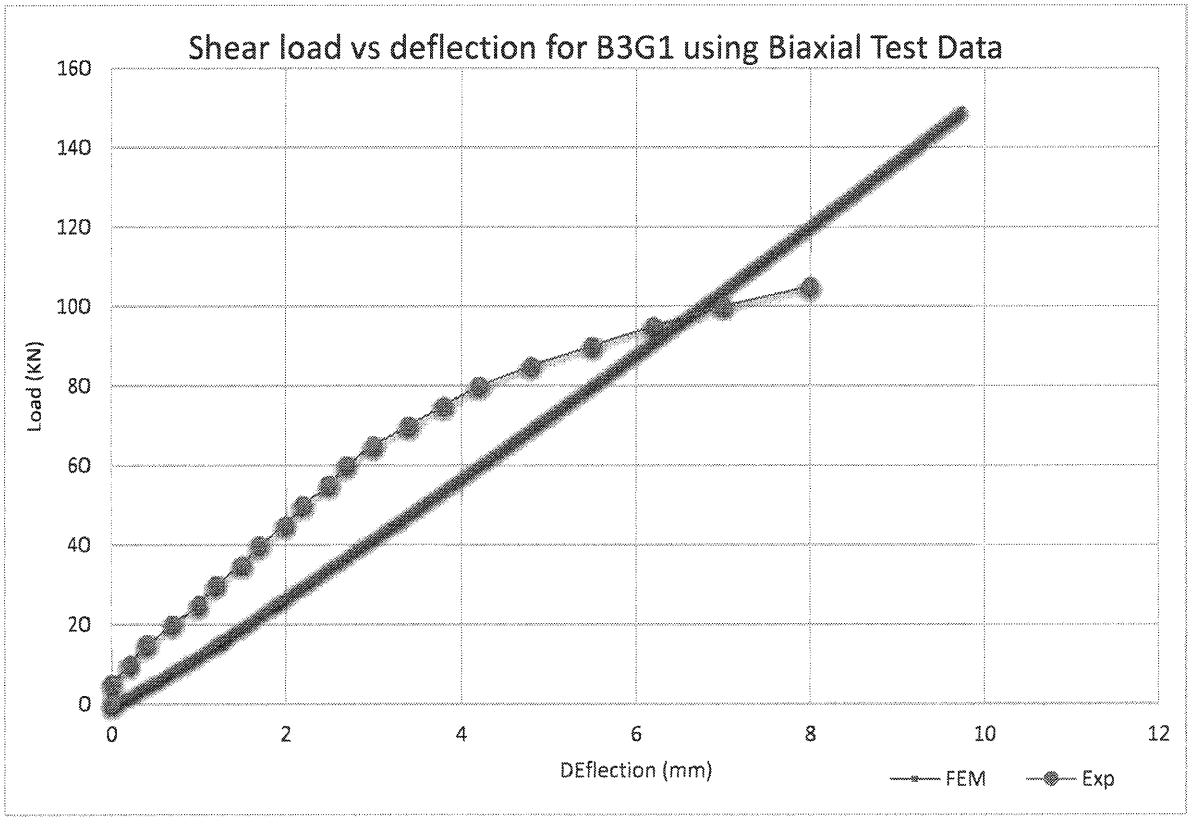


Figure 5.42 Load vs deflection curve for B3G1 using biaxial test data

5.9.3 Menetrey-Wiliam Model after Changing the boundary conditions

Figure 5.43 shows the input data for B3G1 using Menetrey-Wiliam Model after changing the boundary conditions and figure 3.44 shows the load deflection curve.

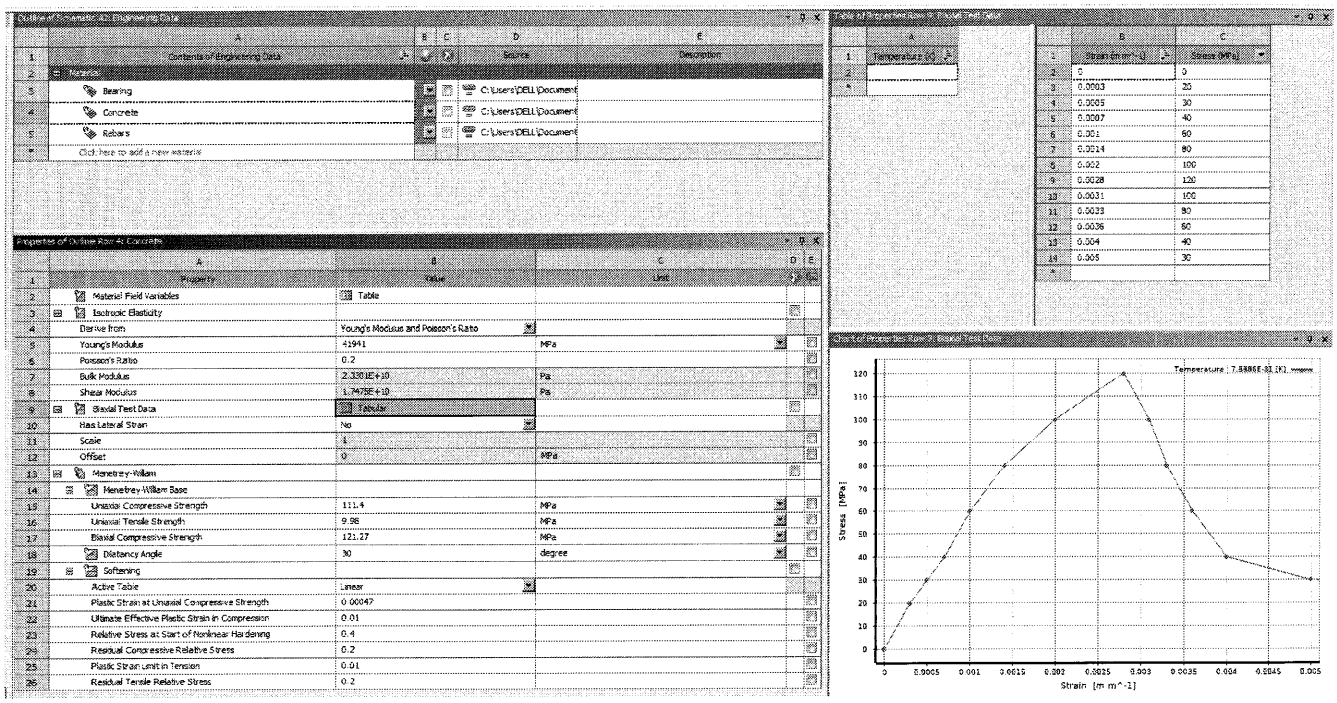


Figure 5.43 Input data for B3G1 using Menetrey-Wiliam Model with changing boundary conditions

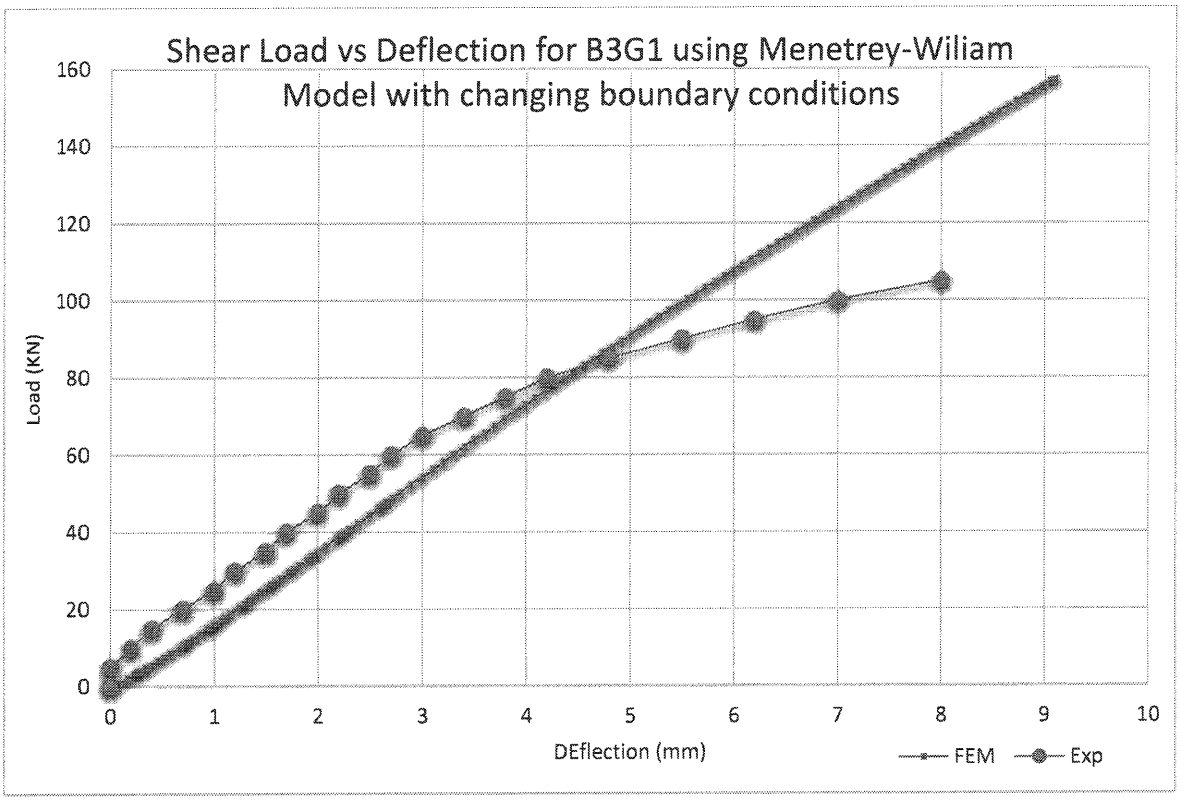


Figure 5.44 Load vs deflection curve for B3G1using Menetrey-Wiliam Model with changing boundary conditions

All the above figures show that the load-deflection relationship curve is linear for higher steel reinforcement ratio when $\rho > \rho_b$ and lower with a/d ratio.

Chapter 6

Data Analysis and Results Discussion

Chapter 6

Data Analysis and Discussion

6.1 Introduction

Researches on reinforced concrete beams made of normal strength concrete and high-strength concrete is widely recorded in literature. However, only a few studies have been carried out on the behavior of ultra-high strength concrete beams.

The advantage of using of an ultra-high strength concrete reinforced with high-strength steel is that the cross-sectional dimensions of structural members can be reduced; thus, reducing the self-weight of the structure and material usage and construction cost too. Hence, there is an increase in the use of ultra-high strength concrete as a structural member. However, despite the benefits of UHSC, its practical applications are still limited because of its complicated and uneconomical production (Chen et al., 2020).

In the present study, the ultra-high strength concrete beams under the action of shear forces have been studied experimentally and numerically to better understand such beam behavior. Shear behavior of UHSC was investigated by testing them under two-point loads then comparing the numerical results using the ANSYS computer program. This arrangement has the advantage of combining two different conditions: Pure bending between the two loads and constant shear forces at the end section.

The span-to-depth ratio (a/d), flexural reinforcement ratio (ρ), and compressive strength of concrete (f_{cu}) are three main variables investigated in this study. Three groups of beams were assigned to study the shear behavior. Groups 1, 2, and 3 (G1, G2, G3) beams were casted without web reinforcement and assigned

to investigate the a/d, ρ, and f_{cu}, respectively. Beams' behavior was studied in terms of crack pattern, load deflection relationships, and shear strength.

6.2 Crack Patterns and General Behavior

The behavior of beams in general can be described based on the results exhibited in chapter 4. In the preliminary stages of loading, the beams were off cracked and acted as a homogeneous composite member composed of concrete and steel.

As the beams were loaded, flexural cracks formed in the tension face of the region with pure bending at a load level of about 35 to 40% of the ultimate load capacity of each beam as shown in figures 4.17 to 4.19 of section 4.5.1. Under further loading, additional flexural cracks formed in the central region and new ones in the shear span between the supports. With further increased of load, flexural cracking increased, and inclined cracks were developed, curving toward the loading points. After cracking, the behavior of the beams was dependent on a/d, ρ, and f_{cu}.

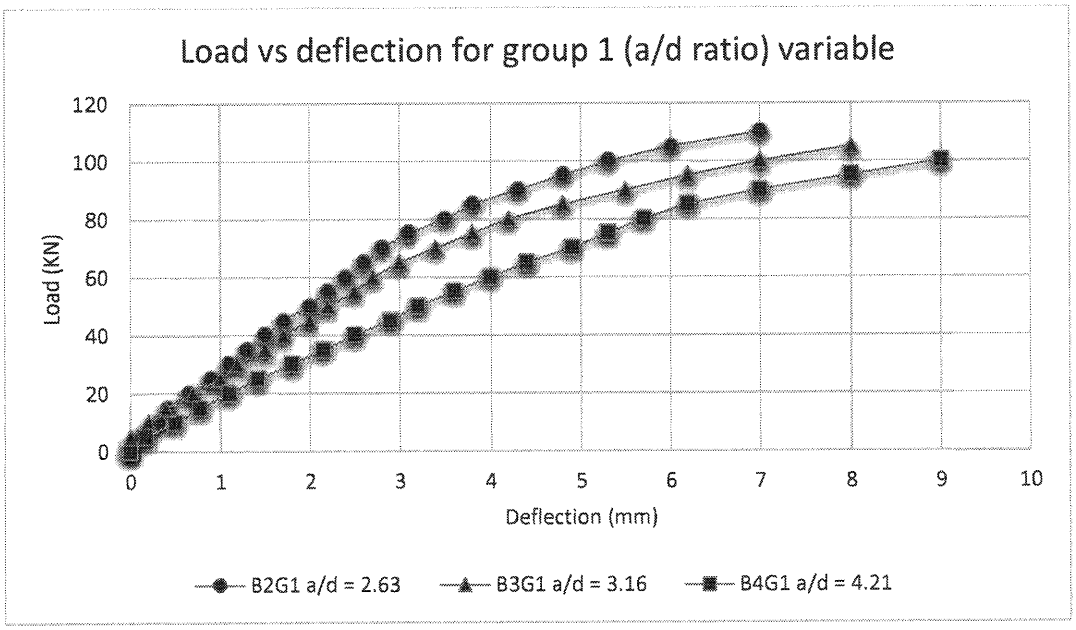


Figure 4.17 Load vs deflection curves for G1 beams (a/d) ratio

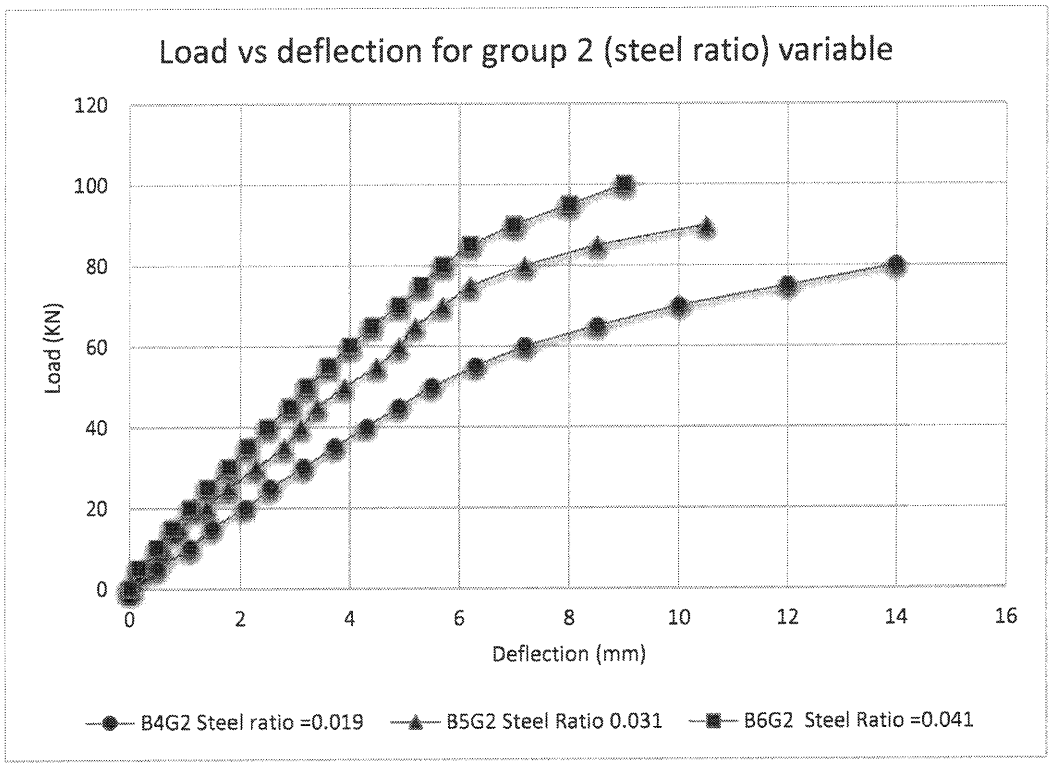


Figure 4.18 Load vs deflection curves for G2 beams (ρ) flexural steel ratio

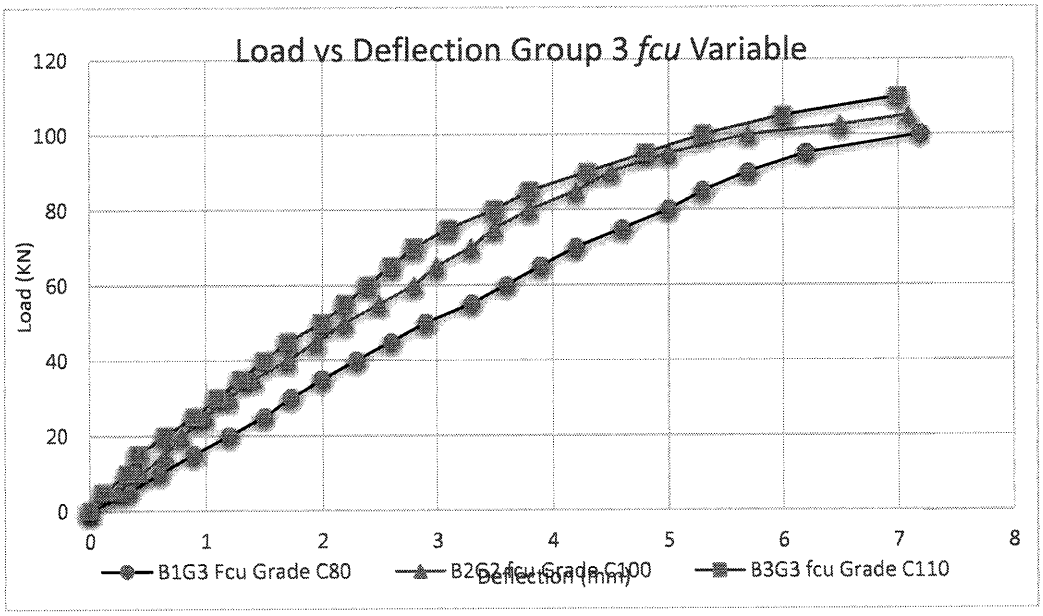


Figure 4.19 Load vs deflection curves for G3 beams (f_{cu}) compressive strength of concrete

For the beams in G1 with (2.63 < a/d < 4.21), ρ = 0.041 and f_{cu} Grade C110, the beam B2G1 in figure 6.1 with a/d =2.63, failure took place shortly after the formation of the critical diagonal tension cracks. The failure occurred because of the horizontal splitting along the tensile reinforcement near the end of the beam. The longitudinal steel for the beam did not yield. This type of failure in beam B2G1 (a/d =2.63) was classified as diagonal tension failure.

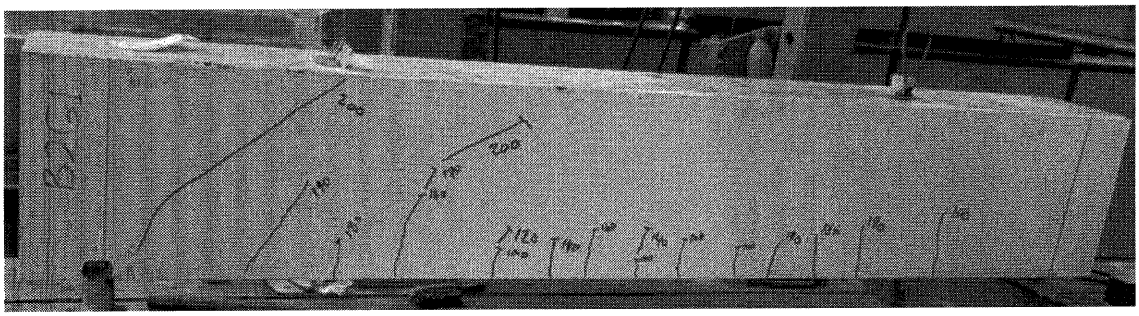


Figure 6.1 Crack pattern and failure in the beam B2G1/B3G3

For the beam B3G1 in figure 6.2 with a/d =3.16, failure took place sustainably greater than the load at which the initial diagonal tension crack occurred and developed without the extensive propagation on flexural cracks in the center portion of the span with crushing in the concrete of the compression zone indicating that the mechanism of failure is that of shear compression.

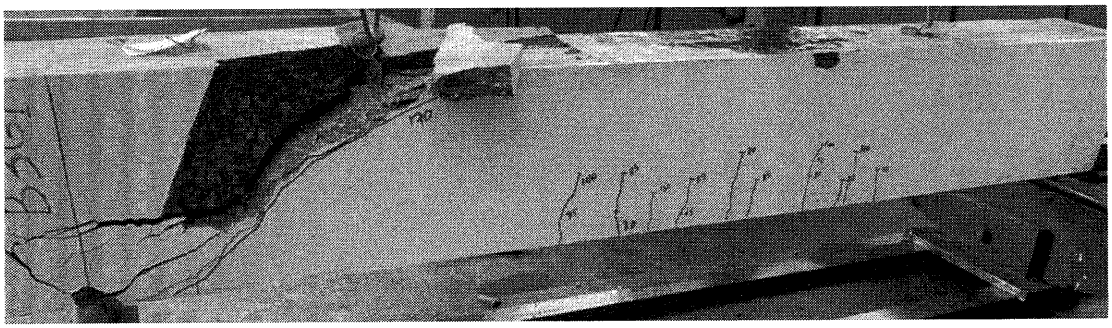


Figure 6.2 (a) Crack pattern and failure in the beam B3G1

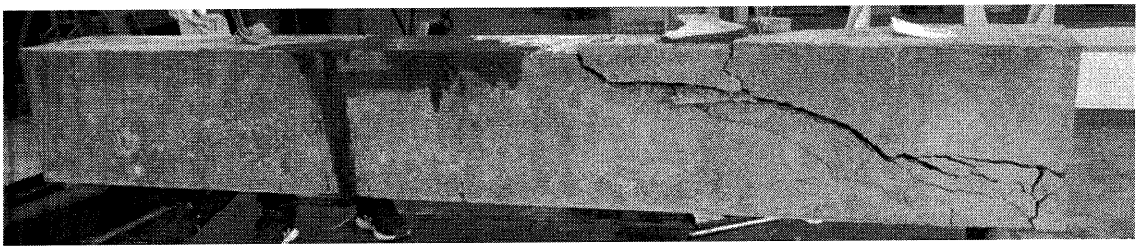


Figure 6.2 (b) Crack pattern and failure in the beam B3G1 (Other side)

For the beam B4G1 in figure 6.3 with a/d = 4.21, formation of inclined cracks corresponded to ultimate capacity and flexural failure was expected. However, the beam failed suddenly in shear and formed a diagonal crack that propagated from the mid-span between the two-point loading toward the mid-third of the shear span.

This type of failure is classified as flexure shear compression failure.

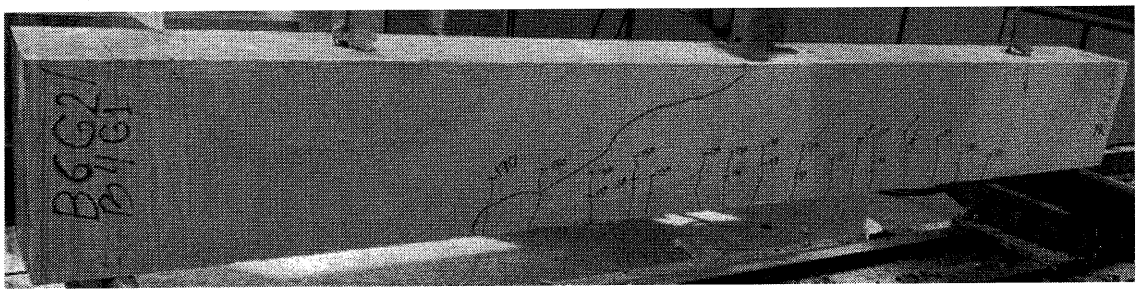


Figure 6.3 Crack pattern and failure in the beam B4G1/B6G

For the beams in G2 with $0.019 < \rho < 0.041$ and a/d = 4.21 and f_{cu} Grade C110, B4G2 in figure 6.4 with $\rho = 0.019$, the crack pattern and general behavior were the same as the beam in B3G1 because the failure took place with crushing in the concrete of the compression zone. The inclined crack that caused the failure propagated from the compression zone near the point load toward the support. The failure is classified as shear compression.

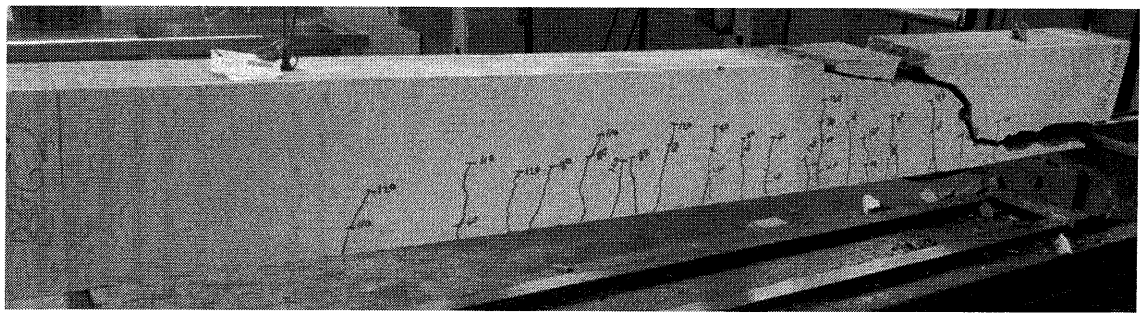


Figure 6.4 Crack a pattern and failure in the beam B4G2

For the B5G2 in figure 6.5 with $\rho = 0.031$, the crack pattern and general behavior were the same as the beam in B4G1, but the inclined crack that caused the failure propagated from the shear span in the compression zone near the point load toward the support. The failure is classified as shear compression.

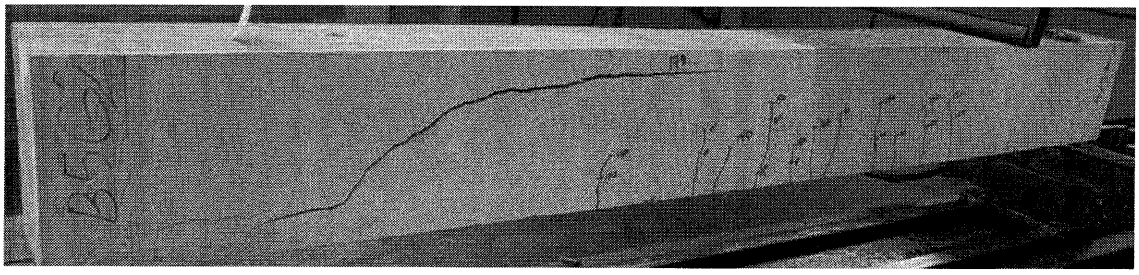


Figure 6.5 Crack pattern and failure in the beam B5G2

B6G2 in figure 6.3 with $\rho = 0.041$ is the same beam B4G1 in G1.

For the beams in G3 with (80 MPa $< f_{cu} <$ 120), (a/d = 3.16), and ($\rho = 0.041$), one-point load at mid-span was used for the two beams in these groups, B1G3 and B2G3, because the machine reached the maximum capacity, then later replaced by one-point load.

B1G3 in figure 6.6 with f_{cu} Grade C80 shows that the crack pattern and general behavior were the same as the beam in B2G1, but the inclined cracks started in the compression zone near the point load at mid span.

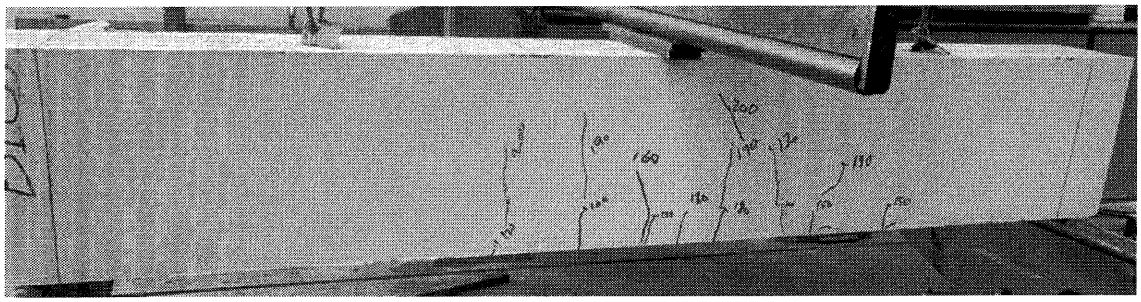


Figure 6.6 Crack pattern in the beam B1G3

B2G3 in figure 6.7 with f_{cu} Grade C100 presents that the crack pattern and general behavior were the same as the beam in B2G1, but the inclined crack that caused the failure propagated from the shear span in the compression zone near the point load at the mid-span toward the support. The failure is classified as shear compression.

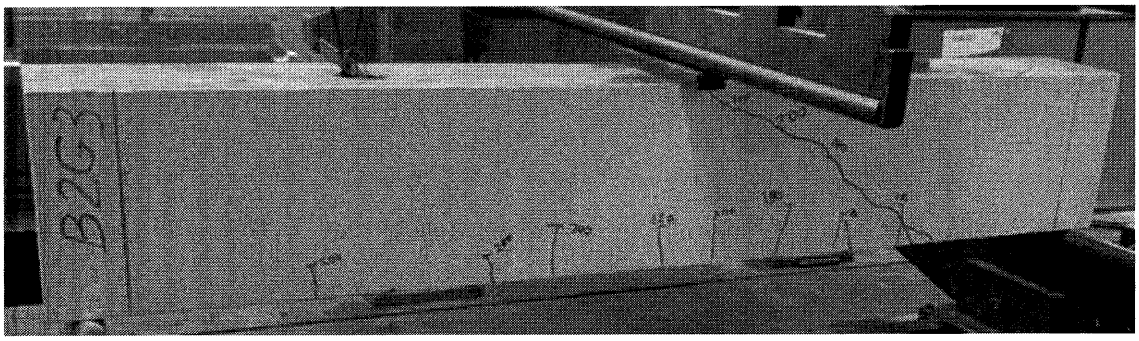


Figure 6.7 Crack pattern and failure in the beam B2G3.

Beam B3G3 in Figure 6.1 with f_{cu} Grade C110 is the same beam B2G1 in G1.

In all the groups, after the first appearance of flexure cracks and as the load increased, additional flexural and diagonal tension cracks were formed, existing cracks were lengthened and widened. Failure occurred when one of the inclined cracks propagated suddenly from shear span in the compression zone near the points loading toward support with an angle approximately 45°.

Figure 6.2 to Figure 6.10 show the crack pattern and failure for G1, G2, and G3. Table 6.1 shows the values of cracking moments, failure load, shear, and maximum moments for the tested beams. In this study, all the beams are without stirrups and the crack pattern was fully developed at a load about 85 to 95% of the ultimate load.

Table 6.1 Cracking moment, failure load, shear, and moment for the tested beams

No.	Beam No.	At First flexure cracking			At First inclined cracking			At Ultimate (failure)			Failure Mode
		P (KN)	V= P/2 (KN)	M= Pa/2 (KN)	P (KN)	V= P/2 (KN)	M= Pa/2 (KN)	P (KN)	V= P/2 (KN)	M= Pa/2 (KN.m)	
1	B2G1	100	50	31.25	190	95	59.38	220	110	68.75	SF
2	B3G1	95	47.5	35.63	180	90	67.5	210	105	78.75	SF
3	B4G1	90	45	45	170	85	85	200	100	100	SF
4	B4G2	40	20	22.1	150	75	88.4	160	80	88.4	SF
5	B5G2	70	35	38.15	170	85	92.65	180	90	98.1	SF
6	B6G2	90	45	45	190	95	95	200	100	100	SF
7	B1G3	90	45	28.13	180	90	56.25	200	100	62.5	SF
8	B2G3	97	48.5	30.31	185	92.5	57.81	210	105	65.63	SF
9	B3G3	100	50	31.25	190	95	59.38	220	110	68.75	SF

6.3 Calculation of Cracking Moments and Stresses

The ACI code, SI units ACI 318-2019 is described in section 2.3. The cracking moment is calculated, and the pre-cracking and post-cracking are shown in table 6.2 below.

Table 6.2 Cracking moment and stresses Calculation

No.	Beam No.	a/d	ρ	f_{cu} (MPa)	$M_{cr, ACI}$ (KN.m)	Stresses before cracking		Stresses after cracking		$M_{cr, test}$ (KN.m)	$M_{cr, test}$ / $M_{cr, ACI}$
						f_c (MPa)	f_s (MPa)	f_c (MPa)	f_s (MPa)		
1	B2G1	2.63	0.041	112.8	23.43	7.49	16.59	10.84	59.11	31.25	1.33
2	B3G1	3.16	0.041	111.4	23.31	7.45	16.58	10.76	58.83	35.63	1.53
3	B4G1	4.21	0.041	106.5	22.89	7.62	16.61	11.07	59.95	45	1.89
4	B4G2	4.21	0.019	107.5	22.22	7.03	22.02	10.72	96.79	22.1	1.00
5	B5G2	4.21	0,031	106.6	23.62	7.35	21.09	9.93	65.64	38.15	1.62
6	B6G2	4.21	0,041	106.5	22.89	7.62	16.61	11.07	59.95	45	1.89
7	B1G3	2.63	0.041	76.8	19.59	6.29	14.98	9.04	51.66	28.13	1.44
8	B2G3	2.63	0.041	102.2	22.51	7.18	16.54	10.26	56.96	30.31	1.35
9	B3G3	2.63	0.041	112.8	23.43	7.49	16.59	10.84	59.11	31.25	1.33

The table shows that the test cracking moment is higher than the one calculated as per the ACI code equations 2.21 to 2.26 shown in chapter 2, section 2.3.

Cracking moment

$$M_{cr} = \frac{f_r . I_{un,tr}}{h - \bar{y}_{tr}} \qquad \ldots (2.21)$$

Stresses before cracking:

$$f_c = \sigma_c = M_{cr} . \frac{\bar{y}_{tr}}{I_{un,tr}} \qquad \ldots (2.23)$$

$$f_s = \sigma_{cs} = n\, M_{cr} . \frac{d - \bar{y}_{tr}}{I_{un,tr}} \qquad \ldots (2.24)$$

Stresses after cracking:

$$f_c = \sigma_c = M_{cr} \cdot \frac{\bar{y}_{cr,tr}}{I_{cr,tr}} \qquad \ldots (2.25)$$

$$f_s = \sigma_{cs} = n\, M_{cr} \cdot \frac{d - \bar{y}_{cr,tr}}{I_{cr,tr}} \qquad \ldots (2.26)$$

6.4 Load Deflection Relationships

The reading of the total applied load (*P*) in this study of the ultra-high strength concrete beam reinforced with high strength is direct from the testing machine, while the vertical deflection of the tested beams is obtained from the dial gage reading, which was placed at the mid-span. The load deflection curve is determined as the applied shear load (*V*); which is (*P/2*) versus the maximum deflection at mid-span beam.

In this study, the variables that influence the load-deflection relationship are the span-to-depth ratio (*a/d*), flexural reinforcement (ρ), and compressive strength of concrete (f_{cu}). The results in the previous chapter (4) and figures 4.11. 4.12, and 4.13 show the load deflection curves of these variables in G1, G2, and G3.

The load deflection curves of all beams show three stages for each beam curve. Pre-cracking stage, post-cracking stage, and failure stage. The load deflection curves may be used to classify the failure type. In the pre-cracking stage, the deflection increases linearly with the loading because the strains in the steel and concrete are small and both materials are in elastic portion of their respective response. In the post-cracking stage, there is a change of slope in the load deflection curve due to cracking, but the deflection again increases linearly with an increasing load before failure. The third portion is an exceedingly small portion because the failure occurs at this stage, the load deflection curves in this portion exhibit some changes in slope.

The main variables that affected the load deflection behavior are discussed in the next sections.

6.4.1 Shear Span-to-Depth Ratio (a/d)

The load deflection curve for G1, which includes the beams B2G1, B3G1, and B4G1 is shown in figure 4.17, where the beam is without shear reinforcement and has the same longitudinal steel ratio $\rho = 0.041$, and compressive strength of concrete f_{cu} = Grade C110, but different shear span-to-depth ratio a/d. The figure shows that the beam with lower a/d ratio has a stiffer response in terms of load deflection behavior. At the same load level as a/d ratio, deflection increases. This is because the depth of the beam is constant, while the shear span increases, the (a/d) ratio increases. The results obtained in this research are similar to the results gathered by other investigators.

Wang et al. (2020) studied the shear performance of reinforced ultra-high-performance concrete rectangular section beams. One of the variables considered was the effect of a/d ratio, and the same results were obtained for load deflection curves with rapidly decreasing curve slopes for beams with large shear-span ratios.

Another research on the shear behavior of ultra-high-performance concrete beams reinforced with high-strength steel bars was conducted by Ahmad et al. (2019). The researchers found a significant reduction in shear capacity of beams with an increase in the a/d ratio. This reduction in the shear capacity of the beams with increase in the a/d may be attributed to the increase in the shear span, a, at the same effective depth, d.

6.4.2 Longitudinal Steel Ratio (ρ)

The load deflection curves of G2 which include B4G2, B5G2, and B6G2 beams without shear reinforcement show that beams have the same f_{cu} = Grade C110 and the same a/d =4.21 ratio but have different amount of longitudinal reinforcement (ρ).

Figure 4.18 presents the comparison of the effect of changing the flexural reinforcement. The findings reveal that the beam with higher steel content has a stiffer response in terms of load deflection behavior. This trend is due to the larger effective moment of inertia in the large amount of tensile reinforcement. For the same load level, the deflection increases as the tensile steel ratio decreases as shown in the same figure. The results obtained in this research are similar to the findings of other investigators.

Ahmad et al. (2019) in their study on the shear behavior of ultra-high-performance concrete beams reinforced with high-strength steel bars, found that the load deflection curve shows the effect of longitudinal reinforcement ratio (ρ). In addition, the results indicate an increase in shear load capacities and mid-span deflections with an increase in longitudinal reinforcement ratio.

Nikbakhta et al. (2019) investigated on the shear and flexural behavior of steel reinforced High-Performance Self-Compacting Concrete (HPSCC) beams and learned that increase in the longitudinal reinforcement resulted to increase in the strength of the beams but reduction in their deformation capacity.

The study of Kodur et al. (2018) presented an analysis of flexural and shear resistance of ultra-high-performance fiber reinforced concrete beams without stirrups and they found that in load deflection curve, a higher reinforcement ratio exhibited higher load.

6.4.3 Compressive Strength of Concrete (f_{cu} for (BS) or f'_c for (ACI))

The last variable in this study refers to the compressive strength of concrete (f_{cu}). Figure 4.19 shows a comparison of load deflection curves for the three beams in G3 which include B1G3, B2G3, and B3G3 beams without shear reinforcement, with the same longitudinal steel ratio $\rho = 0.041$, and shear span-to-depth ratio $a/d = 2.63$, but with different concrete strength.

The figures show that results are similar, but the higher strength concrete suffers very less deflection than a similar member with lower strength concrete at the same load level, which may be attributed to the fact that the higher strength concrete beams are stiffer than lower strength concrete beams since the modulus of elasticity of concrete is larger for the higher strength concrete than for lower strength concrete. The results obtained in this research are similar to the findings of other investigators.

Lai Zhichao et al. (2022) studied the shear behavior of high-strength square concrete filled steel tube members where four values of compressive strength of concrete were investigated: 30, 60, 90, and 120 Mpa. The findings disclosed that load deflection curves have effect of f'_c on the shear strength of high-strength concrete members that increased with increasing f'_c.

Abdullah et al. (2020) examined the reinforced concrete beams capacity with different values of concrete's compressive strength having a maximum of 89 MPa. The curves of load versus central deflection were exhibited in all the tested beams. Through the comparison curves, the findings reveal that the maximum compressive strength value of 89 MPa has a higher deflection value.

The study conducted by Aziz et al. (2013) on the shear strength and behavior of ultra-high strength performance fiber reinforced concrete deep beams without web reinforcement particularly on the three values of concrete's compressive strength: normal strength, high strength, and ultra-high strength of 134.5 Mpa reveal that failure load increased when the compressive strength increased.

6.5 Shear Strength of Beams without Web Reinforcement

6.5.1 General

The beams without shear (web) reinforcement were tested to investigate the concrete shear strength v_c of ultra-high concrete beams reinforced with high strength bars and the effect of shear span-to-depth ratio (a/d), longitudinal reinforcement ratio (ρ), and compressive strength of ultra-high strength concrete (f_{cu}).

The ultimate shear capacity of reinforced concrete beams without shear reinforcement is considered as the shear carried by concrete V_c.

$$V_u = V_c \qquad \ldots\ldots \quad (6.1)$$

ACI code for shear without reinforcement is subjected to shear and flexure only in shear strength. SI units are presented in section 2.5.1.

$$V_c = \lambda \times \left(0.16\sqrt{f'_c} + 17.2\rho_w \frac{V_u d}{M_u}\right) b_w d \qquad \ldots (2.27)$$

BS8110 is presented (In SI units)

$$V_c = 0.79\left(\frac{100A_s}{bd}\right)^{\frac{1}{3}}\left(\frac{400}{d}\right)^{\frac{1}{4}}\left(\frac{f_{cu}}{25}\right)^{\frac{1}{3}}/\Upsilon_m \qquad \ldots (2.30)$$

By using Eurocode 2, the shear capacity of the concrete is given by an empirical expression:

$$V_{Rd,c} = \left[0.12\, k(100\rho_1 f_{ck})^{\frac{1}{3}}\right] b_w d \qquad \ldots (2.31)$$

The above equations for the estimation of concrete shear strength are recommended for normal strength concrete but are considered conservative for high-strength concrete; however, used in this study for ultra-high strength concrete.

The measured shear capacity at ultimate using American ACI 319 Code, British Standard BS 8110, European Standard Eurocode 2 for each tested beam in addition to the values calculated using finite element analysis and experimental analysis are shown in tables 6.3, 6.4, and 6.5.

Experimental shear stress and finite element analysis results are compared with the ultimate shear stress by ACI 318, BS 8110, Euro code 2, and Canadian code CSA S6 using the above equations in terms of shear load and shear stress as shown in table 6.5 where calculation is by dividing the shear capacity by V/ (bw d $\sqrt{fc}$) and in table 6.6 by dividing the width (b) and the effective depth (d) of the beam.

Table 6.3 Experiment and FEA comparison of shear strength with codes

No.	Beam No.	*a/d*	ρ	f_{cu} MPa	Test		FEA		BS 8110		ACI 318		Eurocode 2	
					V_c KN	v_c MPa	V_c KN	v_c MPa	V_c KN	v_c MPa	V_c KN	v_c MPa	V_c KN	v_c MPa
1	B2G1	2.63	0.041	112.8	110	2.316	110	2.316	90.71	1.910	85.03	1.790	84.77	1.785
2	B3G1	3.16	0.041	111.4	105	2.211	105	2.211	90.33	1.902	82.45	1.736	84.42	1.777
3	B4G1	4.21	0.041	106.5	100	2.105	100	2.105	88.99	1.934	78.18	1.718	85.84	1.807
4	B4G2	4.21	0.019	107.5	80	1.524	90	1.714	73.86	1.403	81.9	1.554	68.94	1.313
5	B5G2	4.21	0,031	106.6	90	1.737	95	1.834	86.35	1.666	83.11	1.604	80.77	1.559
6	B6G2	4.21	0,041	106.5	100	2.105	100	2.105	88.99	1.934	78.18	1.718	85.84	1.807
7	B1G3	2.63	0.041	76.8	100	1.895	106	2.232	79.8	1.680	72.4	1.524	74.58	1.570
8	B2G3	2.63	0.041	102.2	105	2.211	106	2.274	87.77	1.848	81.56	1.717	82.3	1.727
9	B3G3	2.63	0.041	112.8	110	2.316	108	2.316	90.7	1.910	85.03	1.790	84.77	1.785

Table 6.4 Comparison the effect of a/d, ρ, and f_{cu} on shear strength with FEA and codes in terms of $(Vc/(bw\ d\ \sqrt{fc})$

No.	Beam No.	a/d	ρ	f_{cu} MPa	f_c' Mpa	$Vc/(bw\ d\ \sqrt{f'c})$				
						Test	FEA	BS	ACI	EC2
1	B2G1	2.63	0.041	112.8	90.24	0.24	0.24	0.20	0.19	0.19
2	B3G1	3.16	0.041	111.4	89.12	0.23	0.23	0.20	0.18	0.19
3	B4G1	4.21	0.041	106.5	85.2	0.22	0.22	0.20	0.18	0.19
4	B4G2	4.21	0.019	107.5	86	0.17	0.18	0.15	0.17	0.14
5	B5G2	4.21	0,031	106.6	85.28	0.19	0.20	0.18	0.17	0.17
6	B6G2	4.21	0,041	106.5	85.2	0.22	0.22	0.20	0.18	0.19
7	B1G3	2.63	0.041	76.8	61.44	0.24	0.28	0.21	0.19	0.20
8	B2G3	2.63	0.041	102.2	81.76	0.24	0.25	0.20	0.19	0.19
9	B3G3	2.63	0.041	112.8	90.24	0.24	0.24	0.20	0.19	0.19

Table 6.5 Comparison the effect of a/d, ρ, and f_{cu} on shear strength and with FEA and codes

Beam No.	a/d	ρ	f_{cu} MPa	f'_c MPa	Ultimate shear stress $v_u = v_c$ (MPa)					Relative shear stress			
					Test	FEA	BS	ACI	EC2	v_{test}/v_{FEA}	v_{test}/v_{BS}	v_{test}/v_{ACI}	v_{test}/v_{EC2}
B2G1	2.63	0.041	112.8	90.24	2.316	2.316	1.910	1.790	1.785	1	1.213	1.294	1.298
B3G1	3.16	0.041	111.4	89.12	2.211	2.211	1.902	1.736	1.777	1	1.162	1.274	1.244
B4G1	4.21	0.041	106.5	85.2	2.105	2.105	1.934	1.718	1.807	1	1.089	1.226	1.165
B4G2	4.21	0.019	107.5	86	1.624	1.714	1.403	1.554	1.313	0.89	1.053	1.001	1.125
B5G2	4.21	0,031	106.6	85.28	1.737	1.834	1.666	1.604	1.559	0.95	1.063	1.083	1.129
B6G2	4.21	0,041	106.5	85.2	2.105	2.105	1.934	1.718	1.807	1	1.089	1.226	1.202
B1G3	2.63	0.041	76.8	61.44	2.105	2.232	1.680	1.524	1.570	0.85	1.128	1.234	1.207
B2G3	2.63	0.041	102.2	81.76	2.211	2.274	1.848	1.717	1.727	0.97	1.196	1.287	1.28
B3G3	2.63	0.041	112.8	90.24	2.316	2.316	1.910	1.790	1.785	1	1.213	1.294	1.298

6.5.2 Effect of the Shear Span-to-Depth Ratio (a/d)

The effect of *a/d* ratio on the shear strength of tested beam with compressive strength f_{cu} Grade C110 and constant flexural steel ratio $\rho = 0.041$ is shown in tables 6.3 to 6.5 and figures 6.8 to 6.10.

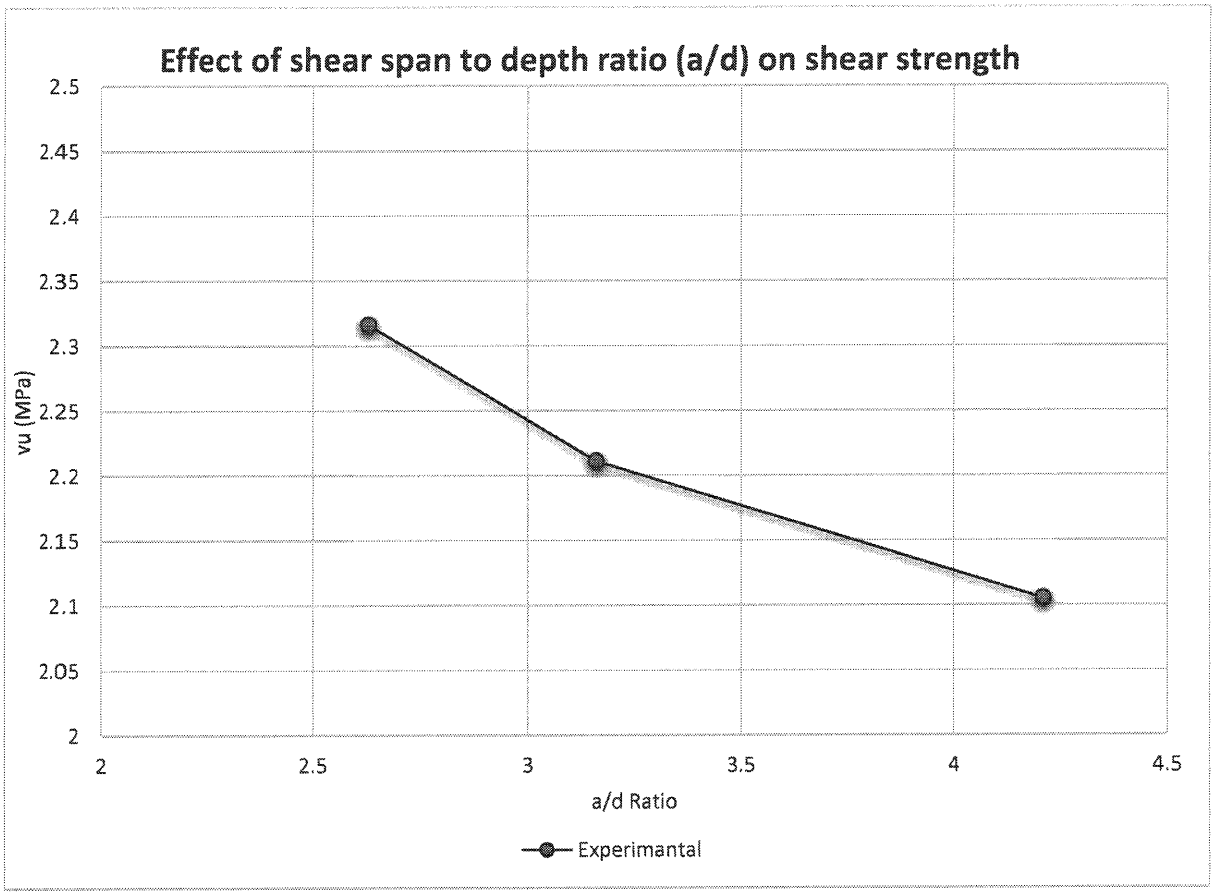


Figure 6.8 The effect of shear spa-to-depth ratio (a/d) on shear strength

The measured concrete shear strength ($V_c = V_u$) decreased sharply with the increase of a/d ratio as shown in figure 16.8. For the same applied load, larger a/d ratio means larger bending moment in the shear span, so that the penetration of the flexural cracks increases as flexural stresses near the crack tip increase. As a/d ratio increases, the flexural crack develops trend incline.

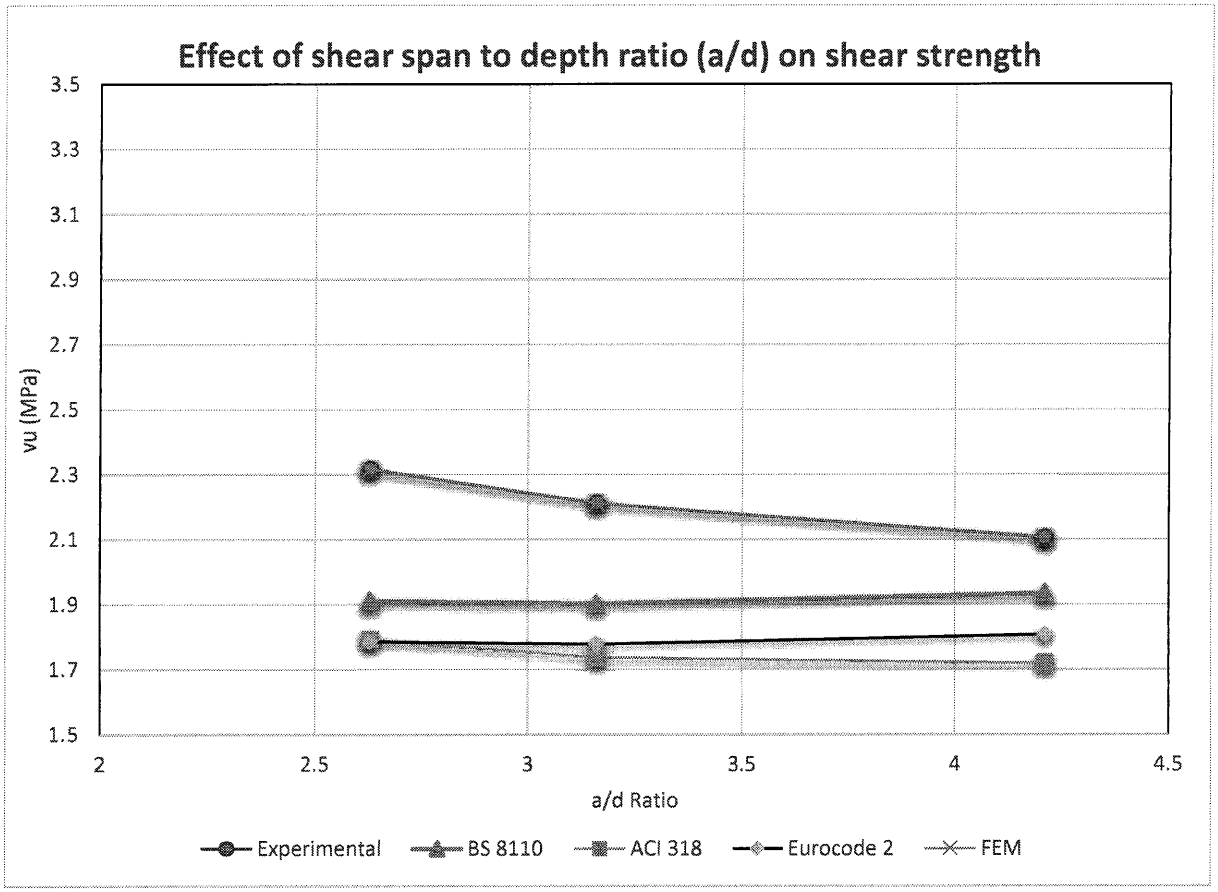


Figure 6.9 The effect of shear span-to-depth ratio (a/d) on shear strength with comparison with codes

The comparison of experimental shear strength v_c with that computed by American code ACI 318, British standard BS 8110, and Eurocode 2 equations are shown in figure 6.9.

Experimental shear strength of concrete results is consistent with ACI 318, BS 8110, and Eurocode 2 results where there is a decrease with the increase of the a/d ratio. ACI 318, BS 8110, and Eurocode 2 v_c values are close to each other, except the experimental results given above by the code equations. FEA results are presented in the next section.

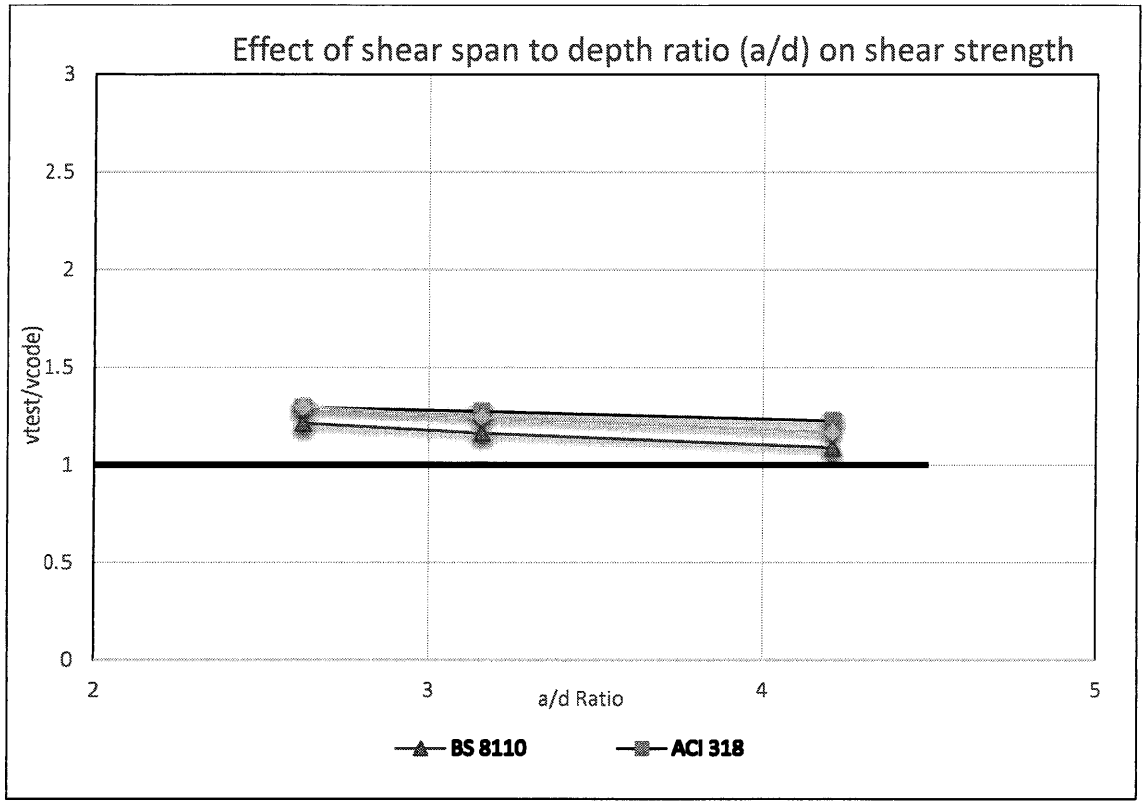


Figure 6.10 The effect of shear span-to-depth ratio (a/d) on concrete shear strength beam $v_{c,\,test}$ / $v_{c,\,BS}$, $v_{c,\,test}$ / $v_{c,\,ACI}$, and $v_{c,\,test}$ / $v_{c,\,EC2}$

Figure 6.10 presents the relative shear strength (vc, test / vc, BS, vc, test / vc, ACI, and vc, test/$v_{c,\,EC2}$) which are shown to decrease as a/d ratio increase. The value increases from 1.089 at a/d equal 4.21 to 1.213 at a/d equal 2.63 using BS 8110 equation. Increase from 1.226 at a/d equal 4.21 to 1.294 at a/d equal 2.63 is shown using ACI equation and increase from 1.165 at a/d equal 4.21 to 1.298 at a/d equal 2.63 is evident when using Eurocode 2.

It can also be seen from the above figures that the measured concrete strength was larger than that computed by ACI, BS, and EC2 equations; that these equations are understanding shear strength for all values of a/d ratio for ultra-high strength

concrete using high-strength steel bars especially at the lower ratio. This reduce factor of safety for beams of ultra-high strength concrete may be because the above building codes do not account the effect of a/d ratio on the shear strength of structural design in an ultra-high strength concrete beams reinforced with high-strength steel bars. The effect of a/d ratio in ACI 318 equation for the two-point loading of beam is denoted by the term (V_u d/M_u), that is equal to d/a, but it has an exceedingly small effect.

The above results are parallel with the findings of Wang et al. (2020) who conducted research on shear performance of reinforced ultra-high-performance concrete rectangular section beams and found that beams' shear span ratio at a certain range can obviously decrease the beams' shear capacity and Bahraq et al. (2019) who conducted an experimental and numerical investigation of shear behavior of RC beams strengthened by ultra-high performance concrete and found that as the *a/d* ratio increased, the shear capacity of the beams decreased. Moreover, other studies which are consistent with the findings of this current study include Wua et al. (2018) who examined the shear strength of reinforced concrete beams with pre-cast high-performance fiber-reinforced cementitious composite permanent found that the shear strength of the specimen with higher shear span-to-depth ratio is higher than the beams with lower shear span-to-depth ratio and finally, Kwak et al. (2002) who investigated the shear strength of steel fiber reinforced concrete beams without stirrups and found that the shear strength of members increased with decreasing span-to-depth ratio.

From the above figures and discussions, it can be deduced that the shear strength of ultra-high strength concrete beams using high steel bars are affected by the shear span-to-depth ratio and hence, must be included in the estimation of shear strength of the beams.

6.5.3 Effect of Steel Ratio (ρ) on Shear Strength

The effect of longitudinal (flexural) steel ratio ρ on the concrete shear strength of the tested beams made of ultra-high strength concrete about 110 MPa without stirrups and with concrete shear span-to-depth ratio (a/d) of 4.21 is shown in tables 6.3 to 6.5 and figures 6.11 to 6.13.

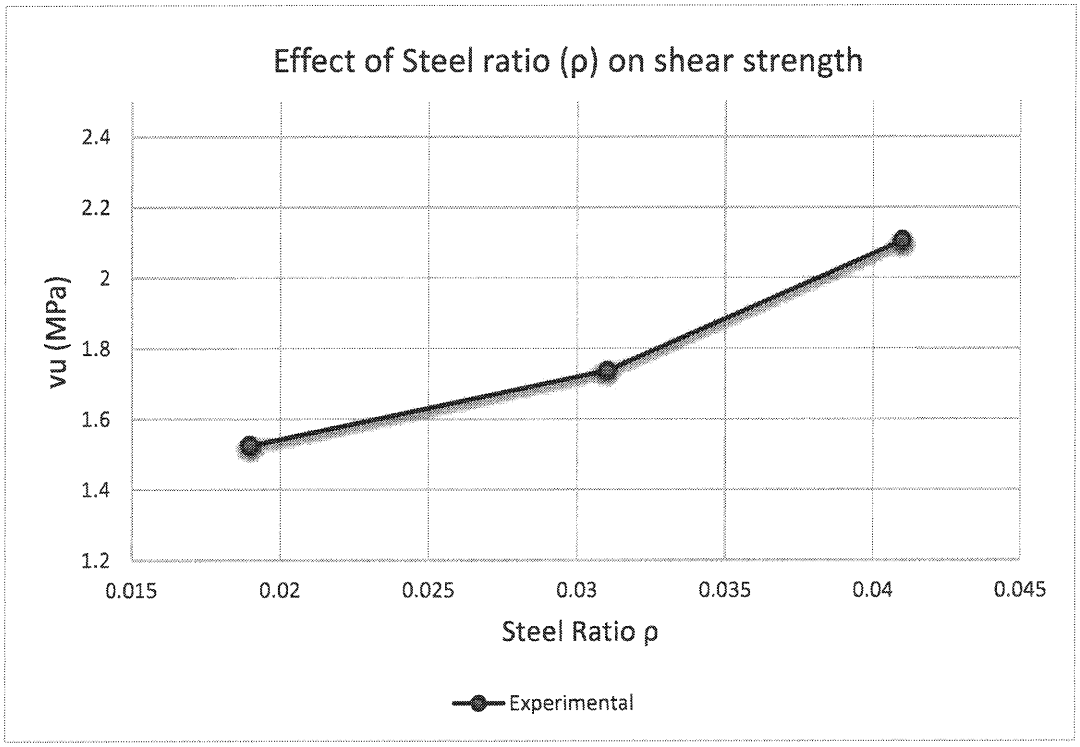


Figure 6.11 The effect of steel ratio (ρ) on shear strength

The measured concrete shear strength V that was obtained by the tested beams as shown in figure 6.11 increased as the longitudinal reinforcement ratio ρ increased.

For a given applied load, larger longitudinal steel ratio ρ means less penetration of the flexural crack. The principal stress above the flexural crack depends on the depth of penetration of the crack. The magnitude of these stresses affected the rate at which the flexural crack developed and inclined near the tip of that crack, so that the less the penetration of the flexure crack, the less the principal stresses. The

applied load must be the shear to cause principal stresses that result in diagonal tension cracking.

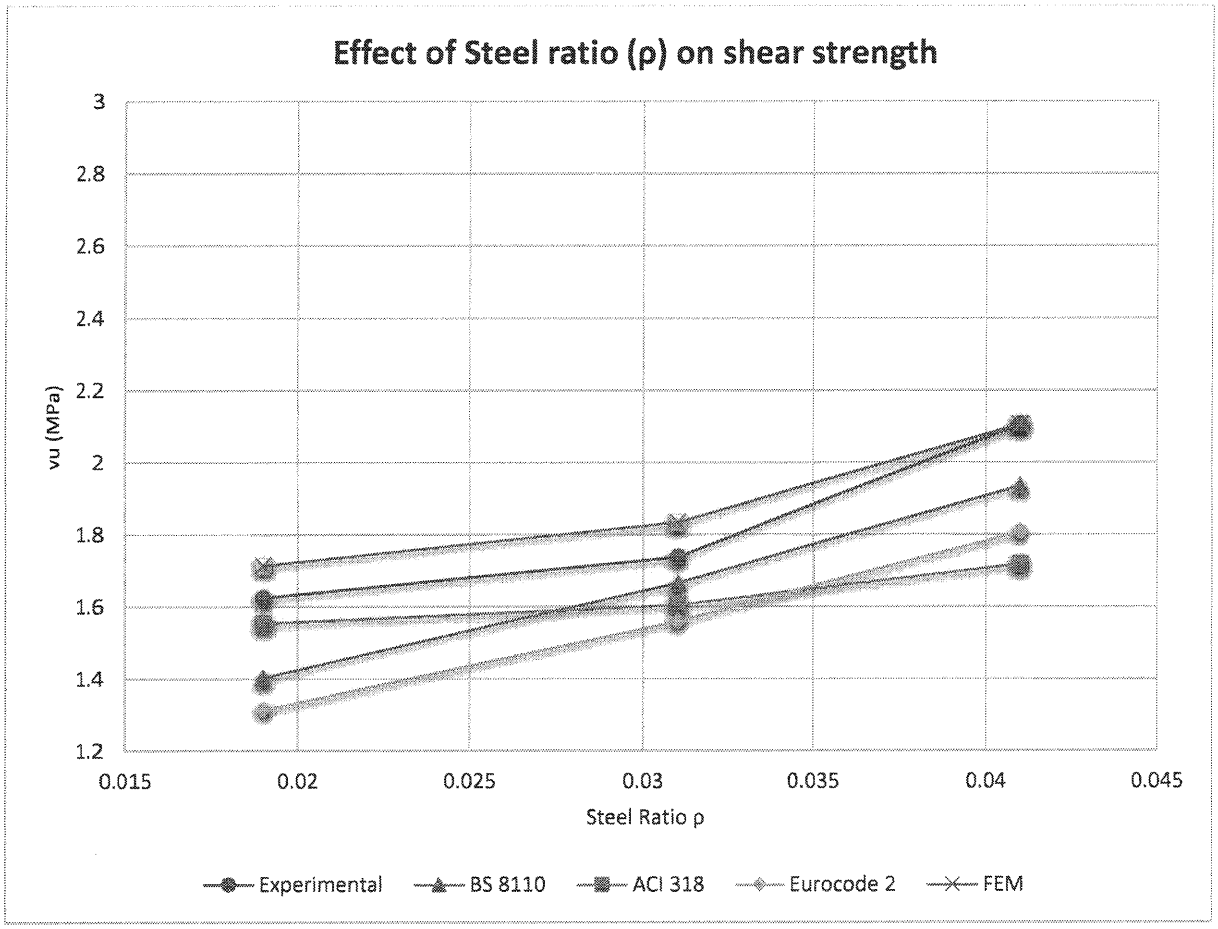


Figure 6.12 The effect of steel ratio (ρ) on shear strength with comparison with codes

The experimental results for concrete shear strength were compared using the American code ACI 318, British standard BS 8110, and Eurocode 2, as shown in figure 6.12.

Experimental shear strength of concrete results is similar with ACI 318, BS 8110, and Eurocode 2 results where there is an increase with the increase of the ρ ratio. ACI 318, BS 8110, and Eurocode 2 v_c values are close to each other as shown

in the experimental results using the code equations except for the lower value of ρ=0.019, which is equal to using ACI 318 equation. FEA results are discussed in the next section.

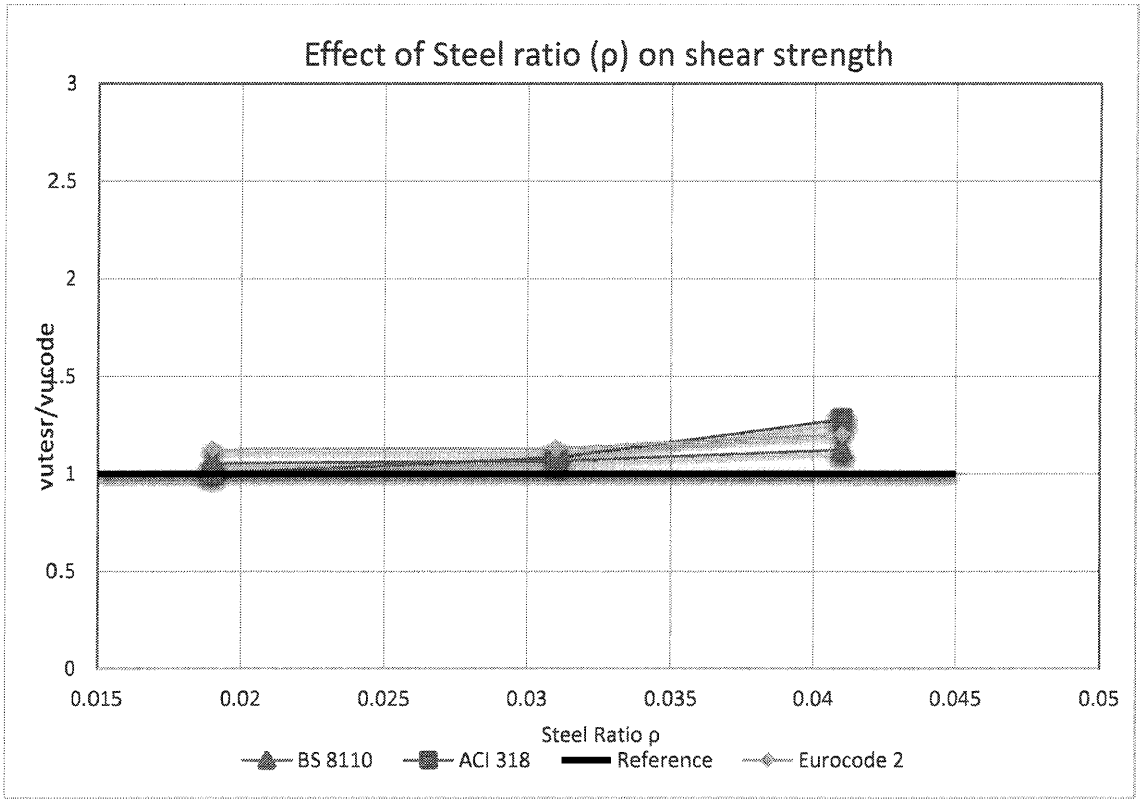


Figure 6.13 The effect of steel ratio (ρ) on concrete shear strength beam $v_{c,\,test}$ / $v_{c,\,BS}$, $v_{c,\,test}$ / $v_{c,\,ACI}$, and $v_{c,\,test}$ / $v_{c,\,EC2}$

The experimental results of concrete shear strength were compared with those computed by ACI 318, BS 8110, and Eurocode 2 equations relative to shear strength. Figure 6.13 shows that the relative shear strength (vc, test / vc, BS, vc, test / vc, ACI, and vc, test / $v_{c,\,EC2}$) increased from 1.053 for ρ equal to 0.019 to 1.123 for ρ equal to 0.041 in BS 8110, increased from 1.001 for ρ equal to 0.019 to 1.279 for ρ equal to 0.041 in ACI 318, and increased from 1.125 for ρ equal to 0.019 to 1.202 for ρ equal to 0.041 in Eurocode 2. Further, it can be seen from the abovementioned figures that the measured concrete shear strength is larger than those computed by

the above code equations and are underestimated for ultra-high strength concrete beams especially for the higher ρ. This is because the effect of ρ on shear strength is disregarded by these structural design codes in ultra-high strength concrete beams reinforced with high-strength steel bars.

The above results are similar with the findings of different researchers including Ahmad et al. (2019) who found that shear load capacity hardly increased with increasing longitudinal reinforcement ratio; Nikbakhta et al. (2019) who concluded from their study on the shear and flexural behavior of steel reinforced HPSCC that the increase in longitudinal reinforcement results to the increase in the strength of the beams; and Kodur et al. (2018) who learned from their study that beams with a higher reinforcement ratio reveal higher load.

It is clear from the above studies that the longitudinal reinforcement ratio affects the concrete shear strength of ultra-high strength concrete beams reinforced with high steel bars.

6.5.4 Effect of Compressive Strength of Concrete on Shear Strength

The concrete shear strength V_c was affected by the uniaxial compressive strength of concrete f_{cu} for the tested beams with f_{cu} ranging from 76.8 to 112.8 MPa with constant a/d ratio of 4.21and constant longitudinal reinforcement ratio ρ of 0.041without stirrups as shown in tables 6.3 to 6.5 and figures 6.14 to 6.16.

The shear strength of concrete V_c of the tested beams increase as the compressive strength of concrete f_{cu} as indicated by BS code or (f'_c as denoted by ACI code) increased as shown in figure 6.20. At the same load level, larger f_{cu}

indicates larger shear strength for the tested beams as expected. The shear is resisted mostly by the concrete's shear stress until the cracking load. Then the aggregate interlocks, dowel action of the longitudinal reinforcing bars and resistance of the beam after the cracking load is still with untracked concrete at the top fiber (Meqdadi., 1993).

According to Elzanaty et al. (1986) the surface roughness and the amount of opening at the crack affects the percentage of the shear resistance carried by the aggregate interlock.

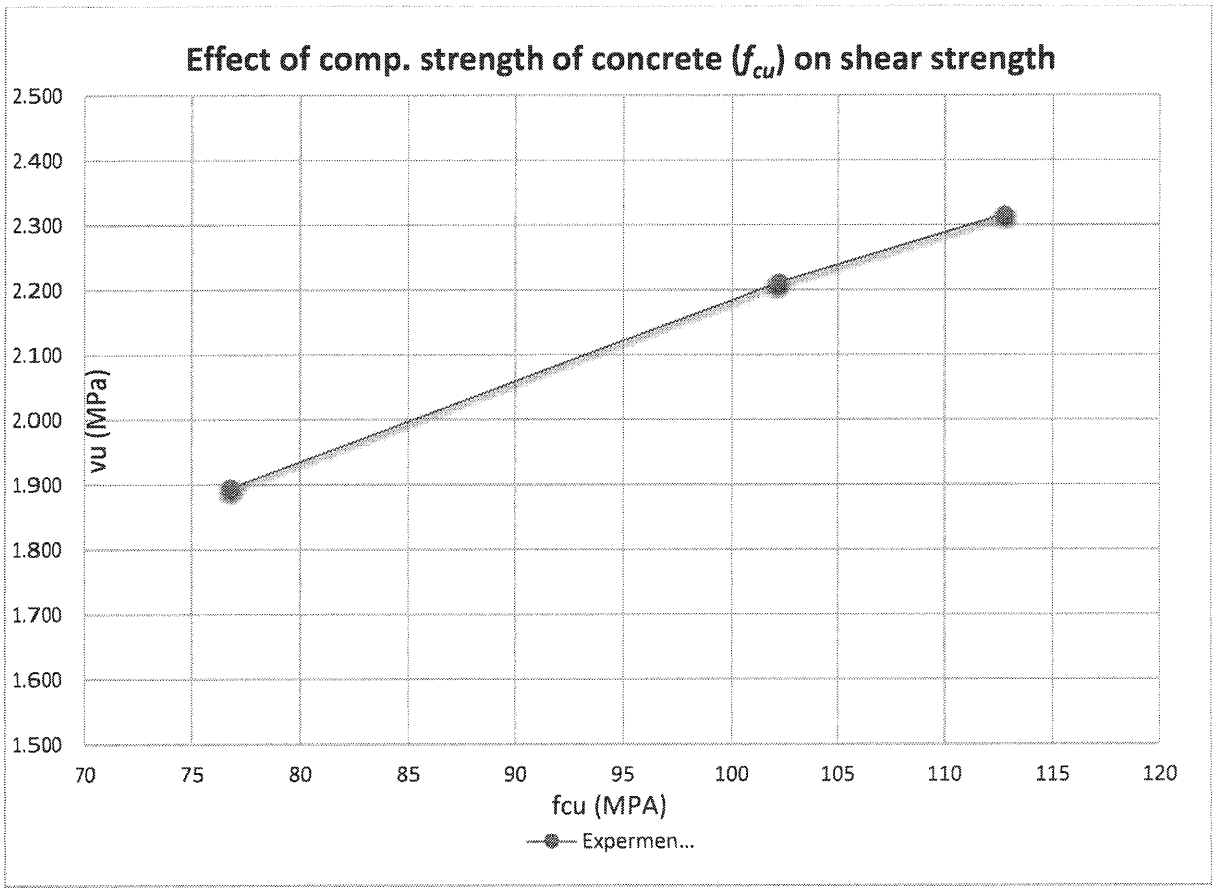


Figure 6.14 The effect of compressive strength of concrete (f_{cu}) on shear strength

The tested beams in this investigation show that the crack surface for higher concrete strength is smoother, indicating that the shear strength carried by aggregate

interlock decreases with increasing f_{cu}. After cracking, part of the shear displacement along the crack is resisted by dowel action of the longitudinal steel giving rise to vertical tension in the surrounding concrete and another part by the untracked concrete, which depends also on f_{cu} as well as on the area of the compression zone above the crack. These three parts that resist shearing are independent and are not easy to separate.

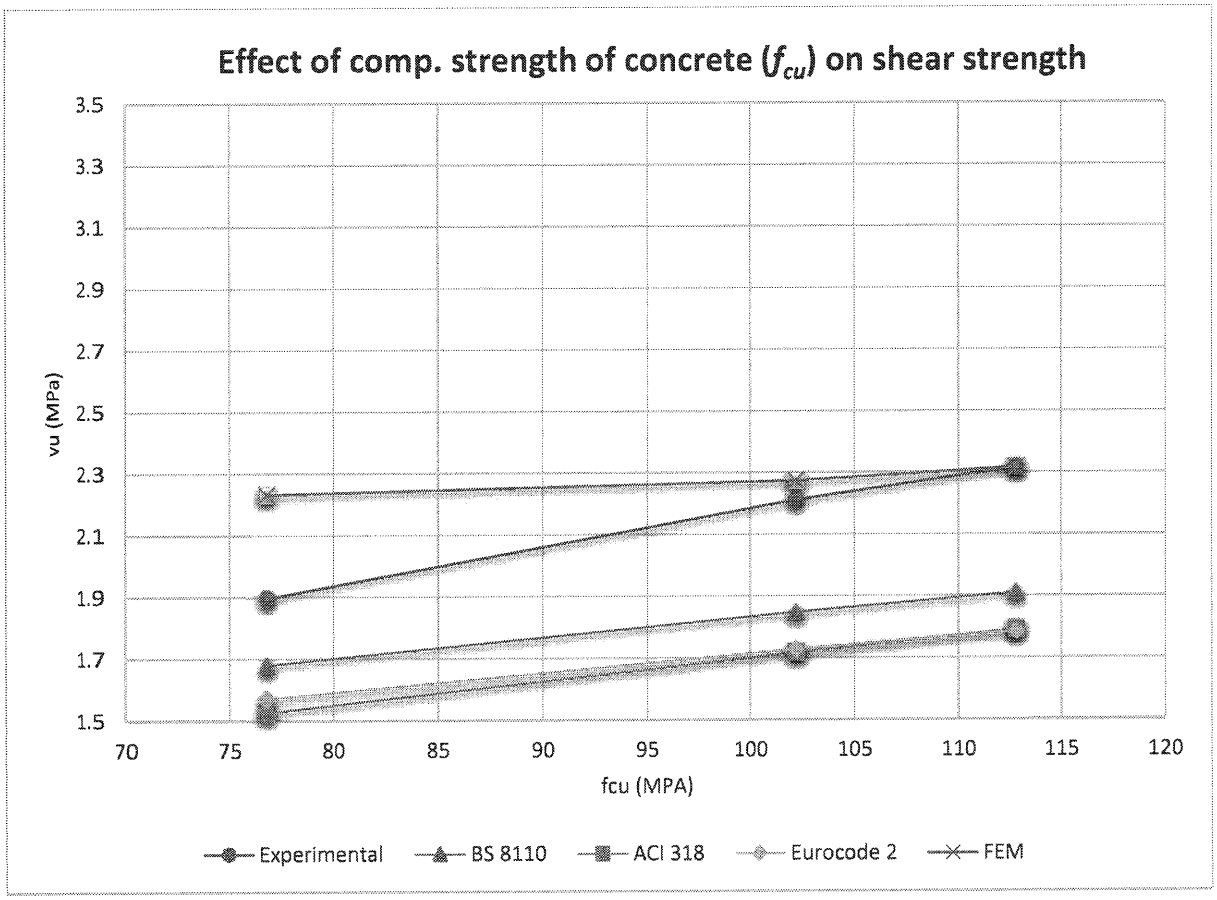


Figure 6.15 The effect of compressive strength of concrete (f_{cu}) on shear strength with comparison with codes V_c

The concrete shear strength test results were compared with those calculated by American code ACI 318, British standard BS 8110, Eurocode 2, and Canadian Standards Association CSA S6 equations as shown in figure 6.18.

The experimental shear strength of concrete results is similar with ACI 318, BS 8110, and Eurocode 2 results where there are increase with the increase in f_{cu}. ACI 318, BS 8110, and Eurocode 2 v_c values are closed to each other as indicated in the experimental results through the given code equations.

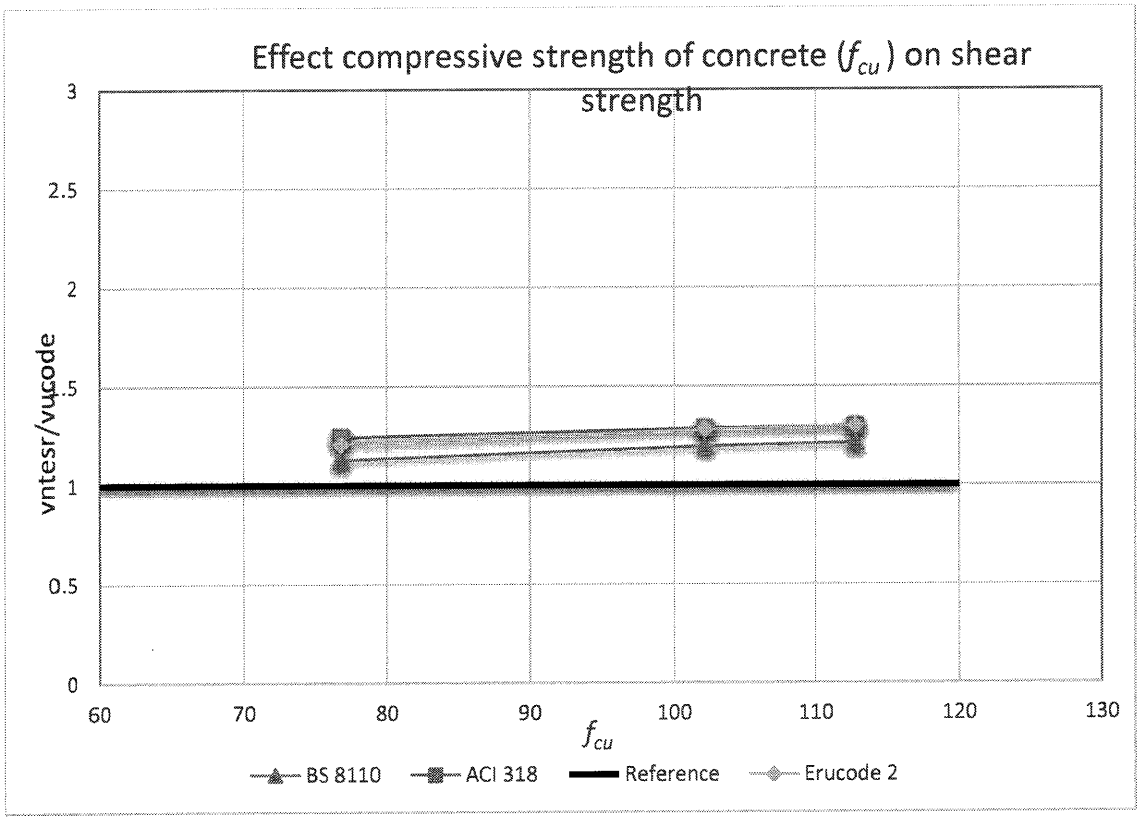


Figure 6.16 The effect of compressive strength of concrete (f_{cu}) on concrete shear strength beam $v_{c,\,test}$ / $v_{c,\,BS}$, $v_{c,\,test}$ / $v_{c,\,ACI}$, and $v_{c,\,test}$ / $v_{c,\,EC2}$

The experimental result for concrete shear strength were compared with the computed by ACI 318, BS 8110 and Eurocode 2 equations as relative shear strength. Figure 6.16 shows that the relative shear strength ($v_{c,\,test}$ / $v_{c,\,BS}$, $v_{c,\,test}$ / $v_{c,\,ACI}$, and $v_{c,\,test}$ / $v_{c,\,EC2}$) increased from 1.128 for f_{cu} equal to 76.8 MPa to 1.213 for f_{cu} equal to 112.8 MPa in BS 8110, increased from 1.243 for f_{cu} equal to 76.8 MPa to 1.294 for f_{cu} equal to 112.8 in ACI 318, and increased from 1.207 for f_{cu} equal to 76.8 MPa to

1.298 for f_{cu} equal to 112.8 MPa in Eurocode 2. Also, it can be seen from the above figures that the measured concrete shear strength was larger than those computed by the above code equations and were underestimated for ultra-high strength concrete beams especially for the higher f_{cu}. This reduces the factor of safety for beams with ultra-high strength concrete. BS 8110 equation gives a better result than ACI code equation because ACI building code related the strength of concrete f_{cu} or f'_c as denoted by ACI through a power equal to the power (0.5) while the BS 8110 related the strength to the power equal to (1/3) that is, the actual increase in shear strength may be closer to $(f_{cu})^{1/3}$ as reported by many investigators (Zsutty, 1968).

The test results of concrete shear strength were compared with those computed by ACI 318, BS 8110, and Eurocode 2 equations relative to shear strength. Figure 6.22 shows that the relative shear strength (vc, test / vc, BS, vc, test / vc, ACI, and vc, test / $v_{c, EC2}$) increased from 1.128 for f_{cu} equal to 76.8 MPa to 1.213 for f_{cu} equal to 112.8 MPa in BS 8110, increased from 1.243 for f_{cu} equal to 76.8 MPa to 1.294 for f_{cu} equal to 112.8 in ACI 318, and increased from 1.207 for f_{cu} equal to 76.8 MPa to 1.298 for f_{cu} equal to 112.8 MPa in Eurocode 2. In addition, it can be seen from the abovementioned figures that the measured concrete shear strength was larger than the ones computed by the above code equations and were underestimated for ultra-high strength concrete beams especially for the higher f_{cu}. This reduces the factor of safety for beams with ultra-high strength concrete. BS 8110 equation gives better result than ACI code equation because ACI building code related the strength of concrete f_{cu} or f'_c as denoted by ACI through a power equal to the power (0.5) while the BS 8110 related the strength to the power equal to (1/3) and that is an actual increase in shear strength which may be closer to $(f_{cu})^{1/3}$ as reflected in various researchers (Theodore, 1968).

BS8110 as shown in the above figures was underestimated for all values of f_{cu} but is more accurate than ACI code and Eurocode 2. Eurocode 2 also related the strength to the power equal to (1/3) for the estimation of the concrete shear strength of the tested beam. This may be because BS 8110 uses the compressive strength of cubes instead of cylinder. Table 6.4 shows that the cylinder compressive strength is about 0.8, the cube compressive strength of concrete.

All the above figures show that the compressive strength of concrete has an effect on concrete shear strength for the structural design of ultra-high strength concrete beams reinforced with high strength steel bars.

The above findings were consistent with research outcomes of Lai et al. (2022) who found that the shear strength of members increased with increasing (f'_c) because the elastic modulus (shear modulus) of concrete increased with increasing(f'_c); Aziz et al. (2013) whose experiment revealed that the failure load increased when the compressive strength increased (shear strength); and Kwak et al. (2002) whose findings indicated that the shear strength of members increased with increasing compressive shear strength.

6.6 Data Analysis and Discussion for FEM Results

6.6.1 General

This section discusses the 3D Finite FEA models in chapter 5 that show the investigation on the shear behavior of ultra-high strength concrete reinforced with high strength bars. The FEA models were developed using ANSYS (2021/R2).

Farooq et al. (2014) explains that ANSYS is a software appropriate in engineering simulation based on finite element methods for it can solve problems from simple linear analyses to the most complicated non-linear simulations.

The models were used in analyzing the shear behavior of the beams and in conducting parametric studies to further investigate the effect of shear span-to-depth ratio (a/d), longitudinal steel reinforcement ratio (ρ), and compressive strength of concrete (f_{cu}).

G1 beams are to study on the shear span-to-depth ratio with beams having (a/d) ratios of (2.63, 3.16 and 4.21), and all with ($\rho = 0.041 = 1.1\ \rho_b$ and fcu Grade C110). G2 beams are to study on the longitudinal steel reinforcement ratio with beams having (ρ) equal to (0.019, 0.031, and 0.041). These values with respect to the (ρ_b) are (0.521 ρ_b, (0.838 ρ_b, and (0. 1.487 ρ_b). G3 beams are to study on the compressive strength of concrete with beams having (f_{cu}) equal to (76.8, 102.2 and 112.8) and all with ($\rho = 0.041 = 1.1\ \rho_b$ and $a/d = 2.63$).

6.6.2 Materials and Modelling

The concrete beam is modeled with an eight-node Solid65 element with three degrees of freedom at each node. Link180 spar element with three degrees of freedom per node is used to model the steel reinforcement. The columns and loading points are modeled with eight-nodded Solid180 elements.

Table 5.1 shows the Menetrey-Wiliam model, softening base for concrete, stress strain for concrete based on the fuzzy model, dilation angle affecting the amount of plastic volume deformation assuming 30°, and other concrete properties while table 5.2 presents the properties of steel reinforcement and figure 5.5. exhibits the properties of steel bearing plate.

A parametric study on the mesh size was carried out in section 5.6.1 with different mesh sizes. A mesh size of 40 mm predicted good post-yield response in the beams selected for validation.

6.6.3 Load Deflection Relationships

The mid-span deflection curves throughout the loading for the tested beams using FEA are presented in section 5.7. In the load-deflection curves of beams without web reinforcements, linear up to failure were noticed in most of the beams especially for beam with high reinforcement steel ratio ($\rho > \rho_b$) and low (a/d) ratio.

6.6.3.1 Shear Span-to-Depth Ratio (a/d)

Figure 5.27 shows the load deflection curves for G1 beams with a/d ratio as a variable and same f_{cu} Grade C110, and $\rho > \rho_b$, B2G1 and B3G1 with a/d =2.63, and 3.16 show linear relationship while B4G1 shows linear up to 70% then start non-linear up to failure, this is because this beam has higher a/d =4.21.

The results show that the beams with a higher a/d ratio experienced a higher deflection than those with a lower a/d ratio. The shear load decreased as a/d ratio increased, and this is in line with the experimental results.

6.6.3.2 Longitudinal Steel Ratio (ρ)

Figure 5.34 shows the load deflection curves for G2 beams with (ρ) ratio as a variable and the same f_{cu} Grade C110 and a/d = 4.21. B4G2 with $\rho = 0.019 < \rho_b$, shows linear up to 55% then start non-linear up to failure. B5G2 with $\rho = 0.031 < \rho_b$, shows linear up to 65% then start non-linear up to failure. B4G1 with $\rho = 0.041 > \rho_b$, shows linear up to 75% then start non-linear up to failure.

The results show that the beams with a higher (ρ) ratio experienced a higher deflection than those with a lower ρ ratio. The shear load increased as (ρ) ratio increased and this is consistent with the experimental results.

6.6.3.3 Compressive Strength of Concrete (f_{cu})

Figure 5.39 shows the load deflection curves for G3 beams with f_{cu} ratio as a variable and the same $\rho = 0.041 > \rho_b$, and $a/d = 2.63$. All beams B1G3, B2G3, and B3G3 show a linear relationship and the results are remarkably close to each other.

The results show that the beams with a higher f_{cu} experienced a little higher deflection than those with a lower f_{cu}. The shear load increased as little f_{cu} increased, and this is parallel with the experimental results.

6.6.4 Shear Strength of Beams without Web Reinforcement

Table 6.3 to table 6.5 show the measured shear capacity at ultimate using American ACI 319 Code, British Standard BS 8110, European Standard Eurocode 2, and Canadian code CSA S6 for each tested beam in addition to the values completed through finite element analysis and experimental analysis.

6.6.4.1 The Effect of the Shear Span-to-Depth Ratio (a/d)

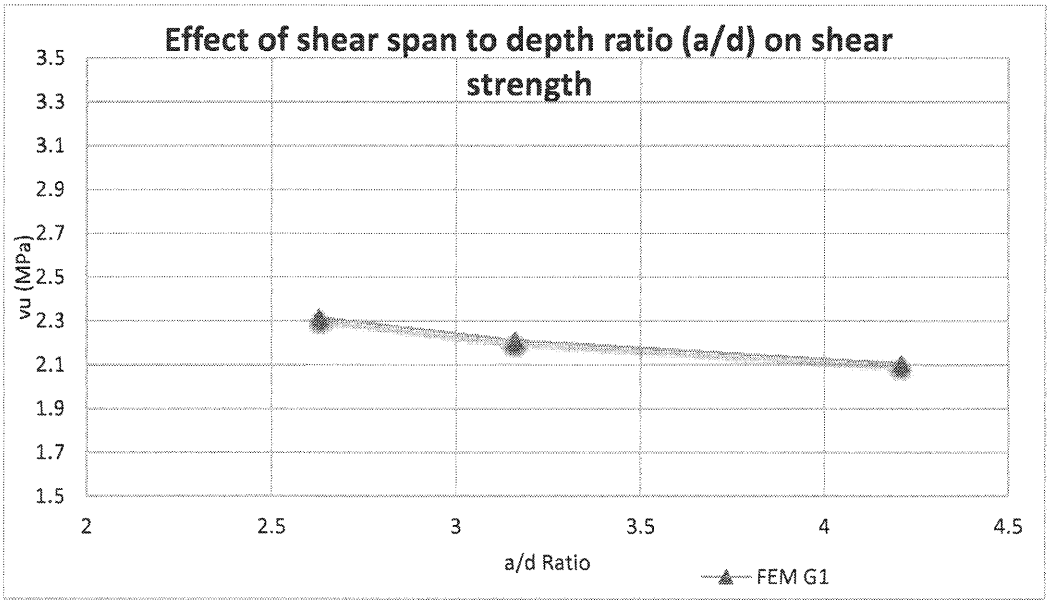


Figure 6.17 The effect of shear span-to-depth ratio (a/d) on shear strength

Figure 6.17 shows the effect of shear span-to-depth ratio a/d on shear strength of ultra-high strength of concrete beams reinforced by high strength steel using finite element analysis. The results indicate the shear strength decreases with increasing a/d; this is aligned with the experimental results.

6.6.4.2 Effect of Steel Reinforcement Ratio (ρ) on Shear Strength

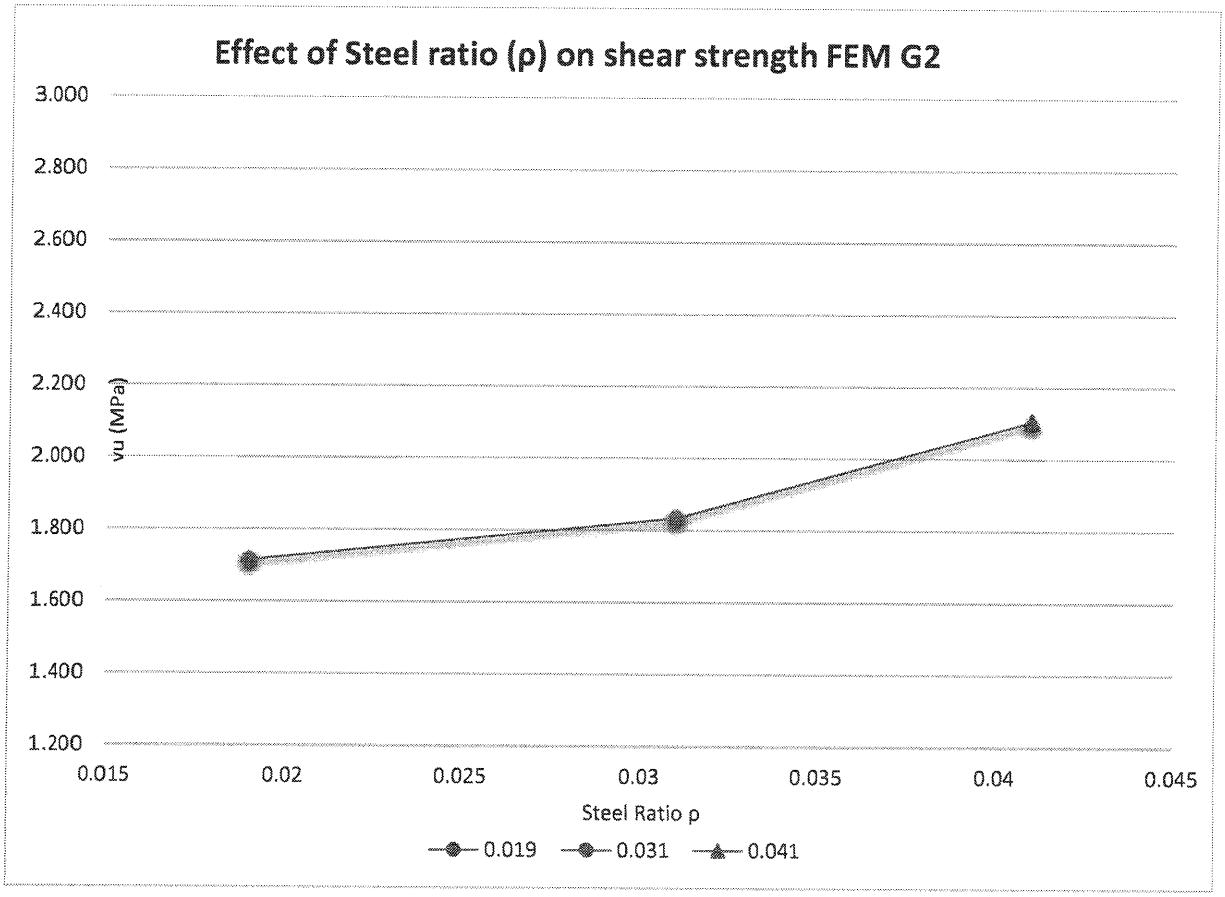


Figure 6.18 The effect of steel ratio (ρ) on shear strength

Figure 6.18 presents the effect of steel ratio (ρ) on shear strength of ultra-high strength of concrete beams reinforced by high strength steel using finite element analysis. The results disclose that the shear strength is increased with increasing (ρ), and this is coherent with the experimental results.

6.6.4.3 Effect of Compressive Strength of Concrete (f_{cu}) on Shear Strength.

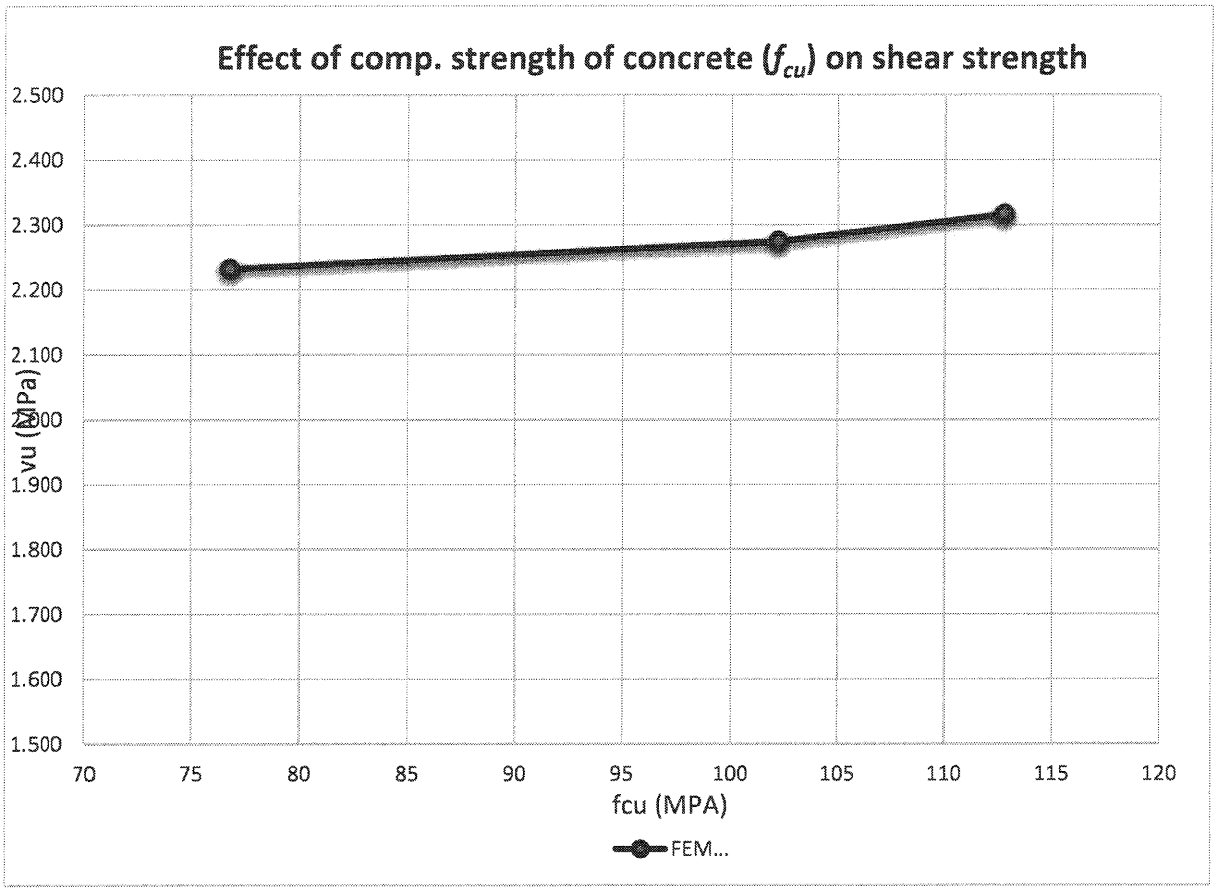


Figure 6.19 The effect of compressive strength of concrete (f_{cu}) on shear strength

Figure 6.19 displays the effect of steel ratio (f_{cu}) on shear strength of ultra-high strength of concrete beams reinforced by high strength steel using finite element analysis. The results reveal that the shear strength is increased with increasing (f_{cu}). The findings are consistent with the experimental results.

6.6.5 FEM Results and Experimental Results Comparison

The aim of this study is to compare the experimental results with numerical results using the finite element method. Experimental analysis is widely done to

study the behavior of shear of reinforced concrete beams under various loading and boundary conditions and the structure's actual behavior.

According to Badiger et al. (2014) FEA is a method used in evaluating structures with an accurate prediction of the component's response subjected to various structural loads. The method is faster and cost-effective compared to the experimental method. On the one hand, FEM is used to model the complex behavior of reinforced concrete beams.

6.6.5.1 Load Deflection Relationships

The effect of span-to-depth ratio in G1 is shown in section 5.7.1. The beams B2G1 and B3G1 presented in figures 5.22 and 5.24 show a linear relationship in FEA but the experimental result shows approximately 60% linear then non-linear up to failure. In the linear part, there is a small difference in reading the deflection for the same applied load. B4G1 in figure 5.26 shows a linear relationship in FEA but the experimental result is up at approximately 80% linear then non-linear up to failure. In the linear part, the reading of deflection is equal to the same applied load.

The effect of longitudinal steel ratio in G2 is shown in section 5.7.2. The beams B4G2 and B5G2 are presented in figures 5.22 and 5.24. The load deflection relationship in FEA is in line with the experimental results where B6G2 is the same beam as B4G1.

The effect of concrete compressive strength in G3 is shown in section 5.7.3 while beams B1G3, B2G3, and B3G3 are shown in figures 5.36, 5.38, and 5.40. The relationship of all beams shown in FEA is linear but the experimental B1G3 up is approximately 90% linear then non-linear up to failure. In the linear part, the deflection readings are aligned with the same applied load. For B2G3 and B3G3, the experimental result is up by approximately 70% linear then non-linear up to failure.

In the linear part, the reading of deflection has some difference with the same applied load for B2G3 and B3G3.

6.6.5.2 Shear Strength of Beams

The comparison of the effect of span-to-depth ratio on concrete strength in the experimental results and finite element method show an ultimate concrete shear strength V_u, which decreased with the increase of a/d ratio as shown in figure 6.20 for the same applied load. The value of shear strength by FEM in this group is match with the value of the experimental method.

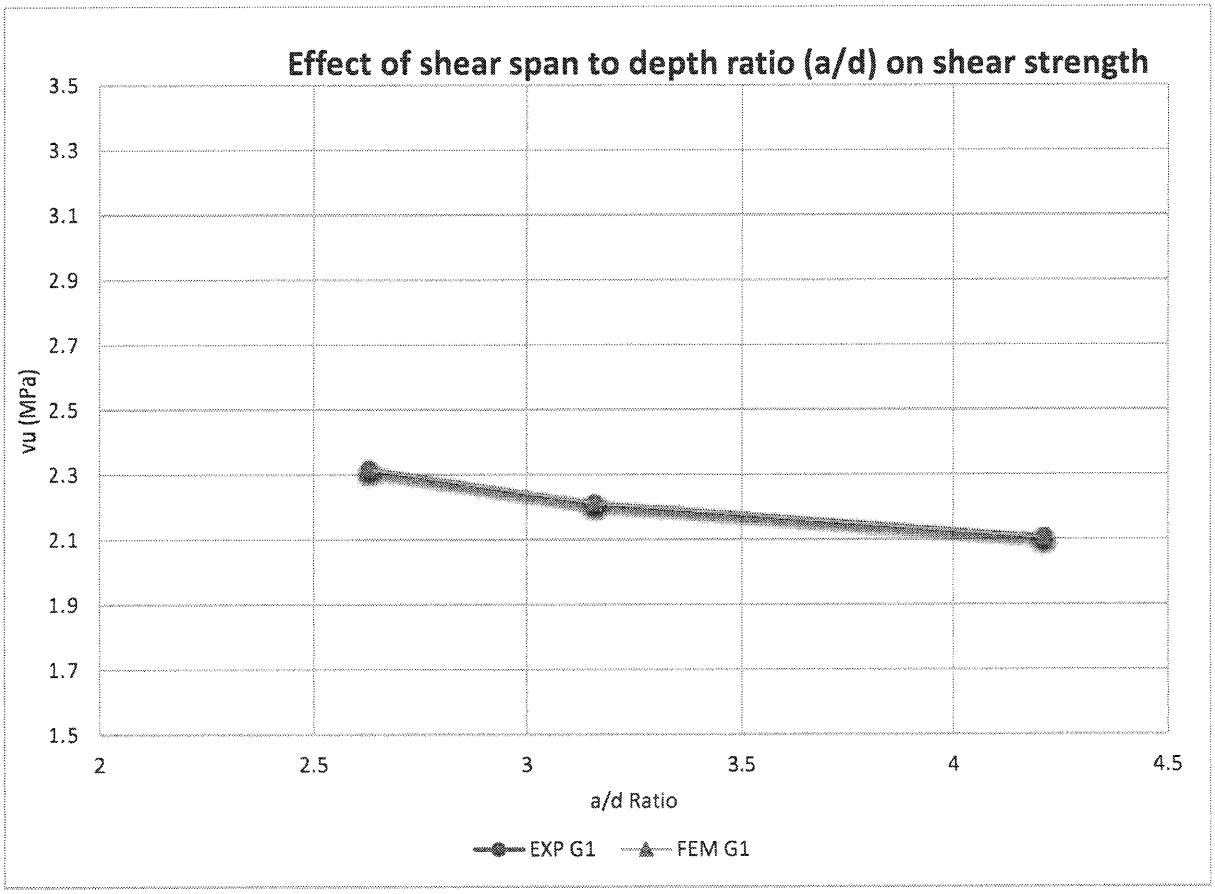


Figure 6.20 Comparison the effect of shear span-to-depth ratio (a/d) on shear strength Experimentally and by using FEM

The comparison of the effect of longitudinal steel ratio on concrete strength present that both experimental results and finite element method show an ultimate concrete shear strength Vu, which increased with the increase of ρ ratio as shown in figure 6.21 for the same applied load. The value of shear strength by FEM in this group is about 6% more than experimental method.

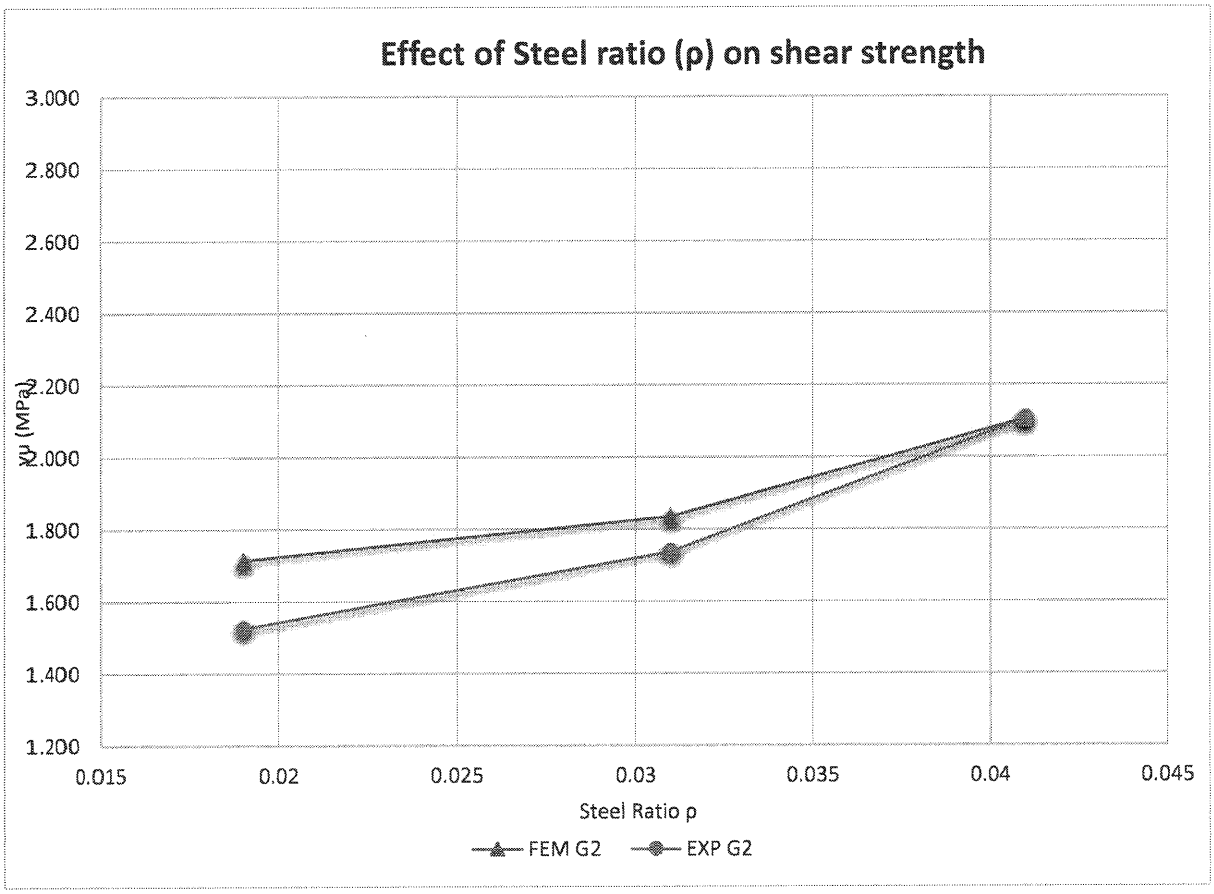


Figure 6.21 Comparison the effect of longitudinal steel ratio (ρ) on shear strength Experimentally and by using FEM

The comparison of the effect of compressive strength on concrete strength shows that both experimental results and finite element method have an ultimate

concrete shear strength V_u, which increased with the increase of f_{cu} as shown in figure 6.22 for the same applied load. The value of shear strength by FEM in this group is about 6.5% more.

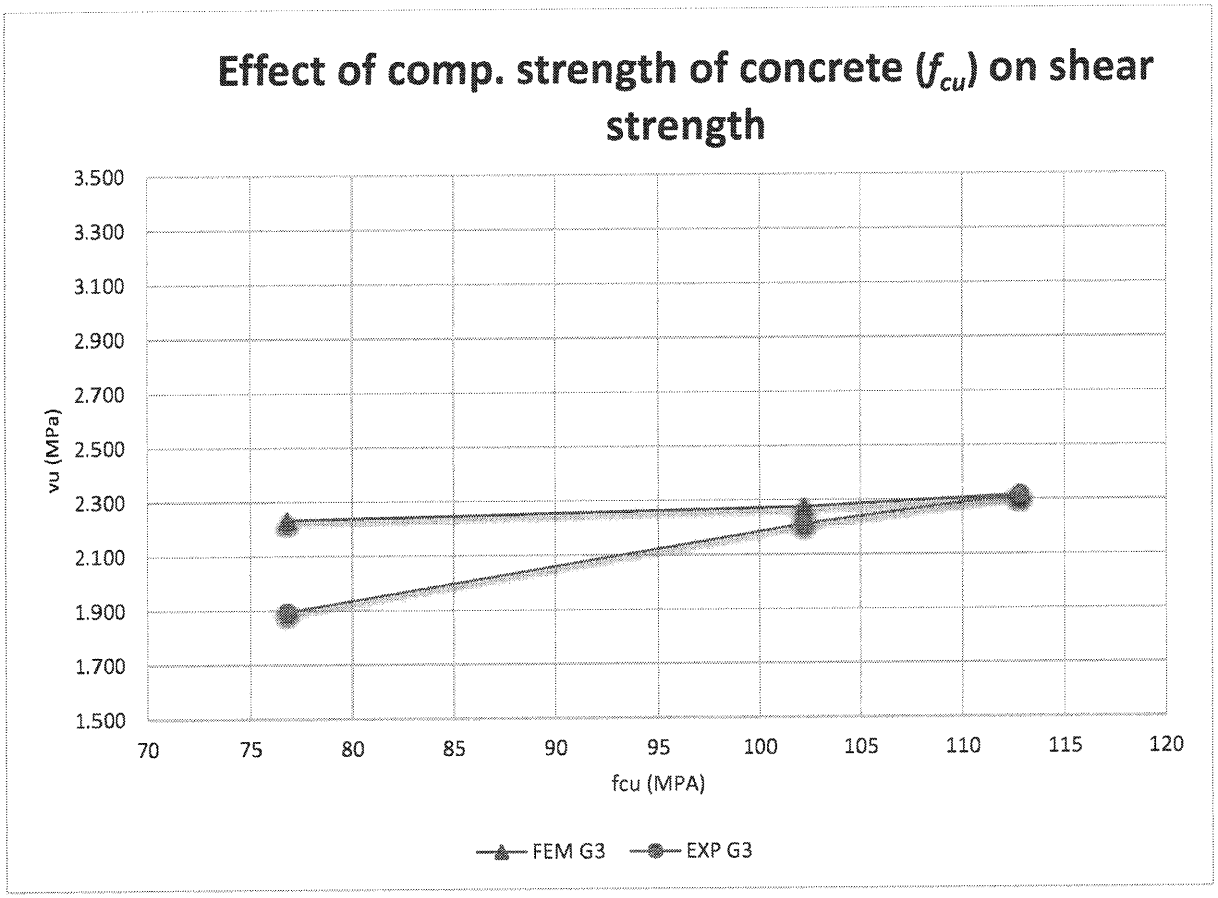


Figure 6.22 Comparison the effect of concrete compressive strength (f_{cu}) on shear strength Experimentally and by using FEM

6.6.6 Linear Relationship from Literature on the Load Deflection Curve

Abd Hamid1 et al. (2018) performed a finite element analysis of a smart reinforced concrete beam with flexible shape memory alloy under stagnant loading for seismic mitigation.

Using FEM modelling in ANSYS for simply supported RC beams with smart rebars, the control beam was subjected to static load where the material employed was the super elastic shape memory alloys (SESMA). The SESMA is a unique alloy that can undergo large deformations and return to an unreformed shape.

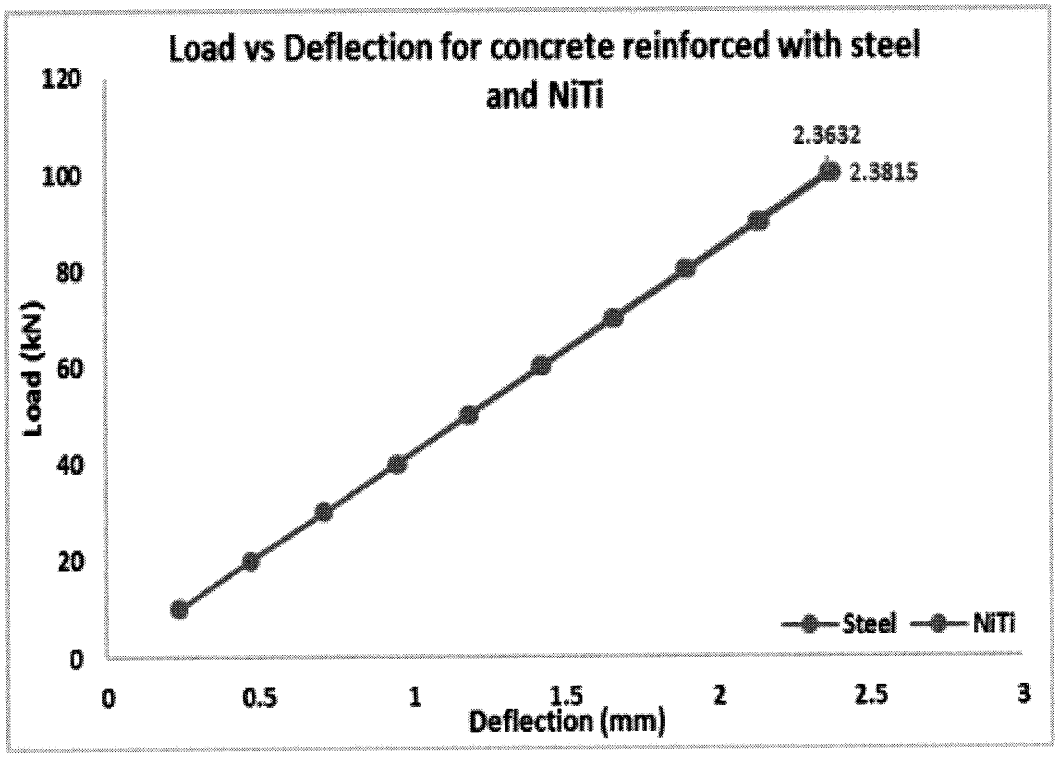


Figure 6.23 Load vs deflection of concrete reinforced with steel and NiTi (Abd Hamid1 et al., 2018)

The deflection of both steel and NiTi reinforced concrete beam with nickel titanium alloy is increasing linearly with the increase of load. The result of the maximum deformation analysis by finite element model on NiTi and conventional reinforced concrete beam are shown in figure 6.23.

Antonio et al. (1998) investigated a reinforced concrete structure using ANSYS non-linear concrete model.

A simply supported reinforced concrete beam was subjected to uniformly distributed loading. Longitudinal reinforcement has been considered and concrete model in ANSYS using Drucker-Prager yielded criterion.

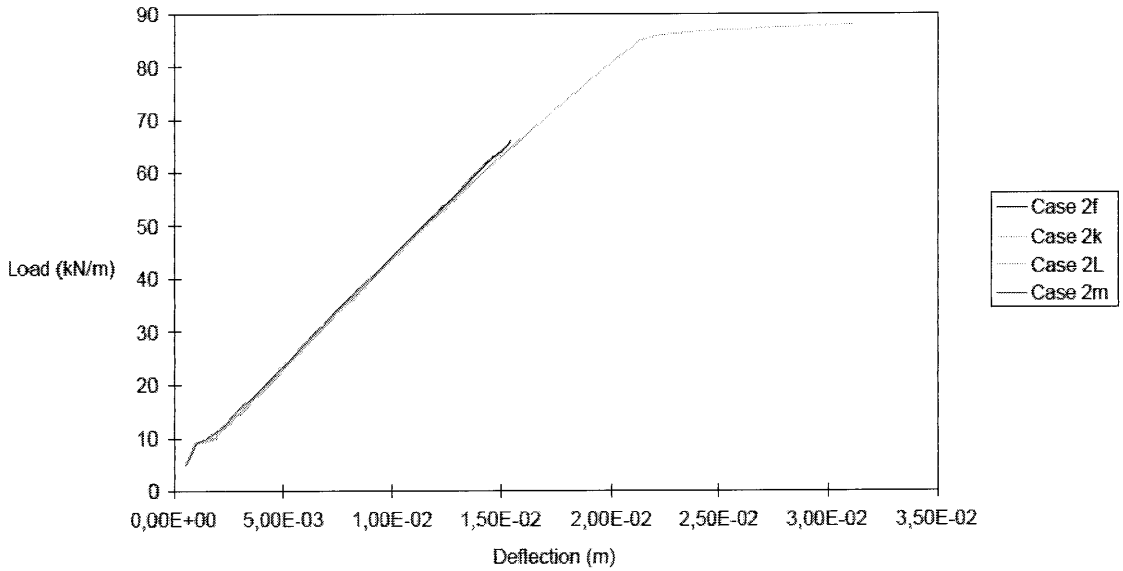


Figure 6.24 Load vs deflection curves for models with discrete reinforcement (Antonio et al.,1998)

The load-deflection curve in figure 6.24 shows a nearly linear curve (Case 2f) that quickly reached failure in the compression zones and cannot converge to a solution. As the steel assumed to behave linearly, failure in these models occurred and as soon as the failure surfaced, it reached the compressed concrete.

Chapter 7

Conclusions, Recommendations and Future Works

Chapter 7

Conclusions, Recommendations and Future Works

Shear behavior of UHSC beams reinforced by HSS bars was studied through the three groups of beams. A total of ten beams were casted at Bahrain Precast Concrete Company and tested in the structural laboratory of Civil Engineering Department at the University of Bahrain. Three beams for each group; with nine beams were assigned in this study, combined with three cubes as a control specimen for each beam.

The main variables investigated in this study are the span-to-depth ratio (a/d), flexural reinforcement ratio (ρ), and compressive strength of concrete (f_{cu}). The following conclusions and recommendations were observed:

7.1 Conclusions

This investigation is to study the shear behavior of UHSC beams reinforced with HSS bars. The variables considered are the shear span-to-depth (a/d) ratio, percentage of longitudinal steel ratio (ρ), and compressive strength of concrete (f_{cu}). The following conclusions are drawn based on the obtained results in this study:

(1) The first crack was observed on the tension face in the region of pure bending at the load level of about 35 to 40% of the ultimate capacity, while the first inclined cracks were observed at about 85 to 95%.

(2) All tested beams exhibited shear failure mode in the critical shear span and the failure is a brittle-type mode which occurs suddenly without advance warning.

(3) Two types of shear failure were observed: The first failure was diagonal tension failure, which was observed on the beams with UHSC *fcu* = 112.8 MPa and

flexural reinforcement ratio of $\rho = 0.041$ and shear span-to-depth ratio of $a/d = 2.62$ without shear reinforcement. The second failure was shear compression failure of UHSC beams, $76.8 \leq fcu \leq 117.1$ MPa, and flexural reinforcement ratio of $0.019 \leq \rho \leq 0.041$ without shear reinforcement.

(4) Shear span-to-depth ratio (a/d), flexural reinforcement ratio (ρ), and compressive strength of concrete (f_{cu}) have affected the behavior of beams during testing until shear failure occurred. Deflection has increased as (a/d) increased or (ρ) or (f_{cu}) decreased.

(5) The shear strength of UHSC beams reinforced with HSS bars without web reinforcement increased with the increase in flexural reinforcement ratio (ρ), or compressive strength of concrete (f_{cu}), and decreased with the decrease of the shear span-to-depth ratio (a/d).

(6) The ratio of the test to predicted shear strength by ACI 318, BS 8110, and Eurocode 2 equations have increased as ρ or f_{cu} increased, or a/d decreased, and was larger than 1 for all the tests.

(7) Using of HSS strongly influenced the shear behavior of the concrete beams tested in the current study and constructed without web reinforcement.

(8) The international codes equations (ACI 318, BS 8110, and Eurocode 2) appeared to underestimate the shear strength of ultra-high strength concrete reinforced with high strength bar without stirrups for all values of a/d, ρ, and f_{cu}.

(9) Load deflection curves in the FEA results show linear relationship for the beams with higher steel ratio of $\rho / \rho_b > 1$ and lower $a/d < 4.21$, where the relationship shows linear up to 60 to 80% then non-linear for lower steel ratio of $\rho / \rho_b < 1$ and higher in $a/d \geq 4.21$.

(10) Shear span-to-depth ratio (a/d), flexural reinforcement (ρ), and compressive strength of concrete (f_{cu}) have affected the behavior of beams using FEA. Deflection have increased as a/d increased or ρ or f_{cu} decreased and this is in line with the experimental results.

(11) The shear stress of UHSC beams reinforced with HSS bars without stirrups using FEA increased with the increase in flexural reinforcement ratio (ρ), or compressive strength of concrete (f_{cu}), and decreased with the decrease in the shear span-to-depth ratio (a/d).

(12) The experimental shear stress is lower in FEA by approximately 6%.

(13) The behavior of the finite element models represented by the load deflection plots at mid-span show good agreement with the test data from the full-scale beam tests in some cases for lower steel ratio of $\rho / \rho_b < 1$ and higher in $a/d \geq 4.21$.

(14) The finite element models show slightly more stiffness than the test data in both the linear and non-linear ranges.

7.2 Recommendations and Future Works

Based on the limited number of tests in this study on the UHSC beams reinforced with HSS bars without stirrups, the following are the recommendations:

(1) ACI 318, BS 8110 and Eurocode 2 equations need some modification to match the specification of the UHSC.

(2) Some modification should be taken for UHSC design because the failure was observed very sudden.

(3) Further investigation on the effect of yield strength of steel (f_y), bar size reinforcement (ϕ_b), width to height (b/h) ratio or width-to-depth (b/d) ratio, tensile strength of concrete (f_t), and compression steel reinforcement (A_s').

(4) Conduct of research on stress-strain relationship for concrete and steel, which requires a computerized testing machine attached with data accession system and with necessary strain gages to measure the strain in steel reinforcement and concrete.

(5) Investigation on shear behavior when using the stirrups, effect of shear reinforcement (V_s), and stirrups spacing (s).

(6) Further studies on using UHSC like flexural behavior, other types of structural members such as columns, slabs, deep beams, etc. as well as other types of materials such as light weight ultra-high strength.

References

Abdel-Jaber Ma'en, Mu'tasim Abdel-Jaber, Hasan Katkhuda, Nasim Shatarat, and Rola El-Nimri. (2021). "Influence of compressive strength of concrete on shear strengthening of reinforced concrete beams with near surface mounted carbon fiber-reinforced polymer". *MDPI building* 2021, 11, 563. https://doi.org/10.3390/buildings 11110563.

Abd Hamid Nubailah, Muhammad Hussain Ismail, and Azmi Ibrahim. (2018). "Finite Element Analysis of Smart Reinforced Concrete Beam with Super Elastic Shape Memory Alloy subjected to Static Loading for Seismic Mitigation". Cite as: AIP Conference Proceedings 1958, 020033 (2018); https://doi.org/10.1063/1.5034564 Published Online: 09 May 2018.

ACI 318-19. American Concrete Institute Committee. (2019). "Building code requirements for structural concrete and commentary". *American Concrete Institute, Farmington Hills, Mich, USA.*

ACI 363R-10. (2015). "Report on high-strength concrete". reported by ACI Committee 363, American Concrete Institute *Advancing concrete knowledge*, 01/26/2015 02:45:36 MST.

ACI PRC-440.2-17, American Concrete Institute Committee. (2017). "Guide for the Design and Construction of Externally Bonded FRP Systems for Strengthening Concrete Structures". *American Concrete Institute,* Farmington Hills, Mich, USA. ISBN: 978-1-945487-59-0.

Ahmed S., S. Bahij, M. A. Al-Osta, S. K. Adekunle, and S. U. Al-Dulaijan. (2019). "Shear Behavior of Ultra-High-Performance Concrete Beams Reinforced with High-Strength Steel Bars". *ACI Structural Journal.* July 2019, Title No. 116-S73.

Al-Kabasi Anas Ammar, Ali Saif Al-Wardi, Qadir Bux alias Imran Latif, and Nasrellah Hassan Ahmed. (2020). "Numerical simulation study On Load deflection of reinforced ultra-high performance fiber reinforced concrete and normal concrete beams under static load". European *Journal of Molecular & Clinical Medicine* ISSN 2515-8260 Volume 07, Issue 08, 2020.

Alsalman Ali, Canh N. Dang, Gary S. Prinz, and W. Micah Hale (2017). "Evaluation of modulus of elasticity of ultra-high-performance concrete". *Elsevier. Construction and Building Materials* 153 (2017) 918–928.

Allena Srinivas, and Craig M. Newtson (2010)". Ultra-High Strength Concrete Mixtures Using Local Materials". *National Ready Mixed Concrete Association*, 2010 Concrete Sustainability Conference.

American Society for Testing of Materials. (2018). *ASTM C150/C150M – 12, ASTM A955/A955M-2009, ASTM C194, ASTM C134, ASTM C138.*

Arafa M., Shihada S., and Karmut M. (2010). "Mechanical Properties of Ultra-High-Performance Concrete Produced I Gaza Strip". *Asian Journal of Material science* 2(1) 1-12, 2010 ISSN 1996-3394 Knowledgia Review Malaysia.

Aziz Omar Qarani, and Msheer Hasan, and Hasnaa Ali. (2013). "Shear strength and behavior of ultra-high performance fiber reinforced concrete (UHPC) deep beams without web reinforcement". *International Journal of Civil Engineering* (IJCE) ISSN 2278-9987 Vol. 2, Issue 3, July 2013, 85-96 © IASET.

Badiger Neha S. (2017). "Study of behavior of reinforced concrete beam Using ANSYS". *International Conference on Emanations in Modern Technology and Engineering* (ICEMTE-2017) ISSN: 2321-8169 26 - 30. Volume: 5 Issue: 3.

Bae Baek-II, Hyun-Ki Choi, and Chang-Sik Choi. (2016). "Flexural strength evaluation of reinforced concrete members with ultra-high-performance Concrete". *Hindawi Publishing Corporation, Advances in Materials Science and Engineering.* Volume 2016, Article ID 2815247, 10 *pages*. http://dx.doi.org/10.1155/2016/2815247.

Bahraq Ashraf Awadh, Mohammed Ali Al-Osta, Shamsad Ahmad, Mesfer Mohammad Al-Zahrani, Salah Othman, Al-Dulaijan, and Muhammad Kalimur Rahman. (2019). "Experimental and Numerical Investigation of Shear Behavior of RC Beams Strengthened by Ultra-High Performance Concrete". *International Journal of Concrete Structures and Materials,* (2019) 13:6. https://doi.org/10.1186/s40069-018-0330-z.

Barbosa Antonio F., and Gabriel O Ribeiro. (1998). "Analysis of reinforced concrete structures using ANSYS nonlinear concrete model". *Computational Mechanics* New Trends and Applications S. Idelsohn, E. Oñate and E. Dvorkin (Eds.) ©CIMNE, Barcelona, Spain 1998.

BS 12:1996, British Standard. (1996). "Specification of Ordinary Portland Cement". *British Standard.*

BS 1881-116, British Standard. (1991). "Testing Concrete Part 116: Method for Determination of Compressive Strength of Concrete Cubes". *British Standard.* 83rd Edition, July 31, 1991.

BS 4449:2005 + A2:2009, British Standard. (2009). "Steel for the reinforcement of Concrete". British Standard.ICS 77.140.15; 91.080.40.

BS 8110-1. British Standard. (1997). "Structural use of Concrete, Part 1: Code of Practice for Design and Construction". *British Standard.*

BS 85002:2015+A2:2019. British Standard. (2019). "Concrete – Complementary British Standard to BS EN 206". *British Standard.*

Bubshait Abdulaziz A. Bassam M. Tahir, and M. O. Jannadi.. (2007). "Use of micro silica in concrete construction". *Building Research & Information.* Pages 41-49. Published online: 08 May 2007.

Chen How-Ji, Yi-Lin Yu, and Chao-Wei Tang. (2020). "Mechanical Properties of Ultra-High-Performance Concrete before and after Exposure to High Temperatures". *MDPI Materials* 2020, 13, 770; doi:10.3390/ma13030770 www.mdpi.com/journal/materials.

Choi Kyoung-Kya, Alaa G. Sheriff, Mahmoud M. Rada Taha, and Lan Chung. (2009). "Shear strength of slender reinforced concrete beams without web reinforcement: A model using fuzzy set theory". *Elsevier. Engineering Structures* 31 (2009) 786-777.

Choi C.-K., and H.-G. Kwak. (1989). "The effect of finite element mesh size in nonlinear analysis of reinforced concrete structures". *Computers &. Wuctures* Vol. 36. No. 5. pp. 807-815, 1990 Printed in Great Britain.

CSA. 2014. A23.3-14. (2014)"Design of concrete structures". *Canadian Standards Association. 5060 Spectrum Way. Suite 100. Mississauga. Ontario. Canada. L4W 5NG.*

Dahmani L., A. Khennane, and S. Kaci. (2010)."Crack identification in reinforced concrete beams using ANSYS software". Strength *of Materials,* Vol. 42, No. 2, 2010 UDC 539.4.

Darwin David, Charles W. Dolan, and Arthur H. Nilson. (2016)."Design of concrete structure". 15th edition. *McGraw-Hill Education: New York.*

Elbahy Y. I., M. A. Youssef, and M. Nehdi. (2009). "Stress block parameters for concrete flexural members reinforced with super elastic shape memory alloys". *Materials and Structures* (2009) 42:1335–1351 DOI 10.1617/s11527-008-9453-z.

Elzanaty Ashraf H, Nilson Arthur H., and Slate Floyd 0. (1986). "Shear Capacity of Reinforced Concrete Beams Using High-Strength Concrete". *ACI JOURNAL* / March-April 1986.

EN 1992-1-2. (2004). (English): Eurocode 2:"Design of concrete structures - Part 1-2: General rules - Structural fire design". *[Authority: The European Union Per Regulation 305/2011, Directive 98/34/EC, Directive 2004/18/EC].*

Farooq Umer, and Mir Aijaz. Ahmad. (2014). "Finite element approach to reinforced concrete using ANSYS". Conference paper March 2014 doi: 10.1314/RG.2.1.4721.9365. National conference on sustainable infrastructure development (NCSID) At: Chandigarh, India.

International Federation for Structural Concrete *(fib).* (2010). fib MC Model Code 2010, Lausanne Switzerland. ISSN 1562-3610, Volume 1 ISBN 978-2-88394-095-6, and Volume 2. ISBN 978-2-88394-096-3.

Florian Hude, and Silva Jaime. (2018). "High strength reinforcement (HSR) – the smart solution for sustainable future". *Building Tomorrow's Society. Fredericton, Canada.* June 13 – June 16, 2018.

Guler Kadir, Fuat Demir, and Ferhat Pakdamar. (2012). "Stress–strain modelling of high strength concrete by fuzzy logic approach". *Construction and Building Materials 37* (2012) 680–684.

Gysel A. Van, and L. Taerwe. (1996). "Analytical Formulation of the Complete Stress-Strain Curve for High Strength Concrete". *Materials and Structures* 1996, 29, 529–533.

Hamrat M. B., Boulekbache, M. Chemrouk, and S. Amziane. (2009.) "Shear behavior of RC beams without stirrups made of normal strength and high strength concretes". *Advances in Structural Engineering* Vol. 13 No. 1 2009.

Hassan Tarek K., Hatem M., Seliem, Hazim Dwairi, Sami H. Rizkalla, and Paul Zia. (2008). "Shear Behavior of Large Concrete Beams Reinforced with High-Strength Steel". *ACI Structural Journal/March-April 2008, Title no. 105-S18.*

Hawileh R.A. (2015). "Finite Element Modeling of reinforced concrete beams with a hybrid combination of steel and aramid reinforcement". *Elsevier. Materials and Design* 65 (2015) 831–839.

Haynes Richard J. (2017). "Significance and Role of Si in Crop Production". *Science Direct, advances in Agronomy.* 2017.

Hung Chung-Chan, Sherif El-Tawil, and Shih-Ho Chao. (2021). "A Review of developments and challenges for UHPC in structural engineering: Behavior, Analysis, and Design". *ASCE J. Struct. Eng.,* 2021, 147(9): 03121001.

Hussein Luaay, and Lamya Amleh. (2015). "Structural behavior of ultra-high performance fiber reinforced concrete-normal strength concrete or high strength concrete composite members". *Elsevier. Construction and Building Materials* 93 (2015) 1105-1116.

Kachlakev Damian, Thomas Miller, and Solomon Yim. (2001). "Finite element modeling of reinforced concrete structures strengthened with FRP laminates". Final Report SPR 316 for *Oregon Department of Transportation, Salem* 97301-5192, and *Federal Highway Administration, Washington,* DC 2059, May 2001.

Kamal M.M., M.A. Safan, Z.A. Etman, R.A. Salama. (2014.)" Behavior and strength of beams cast with ultra-high strength concrete containing different types of fibers". HBRC Journal, (2014)10, 55-63. http://ees.elsevier.com/hbrcj.

Khaksefidi Samaneh, Mansour Ghalehnovi, and Jorge de Brito. (2021). "Bond behavior of high-strength steel rebars in normal (NSC) and ultra-high-performance concrete (UHPC)". *Journal of Building Engineering. Building Materials* 33 (2021) 101592.

Khalil Wasan I. and Tayfur Y. R. (2013). "Flexural Strength of Fibrous Ultra High-Performance Reinforced Concrete Beams". *ARPN Journal of Engineering and Applied Sciences.* VOL. 8. NO. 3.

Khayat Kamal Henri, Weina Menga, Kavya Vallurupallia, and Le Teng. (2019). "Rheological properties of ultra-high-performance concrete — An overview." *Elsevier, Cement and Concrete Research* 124 (2019) 105828.

Khazaal Ammar Saleem. (2008). "Mesh size effects in nonlinear dynamic 3D- analysis of reinforced concrete beam under impact load". Tikrit Journal of Engineering Sciences/Vol.15/No.2/June 2008, (77-93)

Kodur Venkatesh, Roya Solhmirzaei, Ankit Agrawal, Esam M Aziz, and Parviz Soroushian. (2018). "Analysis of flexural and shear resistance of ultra-high-performance fiber reinforced concrete beams without stirrups". *Elsevier. Engineering Structures* 174 (2018) 873-884.

Kwak Yoon-Keun, Marc O. Eberhard, Woo-Suk Kim, and Jubum Kim. (2002). "Shear strength of steel fiber reinforced concrete beams without stirrups". *ACI Structural Journal*, Title no. 99-S55.

Lai Zhichao, Wenbing Han, Ying Wang, Xiaoqiang Yang, and Wenjin Huang. (2022). "Shear behavior of high-strength square concrete filled steel tube members". *Elsevier,* Journal *of Constructional Steel Research* 196 (2022) 107423

Li Chuanxi, Zheng Feng , Lu Ke , Rensheng Pan, and Jie Nie. (2019). "Experimental Study on Shear Performance of Cast-In-Place Ultra-High Performance Concrete Structures". Materials (Basel). 2019 Oct; 12(19): 3254. PMCID: PMC6804125. PMID: 31590407. Published online 2019 Oct 5. doi: 10.3390/ma12193254.

Liu Wing Kam, Shaofan Li, and Harold S. Park. (2022). "Eighty Years of the Finite Element Method: Birth, Evolution, and Future". *Archives of Computational Methods in Engineering* (2022) 29:4431–4453. https://doi.org/10.1007/s11831-022-09740-9.

Machial Robert, M. Shahria Alam, and Ahmad Rteil. (2012). "Revisiting the shear design equations for concrete beams reinforced with FRP rebar and stirrup". *Materials and Structures* RILEM 2012. DOI 10.1617/s11527-012-9859-5.

Mansor Ahmed Abdullah, Ahlam Sader Mohammed, and Maysoon Adullah Mansor. (2020). "Reinforced concrete beams capacity with various concrete compressive strengths". IOP Conf. Series: *Materials Science and Engineering* 978 (2020) 012036 IOP Publishing doi:10.1088/1757-899X/978/1/012036.

Farzad Masha, Mohamadreza Shafieifar, and Atorod Azizinamini. (2019). "Experimental and numerical study on bond strength between conventional concrete and Ultra High-Performance Concrete (UHPC)". *Elsevier, Engineering Structures* 186 (2019) 297-305.

Meqdadi M. Mohammed. (1993). MSc. Thesis. "Shear and Flexural Behavior of High Strength Concrete Beams with Large Span to Depth Ratio". *Jordan University of Science and Technology. Jordan.*

Meszoly Tamas, and Norbert Randl. (2018). "Shear behavior of fiber-reinforced ultra-high performance concrete beams". Elsevier, *Engineering Structures* 168 (2018) 119-127.

Muhammad Jaza Hassan, and Abdulkadir Mohamed Rauof. (2017). "Nonlinear Finite Element Modeling for High Strength Fibrous Reinforced Concrete Beams". Professor Sulaimani Journal for Engineering Sciences / Volume 4 - Number 4 – 2017.

Neville A. M. (2011). "Properties of concrete Fifth Edition". *Published by Pearson Education Limited. London. 2011.*

Nikbakhta Ehsan, Amin Al-Fakiha, Chieng Chew Huia, Lee Yuan Jakea, and Mst. Sadia Mahzabinb. (2019). "An experimental investigation on the shear and flexural behavior of steel reinforced HPSCC beams.". *Elsevier, Structures* 19 (2019) 286-295.

Nguyen Tan-Trac, Huu-Tai Thai, and Tuan Ngo. (2021). "Optimized mix design and elastic modulus prediction of ultra-high strength concrete". *Elsevier. Construction and Building Materials* 302 (2021) 124150.

Pandimani, Markandeya Raju Ponnada, and Yesuratnam Geddada. (2022). "Numerical nonlinear modeling and simulations of high strength reinforced concrete beams using ANSYS". *Journal of Building Pathology and Rehabilitation* (2022) 7:22 https://doi.org/10.1007/s41024-021-00155-w.

Park R., and T. Paulay. (2009). "Reinforced Concrete Structures". *John Wiley & Sons. New York.*

Pradhan Karan Kumar, and Snehashish Chakraverty. (2019). "Finite Element Method". *Computational Structural Mechanics*, 2019.

Perceka Wisena, Wen-Cheng Liao, and Yung-Fu Wu. (2019). "Shear Strength Prediction Equations and Experimental Study of High Strength Steel Fiber-Reinforced Concrete Beams with Different Shear Span-to-Depth Ratios". MDPI Applied Science 2019, 9, 4790; doi:10.3390/app9224790

Rewers Iga. (2019). Numerical Analysis of RC beam with High Strength Steel Reinforcement using CDP model". 2019 *IOP Conf. Ser. Mater. Sci. Eng.* 471 022025.

Rashid M. A., and M. A. Mansur. (2005). "Reinforced High-Strength Concrete Beams in Flexure". *ACI Structural Journal*, May-June, Title no. 102-S47, PP 462-472.

Saeed Moavini. (2020). "Finite Element Analysis Theory and Application with ANSYS". Fifth edition, Pearson, ISBN-13: 978-0-13-521210-3.

Said Asmaa, Mahmoud Elsayed, Ahmed Abd El-Azim, Fadi Althoey, and Bassam A. Tayeh. (2022). "Using ultra-high performance fiber reinforced concrete in improvement shear strength of reinforced concrete beams". *Elsevier, Construction Materials* 16 (2022) e01009.

Shah Surendra P., Stuart E. Swartz, and chengsheng Ouyang. (1995). "Fracture mechanics of concrete: Applications of fracture mechanics to concrete, rock, and other quasi-brittle materials". John Wiley & Sons INC.

Smarzewski Piotr, and Adam Stolarski. (2017). "Numerical Analysis on the High-Strength Concrete Beams Ultimate Behavior". WMCAUS IOP Conf. Series: *Materials Science and Engineering* 245 (2017) 032013 doi:10.1088/1757-899X/245/3/032013.

Solhmirzaei Roya, and Kodur Venkatesh. (2021). "Numerical Model for Tracing Structural Response of Ultra-High Performance Concrete Beams". *MPDI Modelling* 2021, 2, 448–466. https://doi.org/10.3390/modelling2040024

Subramanian N., Krishna N Ramanathan, and A.R. Santhakumar. (2020). "Review of basic codal provisions for the design of reinforced concrete structures". ICI Journal April-June 2020.

Subramani T., R. Manivannan, and M. Kavitha. (2014). "Crack identification in reinforced concrete beams using ANSYS software". *Journal of Engineering Research and Applications* ISSN: 2248-9622, Vol. 4, Issue 6(Version 6), June 2014, pp.133-141.

Tahenni Touhami, Farid Bouziadi, Bensaid Boulekbache, and Sofiane Amziane. (2021). "Experimental and nonlinear finite element analysis of shear behavior of reinforced concrete beams". *Elsevier. Structures* 29 (2021) 1582-1596.

Tanijaya Jonie, Suleman Tappi, and Jabair. (2021). "The mechanical properties of limestone as an aggregate on high strength concrete". IOP Conf. Series: *Materials Science and Engineering* 1088 (2021) 012098.

Tavallali Hooman, Andres Lepage, Jeffrey M. Rautenberg, and Santiago Pujol. (2014). "Concrete Beams Reinforced with High-Strength Steel Subjected to Displacement Reversals". *ACI Structural Journal/September*-October 2014. Title No. 111-S87.

Tjitradi Darmansyah, Eliatun Eliatun, and Syahril Taufik. (2017). "3D ANSYS Numerical Modeling of Reinforced Concrete Beam Behavior under Different Collapsed Mechanisms.". *International Journal of Mechanics and Applications* 2017, 7(1): 14-23 DOI: 10.5923/j.mechanics.20170701.02.

Tibea C., and Dan V. Bompa. (2020). "Ultimate shear response of ultra-high-performance steel fiber-reinforced concrete elements". *Archives of Civil and Mechanical Engineering.* (2020) 20:49. https://doi.org/10.1007/s43452-020-00051-z.

Wakjira Tadesse G, and Usama Ebead. (2020). "Shear span-to-depth ratio effect on steel reinforced grout strengthened reinforced concrete beams". *Elsevier. Engineering Structures* 216 (2020) 110773.

Wang Qiang, Hua-Lin Songb, Chun-Ling Lua, and Ling-Zhi Jinb. (2020). "Shear performance of reinforced ultra-high performance concrete rectangular section beams". *Elsevier. Structures* 27 (2020) 1108-1194.

Wille Kay, Antoine E. Naaman, and Gustavo J. Parra-Montesinos. (2011). "Ultra-High-Performance Concrete with Compressive Strength Exceeding 150 MPa (22 ksi): A Simpler Way". *Publication Materials Journal, Volume: 108, Issue:* 1, Appears on pages(s): 46-54 Date: 1/1/2011.

Wu Xiangguo, Thomas H.-K. Kang, Yang Lin, Hyeon-Jong Hwang. (2018). "Shear strength of reinforced concrete beams with precast high-performance fiber-reinforced cementitious composite permanent form". Elsevier Composite Structures 200 (2018) 829–838.

Xia Jun, Kevin R. Mackiea, Muhammad A. Saleemb, and Amir Mirmiranb. (2011). "Shear failure analysis on ultra-high performance concrete beams reinforced with high strength steel". *Elsevier. Engineering Structures* 33 (2011) 3597-3609.

Yousef Ahmed M., Ahmed M. Tahwia, and Nagat A. Marami. (2018). "Minimum shear reinforcement for ultra-high-performance fiber reinforced concrete deep beams". *Elsevier. Construction and Build. Materials.* 184 (Sep): 177–185.

https://doi.org/10.1016/j.conbuildmat.2018.06.022.

Zhang Zhe, Xu-Dong Shao, and Ping Zhu. (2020)." Direct tensile behaviors of steel-bar reinforced ultra-high performance fiber reinforced concrete: Effects of steel fibers and steel rebar". *Elsevier. Construction and Building Materials* 243 (2020) 118054.

Summary in Arabic

ملخص باللغة العربية

سلوك الجوائز (الجسور الخرسانية) المصنوعة من خرسانة فائقة التحمل المسلحة بقضبان فولاذية عالية القوة تحت تأثير قوى القص

الخلاصة:

الخرسانة فائقة التحمل (UHSC) أو الخرسانة فائقة الأداء (UHPC) هو نوع جديد من المركبات الخرسانية القائمة على الأسمنت مع قوة وصلابة ومتانة عالية والتي تم استخدامها على نطاق واسع في مشاريع الهندسة المدنية مثل هياكل الجسور ومدارج المطارات والسكك الحديدية عالية السرعة وأعمال الإصلاح وما إلى ذلك بسبب خصائصه الممتازة، حيث يستخدم UHSC بدلاً من الخرسانة ذات القوة العادية (NSC).

تتمثل ميزة استخدام UHSC المسلح بقضبان فولاذية عالية القوة (HSS) في أنه يمكن أن يقلل من أبعاد المقطع العرضي للأعضاء الهيكلية؛ لذلك، يقلل من الوزن الذاتي للهيكل. لهذا السبب، هناك حاجة إلى مزيد من البحث حول أعضاء الهيكل باستخدام هذا النوع من المواد.

تمت دراسة سلوك القص للجوائز المصنوعة من UHSC والمسلحة بقضبان HSS من خلال ثلاث مجموعات حيث تم صب عشرة جوائز في شركة البحرين للخرسانة مسبقة الصب واختبارها في المختبر الإنشائي لقسم الهندسة المدنية بجامعة البحرين. وتم تخصيص ثلاثة جوائز لكل مجموعة بمجموع تسعة جوائز تمت دراستها مع ثلاثة مكعبات تحكم لكل جائز لقياس مقدار تحمل الخرسانة.

يهدف هذا البحث الى دراسة سلوك القص في الجوائز الخرسانية المصنوعة من خرسانة فائقة التحمل المسلحة من قضبان عالية القوة من خلال تأثير المتغيرات التالية:

1- نسبة مجاز القص الى العمق الفعال (a/d) في المجموعة الأولى، وقد كانت القيم هي (2.63 و3.16 4.21) اما نسبة التسليح فقد كانت 0.041 وقوة تحمل الخرسانة درجة سي 110

2- كمية تسليح الحديد الطولي المقاوم لقوى القص في منطقة الشد (نسبة التسليح ρ) في المجموعة الثانية، وقد كانت القيم هي (0.041 و0.031 و0.019) اما نسبة المجاز للقص فقد كانت 4.21 وقوة تحمل الخرسانة درجة سي 110

3- مقدار قوة تحمل الخرسانة (f'c أو fcu). في المجموعة الثالثة، وقد كانت القيم هي (76.8 ميجا باسكال، 102.2 ميجا باسكال و112.8 ميجا باسكال) اما نسبة التسليح فقد كانت 0.041 ونسبة المجاز للقص فقد كانت 2.63.

وقد تم صب جميع الجوائز بدون كانات (تسليح الحديد المقاوم لقوى القص) للتحقق من تأثير a/d و ρ و fcu.

تمت دراسة تأثير كل متغير بشكل منفصل، بينما بقيت قيم المتغيرات ثابتة أو شبه ثابتة. جميع الجوائز لها نفس المقطع العرضي بعرض (ملم b = 200) وبعمق (ملم h = 300)، والعمق الفعال (d) يعتمد على قطر القضبان وعدد الطبقات من 230.5 ملم الى 263.5 ملم، وقد تم دعم العارضة بأسطوانة في كلا الطرفين للقضاء على أي تأثير محوري وتحميلها بأحمال من نقطتين مما أعطى ميزة الجمع بين شرطين اختبار مختلفين: الانحناء النقي بين الحملتين وقوة القص الثابتة في المقاطع الطرفية.

تمت دراسة سلوك القص للجوائز المختبرة من حيث نمط الشق، وآليات الفشل، وعلاقات هبوط الحمل، وقوة القص. وقد تم استخدام مقياس لتسجيل الهبوط في الجوائز من المنتصف، وتم توثيق جميع القياسات حتى الفشل، وتم إجراء فحص دقيق لظهور الشقوق.

جميع الجائز في المجموعة الأولى فشلت بواسطة قوى القص حيث فشل الجائز والذي نسبة (a/d = 2.63) بطريقة الفشل من النوع التوتر القطري بينما فشل الجائز والذي نسبة (a/d = 3.16) بطريقة الفشل من نوع فشل ضغط القص والجائز والذي نسبة (a/d = 4.21) بطريقة فشل قص الانعطاف.

أما جوائز المجموعة الثانية فجميعها كذلك فشلت بواسطة قوى القص حيث فشل الجائز والذي نسبة التسليح فيه (ρ= 0.019 و0.031) فقد فشلا بطريقة الفشل من النوع ضغط القص بينما فشل الجائز والذي نسبة (ρ= 0.041) بطريقة الفشل من النوع فشل قص الانعطاف.

جوائز المجموعة الثالثة فجميعها كذلك فشلت بواسطة قوى القص حيث فشل الجائز والذي قوة تحمل الخرسانة (fcu = 76.8 و 102.2 ميجا باسكال) فقد فشلا بطريقة الفشل من النوع ضغط القص بينما فشل الجائز والذي قوة تحمل الخرسانة فيه (ميجا باسكال fcu = 112.8) بطريقة الفشل من النوع فشل قص الانعطاف.

وتظهر النتائج انه عند نفس مستوى الحمل، مع زيادة نسبة a/d يزداد الهبوط وتقل قوة القص وأيضاً مع زيادة fcu و ρ ينخفض الهبوط وتزداد قوة القص.

تمت مقارنة مقاومة القص التجريبية للجوائز المصنوعة من خرسانة فائقة التحمل المسلحة بقضبان عالية القوة بدون استخدام تسليح الحديد المقاوم لقوى القص مع تلك المحسوبة بواسطة معادلات كود المعهد الأمريكي للخرسانة ACI 318 والكود البريطاني BS8110 والكود الاوروبي Eurocode 2. حيث أظهرت النتائج أن مقاومة القص المقاسة كانت أكبر من تلك التي تنبأت بها معادلات الكودات بكميات متفاوتة اعتمادا على نسبة مجاز القص الى العمق الفعال وكمية تسليح الحديد الطولي المقاوم لقوى القص في منطقة الشد ومقدار قوة تحمل الخرسانة، حيث وجدت بانها أقل من النتائج المخبرية وعلية يجب تعديلها لهذا النوع من الخرسانة.

تمت مقارنة مقاومة القص التجريبية للجوائز المصنوعة من خرسانة فائقة التحمل المسلحة بقضبان عالية القوة بدون استخدام تسليح الحديد المقاوم لقوى القص مع تلك المحسوبة رقمياً بواسطة نظرية العناصر الحدية (FEA) باستخدام برنامج ANSYS وقد ظهرت نتائج منحنيات علاقة قوى القص مع الهبوط في الجوائز عند دراسة تأثير (a/d) بأن النتائج المخبرية أعلى من نتائج التحليل بواسطة نظرية العناصر الحدية في الجزء الخطي من المنحنى وأقل منه بعد الجزء الخطي. أما عند دراسة تأثير نسبة التسليح (ρ) فقد أظهرت النتائج المخبرية بانها أقل من طريقة العناصر الحدية خلال الجزء الخطي ولكنها متقاربة النتائج بعد الجزء الخطي. أما تأثير قوة تحمل الخرسانة (fcu) بأن النتائج المخبرية أعلى من نتائج التحليل بواسطة نظرية العناصر الحدية في الجزء الخطي من المنحنى وخاصة عندما تكون قوة تحمل الخرسانة اعلى وتكون متقاربة في حالة ان تكون قوة تحمل الخرسانة أقل. علاوة على ذلك، أظهرت النتائج أن مقاومة القص التجريبية أقل بحوالي 13.5% من FEA.

بشكل عام تظهر نتائج FEA إنه عند مستوى الحمل ومع زيادة نسبة (a/d), يزداد الهبوط وتقل وتقل قوة القص. بالإضافة الى ذلك كلما زادت (ρ) او (fcu) يقل الهبوط، وتزداد قوة القص وهذا يتفق مع النتائج التجريبية. مع ملاحظة ان منحنيات الهبوط مع الحمل في نتائج طريقة العناصر الحدية باستخدام برنامج ANSYS تظهر علاقة خطية للجسور ذات نسبة التسليح العالية ($\rho/\rho_b < 1$) وكذلك عندما تكون نسبة ($a/d < 4.21$), بينما تظهر نتائج المنحنيات علاقة خطية لنسبة بين 60% الى 80% وبعدها تظهر علاقة غير خطية في حالة نسبة التسليح الأقل ($\rho/\rho_b > 1$) وكذلك في حالة نسبة ($a/d \geq 4.21$).

التوصيات:

بناءً على العدد المحدود للاختبارات في هذه الدراسة سلوك الجوائز المصنوعة من خرسانة فائقة التحمل المسلحة بقضبان فولاذية عالية القوة تحت تأثير قوى القص وبدون تسليح الحديد المقاوم لقوى القص، فيما يلي التوصيات:

1- تعديل معادلات كود المعهد الأمريكي للخرسانة ACI 318 والكود البريطاني BS8110 والكود الأوروبي Eurocode 2 لتتناسب مع مواصفات UHSC.

2- نحتاج مزيداً من الدراسات حول هذا الموضوع ومثال على ذلك تأثير مقاومة الخضوع لحديد التسليح (fy) وتأثير زيادة قطر قضبان حديد التسليح (φ_b) وتأثير نسبة عرض الجوائز الى عمقها (b/h) ومقاومة شد الخرسانة (ft) وتأثير كميه حديد التسليح في منطقة الضغط في الجوائز (A's).

3- إجراء بحث حول علاقة الإجهاد والانفعال للخرسانة وحديد التسليح، والتي تتطلب آلة اختبار محوسبة متصلة بنظام وصول البيانات ومعها أجهزة قياس الضغط اللازمة لقياس الضغط في حديد التسليح والخرسانة.

4- دراسات أخرى في سلوك القص عند استخدام حديد التسليح لمقاومة القص (Vs) ودراسة المسافات بين الكانات (s).

5- مزيد من الدراسات حول استخدام UHSC مثل سلوك الانعطاف وأنواع أخرى من العناصر الهيكلية مثل الأعمدة والألواح والعوارض العميقة وما إلى ذلك بالإضافة إلى أنواع أخرى من المواد مثل الوزن الخفيف والمتانة الفائقة.

Appendix

Notifications

a = *Depth of equivalent rectangle stress block in the compression zone (mm)*

a = *Shear span from reaction to the first concentrated load point (m)*

A = *Gross area of the section (mm^2)*

A_s = *Area of tension steel reinforcement (mm^2)*

b = *Width of the rectangular beam (mm)*

c = *Depth of the neutral axis from the top of the beam (mm)*

C = *Compressive concrete force of the beam section (KN)*

d = *Effective depth of the beam from extreme compression fiber to centroid of tension reinforcement (mm)*

a/d = *Span-to-depth ratio*

E = *Modulus of Elasticity (MPa)*

E_c = *Modulus of elasticity for concrete (MPa)*

E_s = *Modulus of elasticity for Steel (MPa)*

f_{2c2} = *Biaxial compressive strength (MPa)*

f_c' = *Uniaxial Compressive strength of Concrete cylinder (Mpa)*

f_{cr} = *Cracking strength of concrete (Mpa)*

f_{cu} = *Uniaxial Compressive strength of Concrete cube correspondence to the concrete in the test beam (Mpa)*

f_r = *Modulus of rupture (Mpa)*

f_s = *Stress of the reinforcing bars (Mpa)*

f_y = *Yield strength of the reinforcing bars (Mpa)*

h = *Total depth of rectangular beam (mm)*

K_{cm} = *Biaxial strain at uniaxial compressive strength*

L = *Length of beam (distance between supports) (m)*

L/h = *Span to total depth ratio*

M = *Bending moment in general (KN.m)*

M_n = *Nominal bending strength in section (KN.m)*

M_u = *Ultimate moment strength of the beam (failure) (KN.m)*

M_{cr} = *Cracking moment in the beam (KN.m)*

n = *Modular ratio (E_s/ E_c)*

P = *Concentrated load in general (KN)*

P_u = *Ultimate failure load of beam (KN)*

V = *Shear load in general (KN)*

V_c = *Shear force carried by concrete (KN)*

V_s = *Nominal shear force provided by stirrups (KN)*

$V_n=V_c+V_s$ = *Nominal sheer force of the beam (KN)*

V_u = *Ultimate shear force in the beam (KN)*

v = *Shear stress in general (KN)*

v_c = *Shear stress carried by concrete (Mpa)*

v_u = *Ultimate shear stress for the beam (Mpa)*

Z = *Lever arm between Tension and Compression forces (mm)*

β_1 = *Concrete property that is the "ratio of depth of rectangular stress block to the depth to the neutral axis*

Υ_m = *Material partial safety factor*

λ = *Concrete design factor*

δ, Δ = *Deflection at md span of the beam (mm)*

ρ = *Steel ratio in tension zone*

ρ_b = *Balanced tensile steel ratio*

ρ' = *Steel ratio compression zone*

ϕ = *Bar diameter (mm)*

φ_c = *Resistance factor for concret*

v = *Poisson's ratio*

ε = *Strain in general (mm/mm)*

ε_c = *Concrete strain*

ε_s = *Steel strain*

ε_{cm}, ε_{cu} = *Maximum (ultimate) strain in concrete*

ε_y = *Yield strain of steel*

جـامعة البحـرين

كلية الهندسة



قسم الهندسة المدنية

سلوك الجوائز (الجسور الخرسانية) المصنوعة من خرسانة فائقة التحمل المسلحة بقضبان فولاذية عالية القوة تحت تأثير قوى القص

أطروحة مقدمة استكمالاً لمتطلبات درجة الدكتوراه في الهندسة المدنية

مقدمة من

محمد موسى محمد مقدادي

الرقم الجامعي: ٢٠١٥٠٠٩٨

المشرف

د. مصطفى ايتكن
(أستاذ)
جامعة البحرين

المشرف

د. م د شاه علام
(أستاذ مساعد)
جامعة البحرين

مـملكة البـــحرين

يناير ٢٠٢٣م